ELECTRONIC CONDUCTION AND HYPERELECTRONIC POLARIZATION IN ELECTRO-ACTIVE POLYACENEQUINONE CLASS OF POLYMERIC SEMICONDUCTORS

By

PORMAMILLA SHAMARAO VIJAYAKUMAR

Bachelor of Engineering
University of Mysore
Mysore, India
1969

Master of Arts
Indiana State University
Terre Haute, Indiana
1973

Submitted to the Faculty of the Graduate College
of the Oklahoma State University
in partial fulfillment of the requirements
for the Degree of
DOCTOR OF PHILOSOPHY
July, 1983

ELECTRONIC CONDUCTION AND HYPERELECTRONIC POLARIZATION IN ELECTRO-ACTIVE POLYACENEQUINONE CLASS OF POLYMERIC SEMICONDUCTORS

Thesis Approved:

Herbert A. Pohl
Thesis Adviser

J. Paul Devlin

J. J. Martin

W. A. Sibley

Norman N. Durham
Dean of the Graduate College

ACKNOWLEDGMENTS

The author wishes to express his sincere gratitude and appreciation to Prof. H. A. Pohl, Thesis Committee Chairman, for his overall guidance, invaluable patience and understanding throughout this study. I am especially thankful to Dr. Pohl for his advice, support, encouragement and drive while writing this thesis. Appreciation is also expressed to other committee members, Professors, J. P. Devlin, E. E. Kohnke, J. J. Martin and W. A. Sibley for their patience, interest and guidance.

He is further indebted to: Professor H. Hall and associates for their assistance in design and construction of pressure cells; Dr. D. Pohl, Dr. J. Kho, Dr. J. Mason and Dr. L. Dunn for synthesizing the polymers studied; Dr. J. L. Tandon for the helpful discussions about electrical circuity; and Dr. K. L. Seshasai and Dr. G. Prakash for their assistance with computer programming.

The author graciously acknowledges financial support of the Physics Department, and Professor W. Hughes, Engineering Energy Lab., of the Electrical Engineering Department at Oklahoma State University; the Piedmont Trust Company, Michigan; and the members of my family.

My special thanks goes to my wife, Geetha, for her patience, understanding, encouragement, and for her typing. Finally, to superboy Santosh, thanks for making it all happen with a smile.

TABLE OF CONTENTS

Chapter Page

LIST OF TABLES

LIST OF FIGURES

Figure Page

Figure Page

CHAPTER I

INTRODUCTION

Organic semiconductors have seen some very exciting developments in the recent years. Several disciplines of science and engineering have contributed to the development of this field.

1.1. Classification of Materials

One can classify all materials in terms of conductivities as metals, inorganic semiconductors, organic semiconductors and insulators as shown in Table I (Gutmann and Lyons, 1967). It is thus seen that the range of conductivities for organic semiconductors is quite large, enabling one to choose the particular type of semiconductor one wants.

The term 'organic conductor' has been used to describe organic solids which contain significant amount of carbon-carbon bonding, and which also supports electronic conduction (Brophy, 1961). For the sake of convenience, one can group the organic semiconducting solids into three categories: (a) Monomeric solids like naphthalene, pyrene etc. (Okamoto and Brenner, 1964); (b) Charge transfer complexes like donor-acceptor (Kanda and Pohl, 1968); and (c) Electro-active organic polymers like polyacenequinone radical (PAQR) type of polymers, pyropolymers etc. (Kanda and Pohl, 1968; and Pohl, 1974).

Figure 1 shows the spectrum of conductivities of some important solids including the special type of pure polymers of PAQR class

TABLE I

TYPICAL VALUES OF CONDUCTANCE PARAMETERS FOR METALS, SEMICONDUCTORS AND INSULATORS

Class of Substance	Typical Values for		
	Conductivity $(ohm\text{-}cm)^{-1}$	Carrier Concentration per cm^3	Mobility $cm^2\ Volt^{-1}\ sec^{-1}$
Metals	10^2 to 10^8	10^{22}	10^3
Inorganic Semiconductors	10^3 to 10^{-10}	10^{11} to 10^{22}	10^5 to 10^{-3}
Organic Semiconductors	10^2 to 10^{-10}	10^6 to 10^{19}	10^2 to 10^{-6}
Insulators	Below 10^{-10}	Below 10^9	Below 10^{-4}

Source: Gutmann and Lyons (1967)

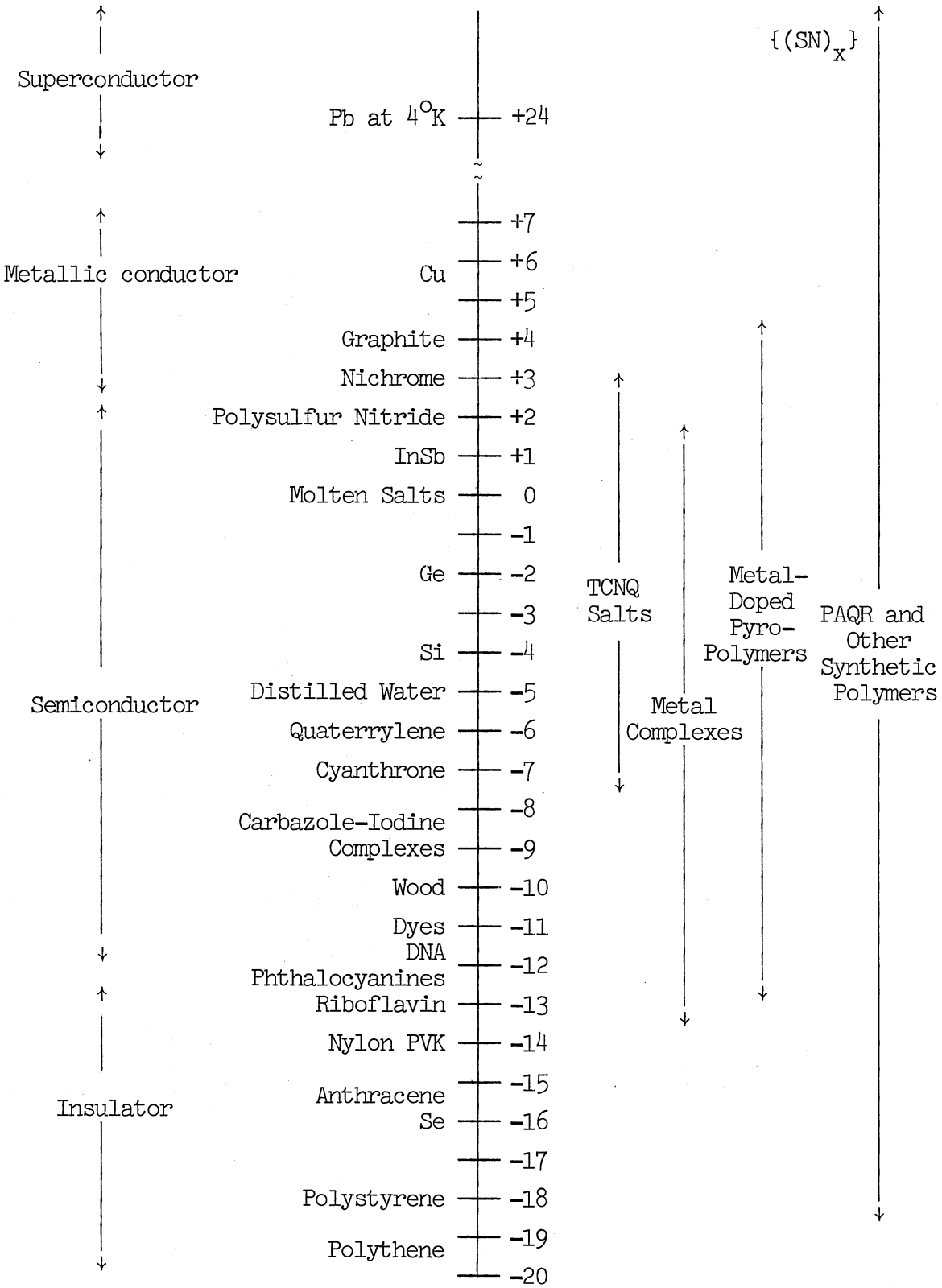

Figure 1. Log (Conductivity)(ohm cm^{-1}) at Room Temperature

(Gutmann and Lyons, 1967; and Goodings, 1975). The finding by Greene et al. (1975) that the crystalline polysulfur nitride $\{(SN)_x\}$ can go superconducting at $0.26^{o}K$ has further enhanced the interest in organic semiconductors.

Most of the organic compounds have been electrical insulators with low dielectric constants (~ 1.8 to 38). In recent years a large number of organic compounds with enhanced electronic properties have been discovered (Inokuchi and Akamatu, 1961; Okamoto and Brenner, 1964; Gutmann and Lyons, 1967; Eley, 1968; Kanda and Pohl, 1968; Pohl, 1968; Boguslavskii and Vannikov, 1970; Paushkin et al., 1974; and Wayne and Street, 1982). One of the unique findings in the PAQR class of polymers is a giant polarization which gives raise to huge dielectric constants (~ 50-100,000) with possibilities to tailor these macromolecular solids to practical needs in the area of dielectrics (Pohl, 1974).

1.2. Hyperelectronic Polarization

Polarization is the result of blocked or restricted motion of charges. There are four recognisable modes of polarization of matter as shown in Figure 2: (a) Electronic polarization is due to the displacement of electrons of the atoms relative to the nucleus as the electric field is applied. This induced moment has all the characteristics of an assembly of dipoles produced by elastic displacement of electrons with natural frequencies equal to or greater than the visible light. This resonance spectra is temperature-independent; (b) Atomic polarization is due to the relative displacement of non-equivalent atoms by an external field with natural frequencies in the infra-red band. This resonance spectra is also temperature-independent. One can separate

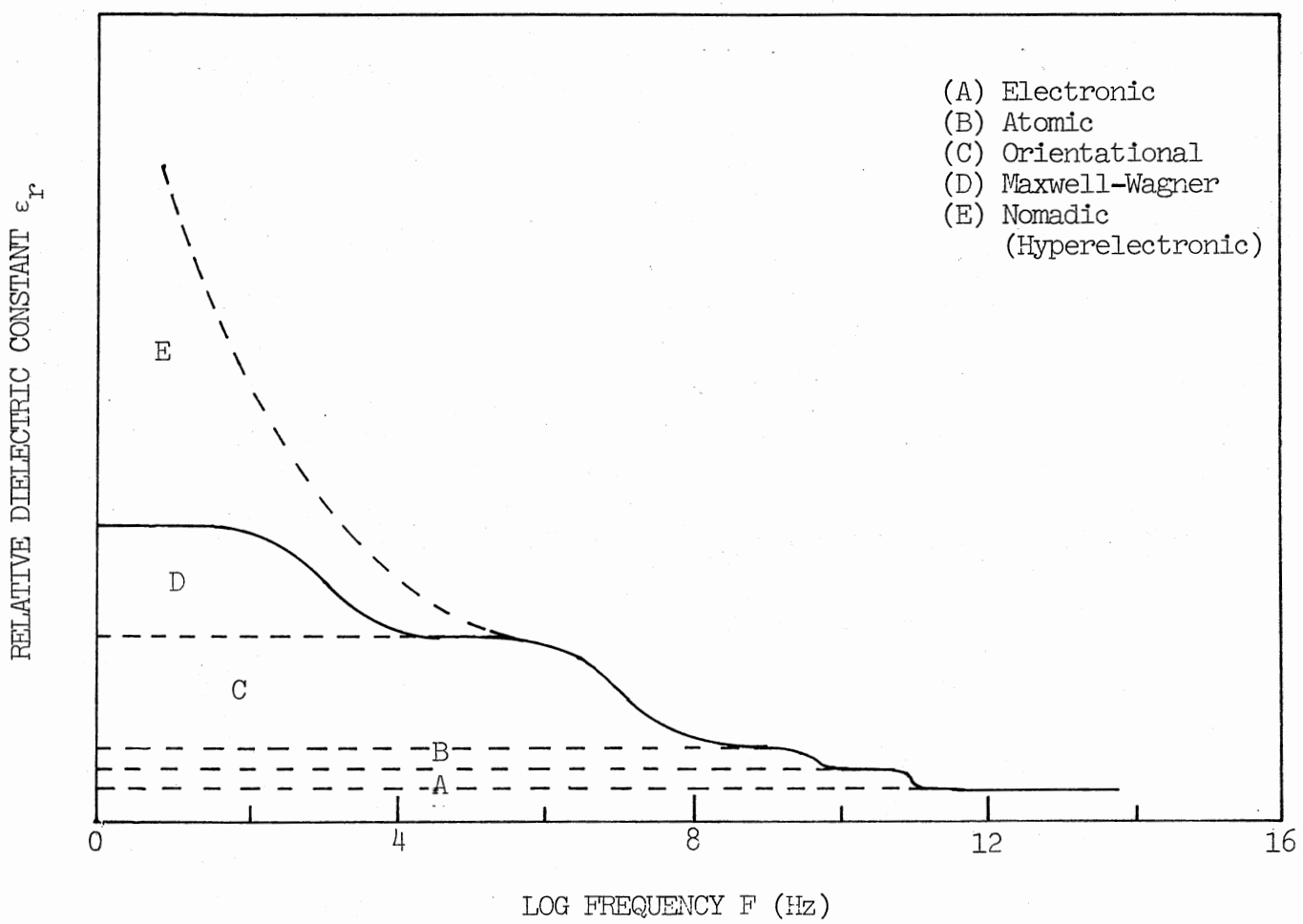

Figure 2. Schematic Diagram of Electrical Polarization Mechanisms

atomic from electronic polarization, by subtracting the dielectric constant ε_r obtained from the Maxwell's relation $n^2 = \varepsilon_r$ (where n is the refractive index) at optical frequencies, from that obtained at infrared frequencies; (c) Orientational polarization is due to the motion of freely rotating dipolar groups. This is a relaxation spectra, with an inverse temperature dependence and thus separating it from the temperature-independent atomic and electronic polarizations; (d) Maxwell-Wagner or Interfacial polarization is due to free charge carriers, which while migrating through a defective crystal get trapped by or pile up against a defect. The net effect is a localized accumulation of charge. This is a macroscopic effect. One can distinguish it from orientational polarization by the behavior of ε_r'' ($\sigma_{AC}/\omega\varepsilon_o$) as a function of frequency. For orientational polarization ε_r'' drops to zero as frequency is decreased, and for interfacial polarization ε_r'' tends to infinity as frequency tends to zero (Anderson, 1964).

In conventional organic polymers, the first three modes of polarization give raise to low dielectric constants (~ 1.8 to 38). Clearly, these phenomena alone cannot account for the huge dielectric constants (~ 50-100,000) observed in the PAQR class of polymers. This giant polarization has been called nomadic polarization by Rosen and Pohl (1966), and this constitutes the fifth (e) mode of polarization as shown in Figure 2. It reflects the response of highly delocalized electrons (thermal, pressure or field generated) in long molecular domains (such as regions of associated π-orbitals in conjugated polymers). If the charge carriers are electrons, it is called as hyperelectronic polarization, and if the charge carriers are protons, it is called as hyperprotonic polarization.

The two prerequisites for the presence of nomadic polarization are: (1) the density of charge carriers must be appreciable; and (2) there must be suitable long domains for the roving charges. The roving charge pairs (electrons and holes) are produced by dissociation of electrons from one molecular chain to a more or less distant molecular chain while leaving a 'hole' in the parent molecular chain as shown in Figure 3. The dissociation energy $\Delta E = W \simeq (I - E_A)$, where I is the ionization energy and E_A is the electron affinity per macromolecule in the solid. For this simple two level process, the Fermi energy $E_F = W/2$, if one assumes that all the macromolecules are equivalent. Of the charge pairs, the intermolecular excitons (Mott) are more effective than the intramolecular excitons (Frenkel) in contributing to nomadic polarization. Hartman and Pohl (1968) have proposed a macromolecular model of polymers made up of long macromolecules of length L and thickness b separated by intermolecular gap as shown in Figure 4. In the presence of an external electric field, the charge pairs on different molecules can give raise to huge dipole moments.

One can separate the nomadic polarization where the dielectric constant shows a strong increase with increasing temperature, from the orientational polarization which decreases with increasing temperature. Since both nomadic and interfacial polarizations are reflected in the lower range of the frequency spectra, it is necessary to establish the criteria for distinguishing the two. Hartman (1968) has shown that for hyperelectronic polarization: (a) ε_r increases with pressure; (b) ε_r strongly increases with temperature; (c) ε_r dependence on electric field strength is non-linear and polarization shows saturation at relatively low field strengths; (d) ε_r dependence upon grain-boundary effects in a

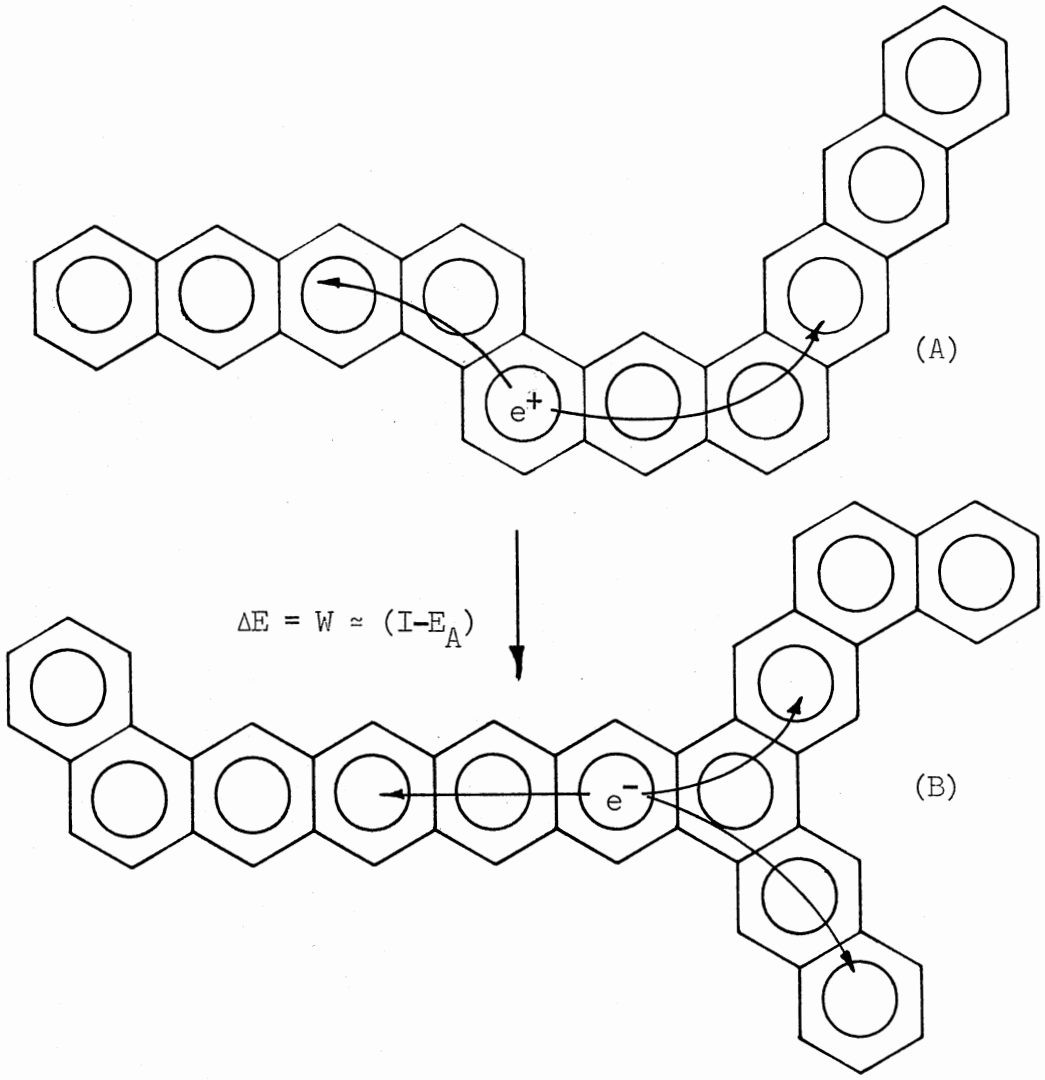

Figure 3. Diagram of Thermal or Field Induced Charge Separation Between Polymer Molecules (A) and (B) of Unlike or Similar Size

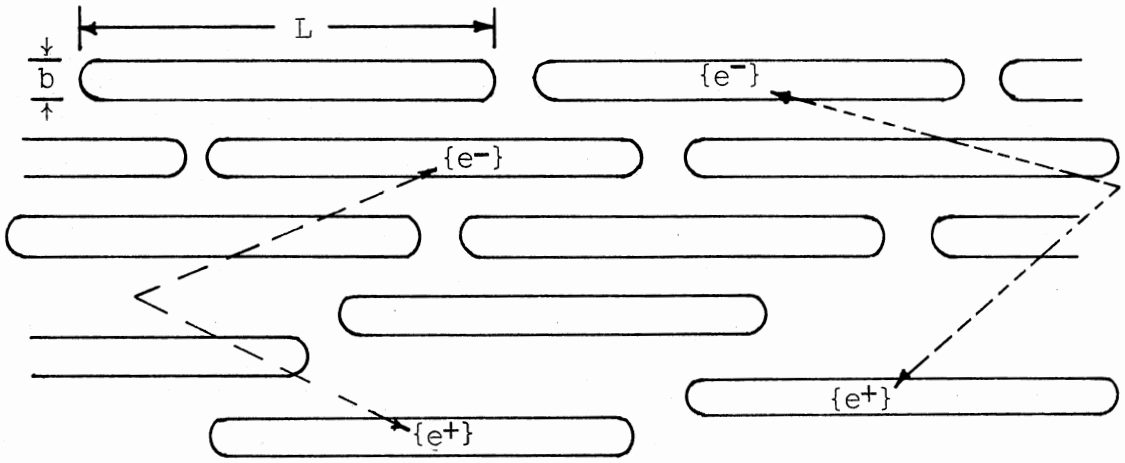

(a) Zero Electric Field

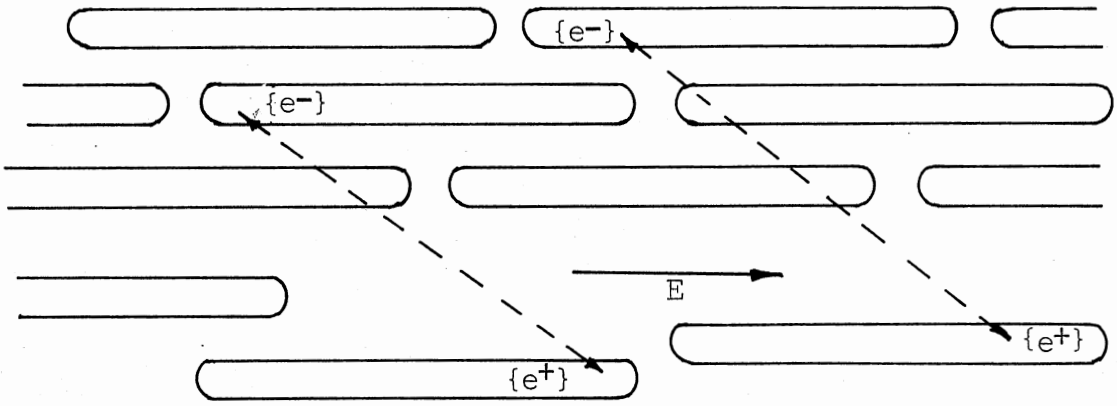

(b) Non-Zero Electric Field

Figure 4. Diagram of Charge Pairs Separated in Long Conjugated Domains (Macromolecules)

polycrystalline sample is negligible; (e) ε_r dependence on shear stress is negligible; and (f) observed relaxation times for the PAQR polymers agree with the model proposed for the nomadic polarization.

Pohl (1974) has shown that for the PAQR class of polymers the conduction is electronic and not electrolytic or ionic for the following reasons: (a) the resistivity is unchanged after passing many coulombs of electrical current; (b) the d.c. resistance is same for reversal of current; (c) the electronic conductivity increases with pressure because of increased orbital overlap, whereas, for ionic conduction, the diffusion of ions require geometric 'holes' for their passage and so increase in pressure should decrease ionic conductivity; and (d) a variety of contacts are satisfactory.

1.2.1. Pollak and Pohl Dielectric Theory (1975)

For a model of a polymer proposed by Pollak and Pohl (1975), a linear polymer of molecular length L = Ns is made of N identical 'mers' or units separated by a distance s. Based on the small polaron theory proposed by Holstein (1959), it is assumed that the carriers responsible for nomadic polarization are small polarons (the polaron is the combination of an electron and its strain field interaction with the elastic lattice), and that a carrier can occupy any one of the equivalent sites in a given polymer. The transport of the small polarons within the polymer chain is postulated as due to thermally activated hopping. The Boltzmann equation for the hopping transport along the macromolecule is represented by a suitable impedance (ladder type R-C) network with generators representing the applied bias voltage. This model predicts the frequency and the electric field dependence of

the real part of the dielectric constant as given by Pollak and Pohl (1975)

$$\text{Re } \varepsilon_r(\omega) = \frac{ne^2L^2K}{6\pi^4kT}\left\{(\text{Coth } \frac{K}{4}) \sum_{\alpha \text{ odd}}^{N} \frac{\alpha^2}{(\bar{K}^2+\alpha^2)^3(1+\omega^2\tau_\alpha^2)} + (\tanh \frac{K}{4}) \sum_{\alpha \text{ even}}^{N} \frac{\alpha^2}{(\bar{K}^2+\alpha^2)^3(1+\omega^2\tau_\alpha^2)}\right\} \quad (1)$$

and the frequency and the electric field dependence of real part of a.c. conductivity as given by Pollak and Pohl (1975)

$$\text{Re } \sigma_{AC}(\omega) = \frac{ne^2\omega^2s^2K}{6\pi^2kT}\left\{(\text{Coth } \frac{K}{4}) \sum_{\alpha \text{ odd}}^{N} \frac{\alpha^2\omega^2\tau_\alpha^2}{(\bar{K}^2+\alpha^2)^2(1+\omega^2\tau_\alpha^2)} + (\tanh \frac{K}{4}) \sum_{\alpha \text{ even}}^{N} \frac{\alpha^2\omega^2\tau_\alpha^2}{(\bar{K}^2+\alpha^2)^2(1+\omega^2\tau_\alpha^2)}\right\} \quad (2)$$

where L = the length of polymer = Ns

N = polymerization index

= number of identical units in L

s = monomer length

α = 1, 2, ----- N

n = n_o exp (-W/2kT) = density of carriers

n_o = density of mers = $1/\pi s^3$

W = activation energy

k = Boltzmann constant

T = temperature

K = d.c. bias electric field parameter = eEL/kT

E = d.c. bias electric field strength

$\bar{K} = K/2\pi$

ω = angular frequency

τ_α = relaxation time = $\dfrac{N^2}{\omega^o \pi^2 (\bar{K}^2 + \alpha^2)}$

$\omega^o = \omega_o \exp(-\varepsilon/kT)$ = hopping rate at temperature T

ε = potential barrier for transition

A representative plot of Log (real part of the dielectric constant ε_r) versus Log (frequency ω) with d.c. bias electric field strength as a parameter (K) as predicted by Equation (1) is given in Figure 5. The real part of the dielectric constant decreases continuously with increasing frequency because the dipoles are unable to follow the variations of higher frequency fields. The hopping rate is independent of the applied low d.c. bias electric field strength. At lower frequencies, the decrease in dielectric constant with higher d.c. bias electric field strengths, is due to the reduction in the effective length as the d.c. bias electric field strength confines the carrier to a limited part of the macromolecule. At higher frequencies and in certain ranges of the d.c. bias electric field strengths, an increase in the dielectric constant for higher d.c. bias electric field strengths is possible due to the enhanced hopping rate by the higher bias d.c. electric field strength. This reversal of dielectric constant with d.c. bias electric field strength, from $(-\partial\varepsilon_r/\partial E)$ to $(+\partial\varepsilon_r/\partial E)$ within a certain range of frequencies is the new prediction as a consequence of this model, which also accounts for the high dielectric constants at unusually low frequencies.

A representative plot of the Log (real part of a.c. conductivity

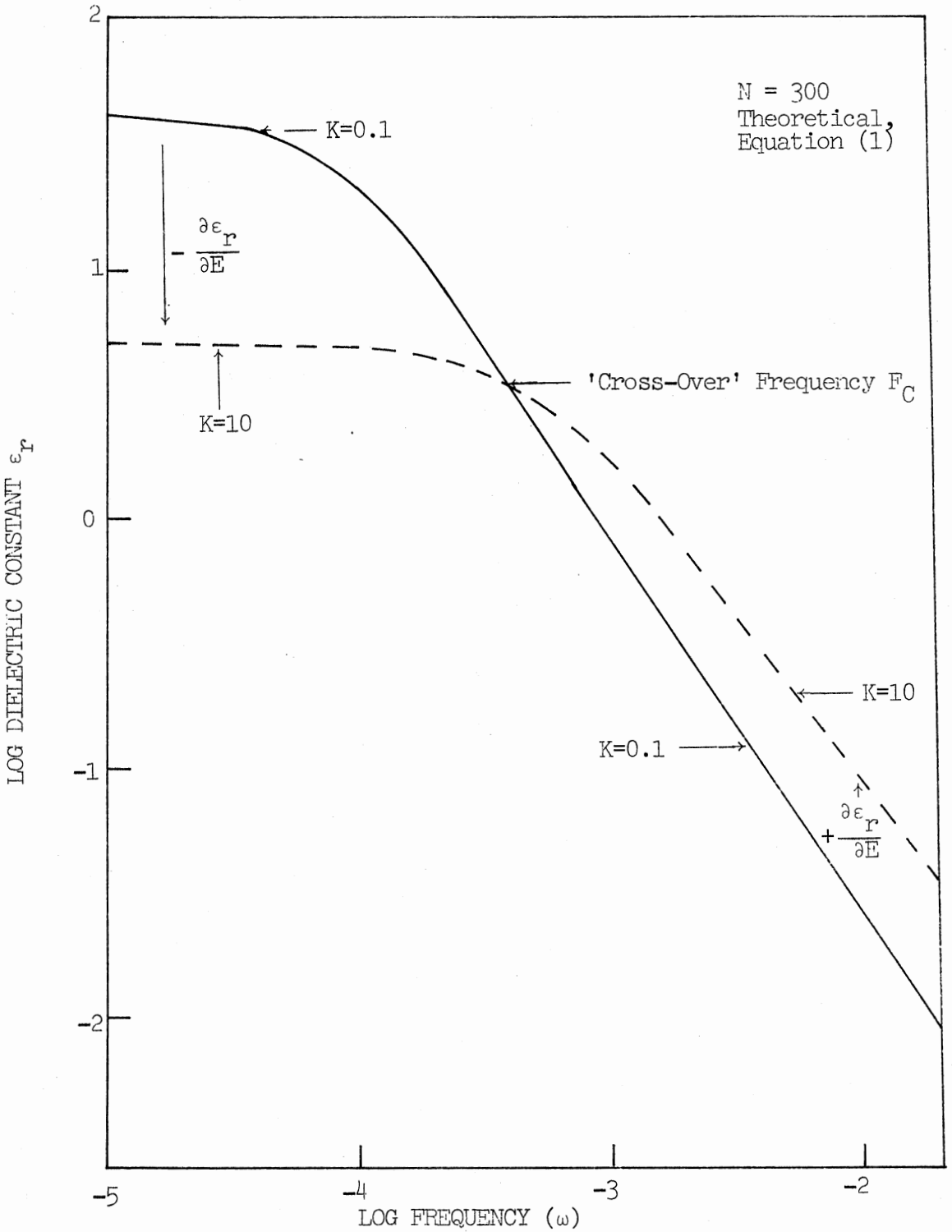

Source: Pollak and Pohl, 1975

Note: The dielectric constant is in units of $(ne^2L^2/6\pi^2kT)$, the frequency ω is in units of ω^o, and the electric field strength parameter K=eEl/kT.

Figure 5. Log (Dielectric Constant) Versus Log (Frequency) (N=300)

σ_{AC}) versus Log (frequency ω) with d.c. bias electric field strength as a parameter (K) as predicted by Equation (2) is given in Figure 6. For the whole range of frequencies, the real part of a.c. conductivity is reduced by the d.c. bias electric field strength, and at higher frequencies it approaches the d.c. conductivity of Einstein relation. As the dominant relaxation time increases as the square of length, this theory also predicts that (a) for long polymers, dispersion is at very low frequencies, and (b) in a real mixture of polymers of varying lengths, the distribution of relaxation times will be broad. This model does not take into account the interaction between the long polarizable centers, which could further increase the relaxation time (Pollak and Pohl, 1975).

1.2.2. Pohl and Pollak Dielectric Theory (1977)

Using the above linear chain model, Pohl and Pollak (1977) have calculated the contribution of nomadic polarization to static dielectric constant. They point out that, in the elongated polymers, where the size of the polarizable center can be larger than the separation between the centers, it is inappropriate to use the Clausius-Mosotti formula. Their calculation is based on a mean field theory as proposed by Pollak (1971), which also includes the interaction between the polarizable macromolecules along with the effects of local electric field rather than the applied electric field.

In this model, a linear polymer of average length L is made of N identical 'mers' or units separated by a distance s, i.e., L = Ns. It is assumed that the wave functions of the carriers responsible for nomadic polarization are localized on a unit, i.e., due to small

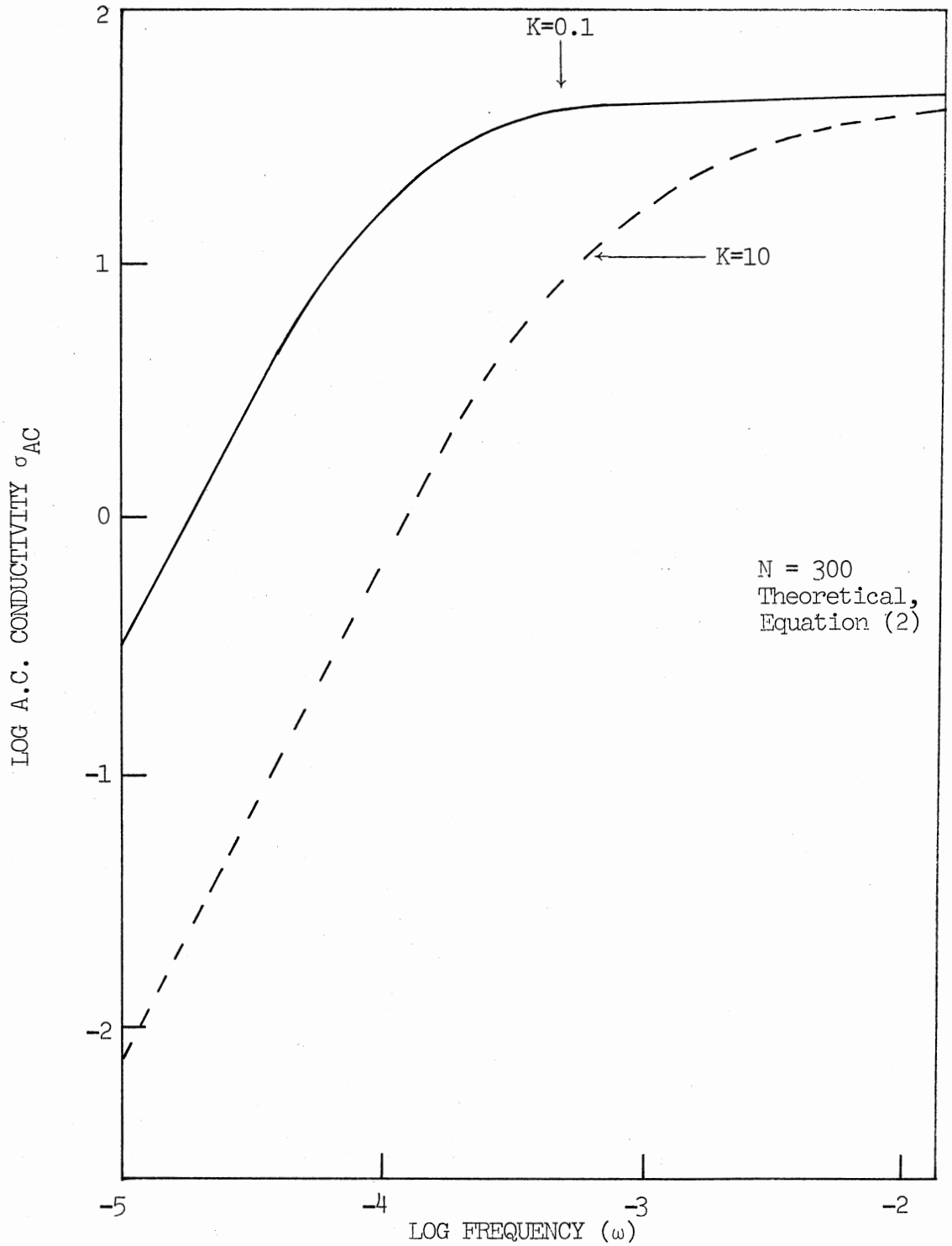

Source: Pollak and Pohl, 1975

Note: The a.c. conductivity is in units of $ne^2\omega^o s^2/6kT$, the frequency is in units of ω^o, and the d.c. bias electric field parameter $K=eEL/kT$.

Figure 6. Log (A.C. Conductivity) Versus Log (Frequency) (N=300)

polaron formation as proposed by Holstein (1959).

In the absence of an external applied electric field, the occupational probability f_k for all sites is the same. When an external electric field is applied, the occupational probability changes. The linear charge density is defined as $\rho(\zeta_k) = ef_k/s$, where e is the charge of an electron, f_k is the occupational probability of site k and ζ_k is the value of the co-ordinate along the polymer at the site k. In a finite electric field strength E,

$$\rho(\zeta) = \rho_o \exp(-eE\zeta/kT) \tag{3}$$

where $\zeta_o = 0$, when a polymer has no carriers, and

$$\rho_o = e\left[\int_{-L/2}^{L/2} \exp(-eE\zeta/kT)\, d\zeta\right]^{-1} \tag{4}$$

$$\rho_o = (e/L)\,(x/\mathrm{Sinh}x) \tag{5}$$

with one carrier, where $x = eEL/2kT$. The induced dipole moment of a polymer molecule is

$$P = \int_{-L/2}^{L/2} \{\rho(\zeta) - (e/L)\}\, \zeta d\zeta \tag{6}$$

$$= (eL/2)\quad(\mathrm{Coth}x - 1/x) \tag{7}$$

At low electric fields, when $x << 1$, polarization P reduces to

$$P_e = (1/12)\,(e^2EL^2/kT) \tag{8}$$

and the polarizability

$$\alpha_e = dP_e/dE = (1/12)\,(e^2L^2/kT) \tag{9}$$

In the general case, the differential polarizability is given by

$$\alpha_d = dP/dE = (e^2L^2/4kT)\,(1/x^2 - 1/\mathrm{Sinh}^2x) \tag{10}$$

$$= (e^2L^2/4kT)\,A_d(x) \tag{11}$$

This is best used in applications to experiments with a large d.c. bias

electric field strength and a small modulating a.c. electric field strength.

The total polarizability is given by

$$\alpha_t = P/E = (e^2L^2/4kT)\,(\mathrm{Coth}x/x - 1/x^2) \tag{12}$$

$$= (e^2L^2/4kT)\,A_t(x) \tag{13}$$

This is useful in application to experiments with large a.c. electric field strengths and no d.c. bias electric field strength. $A_t(x)$ is the Langevin function.

In the mean field dielectric theory proposed by Pollak (1971), the increment in dielectric constant $\Delta\varepsilon$ is given by

$$\Delta\varepsilon = n\langle\alpha\rangle/(1 - nV\langle\beta\rangle) \tag{14}$$

where n is the density of polymer molecules with a carrier, α is the polarizability, $\langle\alpha\rangle$ is α averaged over the orientational distribution of the polymers, β is the reciprocal of the ratio between the external electric field applied to a center and the local electric field induced in it by its polarization charge and averaged over its volume, and $\langle\beta\rangle$ is β averaged over the orientational distribution of the polymer. For an isotropic distribution, $\langle\alpha\rangle = \alpha/3$; $\langle\beta\rangle = \beta/3$; $n = n_o \exp(-W/2kT)$; where $n_o = 1/\pi s^3$; W is the dissociation energy; and $E_F = W/2$, for the two energy level processes.

Using the above equations, the effect of a.c. and d.c. electric field strengths on the increment in static dielectric constant due to nomadic polarization is given by Pohl and Pollak (1977) as

$$\Delta\varepsilon_{t,d}(x,N) = 2N \frac{A_{t,d}(x)}{\frac{6\exp(W/2kT)}{N}\frac{kT}{e^2/4\pi\varepsilon_o^* s} - B_{t,d}(x,N)} \tag{15}$$

where $A_t(x) = \mathrm{Coth}x/x - 1/x^2$

$$A_d(x) = 1/x^2 - 1/\mathrm{Sinh}^2 x$$

$$B_t(x,N) = \frac{1}{xN} \sum_{k=0}^{N} \left[\sum_{j=1}^{k} \frac{\Delta f_j}{(k-j+0.5)^2} - \sum_{j=k+1}^{N} \frac{\Delta f_j}{(k-j+0.5)^2} \right]$$

$$B_d(x,N) = \frac{1}{x} \sum_{k=0}^{N} \left[\sum_{j=1}^{k} \frac{\partial/\partial x(\Delta f_j)}{(k-j+0.5)^2} - \sum_{j=k+1}^{N} \frac{\partial/\partial x(\Delta f_j)}{(k-j+0.5)^2} \right]$$

$$f(j) = \frac{x}{N\mathrm{Sinh}x} \{ \exp(-2jx/N) \}$$

$$\Delta f_j = f_j(x) - f_j(0)$$

$x = eEL/2kT$

t = 'total', i.e., large a.c. electric field strengths with zero d.c. bias electric field strength

d = 'differential', i.e., small a.c. electric field strength with larger d.c. bias electric field strengths

ε_o^* = optical dielectric constant of the medium due to polarizations other than nomadic.

A representative plot of the increment in dielectric constant due to nomadic polarization $\Delta\varepsilon_{t,d}^*$ versus AC/DC electric field strength as predicted by Equation (15) is given in figure 7. It is seen that unless one goes for high electric field strengths, the static dielectric constant is independent of electric field strength. The dielectric constant is reduced by higher d.c. electric field strengths, because the polarons are restricted to move in limited parts of a macromolecule.

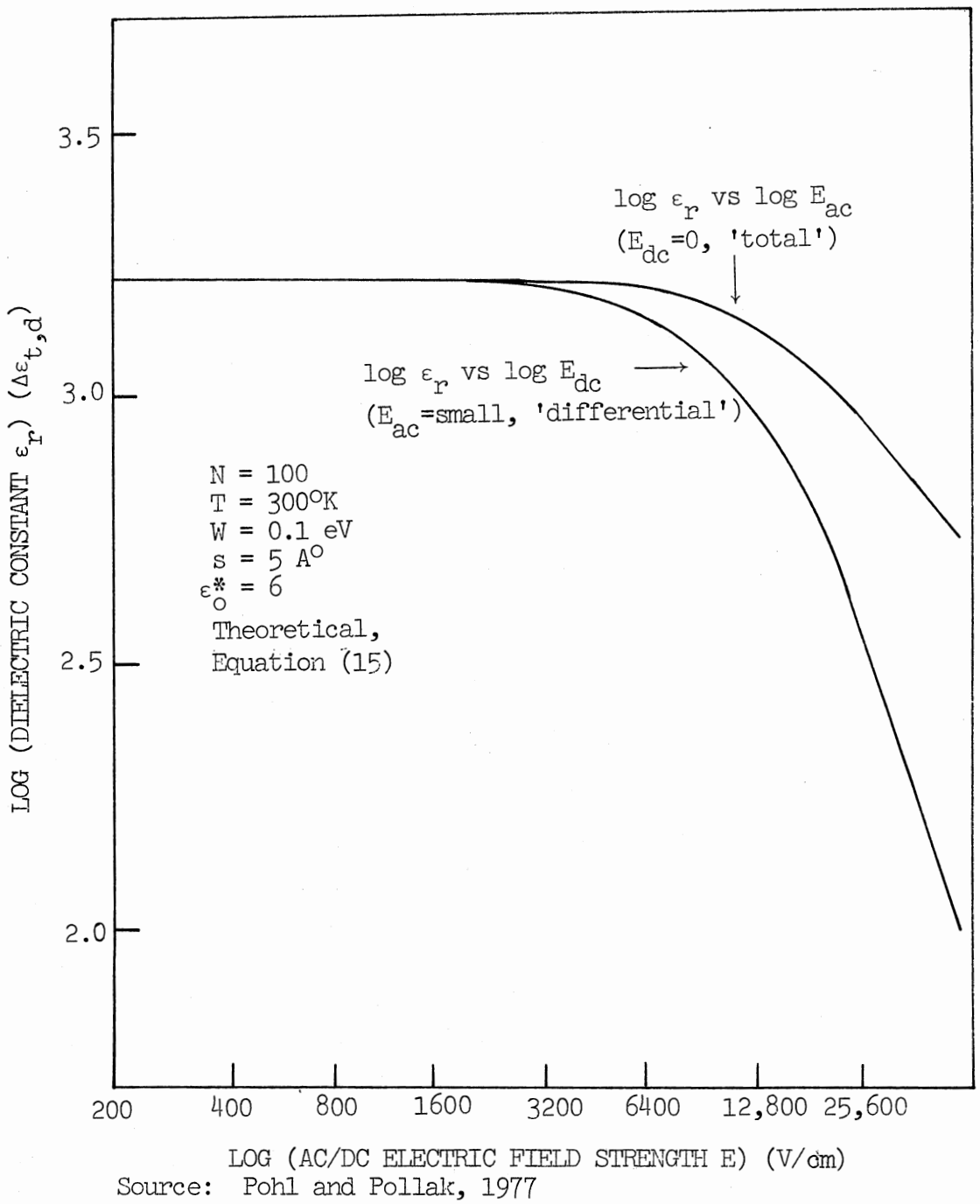

Source: Pohl and Pollak, 1977

Figure 7. Log (Dielectric Constant) Versus AC/DC Electric Field Strength (N=100)

1.3. Purpose of the Study

This thesis is directed towards the study of electronic conduction and hyperelectronic polarization mechanisms in the electro-active polyacenequinone (PAQR) class of polymeric semiconductors. In particular, it attempts to compare the dielectric theories of Pollak and Pohl (1975), and Pohl and Pollak (1977) with the experimental results, through a variation of relevant parameters like pressure, temperature, frequency, a.c. electric field strength and d.c. bias electric field strength.

CHAPTER II

EXPERIMENTAL TECHNIQUES

The electrical properties of the selected polymers were studied as a function of pressure, temperature, frequency, alternating and direct bias voltages.

2.1. Methods of Sample Preparation

The polymers selected for the experimental studies were in the form of polycrystalline powders. These were either in an already finely powdered form, or they were pulverized to a fine powder by the use of an amalgamator (Torit Amalgamator, Torit Manufacturing Company, St. Paul, Minnesota). This type of an amalgamator has an electric vibrator, which rattles a steel capsule into which the coarse sample powder and a steel ball were placed, at a certain rate for a set time. The sample powders were studied in three forms:

(1.) For those sample powders which could be molded into pellets, a pellet press (Parr Instrument Company, Moline, Illinois) was used. Using a six mm diameter punch and die, a compressive force of 20 lbs applied to the hand-pressure lever translated to a 1000 lbs force at the punch through a mechanical advantage ratio of 50 to 1.

(2.) Some of the pellets were silver-painted, which permitted ambient or 'zero' pressure measurements. Highly conductive silver paste Type 57C Parts A and B (Emerson and Cuming Inc., Canton, Massachusetts)

were mixed together in equal quantities and were coated uniformly on both sides of the sample. The setting time for the paint was one hour at 100°C in an oven.

(3.) Many of the polymers would not form into pellets even when subjected to 15,000 atmospheres pressure. These were used as powders in 'sample-holders' like pyrophyllite rings under pressure.

2.2. Pressure Cells

(1.) Figure 8 shows the schematic diagram of the two-terminal Be-Cu pressure cell used in experiments upto 6000 atmospheres pressure. This consisted of two anvils 'high' and 'ground' between which a six mm diameter sample pellet could be sandwiched. The 'high' electrode in the form of a thumb-tack was in contact with the 'high' anvil, which was insulated from the body of the pressure cell by a teflon sleeve at the sides and a mica disc at the top. The body of the cell, the 'ground' T-anvil and the lock-nut formed the 'ground' electrode. To prevent any shear onto the sample while the cell was being 'locked' at the required pressure by the lock-nut, the 'ground' T-anvil was kept from rotating by a screw that extended from the body of the cell into a vertical slot on the side of the T-anvil. The screw was removed after 'locking' the sample.

(2.) Figure 9 shows the schematic diagram of the three-terminal Be-Cu pressure cell used in experiments upto 6000 atmospheres pressure. This consisted of two anvils 'high' and 'ground' between which a six mm diameter sample pellet could be sandwiched. The 'high' electrode in the form of a thumb-tack was in contact with the 'high' anvil. Both these and the 'ground' T-anvil, were insulated from the body of the cell and

SCALE: 4 Cm = 1 Cm

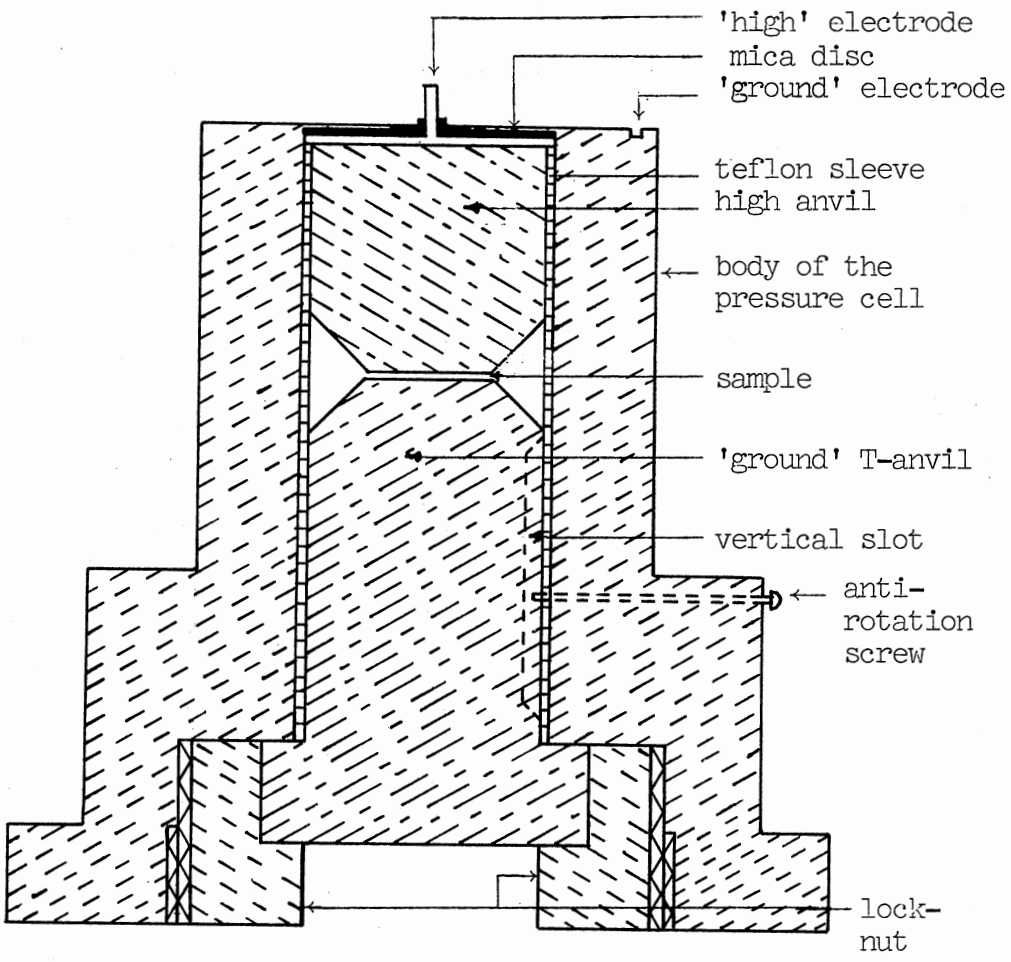

Figure 8. Two-Terminal Be-Cu Pressure Cell

SCALE: 4 Cm = 1 Cm

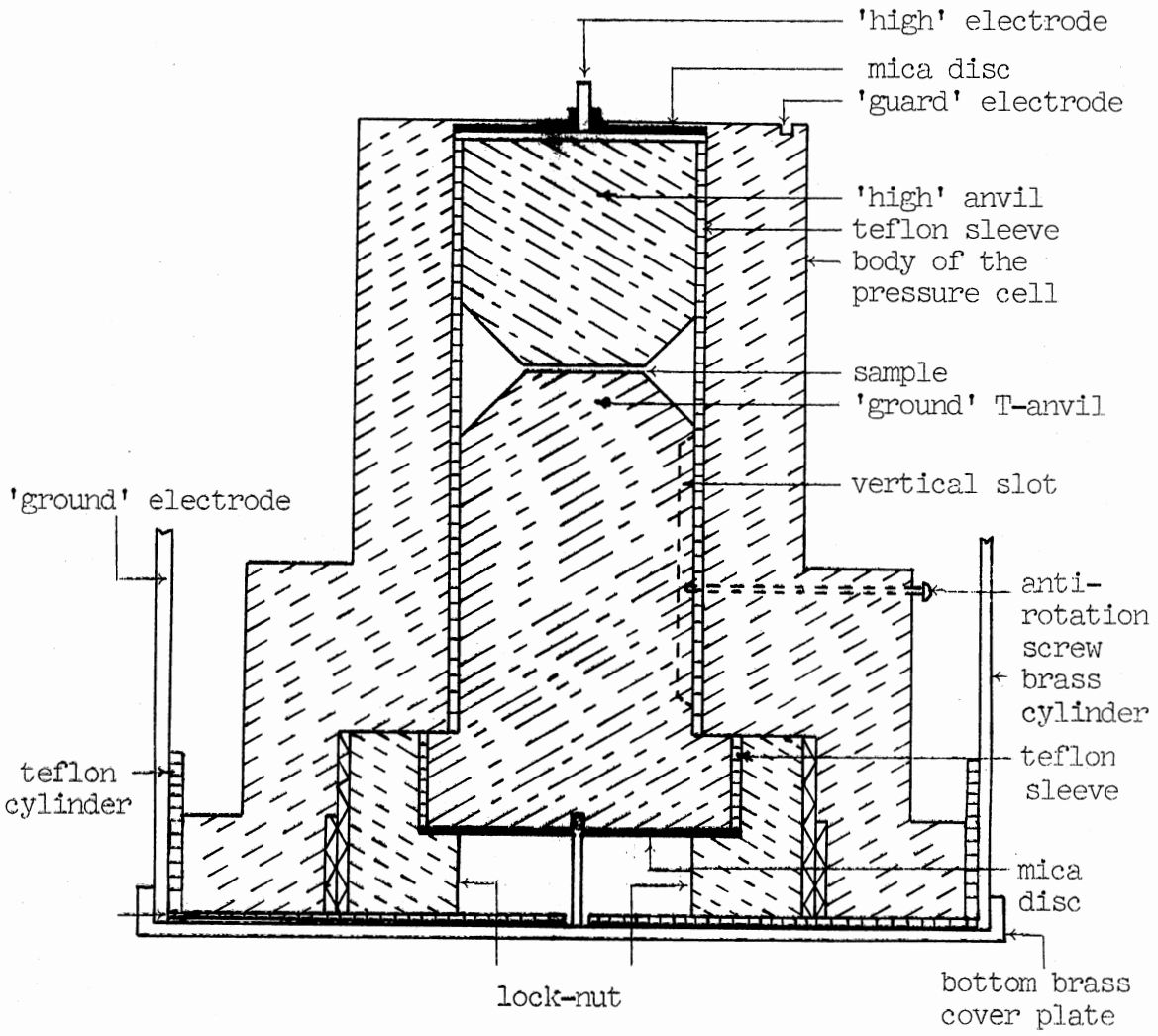

Figure 9. Three-Terminal Be-Cu Pressure Cell

from the lock-nut which formed the 'guard' electrode, by the use of teflon sleeves at the sides, and mica discs at the top and at the bottom. The bottom brass cover plate which was screwed onto the 'ground' T-anvil was insulated from the body of the pressure cell by a teflon disc. The brass cylinder snapped into the bottom brass cover plate. A teflon cylinder insulated the brass cylinder from the body of the cell. To prevent any shear onto the sample while the cell was being 'locked' at the required pressure by the lock-nut, the 'ground' T-anvil was kept from rotating by a screw that extended from the body of the cell into the vertical slot on the side of the T-anvil. The screw was removed after 'locking' the sample.

(3.) Figure 10 shows the schematic diagram of the three-terminal Be-Cu pressure cell used in experiments upto 1500 atmospheres pressure to fit into the cold-end of the Heli-tran. This consisted of a 'guard' cylindrical nut, top end of which had three steel posts embedded 120^{o} apart to form guide posts for the 'ground' and 'high' anvils to snap onto, and also to prevent them from rotating while the cell was being 'locked' to the required pressure. The 'ground' T-anvil was insulated from the top of the 'guard' cylindrical nut by a mica disc, from the steel posts by teflon sleeves, and from its body by a teflon cylinder. The 'high' anvil was insulated from the steel posts of the 'guard' cylindrical nut by the teflon sleeves, and at the top from the 'guard' cylinder by a mica disc. The bottom of the 'ground' T-anvil was screwed into the cold-end of the Heli-tran. The 'guard' cylinder was insulated from the 'ground' of the cold-end of the Heli-tran by a mica disc. The whole assembly was covered by a 'ground' metal cylinder which was screwed onto the cold-end of the Heli-tran.

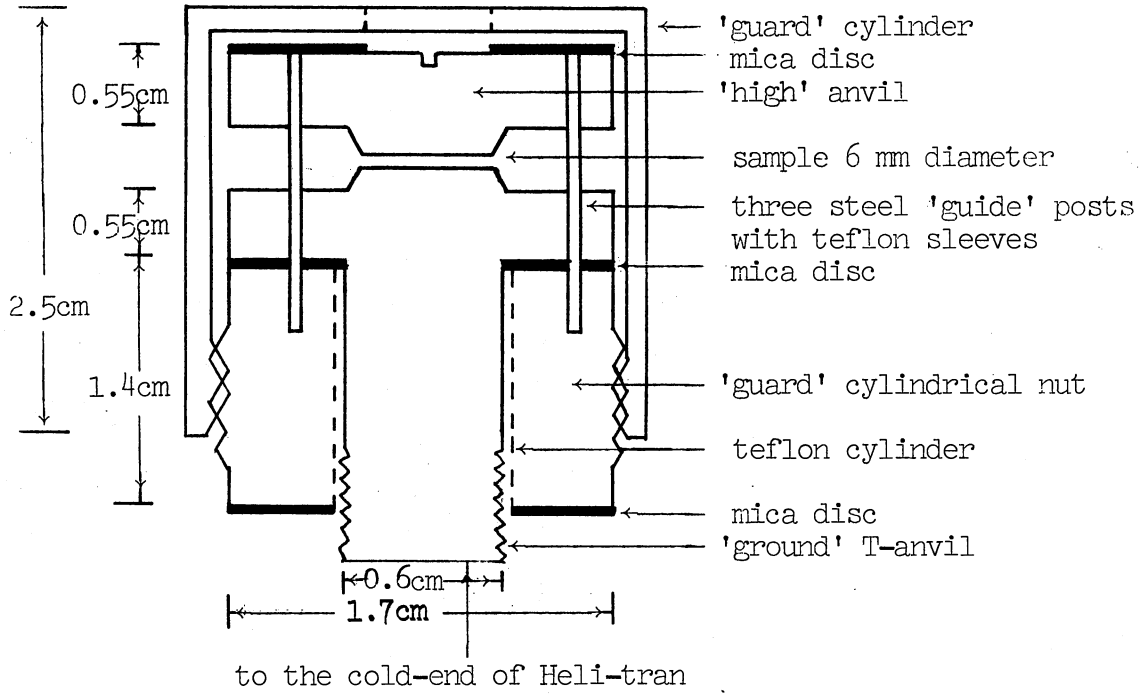

Figure 10. Three-Terminal Be-Cu Pressure Cell for the Heli-Tran

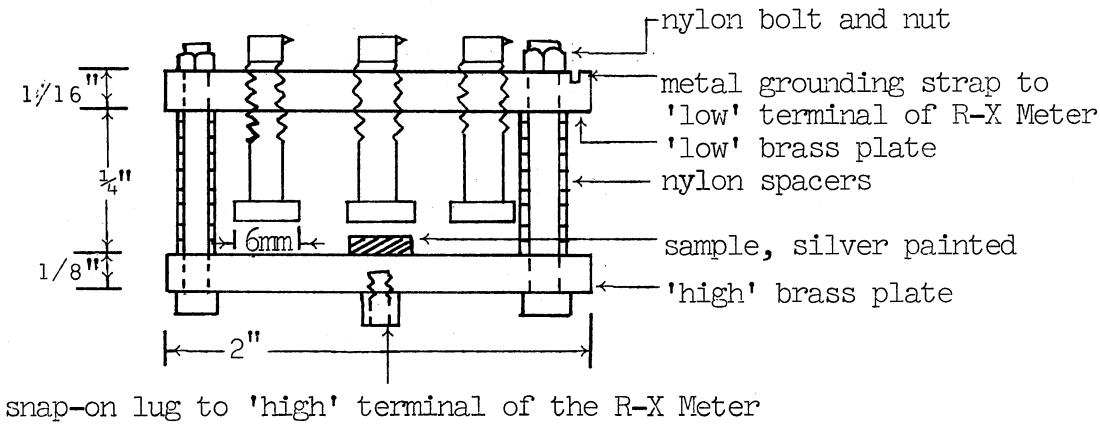

Figure 11. Two-Terminal Brass Parallel Plate Cell for the R-X Meter

(4.) Figure 11 shows the schematic diagram of the two-terminal brass parallel plate cell used with the R-X Meter for silver-painted samples at 'zero' pressure. It consisted of two rectangular brass plates insulated from each other by nylon spacers and held together by two nylon bolts and nuts. It could hold three samples of six mm diameter each. The bottom brass plate was clamped onto the 'high' terminal of the R-X Meter, and the top brass plate was connected to the 'low' terminal of the R-X Meter through a metal grounding strap. The whole assembly was covered with a Faraday cage to eliminate stray pick-up.

2.3. D.C. Conductivity and Pressure

Figure 12 shows a schematic diagram of 'loading' the pressure cell using a hydraulic press (Pasadena Hydraulic Inc., Press, El Monte, California). A three inch diameter piston attached to the bottom platen moved up to apply hydraulic pressure (0 to 3600 psi) against the fixed top platen. To keep the sample void-free, it was subjected to repeated pressures in the required range before the d.c. conductivity was measured as a function of applied pressure. A Weston Model 4444 Auto-Ranging Digital Multimeter (Weston Instruments Inc., Newark, New Jersey) (for resistance range 1 KΩ, accuracy = ±0.05% Rdg ±3 digits; and for resistance ranges 10 KΩ, 100 KΩ, 1 MΩ, accuracy = ±0.05% Rdg ±3 digits), or a Weston Model 4448 Digital Multimeter (for resistance ranges 200 Ω, 2 KΩ, 20 KΩ, 200 KΩ, 2 MΩ, accuracy = ±0.5% Rdg ±3 digits), or a Keithley 602 Electrometer (Keithley Instruments, Cleveland, Ohio) (for resistance range 100Ω to 10^9Ω, accuracy = ±3% full scale, and for resistance range 3×10^9Ω to 10^{13}Ω, accuracy = ±5% full scale) was used

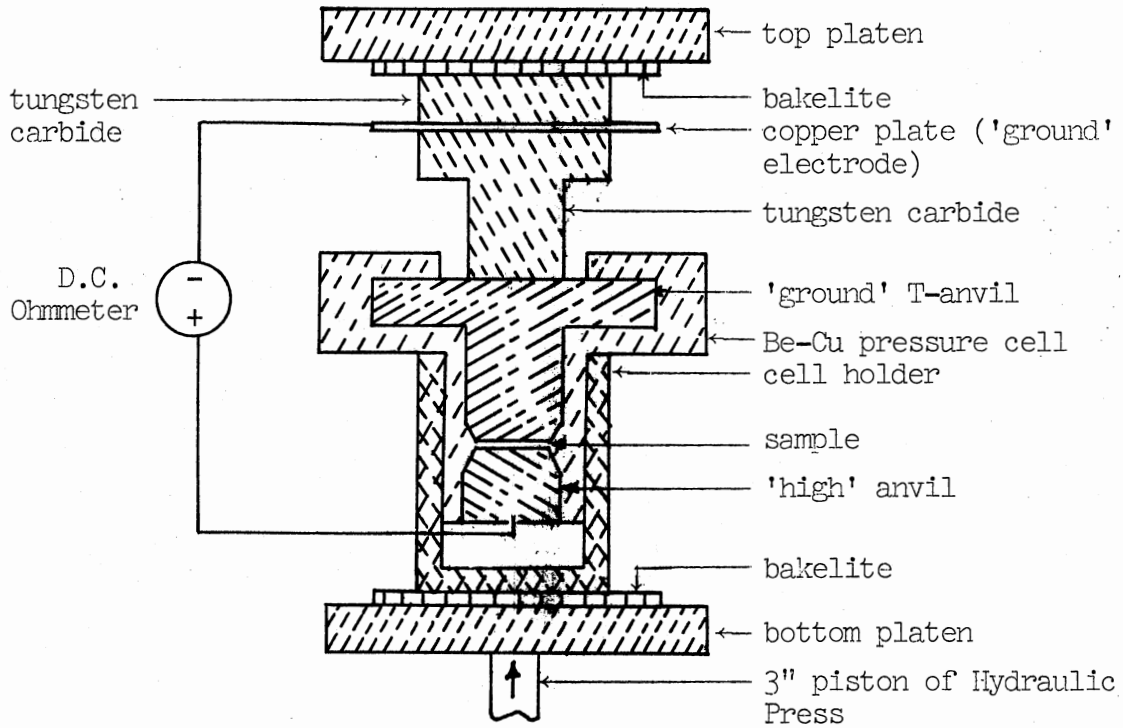

Figure 12. Schematic Diagram of a Pressure Cell Used with the Hydraulic Press

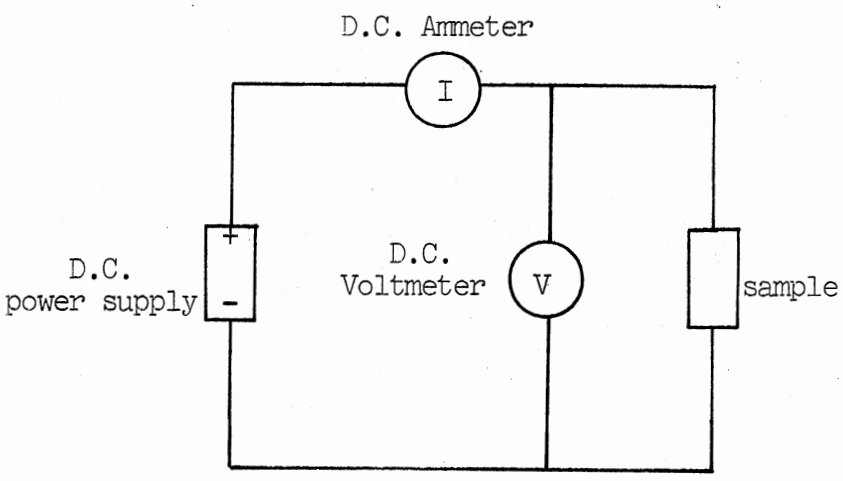

Figure 13. Measurement of D.C. Conductivity

as an Ohmmeter to measure the d.c. conductivity of the sample as a function of pressure. The pressure cell was 'locked' at the required pressure by tightening the lock-nut.

2.4. D.C. Conductivity and D.C. Electric Field

Figure 13 shows a schematic diagram for measuring the d.c. conductivity as a function of applied d.c. voltage, by measuring the current through and the voltage across the sample. A Model IP-27 Heathkit Regulated Power Supply (Heath Company, Benton Harbor, Michigan) (d.c. voltage range 0 to 50 V; and d.c. current range 0 to 1.5 A max) was used as the source with a Weston Model 4444 Auto-Ranging Digital Multimeter (for voltage ranges 100 mV, 1 V, 10 V, accuracy = ±0.02% Rdg ±2 digits; for voltage range 100 V, accuracy = ±0.03% Rdg ±1 digit; and for current ranges 10 μA, 100 μA, 1 mA, accuracy = ±0.05% Rdg ±3 digits), or a Weston Model 4448 Digital Multimeter (for voltage ranges 200 mV, 2 V, 20 V, 100 V, accuracy = ±0.3% Rdg ±1 digit; and for current range 1 to 200 μA, accuracy = ±0.4% Rdg ±1 digit), or a Keithley Model 602 Electrometer (for voltage range 0 to 10 V, accuracy = ±1% full scale; for current range 0.3 A to 10^{-11} A, accuracy = ±2% full scale; and for current range 3×10^{-12} A to 10^{-14} A, accuracy = ±4% full scale) was used either as a Voltmeter or as an Ammeter.

To avoid excessive heating in a sample of resistance R, the maximum applied voltage V_m was chosen such that the power dissipated in the sample $V_m^2/R < 0.1$ watt.

2.5. Temperature

2.5.1. Fixed Point Temperatures

To eliminate the fluctuations of room temperature, a Haake Model KT-62 Thermostat (Gebruder Haake KG, Brinkmann, Wesbury, New York) was used ($T = 300^{o}K$, accuracy = $\pm 0.25^{o}K$). Other fixed point temperatures used were ice point ($T = 273^{o}K$), dry ice ($T = 195^{o}K$) and liquid nitrogen ($T = 77^{o}K$). The sample was kept dry in the pressure cell by passing dry nitrogen gas. It was not possible to attach a thermo-couple to the sample in the pressure cell. As the samples were highly sensitive to temperature changes, a steady state temperature of the surrounding fixed point temperature bath was reached by the sample, when its d.c. resistance showed no further change. It usually took two to three hours to reach steady state in temperature.

2.5.2. Heli-Tran Cryogenic System

Figure 14 shows the schematic diagram of the Heli-tran cryogenic system to achieve a continuous temperature range from $77^{o}K$ to $300^{o}K$. The Heli-tran Model LT-3-110 transfer system (Air Products and Chemicals, Allentown, Pennsylvania) brings a liquid cryogenic from a storage container to the Heli-tran refrigerator to provide a controlled sample temperature.

The starting procedure was as follows: The foreline mechanical pump (The Welch Scientific Company, Chicago, Illinois) was switched on with air outlet valve closed, and valves 1 and 2 open. When the Hastings Vacuum Gage (Hastings-Ray Inc., Hampton, Virginia) read 50 to 100 microns of mercury, valve 3 was opened. Water flow to Model M-2

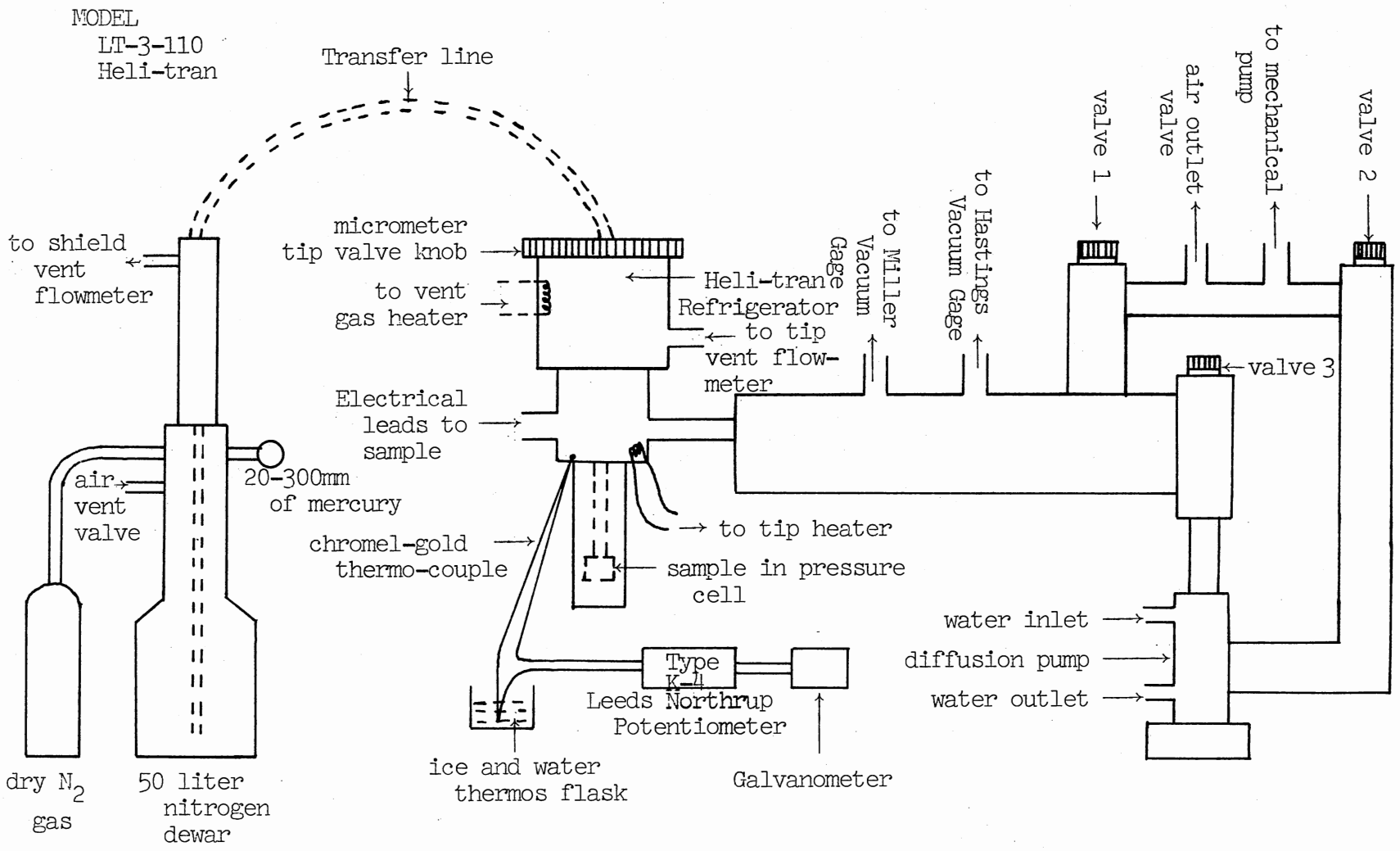

Figure 14. Schematic Diagram of the Heli-Tran Cryogenic System

diffusion pump (Varian NRC Products, Lexington, Massachusetts) was turned on, and the diffusion pump was turned on. When the pressure reached 0.5×10^{-5} mm of mercury as read by Miller Vacuum Gage, shield and tip vents were opened at flowmeters. The Micrometer valve was opened and transfer line was inserted into the liquid nitrogen dewar. The dewar was pressurized to ten inches of mercury using nitrogen gas from the cylinder, and the vent gas heater was turned on. Once frost formed on the transfer line, using the low pressure air vent valve the pressure in the dewar was reduced to five inches of mercury (127 mm). A chromel vs gold 0.07 atomic % iron thermo-couple attached to the cold-end of the Heli-tran was connected to Type K-4 Potentiometer (Leeds and Northrup, Philadelphia, Pennsylvania) through a reference junction of ice and water. A nanovolt null detecting galvanometer (Rubicon Instruments, Philadelphia, Pennsylvania) connected to the potentiometer read the unbalanced thermo-emf. By adjusting the Micrometer tip valve and the electrical power to the tip heater, a temperature stability of $\pm 0.5^{\circ}K$ was achieved in the range from $77^{\circ}K$ to $300^{\circ}K$. The Be-Cu pressure cell designed to be used with the Heli-tran has been described in Section 2.2., Paragraph (3.) and in Figure 10.

2.6. Alternating Current Bridges

Alternating current bridges were used to measure the response of the sample to alternating currents. The sample could be represented in a series or a parallel mode as shown in Figure 15. Both configurations give the same loss tangent $\tan\delta$. In general, $(C_{xs}/C_{xp}) = (1 - \mathrm{Sin}^2\delta)$ and $(R_{xp}/R_{xs}) = \mathrm{Sin}^2\delta$.

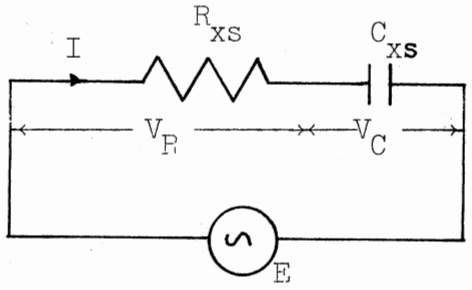

I is common to both R_{xs} and C_{xs}

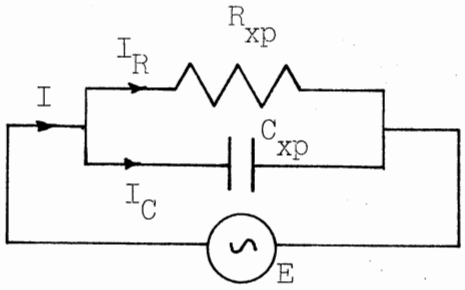

E is common to both R_{xp} and C_{xp}

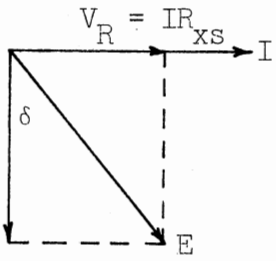

$$I \frac{1}{j\omega C_{xs}} = V_C$$

Dissipation Factor = V_R/V_C

$D_{xs} = \tan\delta_{xs} = \omega C_{xs} R_{xs}$

(a) Series Circuit

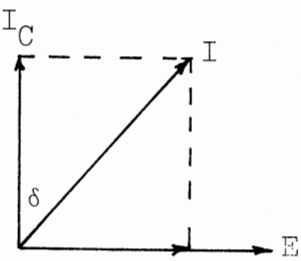

$$I_R = \frac{E}{R_{xp}}$$

Dissipation Factor = I_R/I_C

$D_{xp} = \tan\delta_{xp} = 1/(\omega C_{xp} R_{xp})$

(b) Parallel Circuit

Figure 15. Series and Parallel Circuits

2.6.1. Schering Bridge

Figure 16 shows the schematic diagram for the GRC (General Radio Company, Concord, Massachusetts) Type 716-C capacitance bridge used to measure the equivalent two-terminal capacitance (C_{xp}) and resistance (R_{xp}) of the sample in the two-terminal Be-Cu pressure cell (Figure 8) in the frequency range of 10 Hz to 150 KHz.

(A) This is a modified Schering bridge, which can measure a series capacitance C_{xs} (for equivalent parallel capacitance C_{xp} in the range 100 to 1150 PF) and a series resistance R_{xs} (for equivalent parallel resistance R_{xp} in the range 3 KΩ to 800 KMΩ) in the series mode when the sample is non-lossy, and when the sample is lossy, the ranges of C_{xp} and R_{xp} could be extended in the parallel substitution mode through C_1 (GRC Type 1412-BC decade capacitor, range = 50 PF to 1.11110 μF) and R_1 (GRC Type 1434-G decade resistor, range = 0 to 1.111110 MΩ).

(B) From the balancing condition for the series mode $Z_N Z_B = Z_A Z_{xs}$, $R_{xs} = (R_B)(C_A/C_N)$ and $C_{xs} = (C_N)(R_A/R_B)$. The dissipation factor $D_{xs} = \tan\delta_{xs} = \omega C_{xs} R_{xs}$. In effect C_A controls the dissipation factor and C_N controls C_{xs}. The equivalent parallel values are $C_{xp} = C_s/(1 + \tan^2\delta_{xs})$ and $R_{xp} = R_{xs}(1 + \tan^2\delta_{xs})/(\tan^2\delta_{xs})$. In parallel substitution mode, if $R_A = R_B$, then, $R_{xp} = R_1$ and $C_{xp} = (C_1 + C_N)$. The dissipation factor $D_{xp} = \tan\delta_{xp} = 1/(\omega C_{xp} R_{xp})$.

(C) A HP (Hewlett-Packard Company, Palo Alto, California) Type 200-CD Wide Range Oscillator (frequency range, 5 Hz to 600 KHz) was used as the source generator and a PAR (Princeton Applied Research Corp., Princeton, New Jersey) HR-8 Lock-In Amplifier with the Type D Pre-amplifier (Input impedance, 100 MΩ, 10 PF) was used as a null detector

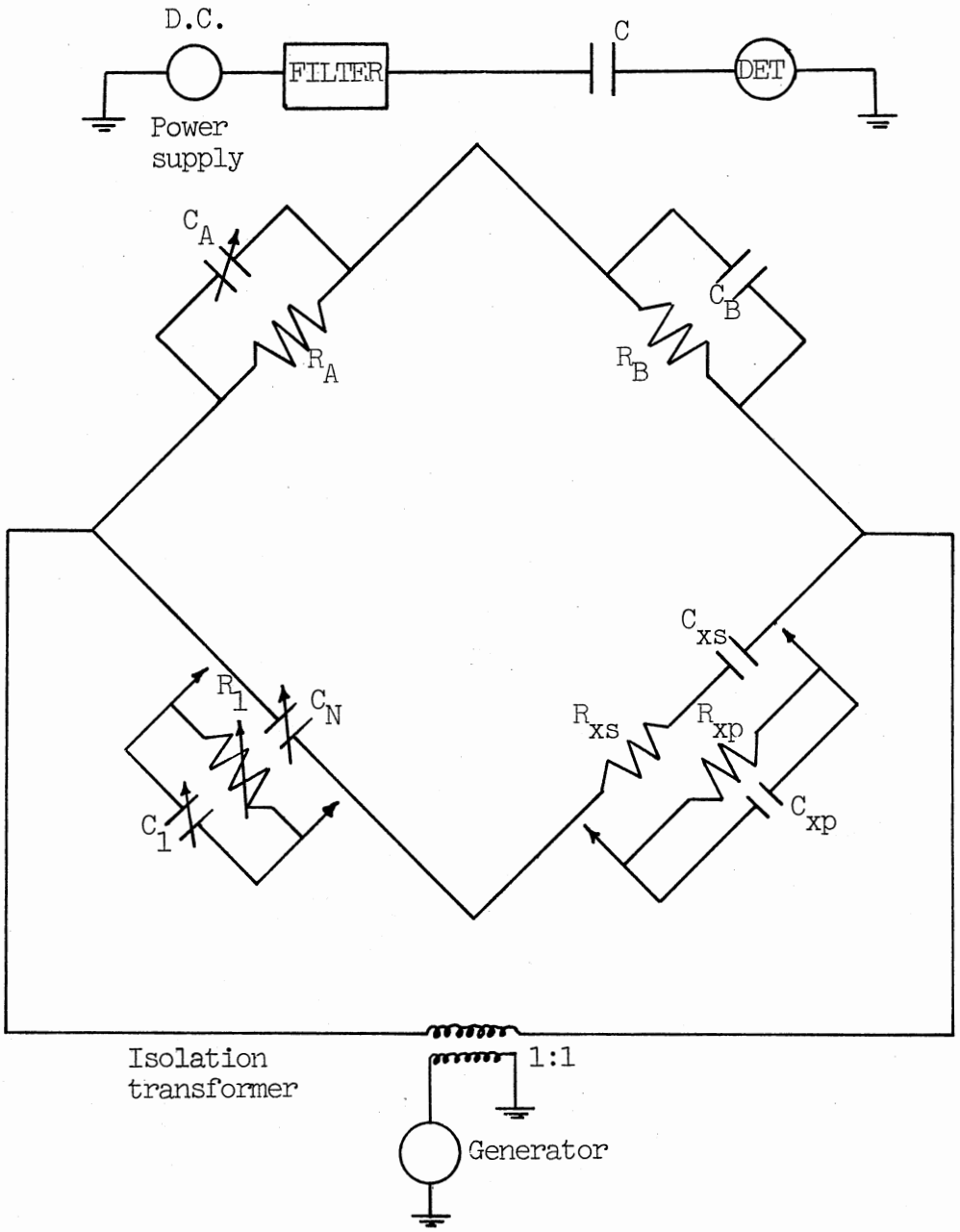

Figure 16. Schematic Diagram of the Schering Bridge with D.C. Bias Voltage

(noise level of the amplifier ≃7 nV). An IP-27 Heathkit Regulated Power Supply (Heath Company, Benton Harbor, Michigan) (voltage range, 0 to 1.5 A max) was used to provide the d.c. bias voltage to the sample. A hum reduction filter was used which reduced 60 Hz hum of the d.c. power supply from 700 nV to 8 nV at low d.c. outputs. A blocking capacitor C was used to isolate the detector from the d.c. power supply. A dual beam Type 533A Tektronix (Tektronix Inc., Beaverton, Oregon) Oscilloscope was used to monitor the output signal from the detector and to measure both the applied a.c. and d.c. bias voltages across the sample. Whenever the sample impedance was comparable to the input impedance (1 MΩ, 20 PF) of the Oscilloscope, the leads to the scope were disconnected for bridge balance. Since the d.c. bias voltage to the sample was applied through detector terminals, the ratio R_A/R_B was kept at unity so that no unbalance d.c. current flowed into the secondary winding of the isolation transformer.

(D) In the substitution mode, the decade resistor R_1 (GRC Type 1434-G) was connected in parallel with capacitor C_N. It was found that the stray capacitance of the decade resistor R_1 varied depending on the resistance setting and the frequency used. This stray capacitance effect was eliminated by connecting 1% precision resistor whose value was close to that of the decade resistor, across the unknown arm of the bridge while measuring the leads impedance.

(E) The accuracies of the bridge in the series mode are ±0.1% ±0.6 PF for capacitance, and ±0.0005 or ±2% of the dissipation factor dial reading whichever is larger. The accuracies in the substitution mode are ±0.05% ±0.6 PF for capacitance, and ±1% for resistance. The overall accuracy of the measurement is limited by the accuracy with which the

cell capacitance can be measured.

(F) To check the reproducibility of the experimental results for the selected polymers, the sample LD-2 was chosen as it was one of the more difficult samples to measure because of its large dielectric constant. As the sample would not form pellets, a pyrophyllite ring was used as a 'sample-holder'. Starting from the process of 'loading' the pressure cell with the sample LD-2, and the measurement of dielectric constant and conductivity was repeated four times, each time with a fresh sample of LD-2. It was found that the % error for the conductivity was 16%, and 20 % for the dielectric constant at V_{ac} = 0.1 V_{pp} and F = 1.0 KHz.

2.6.2. Schering Bridge with Guard Circuit

Figure 17 shows a schematic diagram of Schering bridge with a fifth 'guard' point G created. The conditions for bridge balance are A/N = B/P. By connecting the guard point G to the junction of B and P, F-H (coupling circuit) is in parallel with BP and S is in parallel with the source generator. Bridge is balanced by A/N = {(F||B)/(H||P)} = {(FB)/(F+B) x (H+P)/(HP)}, which gives B/P = F/H. Successive balance gives A/N = B/P = F/H, and this eliminates 'high' to 'guard' capacitance T (in Figure 17) or C_{AG} (in Figure 18).

Similarly, by connecting the guard point G to the junction of N and P, S-T (guard circuit) is in parallel with the detector. Bridge is now balanced by A/B = {(S||N)/(T||P)} = {(SN)/(S+N) x (T+P)/(TP)}, which gives N/P = S/T. Successive balance gives A/B = N/P = S/T, and this eliminates 'guard' to 'ground' capacitance H (in Figure 17) or C_{GB} (in Figure 18).

Figure 18 shows the schematic diagram of the Schering bridge with

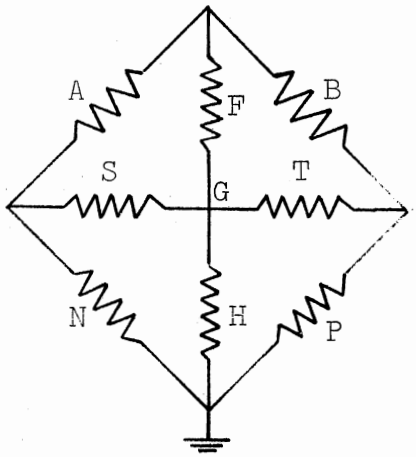

Figure 17. Schematic Diagram of the Schering Bridge with 'Guard' Point

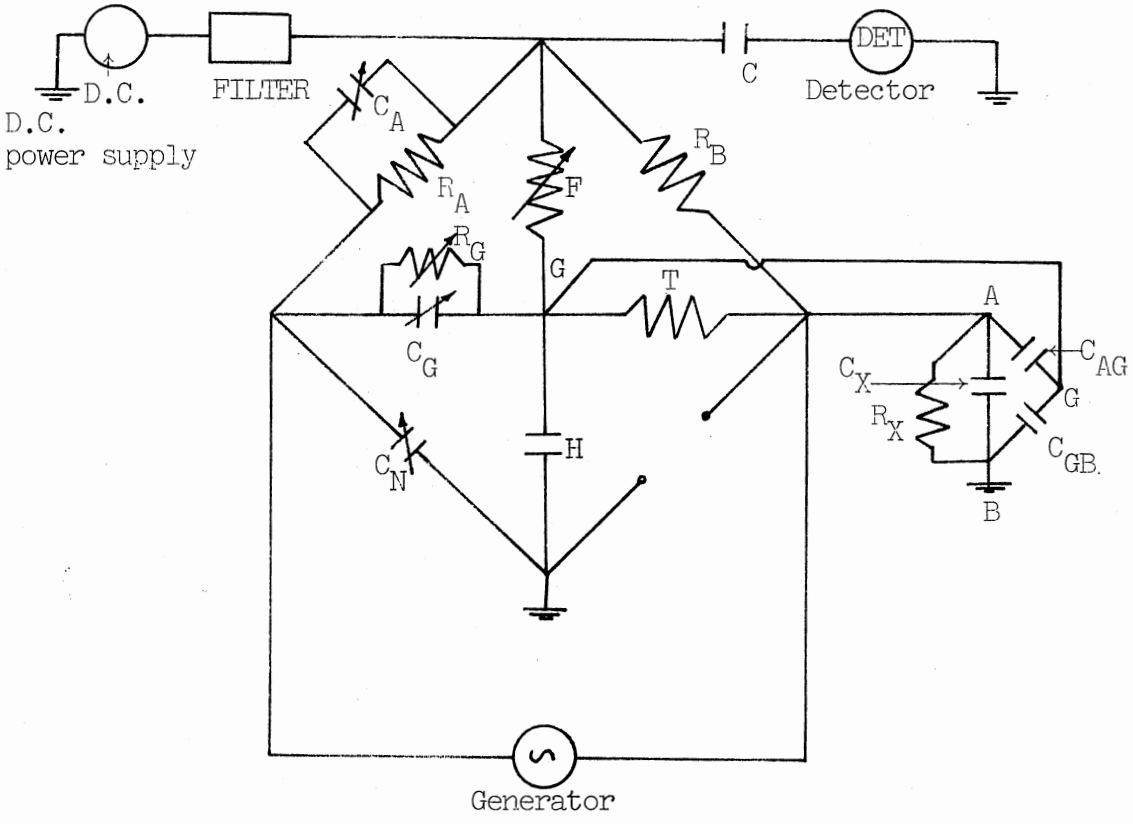

Figure 18. Schematic Diagram of the Schering Bridge with 'Guard' Point and the Three-Terminal Pressure Cell with D.C. Bias Voltage

guard point and the three-terminal Be-Cu pressure cell {Section 2.2., Paragraph (2.) and Figure 9} with d.c. bias voltage.

Figure 19 shows the diagram of connections of the GRC Type 716-C capacitance bridge together with the GRC Type P4 guard circuit which permits a three-terminal measurement of unknown sample in the frequency range of 10 Hz to 150 KHz. With the use of guard circuit and doubly shielded wires to the sample in a 'guarded' Be-Cu three-terminal pressure cell, the effects of stray and lead capacitances, and the effects of temperature and humidity on the lead cables from the bridge to the sample were eliminated.

Paragraphs labelled (A), (B), (C), (D), and (E) of Section 2.6.1. are equally applicable to Section 2.6.2.

2.6.3. The R-X Meter

Figure 20 shows a schematic diagram of a Type 250-A R-X Meter (Boonton Radio Corp., Boonton, New Jersey) along with the d.c. bias circuit. The R-X Meter is a wide frequency (0.5 to 250 MHz) Schering bridge which measures the equivalent two-terminal parallel resistance (range, 15 Ω to 100 KΩ) and parallel capacitance (range, 0 to 20 PF, which could be extended to 120 PF using auxiliary resonating coils) of the unknown sample connected between the terminals CD. A R.F. voltage of approximately 0.1 to 0.5 volts appears across CD. The d.c. resistance looking into these terminals is approximately 66 Ω. The null detector is a Microammeter (0 to 200 μA), which reads the amplified unbalance current.

The balancing conditions obtained from $Z_{AB}Z_{CD} = Z_{AD}Z_{BC}$ are $R_2/C_4 = R_3/C_1 = R_4/C_2$. To operate the bridge, it is balanced first by using C_2

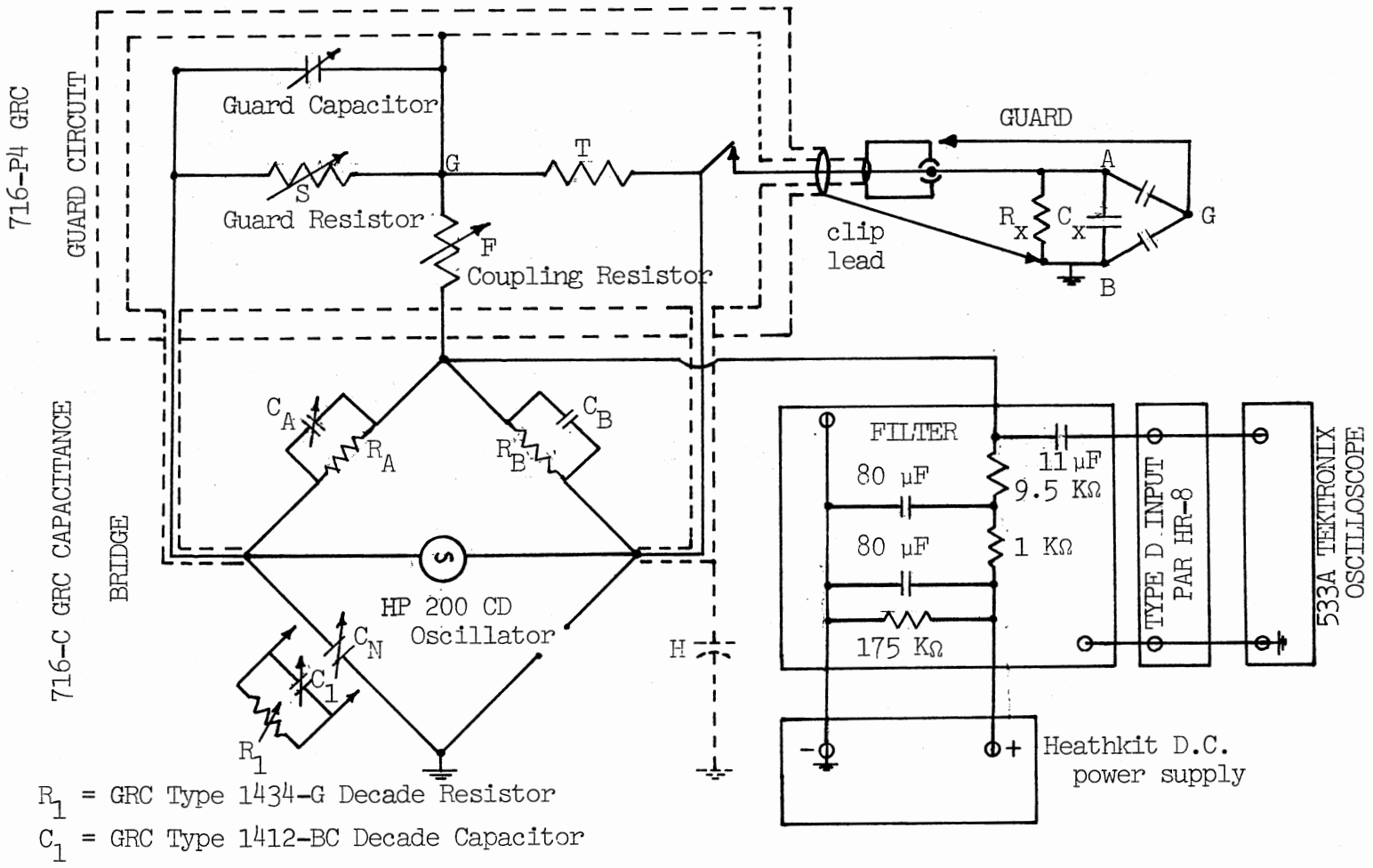

R_1 = GRC Type 1434-G Decade Resistor

C_1 = GRC Type 1412-BC Decade Capacitor

Figure 19. Diagram of Connections of the Schering Bridge with the 'Guard' Circuit and the Three-Terminal Pressure Cell with D.C. Bias Voltage

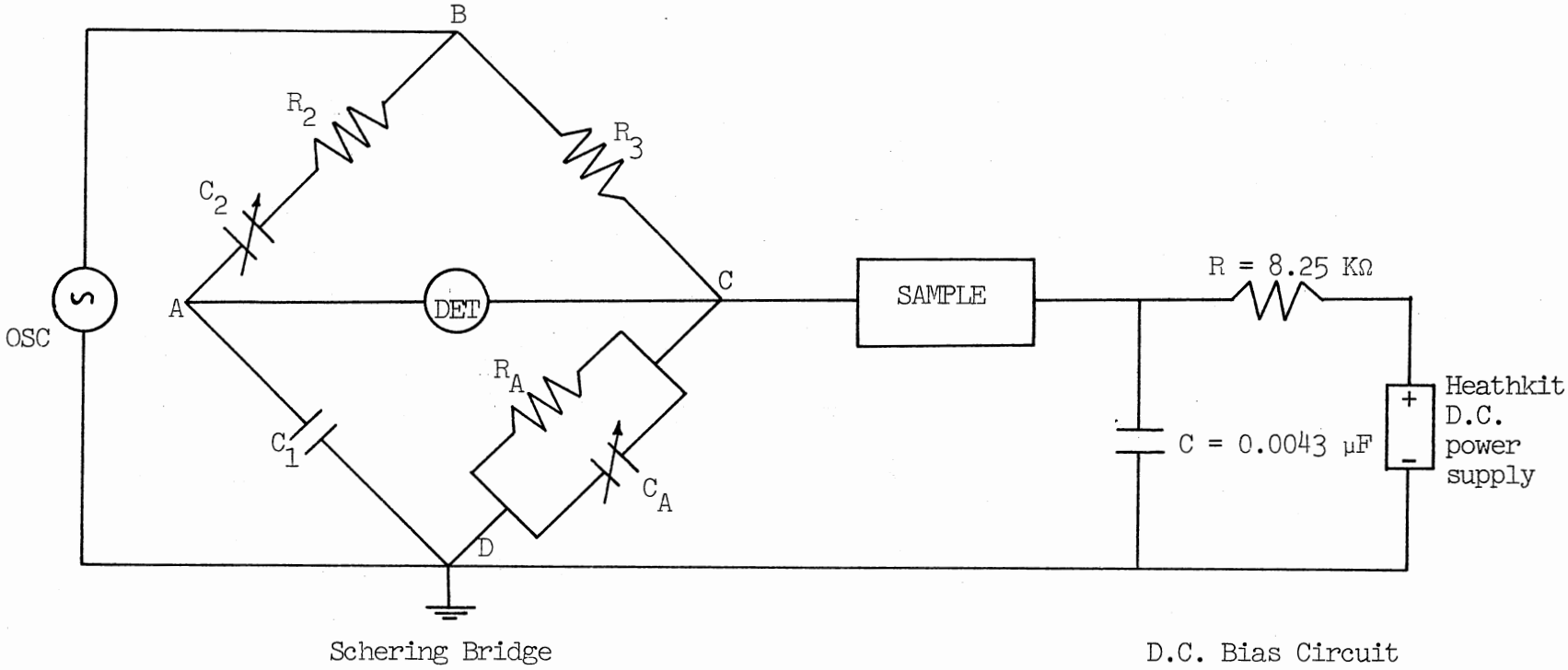

Figure 20. Diagram of Connections for the R-X Meter with the D.C. Bias Circuit

and C_4. With the unknown sample connected across CD, the bridge is unbalanced. The incremental changes ΔC_4 and ΔC_2 necessary to restore the balance are calibrated in terms of equivalent parallel resistance R_p and equivalent parallel capacitance C_p. An equivalent network as given by Sachs and Spiegler (1964) of the unknown sample in a sample holder can be written as shown in Figure 21, where Z_{tr} = line impedance, C_t = stray capacitance, R_s = parallel resistance and C_s = parallel capacitance of the sample.

The d.c. bias circuit shown in Figure 20 allows a method of applying d.c. bias voltage to the sample, for currents less than 50 mA which may be passed directly through the R-X Meter. The value of R is made large enough to present negligible reactance at the range of measuring frequencies (0.5 to 100 MHz), as well as to maximize the d.c. bias voltage to the sample. The accuracy of the bridge measurements are $\pm(2+f/200+R_p/5000+Q/20)\%$ $\pm 0.2\ \Omega$ for resistance, and $\pm(0.5+0.5F^2 x C_p x 10^{-5})$ % ± 0.15 PF for capacitance where, $Q = R_p/X_p$ and F = frequency in MHz.

The main source of error in the measurements with the R-X Meter was the series inductance of the cell used to hold the sample {Section 2.2., Paragraph (4.) and Figure 11}. If C_m = measured parallel capacitance, C_t = true value of parallel capacitance, L_s = series inductance of the sample holder and ω = angular frequency, then

$$C_t = \frac{C_m}{(1 + \omega^2 L_s C_m)} \quad \text{or} \quad C_m = \frac{C_t}{(1 - \omega^2 L_s C_t)} \tag{16}$$

To illustrate the above correction, referring to Table II, the 'open' cell capacitance at f = 1 MHz is C_m = 5.80 PF, and at f = 150 MHz C_m = 7.90 PF. Let us assume that $C_m = C_t$ = 5.80 PF, that is, L_s = 0 at

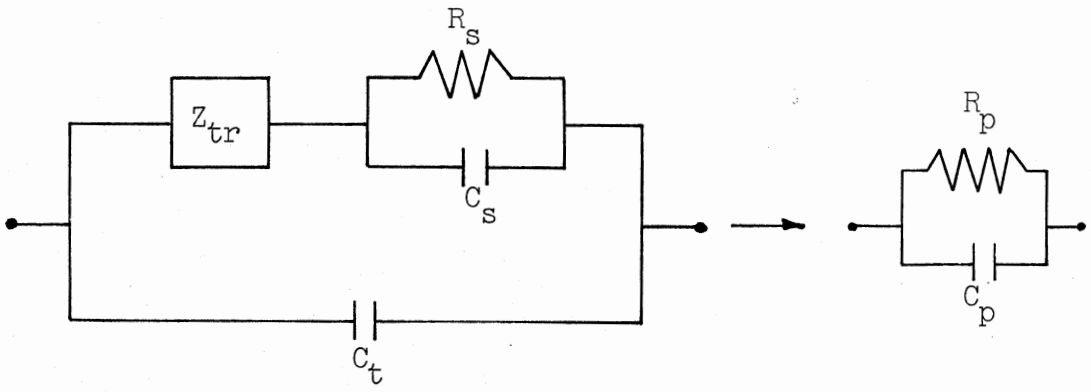

Figure 21. Equivalent Network of the Sample Holder for the R-X Meter

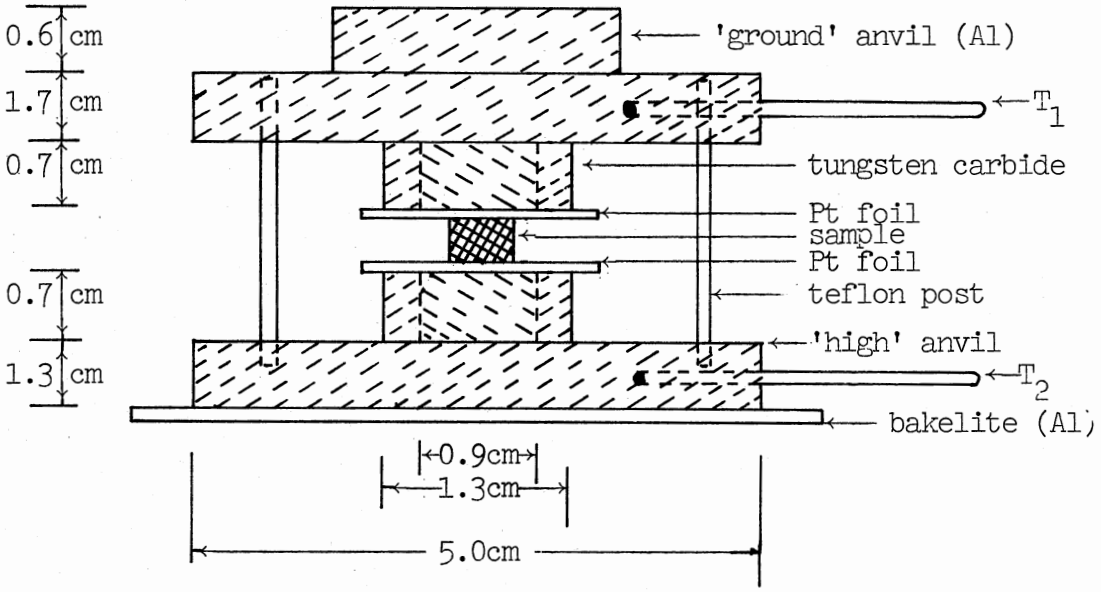

Figure 22. Thermoelectric Power Assembly

TABLE II

EFFECT OF SERIES INDUCTANCE ON CELL CAPACITANCE

Frequency (MHz)	Measured 'Open' Cell Capacitance C_m (PF)	Corrected True 'Open' Cell Capacitance C_t (PF)
1.0	5.80	5.80
10	5.98	5.97
50	6.18	5.99
100	6.52	5.75
120	6.98	5.78
150	7.90	5.79

the low frequency of 1 MHz. At high frequency f = 150 MHz, C_t should also be 5.80 PF, but C_m = 7.90 PF because of inductive effect. Therefore substituting C_m = 7.90 PF, C_t = 5.80 PF and f = 150 MHz in Equation (16), the series inductance L_s = 0.052 μH. With this value for L_s, Table II shows the calculated C_t's which are consistant for the whole range of frequencies. Similarly, if R_m = measured parallel resistance, and R_t = true value of parallel resistance, L_s = series inductance of the sample holder and ω = angular frequency, then,

$$R_t = R_m \times (1 + \omega^2 L_s C_t) \qquad (17)$$

The size of the samples chosen was determined by the maximum capacitance (20 PF) that can be balanced by the bridge in the R-X Meter. The d.c. resistance of the 'open' cell was greater than 10 MΩ. The a.c. resistance of the 'open' cell was greater than 1 MΩ up to 10 MHz, dropped to 10 KΩ at 50 MHz and to 3 KΩ at 100 MHz. This is mainly due to the effect of inductive reactance of the sample holder and the binding posts at higher frequencies. To ensure reliability and good bridge balance, measurements were confined to a frequency range of 0.5 MHz to 100 MHz.

2.7. Thermoelectric Power Measurement

Figure 22 shows an Aluminum pressure cell used in the measurement of thermoelectric power of the samples up to a pressure of 1000 atmospheres. The sample with platinum foils as electrodes was sandwiched between the 'ground' anvil and the 'high' anvil. Two teflon posts embedded in the high anvil served as guide posts to seat the 'ground' anvil. At the center of both anvils, tungsten carbide cylinders were embedded in the recessed aluminum. The 'ground' anvil was in contact

with the upper platen of the hydraulic press and the 'high' anvil was insulated from the lower platen of the hydraulic press by a bakelite disc. The whole assembly was enclosed in a Faraday cage. The two platens of the press could be heated independently. The two thermometers embedded in the aluminum anvils measured the temperature gradient across the sample. The thermoelectric emf generated across the sample was measured by connecting the two platinum electrodes to a Keithley Model 150A D.C. Microvoltmeter.

CHAPTER III

EXPERIMENTAL RESULTS

3.1. D.C. Conductivity and Pressure

For organic semiconductors, the d.c. conductivity is enormously enhanced by the application of pressure. This effect has been associated with the decrease in the activation energy of the formation of carriers due to an increase in the overlap of intermolecular electronic orbitals. Pohl et al. (1962) have developed a theory for the pressure effects based on the theory of absolute reaction rates by Glasstone et al. (1941) giving a d.c. conductivity σ_{DC} increasing with increasing pressure P of the form

$$\sigma_{DC}(P,T) = \sigma(0,T) \exp \{\frac{P^{\frac{1}{2}}}{k} (b'' + b_o'/T)\} \qquad (18)$$

and the activation energy decreasing with increasing pressure as

$$E_P = E_o - bP^{\frac{1}{2}} \qquad (19)$$

where b'', b_o' and b are constants, k = Boltzmann's constant and T = temperature.

Plots of log (d.c. conductivity σ_{DC}) versus (pressure P)$^{\frac{1}{2}}$ are shown in Figure 23 for polymers DP-1A, JK-64 and JM-85A at T = 303^{o}K, in Figure 24 for polymer VJ-1 at T = 296^{o}K, in Figure 25 for polymers LD-5, LD-6, LD-7 and LD-40 at T = 296^{o}K, in Figure 26 for polymers LD-2, LD-3, LD-8, LD-12, LD-19, LD-20, LD-31, LD-32, LD-33, LD-35,

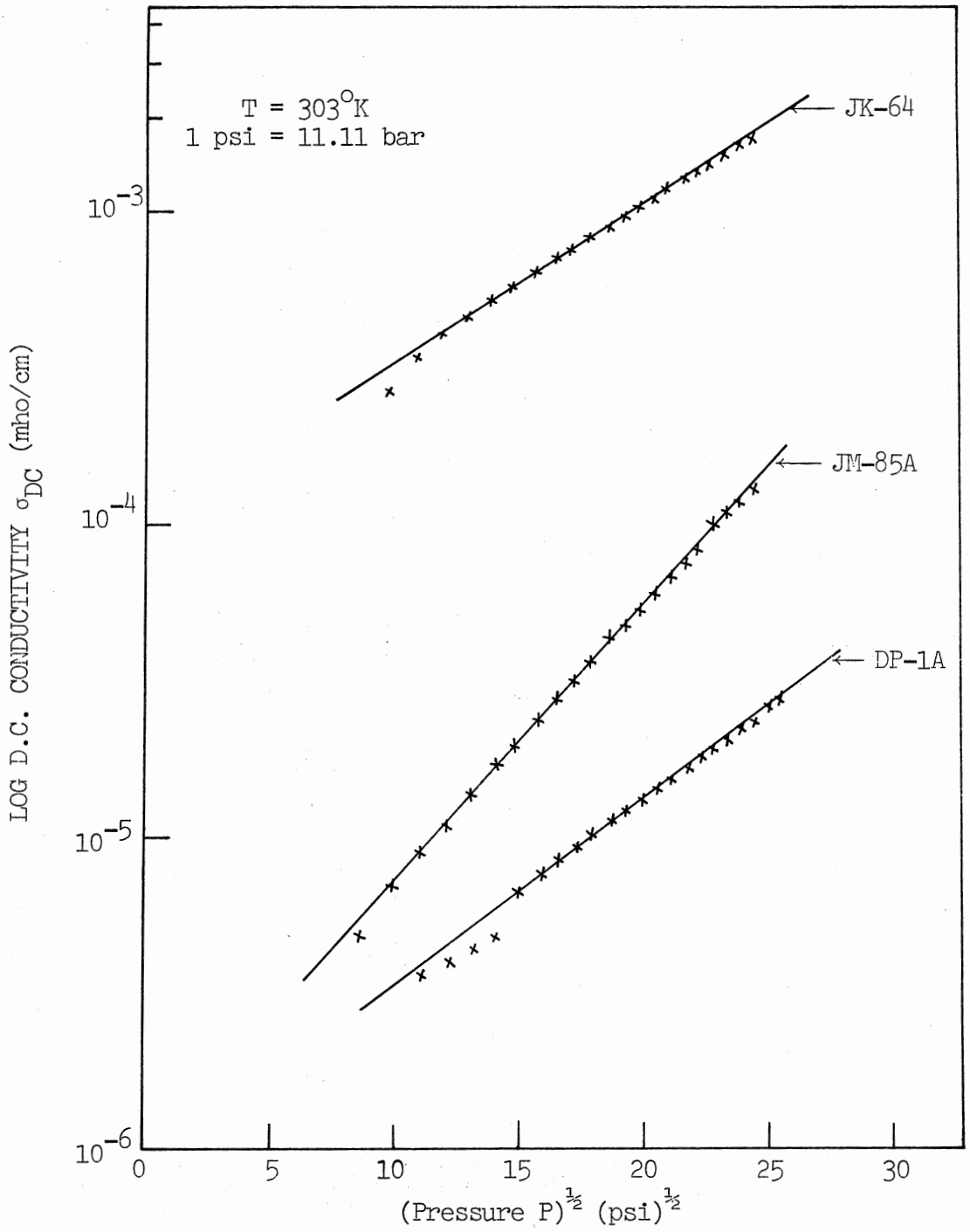

Figure 23. Log (D.C. Conductivity) Versus (Pressure)$^{\frac{1}{2}}$
(Polymers DP-1A, JK-64 and JM-85A)

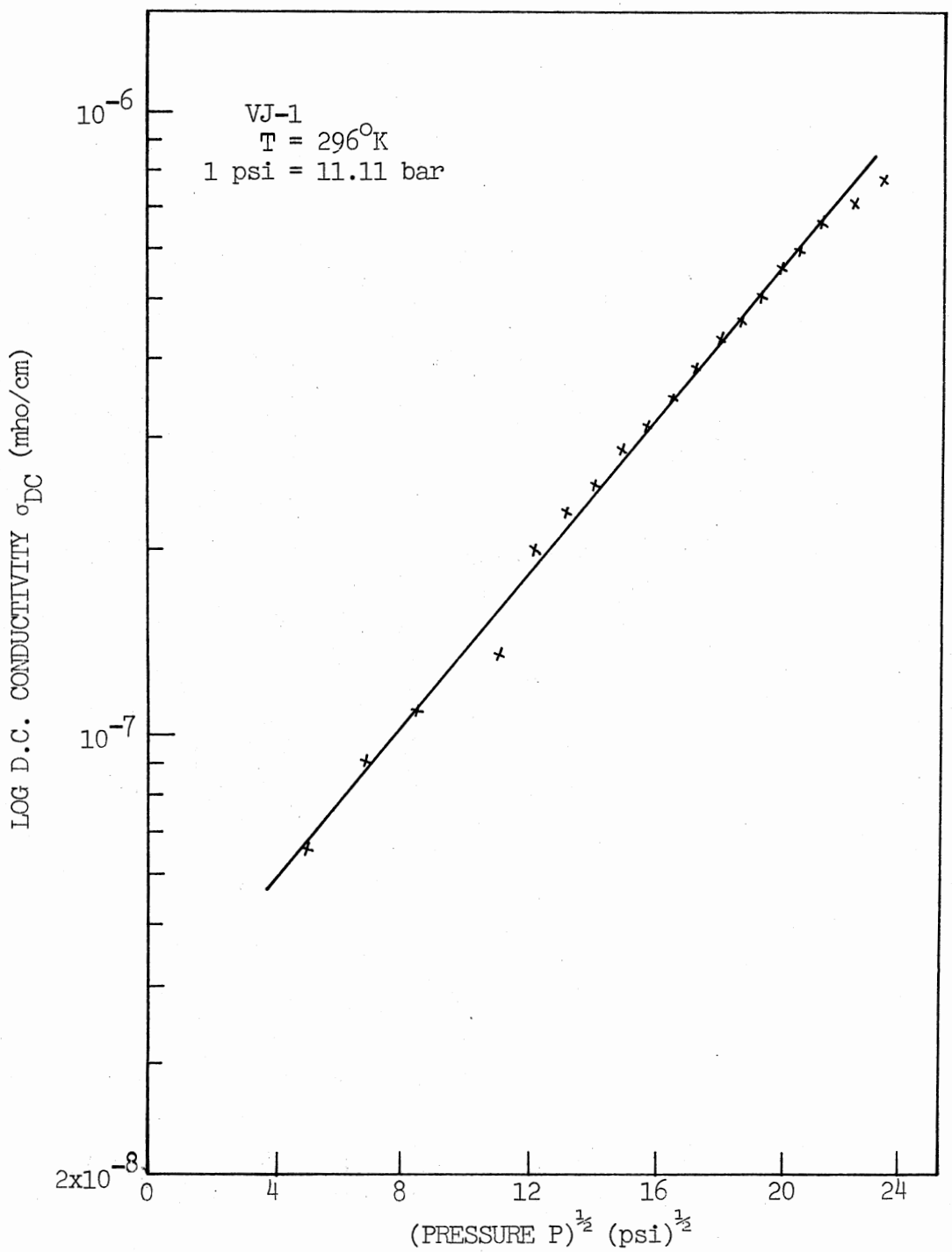

Figure 24. Log (D.C. Conductivity) Versus (Pressure)$^{\frac{1}{2}}$
(Polymer VJ-1)

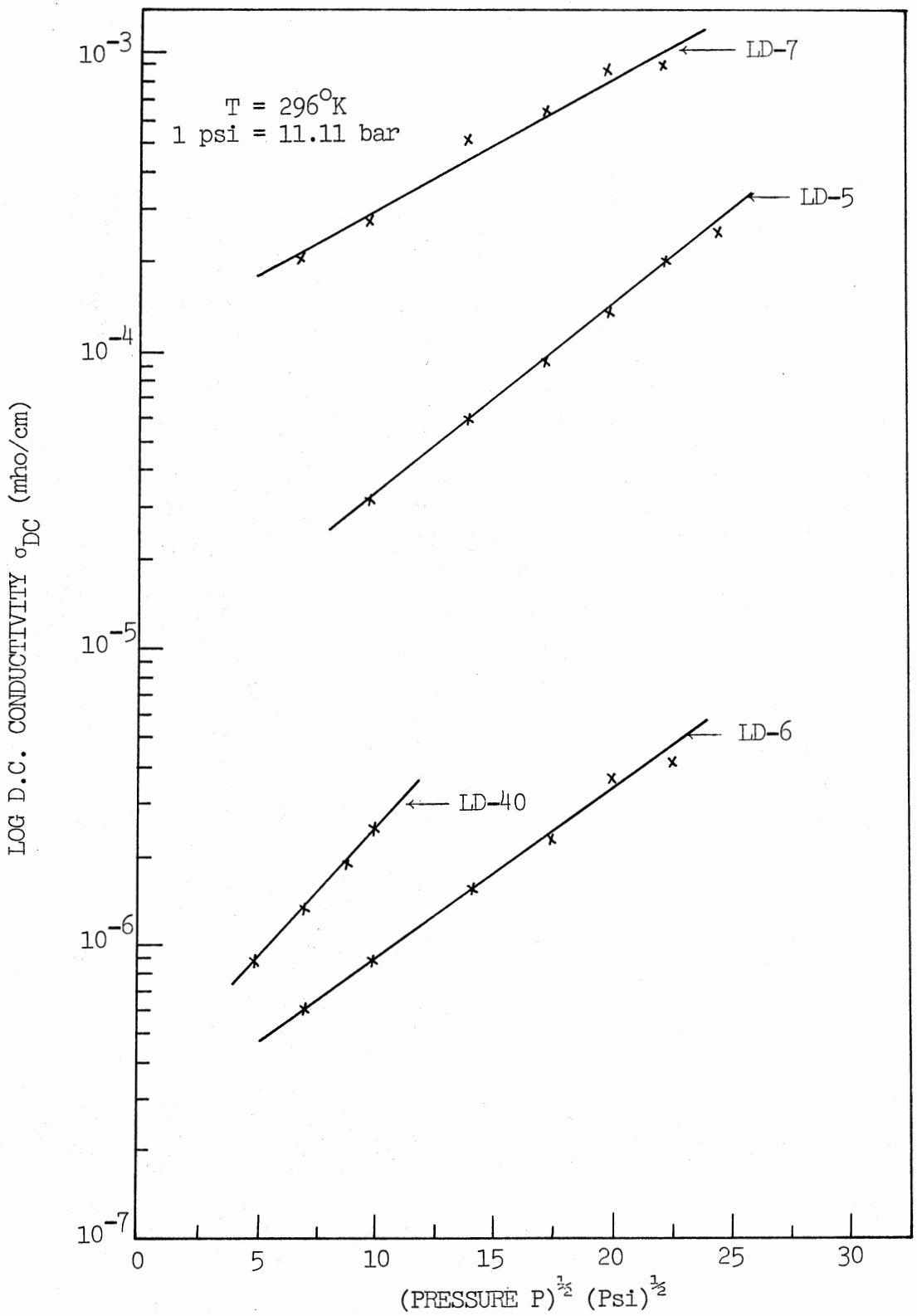

Figure 25. Log (D.C. Conductivity) Versus (Pressure)$^{\frac{1}{2}}$ (Polymers LD-5, LD-6, LD-7 and LD-40)

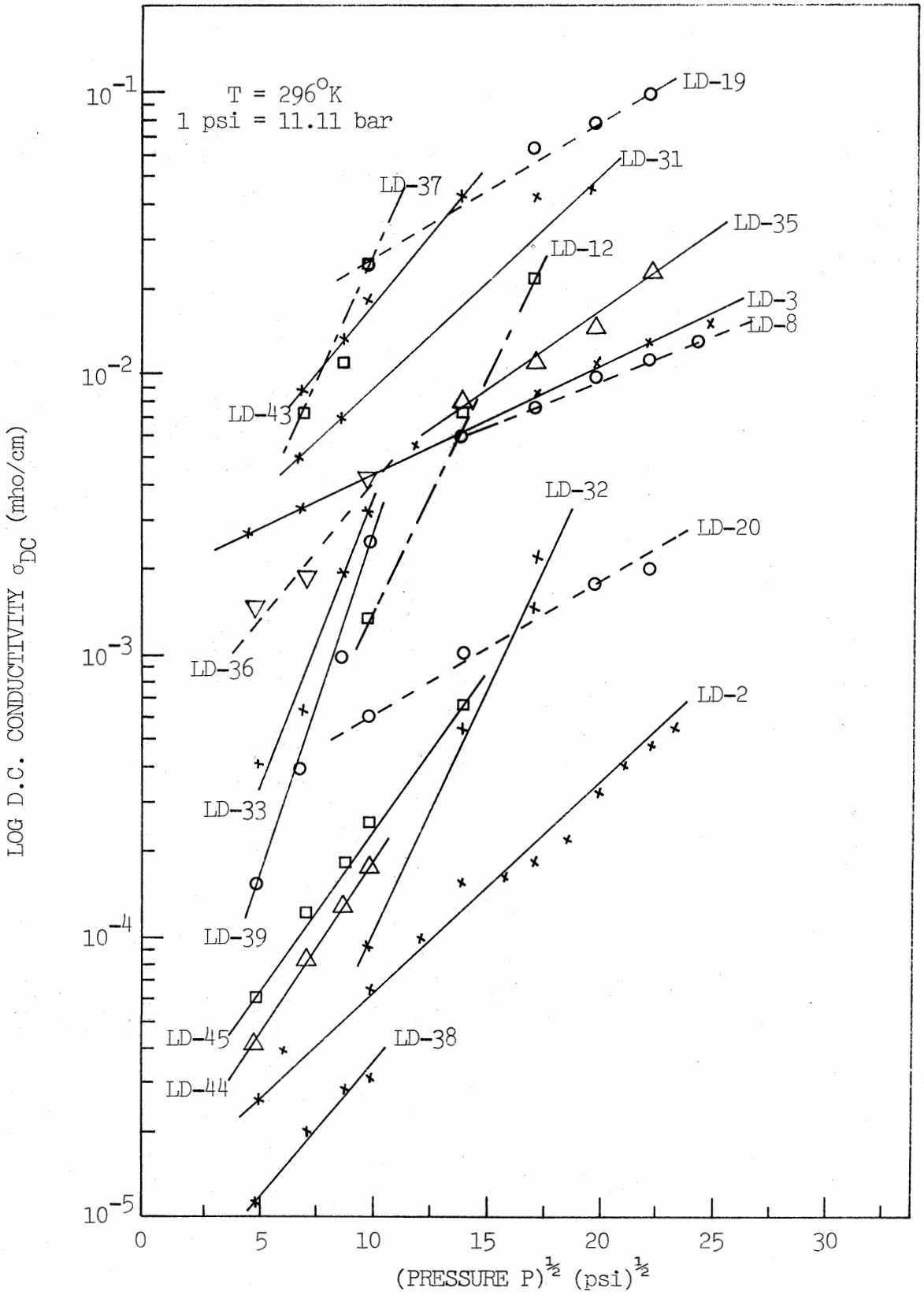

Figure 26. Log (D.C. Conductivity) Versus (Pressure)$^{\frac{1}{2}}$
(LD Series of Polymers - Batch I)

LD-36, LD-37, LD-38, LD-39, LD-43, LD-44 and LD-45 at T = 296°K, and in Figure 27 for polymers LD-4, LD-10, LD-11, LD-21, LD-22, LD-23, LD-24, LD-25, LD-27, LD-28, LD-29, LD-30, LD-34, LD-41, LD-42, LD-47 and LD-48 at T = 296°K. Typical values of the d.c. conductivities for these polymers are listed in Table III. Taking logarithms of Equation (18)

$$\ln (\sigma_{DC}/\sigma_o)_T = (b_T^{\sigma_{DC}}/k)\, P^{\frac{1}{2}} \qquad (20)$$

where $b_T^{\sigma_{DC}}$ is the pressure coefficient of d.c. conductivity at temperature T. These are listed in Table IV for polymers studied at room temperature.

3.2. A.C. Conductivity and Pressure

Based on the theory developed by Pohl et al. (1962) for the effect of pressure on d.c. conductivity, the a.c. conductivity σ_{AC} increases with increasing pressure P as

$$\ln (\sigma_{AC}/\sigma_o)_T = (b_T^{\sigma_{AC}}/k)\, P^{\frac{1}{2}} \qquad (21)$$

where $b_T^{\sigma_{AC}}$ is the pressure coefficient of a.c. conductivity at temperature T.

Plots of log (a.c. conductivity σ_{AC}) versus (pressure P)$^{\frac{1}{2}}$ are shown in Figure 28 for polymer DP-1A for frequencies F = 0.10 KHz, 1.0 KHz, 10.0 KHz and 100 KHz at T = 303°K, 273°K and 195°K, in Figure 29 for polymer JK-64 for F = 10.0 KHz and 100 KHz at T = 303°K and 273°K, and for F = 1.0 KHz, 10.0 KHz and 100 KHz at T = 77°K, in Figure 30 for polymer JM-85A for F = 0.15 KHz, 1.0 KHz, 10.0 KHz and 100 KHz at T = 300°K, 273°K and 195°K, and for F = 100 KHz at T = 77°K, and in Figure 31 for polymers LD-5, LD-6, LD-7, LD-10, LD-11, LD-21, LD-22, LD-23,

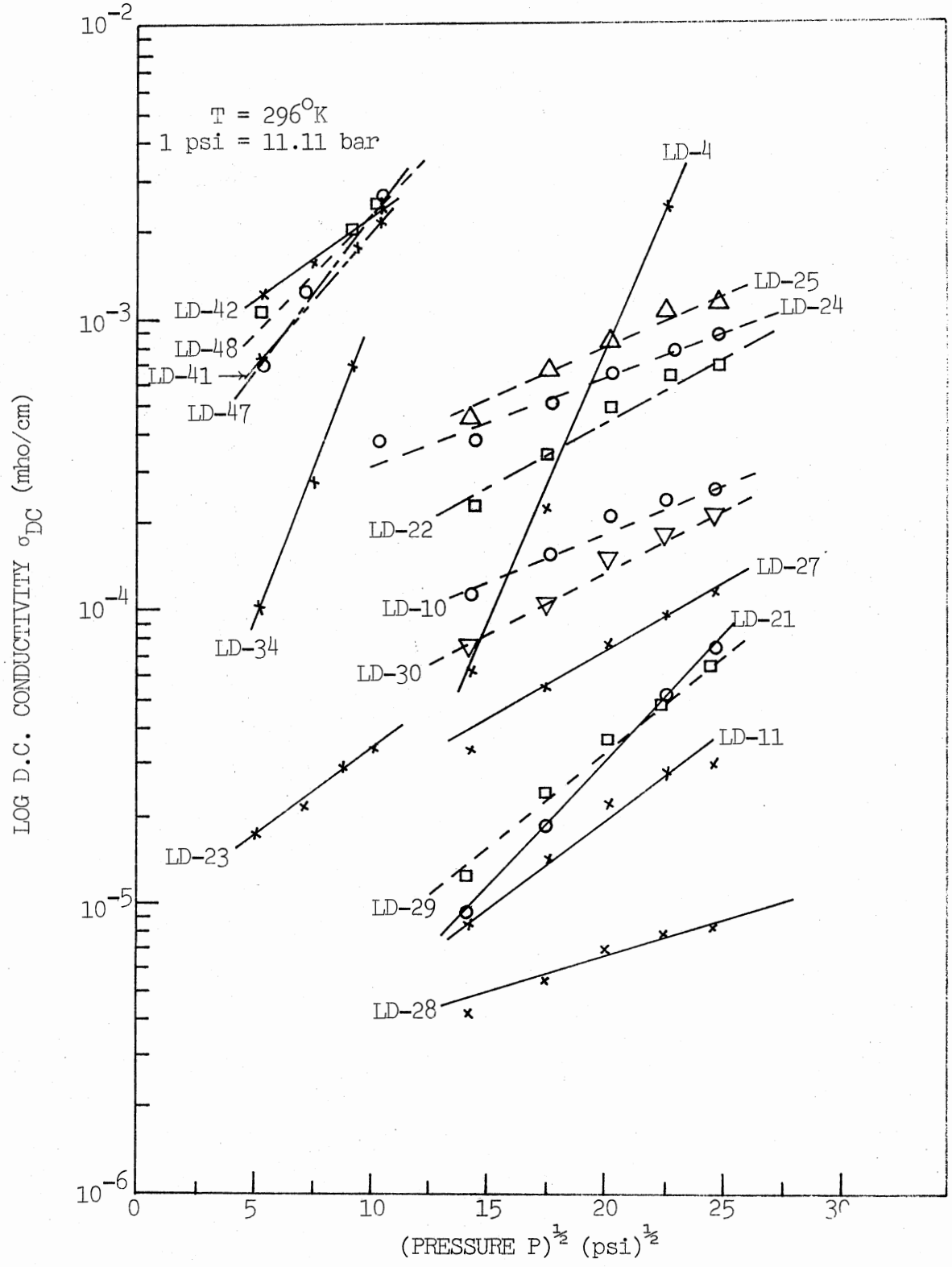

Figure 27. Log (D.C. Conductivity) Versus (Pressure)$^{\frac{1}{2}}$
(LD Series of Polymers - Batch II)

TABLE III

ELECTRICAL PROPERTIES OF ELECTRO-ACTIVE PAQR POLYMERS

Sample Number	Sample Name	Sample Size	Pressure (Kbar)	Temperature (^{o}K)	Frequency	σ_{DC} (mho/cm)	σ_{T} (mho/cm)	σ_{AC} (mho/cm)	ε_{r}	tanδ
1	DP-1A	d=6.0mm Th=9.9mils	8.0	303	1.0 KHz	3.28×10^{-5}	3.386×10^{-5}	1.03×10^{-6}	2481	2.45×10^{1}
				273	1.0 KHz	1.62×10^{-5}	1.673×10^{-5}	5.26×10^{-7}	1815	1.66×10^{1}
				195	1.0 KHz	1.35×10^{-5}	1.551×10^{-6}	2.04×10^{-7}	383.9	7.26×10^{0}
				77	1.0 KHz	2.53×10^{-11}	3.20×10^{10}	2.95×10^{-10}	6.45	8.92×10^{-2}
			3.9	303	1.0 KHz	1.11×10^{-5}	1.169×10^{-5}	5.75×10^{-7}	1720	1.22×10^{1}
				273	1.0 KHz	5.61×10^{-6}	6.134×10^{-6}	5.22×10^{-7}	880.0	1.25×10^{1}
				195	1.0 KHz	4.06×10^{-7}	5.151×10^{-7}	1.09×10^{-7}	115.9	7.99×10^{0}
				77	1.0 KHz	2.02×10^{-11}	2.990×10^{-10}	2.78×10^{-10}	6.30	8.53×10^{-2}
			1.1	303	1.0 KHz	3.05×10^{-6}	3.301×10^{-6}	2.46×10^{-7}	519.8	1.14×10^{1}
				273	1.0 KHz	1.30×10^{-6}	1.459×10^{-6}	1.57×10^{-7}	289.3	9.06×10^{0}
				195	1.0 KHz	7.27×10^{-8}	9.369×10^{-8}	2.10×10^{-8}	24.75	6.80×10^{0}
				77	1.0 KHz	3.50×10^{-12}	2.165×10^{-10}	2.13×10^{-10}	6.15	6.22×10^{-2}

TABLE III (Continued)

Sample Number	Sample Name	Sample Size	Pressure (Kbar)	Temperature (^{o}K)	Frequency	σ_{DC} (mho/cm)	σ_{T} (mho/cm)	σ_{AC} (mho/cm)	ε_r	tanδ
1	DP-1A	d=6.0mm Th=9.9mils	0.46	303	1.0 KHz	8.15×10^{-7}	9.02×10^{-7}	8.76×10^{-8}	203.8	7.96×10^{0}
				273	1.0 KHz	3.03×10^{-7}	3.932×10^{-8}	9.04×10^{-8}	114.9	6.15×10^{0}
				195	1.0 KHz	1.08×10^{-8}	1.974×10^{-8}	8.91×10^{-9}	8.96	3.96×10^{0}
		d=2.8mm Th=11.1mils	3.3	300	10 MHz	1.15×10^{-5}	2.813×10^{-5}	1.66×10^{-5}	18.77	2.69×10^{-1}
			2.1	300	10 MHz	9.60×10^{-6}	2.483×10^{-5}	1.52×10^{-5}	18.77	2.38×10^{-1}
			1.1	300	10 MHz	7.44×10^{-6}	1.944×10^{-5}	1.20×10^{-5}	18.41	1.90×10^{-1}
			0.32	300	10 MHz	4.59×10^{-6}	1.451×10^{-5}	9.92×10^{-6}	16.70	1.56×10^{-1}
2	JK-64	d=6.0mm Th=8.5mils	6.0	303	10 KHz	1.02×10^{-3}	1.131×10^{-3}	1.06×10^{-4}	-	-
				273	10 KHz	6.38×10^{-4}	6.501×10^{-4}	1.18×10^{-5}	-	-
				195	10 KHz	1.27×10^{-4}	1.448×10^{-4}	1.75×10^{-5}	609.9	4.29×10^{1}
				77	1.0 KHz	3.65×10^{-7}	4.141×10^{-7}	4.86×10^{-8}	108.3	6.87×10^{0}

TABLE III (Continued)

Sample Number	Sample Name	Sample Size	Pressure (Kbar)	Temperature (^{o}K)	Frequency	σ_{DC} (mho/cm)	σ_{T} (mho/cm)	σ_{AC} (mho/cm)	ε_r	tanδ
2	JK-64	d=6.0mm Th=8.5mils	3.7	303	10 KHz	7.69×10^{-4}	8.038×10^{-4}	3.43×10^{-5}	1300	1.11×10^{2}
				273	10 KHz	4.90×10^{-4}	5.006×10^{-4}	9.60×10^{-6}	1147	7.84×10^{1}
				195	1.0 KHz	7.58×10^{-5}	8.010×10^{-5}	4.32×10^{-6}	1399	1.03×10^{2}
				77	1.0 KHz	1.71×10^{-7}	2.079×10^{-7}	3.64×10^{-8}	75.76	4.93×10^{0}
			2.2	300	10 KHz	4.25×10^{-4}	4.334×10^{-4}	8.08×10^{-6}	576.5	1.35×10^{2}
				273	10 KHz	2.63×10^{-4}	2.649×10^{-4}	2.00×10^{-6}	556.4	8.56×10^{1}
				77	1.0 KHz	9.69×10^{-8}	1.276×10^{-7}	3.07×10^{-8}	69.77	3.29×10^{0}
		d=4.1mm Th=26.6mils Silver-Painted	0.0	294	1.0 KHz	9.92×10^{-6}	9.783×10^{-6}	3.04×10^{-7}	3848	4.57×10^{0}
				270	1.0 KHz	5.92×10^{-6}	6.269×10^{-6}	4.82×10^{-7}	3742	3.01×10^{0}
				250	1.0 KHz	3.75×10^{-6}	4.056×10^{-6}	4.66×10^{-7}	3510	2.08×10^{0}
				230	1.0 KHz	2.04×10^{-6}	2.700×10^{-6}	5.95×10^{-7}	3105	1.56×10^{0}
				210	1.0 KHz	1.22×10^{-6}	1.829×10^{-6}	6.52×10^{-7}	2504	1.31×10^{0}
				190	1.0 KHz	6.70×10^{-7}	1.329×10^{-6}	6.97×10^{-7}	1911	1.25×10^{0}
				170	1.0 KHz	3.16×10^{-7}	8.846×10^{-7}	2.16×10^{-7}	1124	1.41×10^{0}

TABLE III (Continued)

Sample Number	Sample Name	Sample Size	Pressure (Kbar)	Temperature (^{o}K)	Frequency	σ_{DC} (mho/cm)	σ_{T} (mho/cm)	σ_{AC} (mho/cm)	ε_r	tanδ
2	JK-64	d=4.1mm	0.0	150	1.0 KHz	1.11×10^{-7}	4.763×10^{-7}	1.69×10^{-7}	478.7	1.79×10^{0}
				130	1.0 KHz	3.80×10^{-8}	1.944×10^{-7}	1.00×10^{-7}	217.0	1.61×10^{0}
				110	1.0 KHz	9.27×10^{-9}	6.773×10^{-8}	2.51×10^{-8}	95.78	1.27×10^{0}
				90	1.0 KHz	2.48×10^{-9}	2.657×10^{-8}	1.53×10^{-8}	49.53	9.64×10^{-1}
				77	1.0 KHz	3.18×10^{-10}	9.928×10^{-9}	9.68×10^{-9}	23.17	7.70×10^{1}
				294	10 MHz	9.92×10^{-6}	2.219×10^{-4}	2.12×10^{-4}	18.56	2.15×10^{-1}
3	JM-85A	d=3.0mm Th=10.3mils	6.1	300	1.0 KHz	1.73×10^{-4}	1.9479×10^{-4}	2.14×10^{-5}	1492	2.35×10^{2}
				273	1.0 KHz	8.06×10^{-6}	8.743×10^{-5}	6.78×10^{-6}	821.0	1.91×10^{2}
				195	1.0 KHz	3.03×10^{-6}	3.333×10^{-6}	3.08×10^{-7}	138.2	4.33×10^{1}
				77	1.0 KHz	1.39×10^{-10}	9.006×10^{-10}	7.61×10^{-10}	11.55	1.40×10^{-1}
			2.8	300	1.0 KHz	2.69×10^{-5}	3.188×10^{-5}	5.01×10^{-6}	697.0	8.22×10^{1}
				273	1.0 KHz	1.16×10^{-5}	1.2542×10^{-5}	9.12×10^{-7}	363.4	6.20×10^{1}
				195	1.0 KHz	3.56×10^{-7}	4.7838×10^{-7}	1.22×10^{-7}	83.50	1.03×10^{1}

TABLE III (Continued)

Sample Number	Sample Name	Sample Size	Pressure (Kbar)	Temperature (^{o}K)	Frequency	σ_{DC} (mho/cm)	σ_{T} (mho/cm)	σ_{AC} (mho/cm)	ε_{r}	tanδ
3	JM-85A	d=3.0mm Th=10.30mils	2.8	77	1.0 KHz	1.40×10^{-11}	9.1013×10^{-11}	7.70×10^{-11}	9.30	1.76×10^{-2}
			0.86	300	1.0 KHz	5.51×10^{-6}	6.4548×10^{-6}	9.49×10^{-7}	214.0	5.42×10^{1}
				273	1.0 KHz	1.83×10^{-6}	1.9460×10^{-6}	1.15×10^{-7}	109.2	3.20×10^{1}
				195	1.0 KHz	1.98×10^{-8}	2.098×10^{-8}	2.23×10^{-9}	10.50	3.59×10^{0}
				77	1.0 KHz	1.76×10^{-12}	5.177×10^{-11}	5.00×10^{-11}	6.58	1.41×10^{-2}
4	VJ-1	d=6.0mm Th=20.7mils	5.5	297	-	7.72×10^{-7}	-	-	-	-
			2.2	297	-	2.50×10^{-7}	-	-	-	-
5	LD-2	d=4.7mm Th=15.0mils	5.5	298	1.0 KHz	4.54×10^{-4}	1.932×10^{-4}	$\sim4.54\times10^{-4}$	287000	$\sim1.21\times10^{0}$
			2.2	298	1.0 KHz	1.52×10^{-4}	1.105×10^{-4}	$\sim1.52\times10^{-4}$	239000	$\sim8.31\times10^{-1}$
6	LD-3	d=3.2mm Th=10.0mils	5.5	298	1.0 KHz	1.24×10^{-2}	1.232×10^{-2}	$\sim1.24\times10^{-2}$	9637	$\sim2.30\times10^{3}$
			2.2	298	1.0 KHz	5.42×10^{-3}	5.211×10^{-3}	$\sim5.42\times10^{-3}$	5325	$\sim1.76\times10^{3}$
7	LD-4-43	d=3.0mm Th=12.5mils	1.1	296	1.0 KHz	2.93×10^{-6}	3.37×10^{-6}	4.36×10^{-7}	276.7	2.19×10^{1}

TABLE III (Continued)

Sample Number	Sample Name	Sample Size	Pressure (Kbar)	Temperature (^{o}K)	Frequency	σ_{DC} (mho/cm)	σ_{T} (mho/cm)	σ_{AC} (mho/cm)	ε_{r}	tanδ
8	LD-5	d=3.0mm Th=9.0mils	5.5	298	1.0 KHz	1.93×10^{-4}	2.265×10^{-4}	3.37×10^{-5}	3072	1.32×10^{0}
			2.2	298	1.0 KHz	5.89×10^{-5}	7.333×10^{-5}	1.44×10^{-5}	1691	7.79×10^{1}
9	LD-6	d=3.0mm Th=8.9mils	5.5	298	1.0 KHz	3.05×10^{-6}	3.342×10^{-6}	2.91×10^{-7}	344.9	1.74×10^{1}
			2.2	298	1.0 KHz	1.53×10^{-6}	1.012×10^{-6}	1.36×10^{-7}	106.2	1.71×10^{1}
10	LD-7	d=3.0mm Th=9.8mils	5.5	298	1.0 KHz	8.80×10^{-4}	9.905×10^{-4}	1.10×10^{-4}	22400	7.94×10^{1}
			2.2	298	1.0 KHz	5.08×10^{-4}	3.266×10^{-4}	5.17×10^{-5}	8379	7.01×10^{1}
11	LD-8	d=3.0mm Th=11.1mils	5.5	294	-	1.11×10^{-2}	-	-	-	-
			2.2	294	-	5.59×10^{-3}	-	-	-	-
12	LD-10	d=3.0mm Th=12.1mils	5.5	297	1.0 KHz	2.45×10^{-4}	2.472×10^{-4}	2.20×10^{-6}	2961	1.50×10^{2}
			2.2	297	1.0 KHz	1.16×10^{-4}	1.98×10^{-4}	3.80×10^{-6}	2293	1.55×10^{2}
13	LD-11	d=3.0mm Th=12.6mils	5.5	296	1.0 KHz	2.90×10^{-5}	3.14×10^{-5}	2.40×10^{-6}	5831	9.68×10^{0}
			2.2	296	1.0 KHz	8.60×10^{-6}	1.03×10^{-5}	1.70×10^{-6}	3215	5.76×10^{0}

TABLE III (Continued)

Sample Number	Sample Name	Sample Size	Pressure (Kbar)	Temperature (^{o}K)	Frequency	σ_{DC} (mho/cm)	σ_{T} (mho/cm)	σ_{AC} (mho/cm)	ε_{r}	tanδ
14	LD-12-43	d=3.0mm Th=9.1mils	5.5	294	-	2.30×10^{-2}	-	-	-	-
			2.2	294	-	7.20×10^{-3}	-	-	-	-
15	LD-19-41	d=3.0mm Th=12.2mils	5.5	294	-	9.74×10^{-2}	-	-	-	-
			2.2	294	-	4.34×10^{-2}	-	-	-	-
16	LD-20-39	d=3.0mm Th=7.1mils	5.5	294	-	1.93×10^{-2}	-	-	-	-
			2.2	294	-	1.05×10^{-3}	-	-	-	-
17	LD-21	d=3.0mm Th=6.2mils	5.5	295	1.0 KHz	5.33×10^{-5}	5.49×10^{-5}	1.66×10^{-6}	2199	4.49×10^{1}
			2.2	295	1.0 KHz	8.98×10^{-6}	9.40×10^{-6}	4.60×10^{-6}	673.7	2.51×10^{1}
18	LD-22	d=3.0mm Th=10.4mils	5.5	295	1.0 KHz	6.48×10^{-4}	6.52×10^{-4}	4.75×10^{-6}	2599	4.51×10^{2}
			2.2	295	1.0 KHz	2.27×10^{-4}	2.29×10^{-4}	1.67×10^{-6}	1298	3.17×10^{2}
19	LD-23	d=3.0mm Th=13.2mils	1.1	296	1.0 KHz	3.41×10^{-5}	3.48×10^{-5}	7.01×10^{-7}	993.3	6.30×10^{1}

TABLE III (Continued)

Sample Number	Sample Name	Sample Size	Pressure (Kbar)	Temperature (^{o}K)	Frequency	σ_{DC} (mho/cm)	σ_{T} (mho/cm)	σ_{AC} (mho/cm)	ε_{r}	tanδ
20	LD-24	d=3.0mm Th=12.4mils	5.5	296	1.0 KHz	8.03×10^{-4}	8.06×10^{-4}	3.49×10^{-6}	647.8	2.24×10^{3}
			2.2	296	1.0 KHz	3.85×10^{-4}	3.85×10^{-4}	3.49×10^{-6}	494.7	1.40×10^{3}
21	LD-25-64	d=3.0mm Th=13.2mils	5.5	296	1.0 KHz	1.07×10^{-3}	1.08×10^{-3}	4.39×10^{-6}	865.0	2.24×10^{3}
			2.2	296	1.0 KHz	4.47×10^{-4}	4.51×10^{-4}	4.67×10^{-6}	337.9	2.40×10^{3}
22	LD-27-65	d=3.0mm Th=12.5mils	5.5	296	1.0 KHz	9.85×10^{-5}	9.99×10^{-5}	1.40×10^{-6}	528.5	1.17×10^{2}
			2.2	296	1.0 KHz	3.35×10^{-5}	3.44×10^{-5}	9.75×10^{-7}	361.5	1.71×10^{2}
23	LD-28-65	d=3.0mm Th=7.4mils	5.5	296	1.0 KHz	8.13×10^{-6}	1.05×10^{-5}	2.34×10^{-6}	2338	8.07×10^{0}
			2.2	296	1.0 KHz	4.22×10^{-6}	5.59×10^{-6}	1.36×10^{-6}	1672	6.01×10^{0}
24	LD-29-65	d=3.0mm Th=13.2mils	5.5	296	1.0 KHz	4.81×10^{-5}	5.07×10^{-5}	2.62×10^{-6}	1210	7.53×10^{1}
			2.2	296	1.0 KHz	1.22×10^{-5}	1.62×10^{-5}	3.99×10^{-6}	480.1	6.06×10^{1}
25	LD-30-66	d=3.0mm Th=13.1mils	5.5	296	1.0 KHz	1.83×10^{-4}	1.87×10^{-4}	3.86×10^{-6}	1024	3.28×10^{2}
			2.2	296	1.0 KHz	7.62×10^{-5}	7.85×10^{-5}	2.30×10^{-6}	381.5	3.70×10^{2}

TABLE III (Continued)

Sample Number	Sample Name	Sample Size	Pressure (Kbar)	Temperature (^{o}K)	Frequency	σ_{DC} (mho/cm)	σ_{T} (mho/cm)	σ_{AC} (mho/cm)	ε_{r}	tanδ
26	LD-31	d=3.0mm Th=7.1mils	5.5	297	-	4.47×10^{-2}	-	-	-	-
			2.2	297	-	4.11×10^{-2}	-	-	-	-
27	LD-32	d=3.0mm Th=13.2mils	5.5	297	-	3.23×10^{-2}	-	-	-	-
			2.2	297	-	5.51×10^{-3}	-	-	-	-
28	LD-33	d=3.0mm Th=6.2mils	1.1	297	-	3.25×10^{-3}	-	-	-	-
29	LD-34	d=3.0mm Th=9.2mils	1.1	297	-	9.44×10^{-2}	-	-	-	-
30	LD-35	d=3.0mm Th=12.2mils	5.5	297	-	2.17×10^{-2}	-	-	-	-
			2.2	297	-	7.69×10^{-3}	-	-	-	-
31	LD-36	d=3.0mm Th=12.4mils	1.1	297	-	4.01×10^{-3}	-	-	-	-
32	LD-37	d=3.0mm Th=14.7mils	5.5	297	-	2.78×10^{-1}	-	-	-	-
			2.2	297	-	2.41×10^{-2}	-	-	-	-

TABLE III (Continued)

Sample Number	Sample Name	Sample Size	Pressure (Kbar)	Temperature (^{o}K)	Frequency	σ_{DC} (mho/cm)	σ_{T} (mho/cm)	σ_{AC} (mho/cm)	ε_{r}	tanδ
33	LD-38	d=3.0mm Th=19.4mils	1.1	297	-	3.15×10^{-5}	-	-	-	-
34	LD-39	d=3.0mm Th=11.6mils	5.5	297	-	9.47×10^{-2}	-	-	-	-
			2.2	297	-	3.28×10^{-3}	-	-	-	-
35	LD-40	d=3.0mm Th=10.1mils	1.1	297	1.0 KHz	2.38×10^{-6}	2.41×10^{-6}	2.80×10^{-8}	347.3	1.25×10^{1}
36	LD-41	d=3.0mm Th=8.5mils	1.1	297	-	2.18×10^{-3}	-	-	-	-
37	LD-42	d=3.0mm Th=5.6mils	1.1	297	-	2.45×10^{-3}	-	-	-	-
38	LD-43	d=3.0mm Th=13.2mils	5.5	296	-	3.95×10^{-1}	-	-	-	-
			2.2	296	-	3.95×10^{-2}	-	-	-	-
39	LD-44	d=3.0mm Th=6.1mils	5.5	296	-	1.83×10^{-1}	-	-	-	-
			2.2	296	-	2.25×10^{-3}	-	-	-	-

TABLE III (Continued)

Sample Number	Sample Name	Sample Size	Pressure (Kbar)	Temperature (^{o}K)	Frequency	σ_{DC} (mho/cm)	σ_{T} (mho/cm)	σ_{AC} (mho/cm)	ε_{r}	tanδ
40	LD-45	d=3.0mm Th=10.6mils	5.5	296	-	1.86×10^{-3}	-	-	-	-
			2.2	296	-	6.49×10^{-4}	-	-	-	-
41	LD-47	d=3.0mm Th=11.6mils	1.1	296	-	2.65×10^{-3}	-	-	-	-
42	LD-48	d=3.0mm Th=12.0mils	1.1	296	-	2.42×10^{-3}	-	-	-	-

Note: Applied a.c. voltage $V_{ac}=0.1\ V_{pp}$; a.c. electric field strength $E_{ac}=V_{ac}/Th$; a.c. conductivity $\sigma_{AC}=\sigma_{T}-\sigma_{DC}$, where d.c. conductivity $\sigma_{DC}=Th/(R_{DC}A)$, Th=thickness of the sample, A=area of the sample and R_{DC}=d.c. resistance of the sample; total conductivity $\sigma_{T}=Th/(R_{T}A)$, R_{T}=resistance of the sample as measured by the a.c. bridge; relative dielectric constant $\varepsilon_{r}=(C)(Th)/(\varepsilon_{o}A)$, where C=capacitance as measured by the a.c. bridge; and loss tangent $\tan\delta=\sigma_{T}/(\omega\varepsilon_{r}\varepsilon_{o})$.

TABLE IV

PRESSURE COEFFICIENTS OF ELECTRO-ACTIVE
PAQR POLYMERS AT ROOM TEMPERATURE

Sample Number	Sample Name	Temperature T (^{o}K)	Pressure Coefficients x 10^{-6} $\frac{eV}{(bar)^{\frac{1}{2}}\ ^{o}K}$		
			σ_{DC} b_T	σ_{AC} (f=1.0 KHz) b_T	ε b_T
1	DP-1A	303	3.80	2.45	3.25
2	JK-64	303	4.44	5.87 (f=10.0 KHz)	2.08 (f=10.0 KHz)
3	JM-85A	300	5.18	5.22	3.05
4	VJ-1	297	3.60	-	-
5	LD-2	298	4.39	-	0.827
6	LD-3	298	2.39	-	2.53
7	LD-4-43	296	10.9	-	-
8	LD-5	298	3.73	1.63	1.40
9	LD-6	298	1.27	2.03	3.96
10	LD-7	298	2.58	2.41	2.54
11	LD-8-43	294	1.91	-	-
12	LD-10	297	1.96	3.04	0.755
13	LD-11	296	3.58	2.33	2.17
14	LD-12-43	294	9.92	-	-
15	LD-19-41	294	2.76	-	-
16	LD-20-39	294	2.83	-	-
17	LD-21	295	5.20	3.30	3.91
18	LD-22	295	2.70	2.16	2.31
19	LD-23	296	3.69	8.85	1.84
20	LD-24	296	1.84	5.16	0.786

TABLE IV (Continued)

Sample Number	Sample Name	Temperature T (^{o}K)	Pressure Coefficients x 10^{-6} $\frac{eV}{(bar)^{\frac{1}{2}}\,{}^{o}K}$ (f=1.0 KHz)		
			$b_T^{\sigma_{DC}}$	$b_T^{\sigma_{AC}}$	b_T^{ε}
21	LD-25-64	296	2.11	5.63	1.54
22	LD-27-65	296	2.90	0.706	0.963
23	LD-28-65	296	1.52	1.81	1.06
24	LD-29-65	296	3.93	0.904	2.70
25	LD-30-66	296	2.56	1.45	2.89
26	LD-31	297	4.48	-	-
27	LD-32	297	10.3	-	-
28	LD-33	297	11.9	-	-
29	LD-34	297	12.3	-	-
30	LD-35	297	3.29	-	-
31	LD-36	297	5.97	-	-
32	LD-37	297	10.3	-	-
33	LD-38	297	5.78	3.04	3.00
34	LD-39	297	14.3	-	-
35	LD-40	297	4.48	4.19	7.78
36	LD-41	297	5.72	-	-
37	LD-42	297	3.48	-	-
38	LD-43	296	5.92	-	-
39	LD-44	296	7.17	-	-
40	LD-45	296	6.71	-	-
41	LD-47	296	7.10	-	-
42	LD-48	296	5.26	-	-

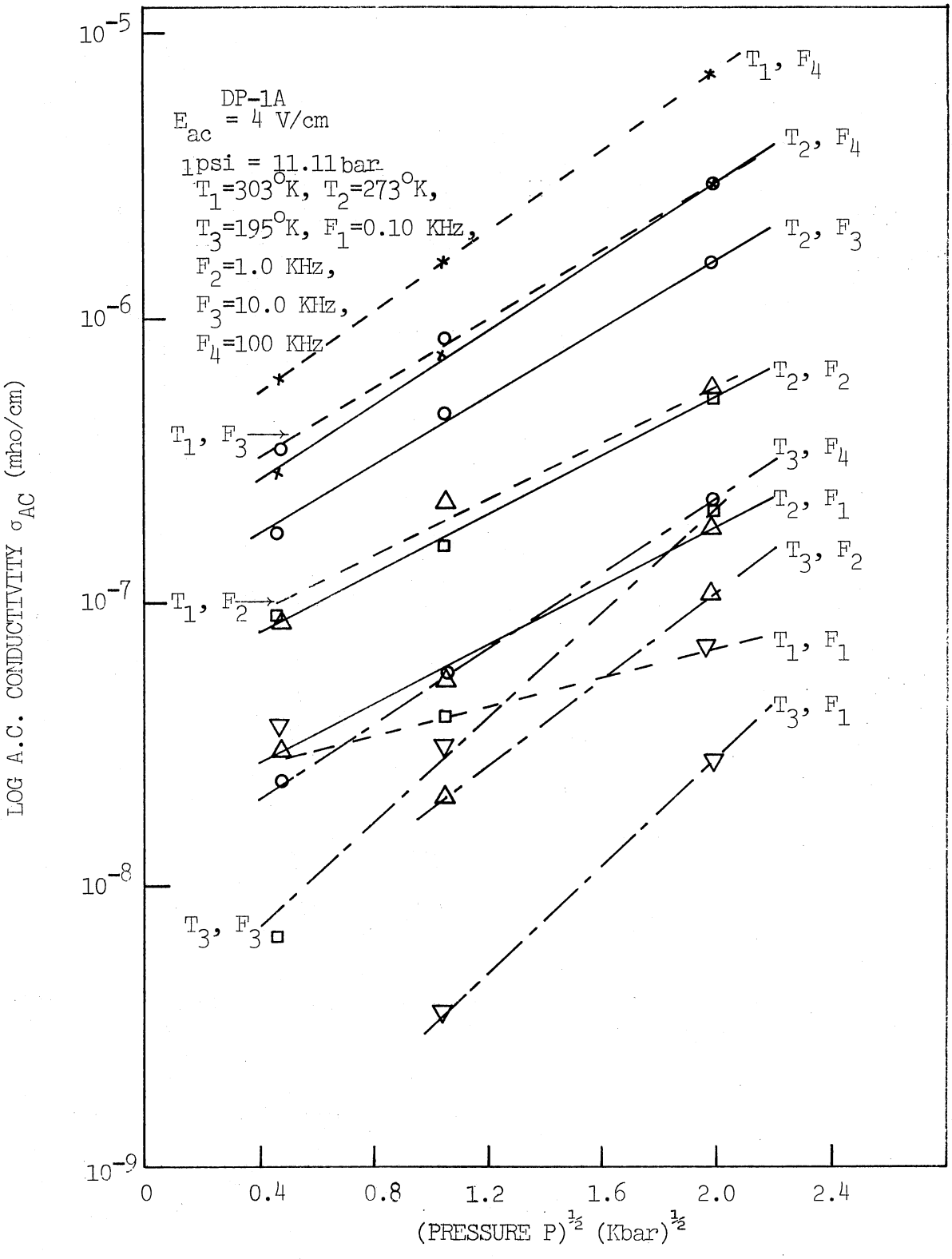

Figure 28. Log (A.C. Conductivity) Versus (Pressure)$^{\frac{1}{2}}$ (Polymer DP-1A)

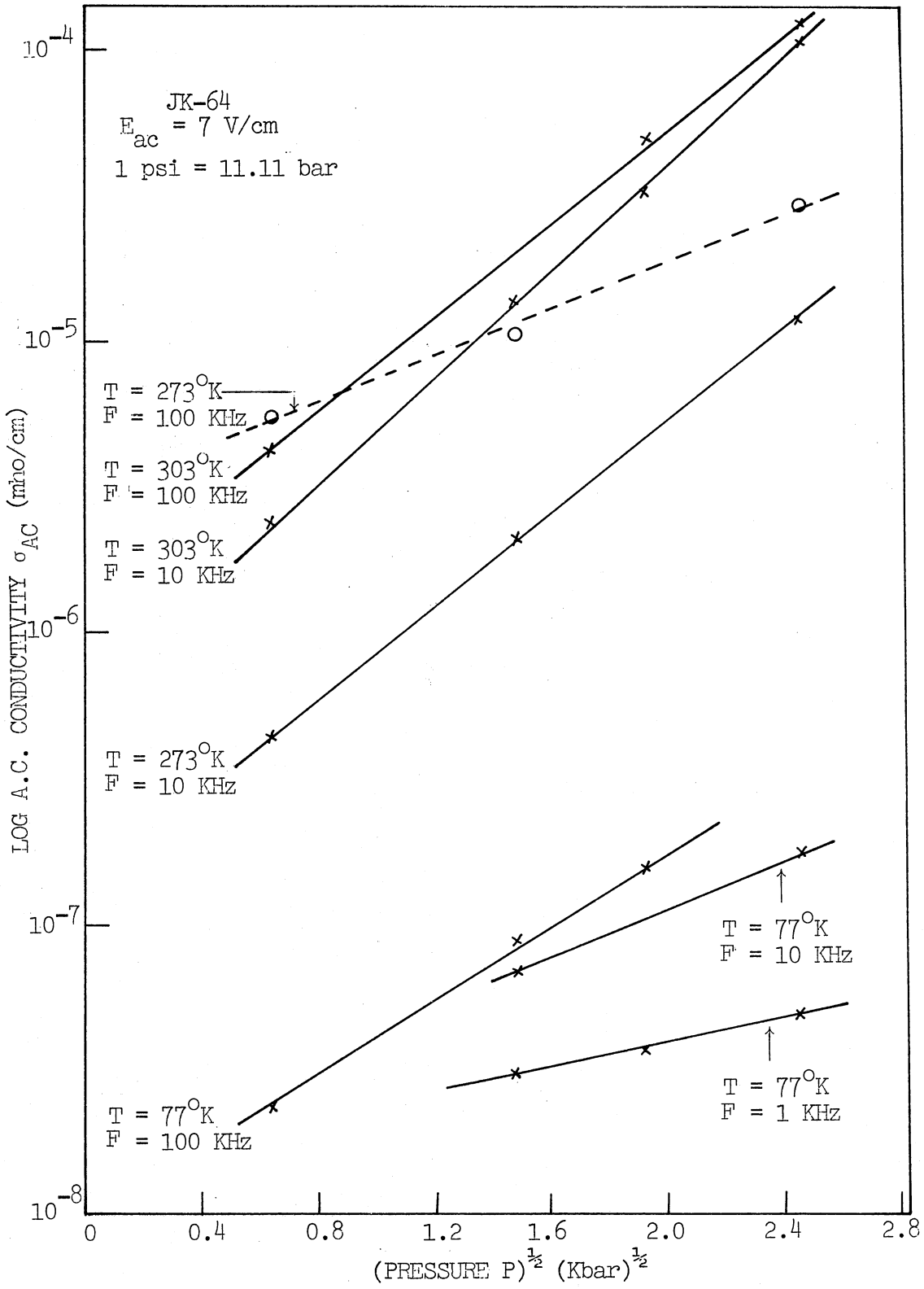

Figure 29. Log (A.C. Conductivity) Versus (Pressure)$^{\frac{1}{2}}$ (Polymer JK-64)

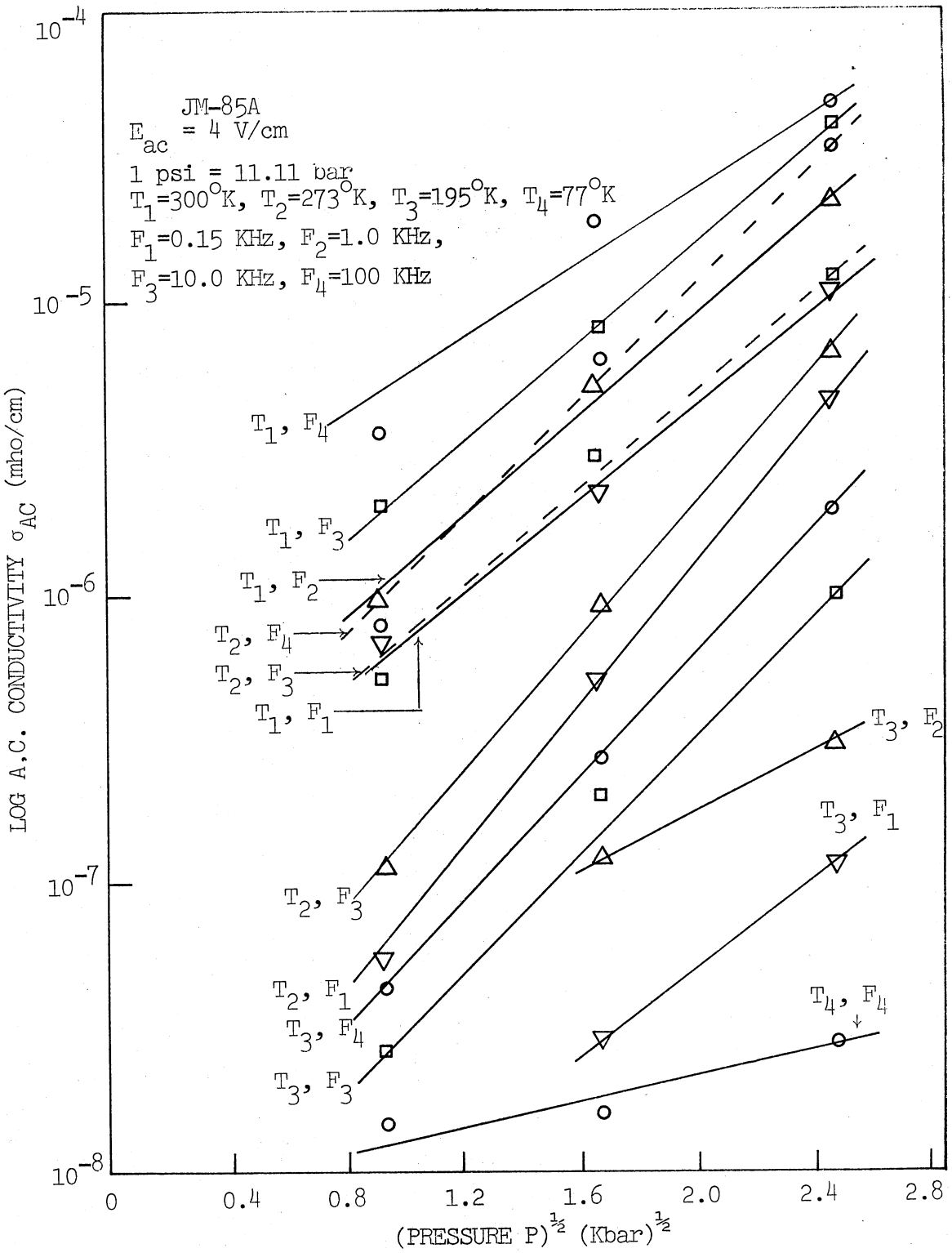

Figure 30. Log (A.C. Conductivity) Versus (Pressure)$^{\frac{1}{2}}$ (Polymer JM-85A)

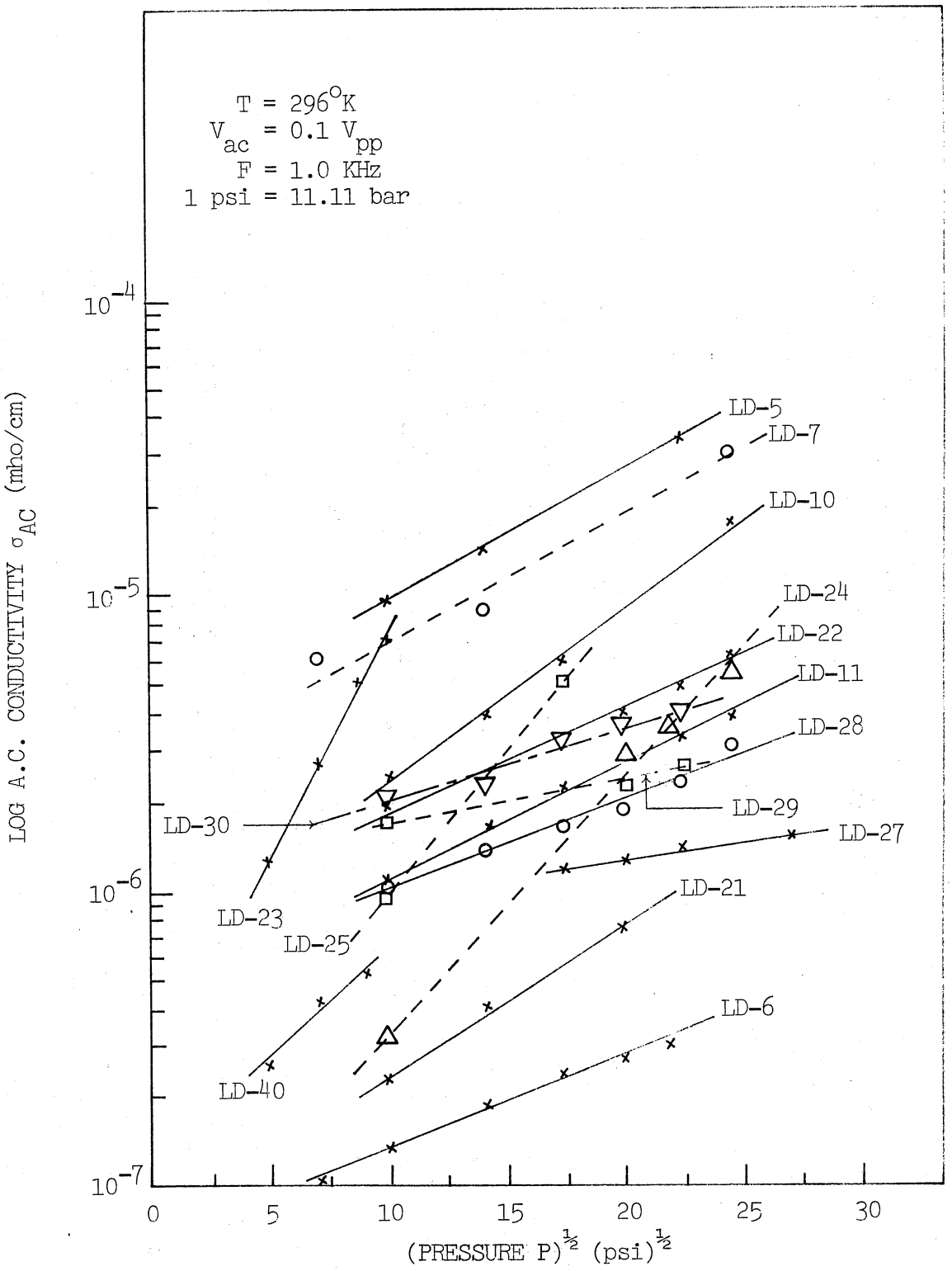

Figure 31. Log (A.C. Conductivity) Versus (Pressure)$^{\frac{1}{2}}$
(LD Series of Polymers)

LD-24, LD-25, LD-27, LD-28, LD-29, LD-30 and LD-40 for F = 1.0 KHz at T = 296°K.

Typical values of a.c. conductivities for these polymers are listed in Table III. The pressure coefficients for a.c. conductivity at room temperature are listed in Table IV. Table V lists the pressure coefficients for a.c. conductivity for polymers DP-1A, JK-64 and JM-85A for various frequencies and temperatures.

3.3. Dielectric Constant and Pressure

By analogy to the equations of conductivity and pressure effects developed by Pohl et al. (1962) {Equation (18)}, Wyhof and Pohl (1970) suggest the equation for increasing relative dielectric constant ε_r with increasing pressure P as

$$\varepsilon_r(P,T) = \varepsilon_r(0,0) \{\exp(-W_\varepsilon/kT)\} \{\exp(b_T^\varepsilon P^{\frac{1}{2}}/k)\} \quad (22)$$

where W_ε is the activation energy for the dielectric constant and b_T^ε is the pressure coefficient for the dielectric constant.

Plots of log (relative dielectric constant ε_r) versus (pressure P)$^{\frac{1}{2}}$ are shown in Figure 32 for polymer DP-1A for F = 0.10 KHz, 1.0 KHz, 10.0 KHz and 100 KHz at T = 303°K, 273°K and 195°K, in Figure 33 for polymer JK-64 for F = 10.0 KHz and 100 KHz at T = 303°K and 273°K, and for F = 0.15 KHz, 1.0 KHz, 10.0 KHz and 100 KHz at T = 77°K, in Figure 34 for polymer JM-85A for F = 0.15 KHz, 1.0 KHz, 10.0 KHz and 100 KHz at T = 300°K, 273°K, 195°K and 77°K, in Figure 35 for polymers LD-2, LD-3, LD-5, LD-6, LD-7, LD-10, LD-11 and LD-21 for F = 1.0 KHz at T = 296°K, in Figure 36 for polymers LD-22, LD-24, LD-25, LD-28, LD-29, LD-30 and LD-38 for F = 1.0 KHz at T = 296°K.

Typical values of relative dielectric constant for these polymers

TABLE V

PRESSURE COEFFICIENTS OF SELECTED POLYMERS
FOR A.C. CONDUCTIVITY

Sample Name	Frequency (KHz)	$b_T^{\sigma_{AC}} \times 10^{-6}$ $\frac{eV}{(bar)^{\frac{1}{2}}\ ^oK}$			
		T=303°K	T=273°K	T=195°K	T=77°K
DP-1A	0.10	2.94	7.22	5.96	-
	1.0	2.45	3.47	4.77	0.720
	10.0	3.65	3.59	5.02	0.250
	100	4.35	3.93	4.27	1.87
JK-64	0.15	-	-	-	-
	1.0	-	-	-	1.29
	10.0	5.87	5.10	-	2.67
	100	5.10	2.62	-	3.92
JM-85A	0.15	5.00	7.65	5.13	3.39
	1.0	5.22	7.18	3.08	4.82
	10.0	5.26	4.72	6.30	1.61
	100	3.94	6.79	6.68	1.29

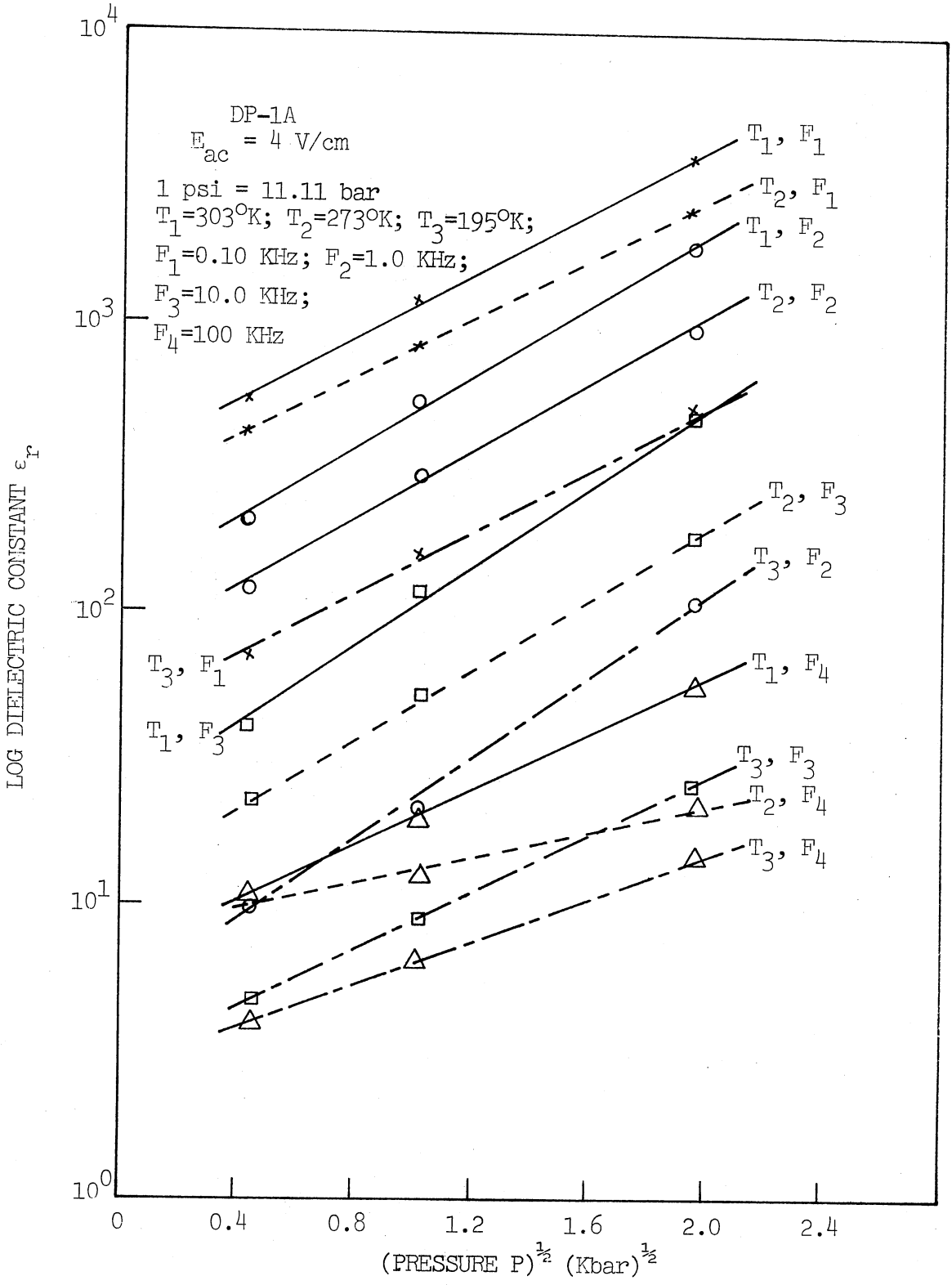

Figure 32. Log (Dielectric Constant) Versus (Pressure)$^{\frac{1}{2}}$ (Polymer DP-1A)

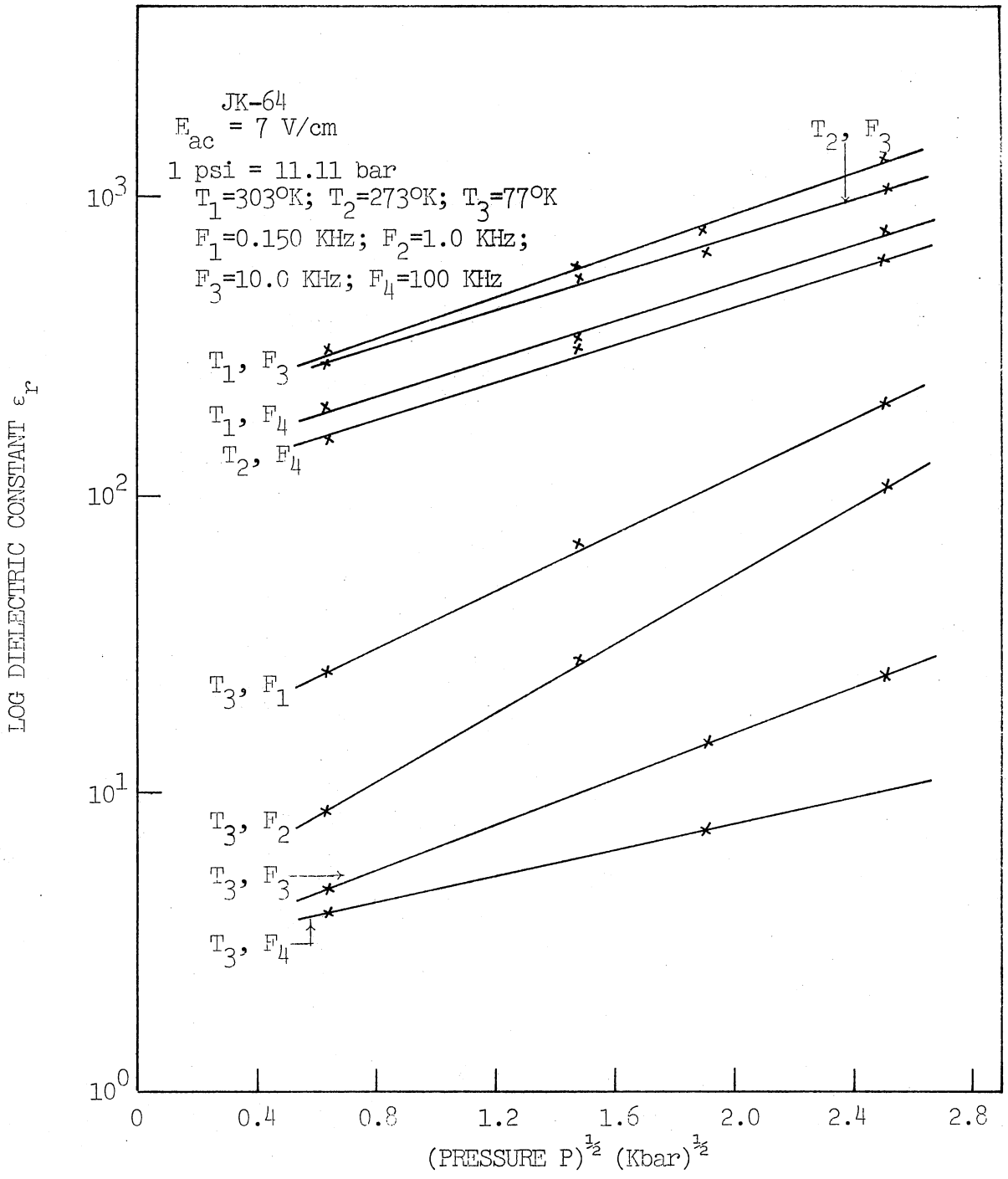

Figure 33. Log (Dielectric Constant) Versus (Pressure)$^{\frac{1}{2}}$ (Polymer JK-64)

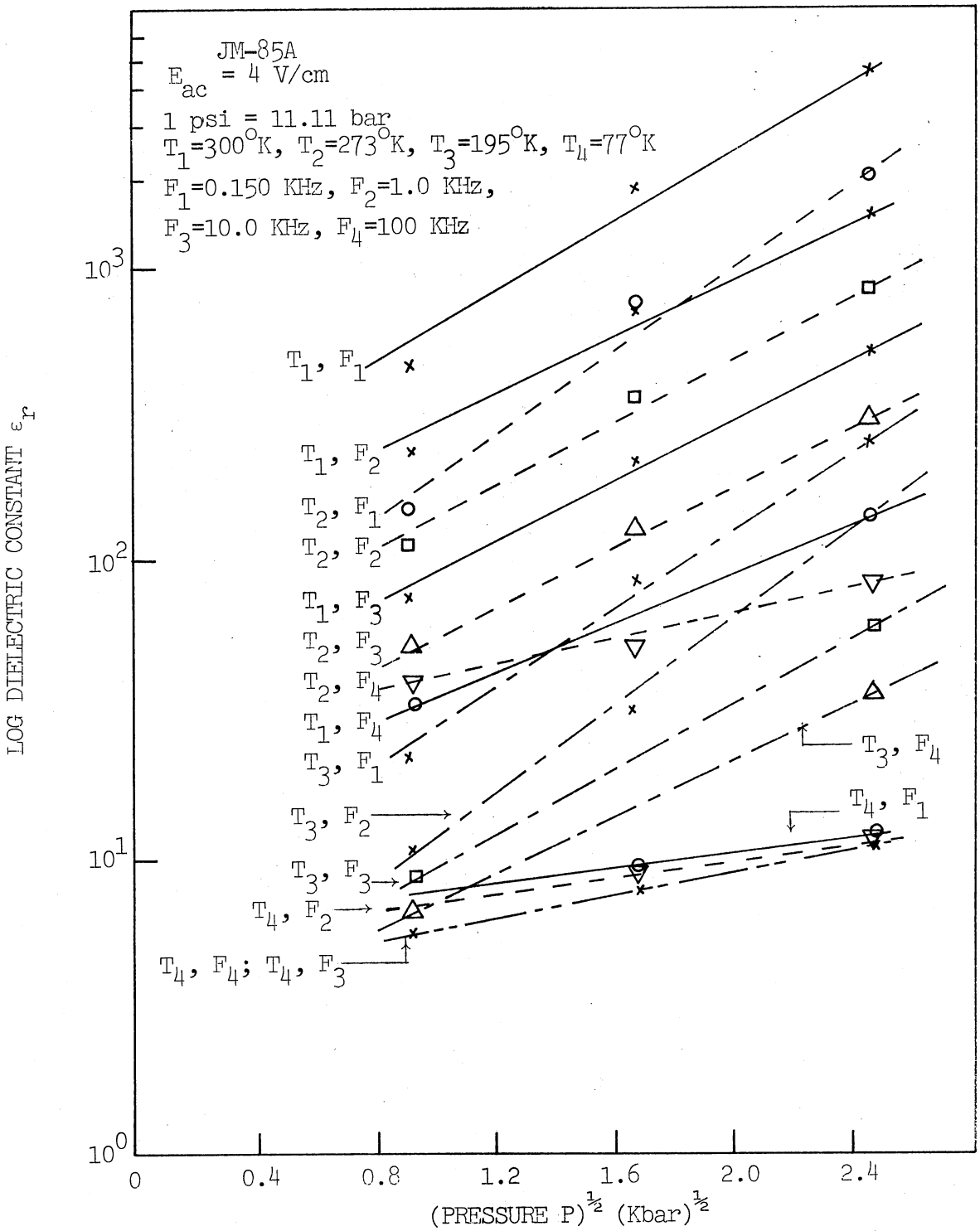

Figure 34. Log (Dielectric Constant) Versus (Pressure)$^{\frac{1}{2}}$ (Polymer JM-85A)

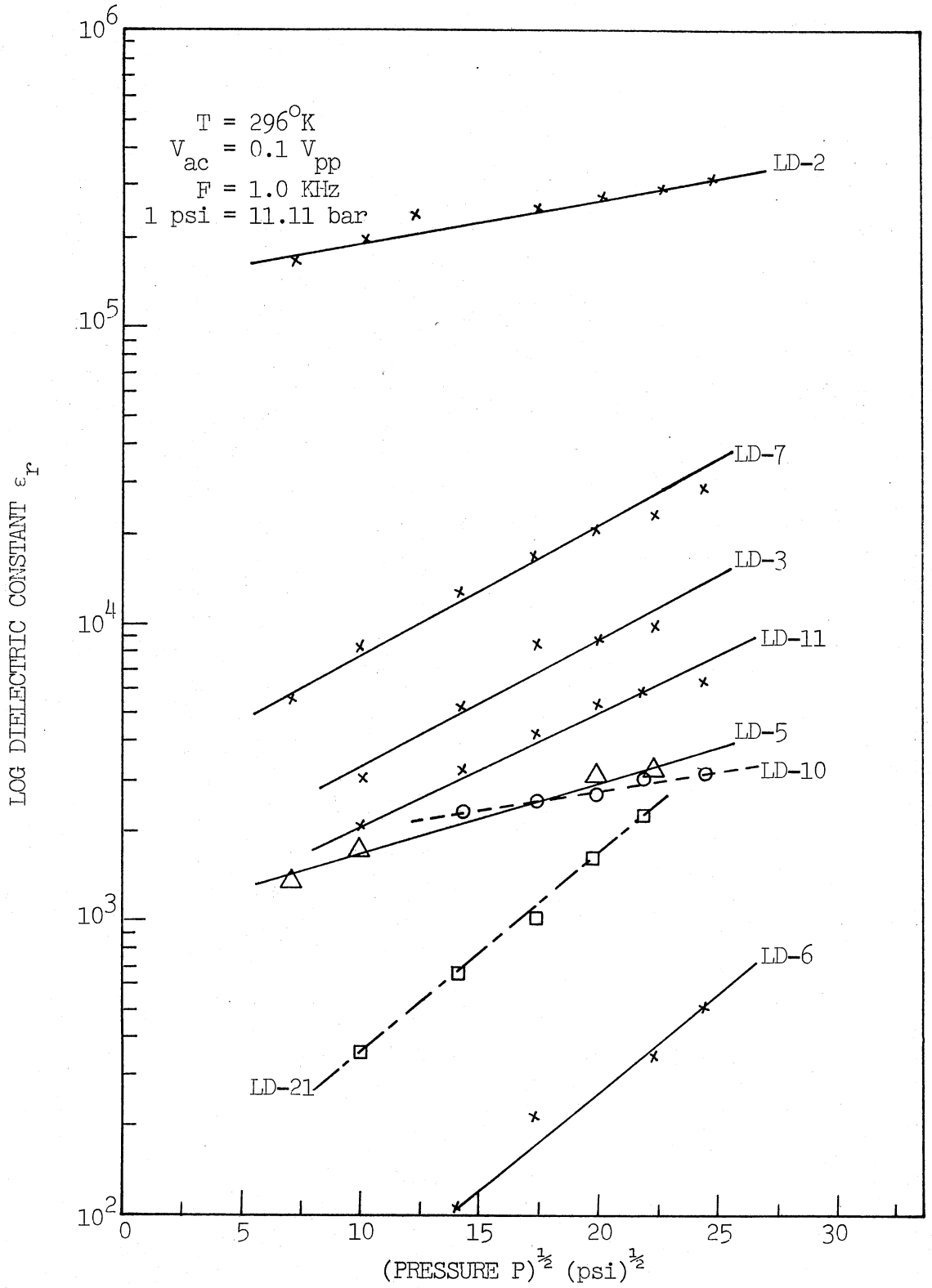

Figure 35. Log (Dielectric Constant) Versus (Pressure)$^{\frac{1}{2}}$
(LD Series of Polymers - Batch I)

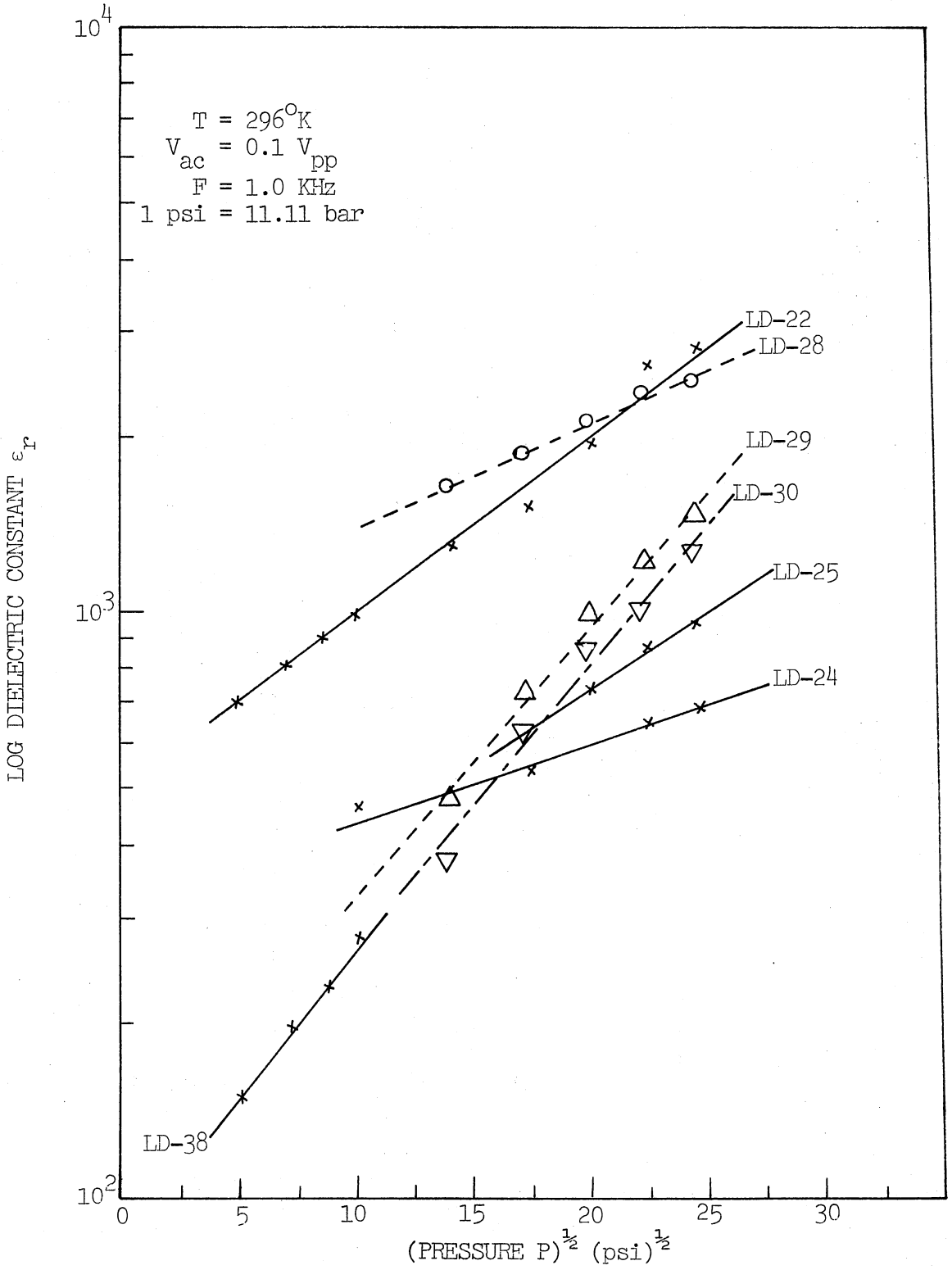

Figure 36. Log (Dielectric Constant) Versus (Pressure)$^{\frac{1}{2}}$ (LD Series of Polymers - Batch II)

are listed in Table III. The pressure coefficients for dielectric constant at room temperature are listed in Table IV. Table VI lists the pressure coefficients for dielectric constant for polymers DP-1A, JK-64 and JM-85A for various frequencies and temperatures.

3.4. D.C. Conductivity and Temperature

In general conductivity depends on the concentration of charge carriers n, their charge e and their mobility by the equation $\sigma = ne\mu$. Assuming that the concentration of carriers (electrons), and hence the semiconductivity increases with increasing temperature according to a Boltzmann type distribution with activation energy E_a

$$\sigma_{DC} = ne\mu(T) \{\exp(-E_a/kT)\} = \sigma_o(T) \{\exp(-E_a/kT)\} \qquad (23)$$

Plots of log (d.c. conductivity σ_{DC}) versus (temperature T)$^{-1}$ are shown in Figure 37 for polymer DP-1A at pressures P = 0.46 Kbar, 1.1 Kbar, 3.9 Kbar and 8.0 Kbar for temperatures ranging from T = 77^{o}K to 300^{o}K, in Figure 38 for polymer DP-1A at 'zero' pressure P = 0 for temperatures ranging from T = 300^{o}K to 350^{o}K, for polymer JK-64 in Figure 39 at P = 0.41 Kbar, 2.2 Kbar, 3.7 Kbar and 6.0 Kbar, and in Figure 40 at P = 0 for temperatures ranging from T = 77^{o}K to 300^{o}K, and in Figure 41 at P = 0 for temperatures ranging from 300^{o}K to 350^{o}K, and in Figure 42 for polymer JM-85A at P = 0.86 Kbar, 2.8 Kbar and 6.1 Kbar for temperatures ranging from T = 77^{o}K to 300^{o}K. The d.c. activation energies for these polymers are listed in Table VII. Figure 43 shows the plots of d.c. activation energy E_a versus (pressure P)$^{\frac{1}{2}}$ as given by Equation (19) in Section 3.1. for polymers DP-1A and JK-64.

It was shown by Mott (1969a and 1972) that the d.c. conductivity

TABLE VI

PRESSURE COEFFICIENTS OF SELECTED POLYMERS
FOR DIELECTRIC CONSTANT

Sample Name	Frequency (KHz)	$b_T^{\varepsilon} \times 10^{-6}$ $\frac{eV}{(bar)^{\frac{1}{2}}\ ^oK}$			
		T=303°K	T=273°K	T=195°K	T=77°K
DP-1A	0.10	2.44	3.04	3.28	1.17
	1.0	3.65	3.63	4.25	2.40
	10.0	4.07	3.63	3.06	2.57
	100	2.84	0.92	2.39	2.67
JK-64	0.15	-	-	-	2.94
	1.0	-	-	-	3.61
	10.0	2.08	1.94	-	2.38
	100	1.88	1.99	-	1.81
JM-85A	0.15	4.13	4.48	4.03	0.81
	1.0	3.05	3.31	3.94	0.90
	10.0	3.18	3.12	3.34	1.22
	100	2.42	1.35	2.96	1.22

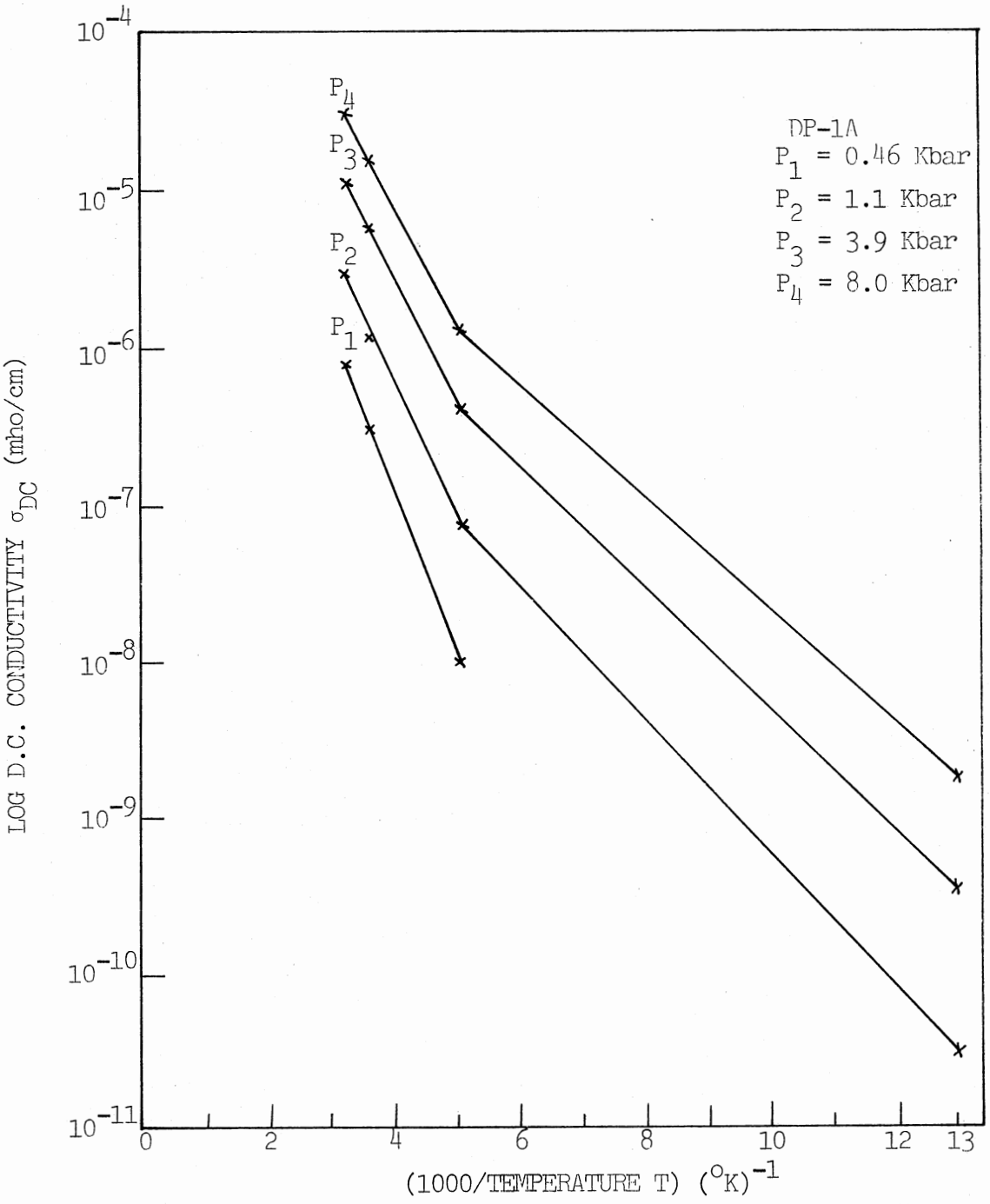

Figure 37. Log (D.C. Conductivity) Versus (1000/Temperature) (Polymer DP-1A)

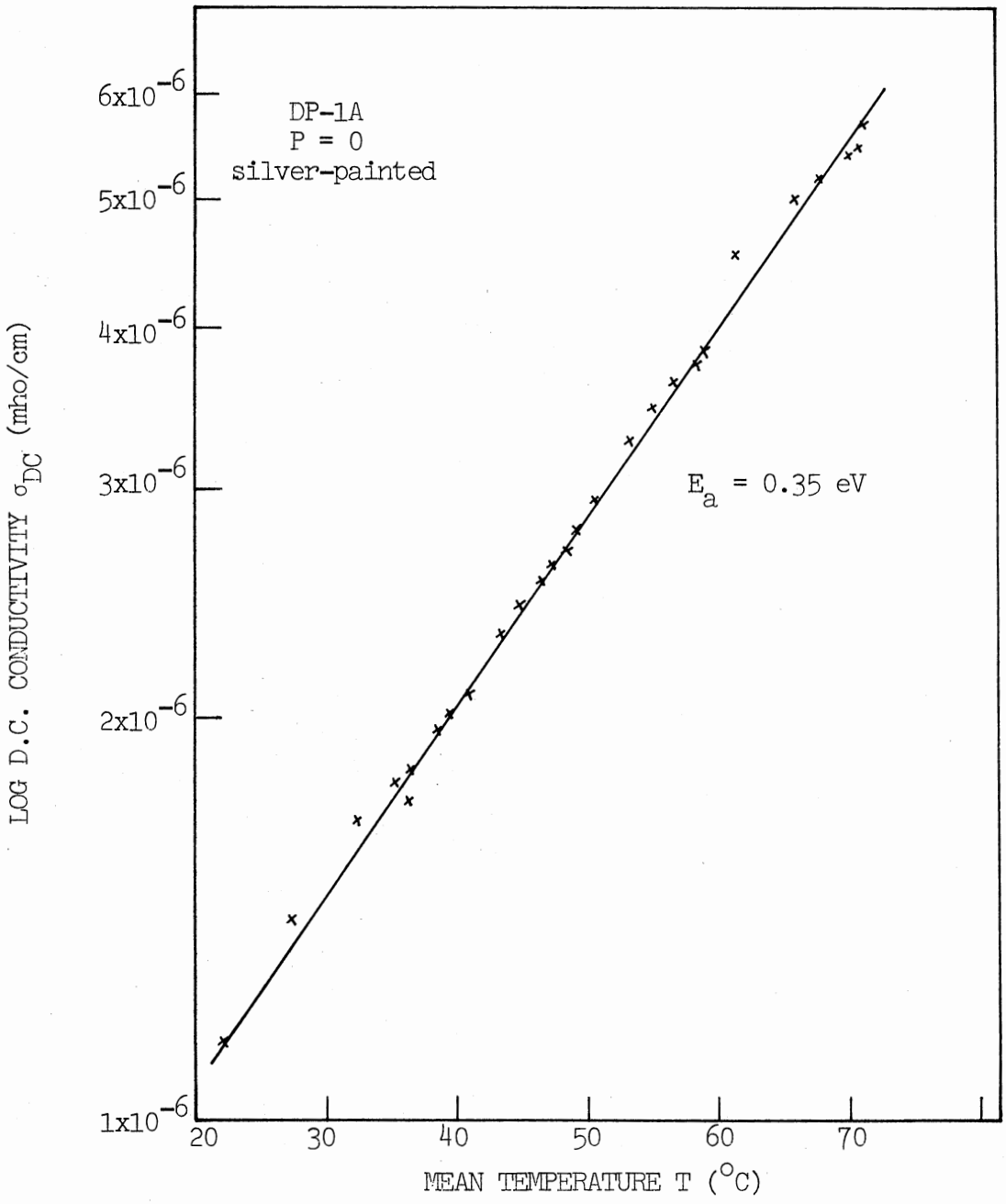

Figure 38. Log (D.C. Conductivity) Versus Mean Temperature (Polymer DP-1A)

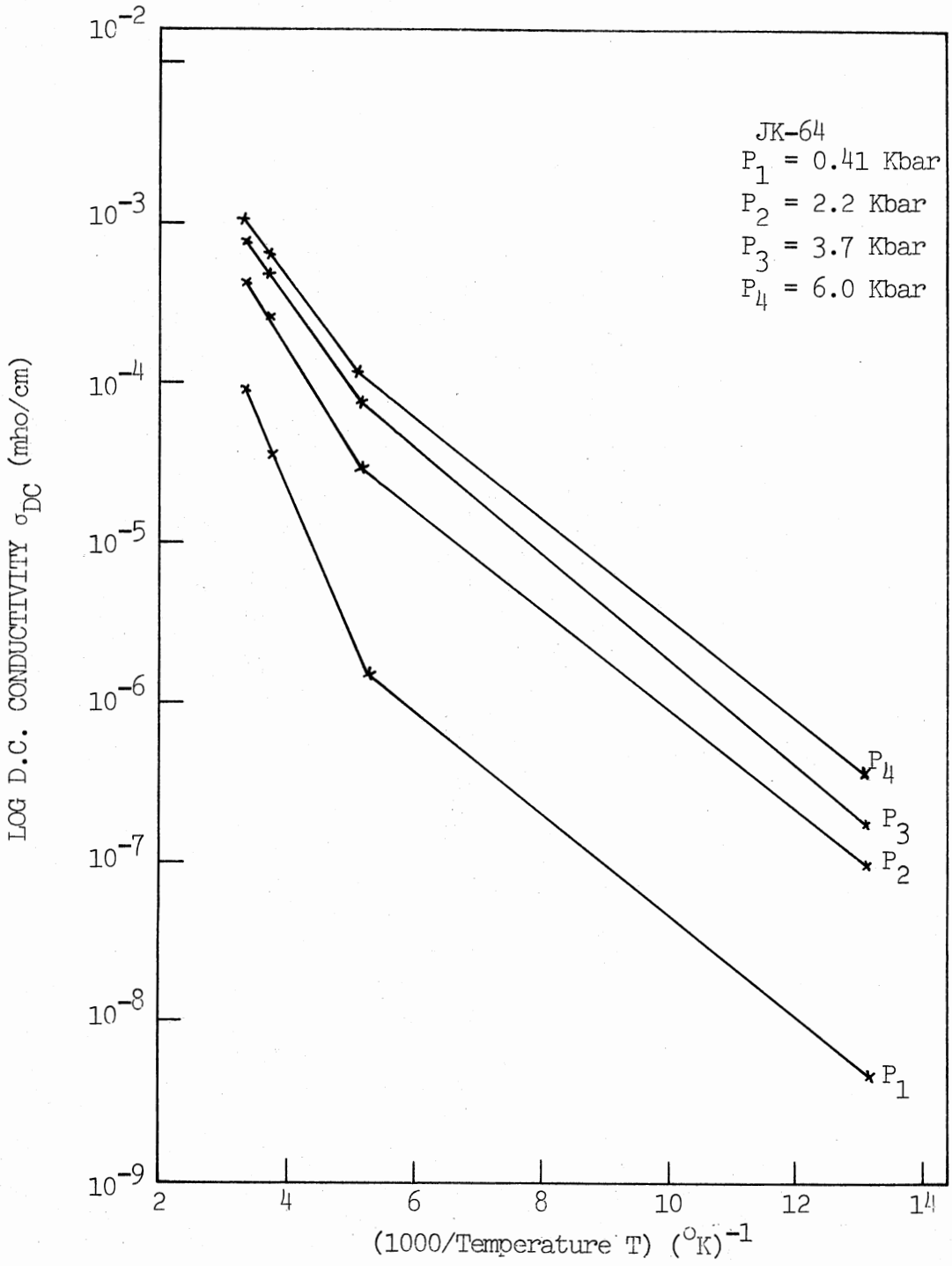

Figure 39. Log (D.C. Conductivity) Versus (1000/Temperature) (Polymer JK-64)

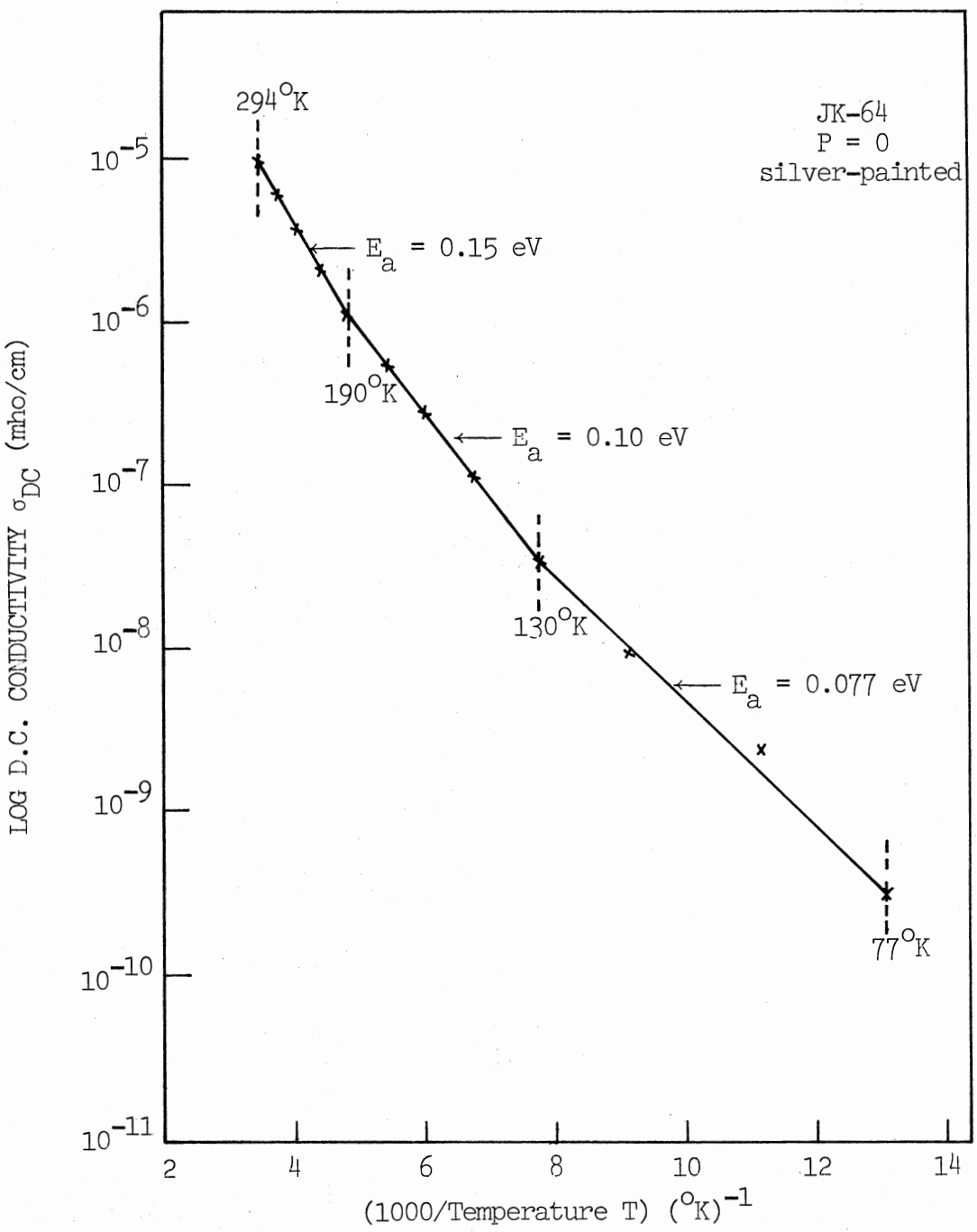

Figure 40. Log (D.C. Conductivity) Versus (1000/Temperature) (Polymer JK-64 at Pressure P=0)

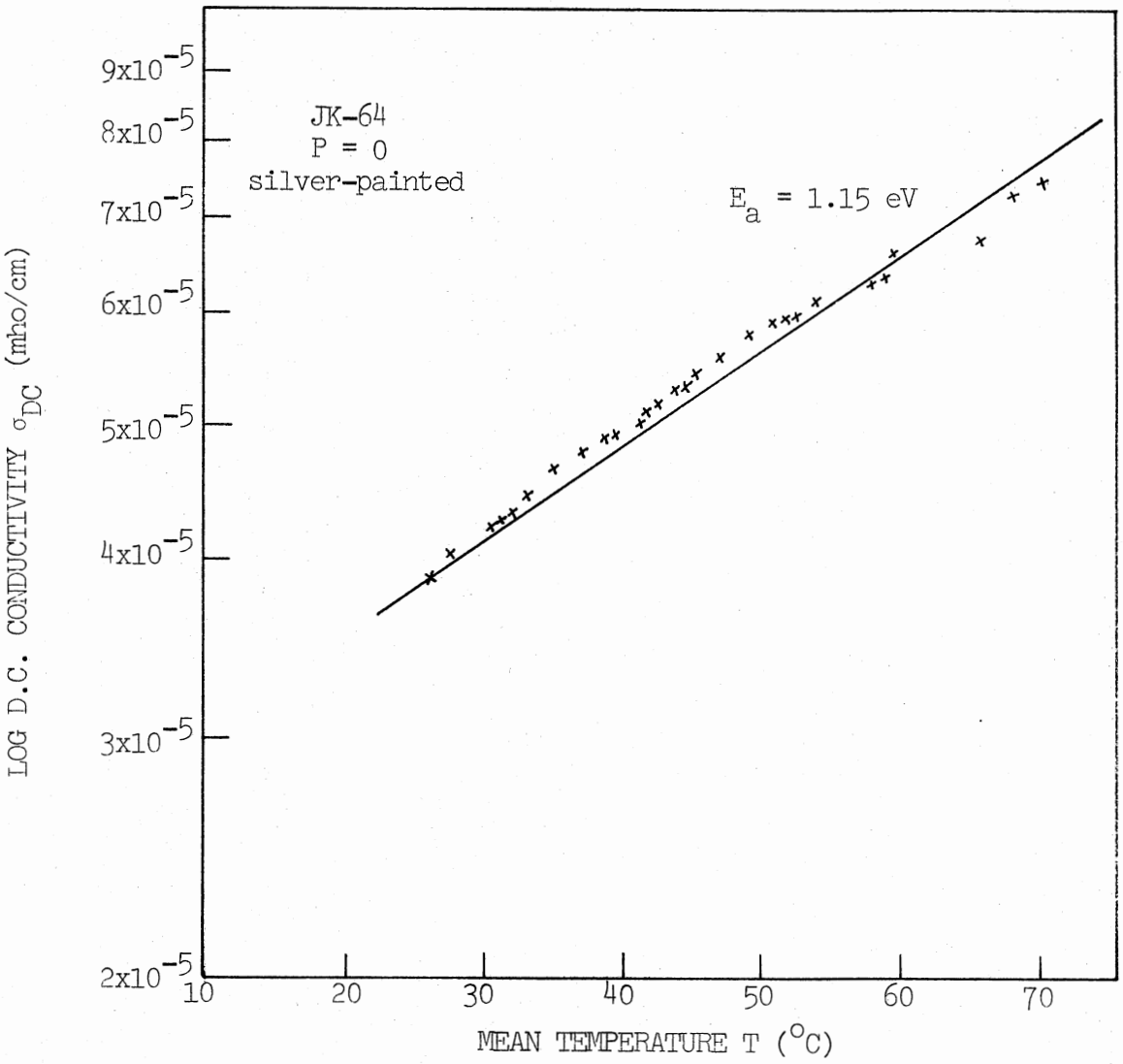

Figure 41. Log (D.C. Conductivity) Versus Mean Temperature (Polymer JK-64)

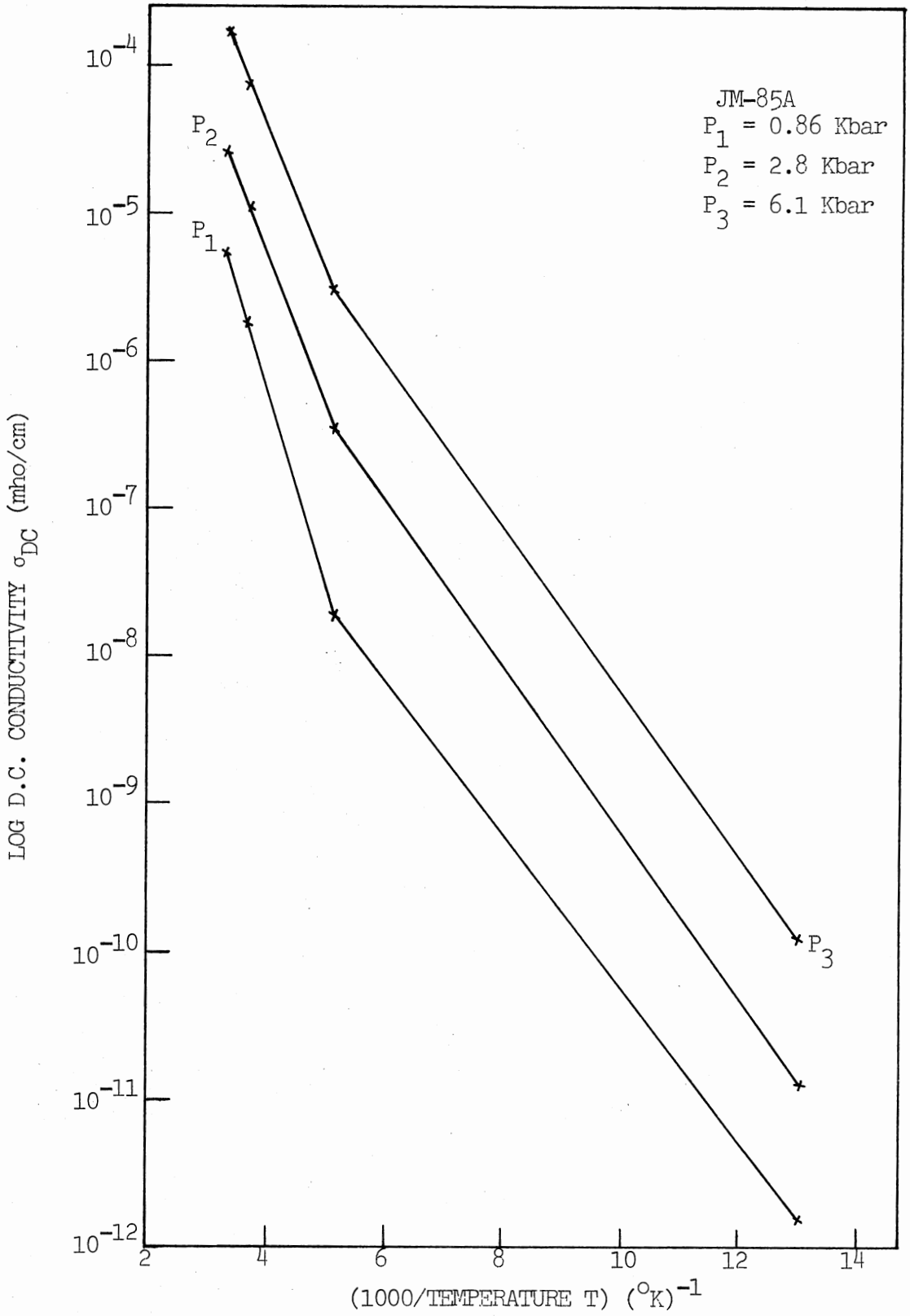

Figure 42. Log (D.C. Conductivity) Versus (1000/Temperature) (Polymer JM-85A)

TABLE VII

ACTIVATION ENERGIES OF SELECTED POLYMERS

Sample Name	Pressure (Kbar)	Temperature Range (^{o}K)	Activation Energy E_a (eV)							
			From $\sigma_{DC} \propto e^{-Ea/kT}$	From $\sigma_{AC} \propto e^{-Ea/kT}$			From $\sigma_{AC} \propto e^{-Ea/kT}$			
				f=0.10 KHz	f=1.0 KHz	f=10.0 KHz	f=100 KHz	f=0.10 KHz	f=1.0 KHz	f=10.0 KHz	f=100 KHz
DP-1A	0.0	300-350	0.35	-	-	-	-	-	-	-	-
	0.46	200-300	0.21	0.055	0.14	0.14	-	0.052	-	0.16	0.18
		77-200	-	-	-	-	-	0.091	-	-	-
	1.1	200-300	0.18	0.089	0.14	0.19	0.11	0.13	0.11	0.15	0.18
		77-200	0.11	0.036	0.020	0.015	0.011	0.053	-	-	-
	3.9	200-300	0.16	0.10	0.16	0.23	0.21	0.10	0.023	0.15	0.21
		77-200	0.10	0.047	0.032	0.015	0.0011	0.077	0.065	0.067	0.034
	8.0	200-300	0.15	0.054	0.098	0.013	0.12	0.55	0.16	0.10	0.12
		77-200	0.097	0.54	0.046	0.026	0.011	0.060	0.072	0.075	0.05
JK-64	0.0	200-350	0.15	0.11	0.048	0.040	0.096	0.0086	0.027	0.095	0.072
		100-200	0.10	0.011	0.066	0.072	0.045	0.085	0.088	0.078	0.0060
		77-100	0.077	0.031	0.021	0.021	0.018	0.038	0.029	0.013	0.072
	0.41	200-300	0.15	-	-	0.43	0.065	-	-	0.046	0.034
		77-200	0.076	-	0.040	0.038	0.051	-	0.034	0.038	0.023

TABLE VII (Continued)

Sample Name	Pressure (Kbar)	Temperature Range (°K)	Activation Energy E_a (eV)							
			From $\sigma_{DC} \propto e^{-Ea/kT}$	From $\sigma_{AC} \propto e^{-Ea/kT}$			From $\sigma_{AC} \propto e^{-Ea/kT}$			
				f=0.10 KHz	f=1.0 KHz	f=10.0 KHz	f=100 KHz	f=0.10 KHz	f=1.0 KHz	f=10.0 KHz	f=100 KHz
JK-64	2.2	200-300	0.11	-	-	0.037	0.067	-	-	0.0094	0.024
		77-200	0.069	-	-	0.031	0.045	-	-	0.028	0.042
	3.7	200-300	0.11	-	-	0.31	0.095	-	-	0.033	0.035
		77-200	0.069	-	0.053	0.045	0.050	-	0.032	0.043	0.059
	6.0	200-300	0.099	-	-	0.053	0.059	-	-	0.053	-
		77-200	0.064	-	-	0.051	-	-	-	0.035	-
JM-85A	0.86	200-300	0.28	-	0.29	0.25	0.21	0.14	0.14	0.10	0.091
		77-200	0.10	-	0.042	0.022	0.012	0.11	0.0052	0.0046	0.0017
	2.8	200-300	0.21	0.21	0.12	0.12	0.11	0.11	0.10	0.077	0.013
		77-200	0.11	0.070	0.062	0.056	0.037	0.032	0.024	0.017	0.013
	6.1	200-300	0.20	0.22	0.21	0.18	0.16	0.14	0.11	0.10	0.165
		77-200	0.11	0.070	0.067	0.061	0.046	0.033	0.027	0.018	0.013

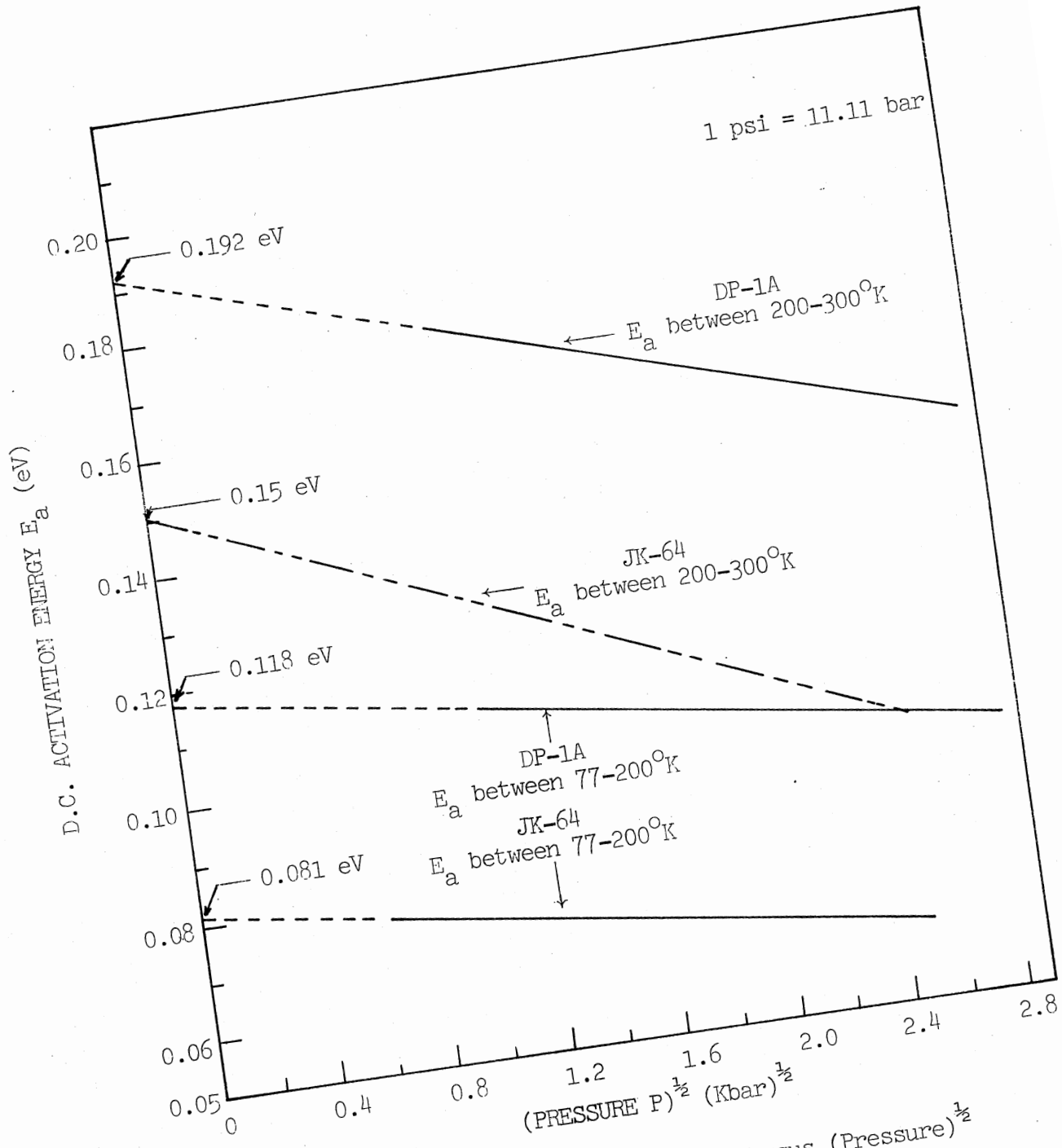

Figure 43. D.C. Activation Energy Versus (Pressure)$^{\frac{1}{2}}$ (Polymers DP-1A and JK-64)

of amorphous solids due to a 'variable range hopping' process is given by

$$\sigma_{DC} = \sigma_o \exp \{-(T_o/T)^{\frac{1}{4}}\} \qquad (24)$$

where $T_o = (16\alpha^3/kN)$; $\sigma_o \simeq \{N/(2\pi\alpha kT)\}^{\frac{1}{2}}(3e^2\nu\Phi_o/2)$; α = coefficient of decaying wave function $\{\exp(-\alpha r)\}$ of a localized state near the Fermi energy level; N = density of states per unit volume per energy interval; ν = phonon frequency; $\Phi_o \simeq 1$; $\alpha^{-1} \simeq 10$ A^o and hence $\alpha = 10^7$ cm^{-1}. Therefore, the slope of log $(\sigma_{DC}T^{\frac{1}{2}})$ versus $T^{-\frac{1}{4}}$ is $T_o^{\frac{1}{4}}$, from which the density of states N can be calculated.

Plots of log $(\sigma_{DC}T^{\frac{1}{2}})$ versus $T^{-\frac{1}{4}}$ are shown in Figure 44 for polymer DP-1A at pressures P = 0.46 Kbar, 1.1 Kbar, 3.9 Kbar and 8.0 Kbar for temperatures ranging from T = 77^{o}K to 300^{o}K, in Figure 45 for polymer JK-64 at 'zero' pressure P = 0 for temperatures ranging from T = 77^{o}K to 300^{o}K, in Figure 46 for polymer JK-64 at P = 0.41 Kbar, 2.2 Kbar, 3.7 Kbar and 6.0 Kbar for temperatures ranging from T = 77^{o}K to 300^{o}K, and in Figure 47 for polymer JM-85A at P = 0.86 Kbar, 2.8 Kbar and 6.1 Kbar for temperatures ranging from T = 77^{o}K to 300^{o}K. The density of states for these three polymers at various pressures are listed in Table VIII.

3.5. A.C. Conductivity and Temperature

By analogy to the relation between d.c. conductivity and temperature {Equation (23) in Section 3.4.}, the equation for increasing a.c. conductivity σ_{AC} with increasing temperature T is of the form

$$\sigma_{AC} = \sigma_o \{\exp(-E_a/kT)\} \qquad (25)$$

Plots of log (a.c. conductivity σ_{AC}) versus (temperature T)$^{-1}$ are shown in Figure 48 for polymer DP-1A for frequencies F = 0.10 KHz, 1.0 KHz, 10.0 KHz and 100 KHz at P = 3.9 Kbar and 8.0 Kbar, in Figure 49 for

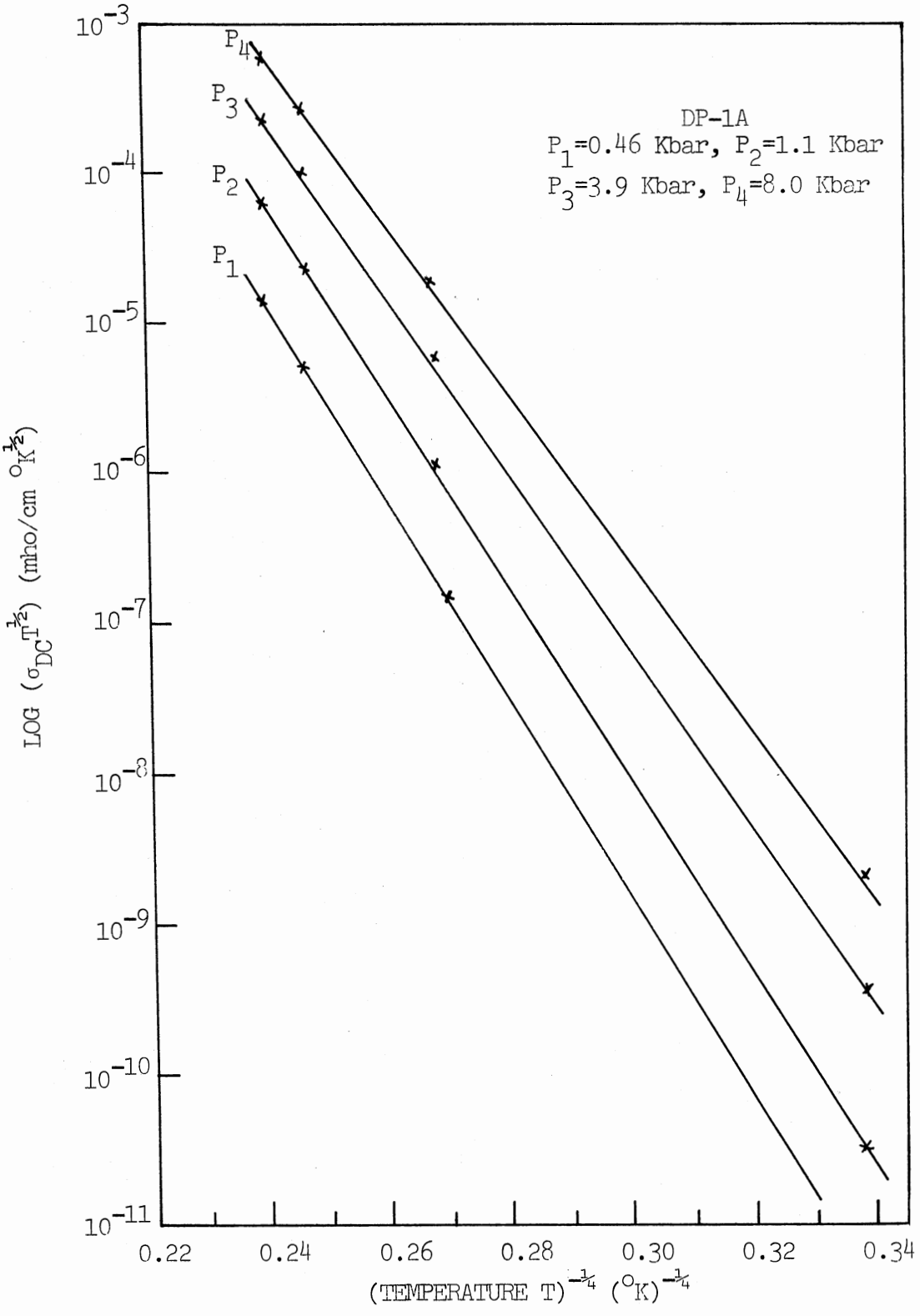

Figure 44. Log ($\sigma_{DC}T^{\frac{1}{2}}$) Versus $T^{-\frac{1}{4}}$ (Polymer DP-1A)

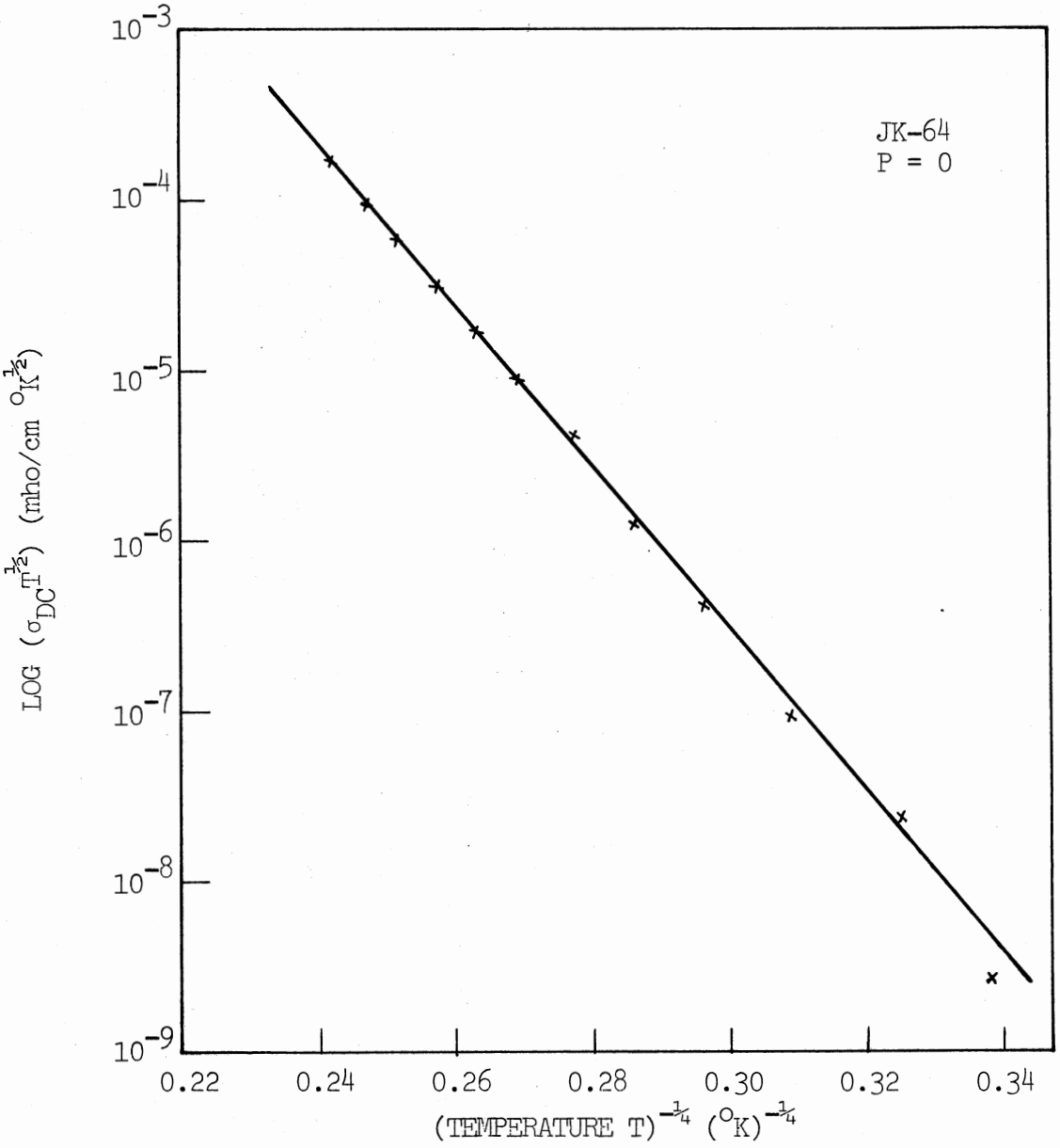

Figure 45. Log ($\sigma_{DC}T^{\frac{1}{2}}$) Versus $T^{-\frac{1}{4}}$
(Polymer JK-64 at P=0)

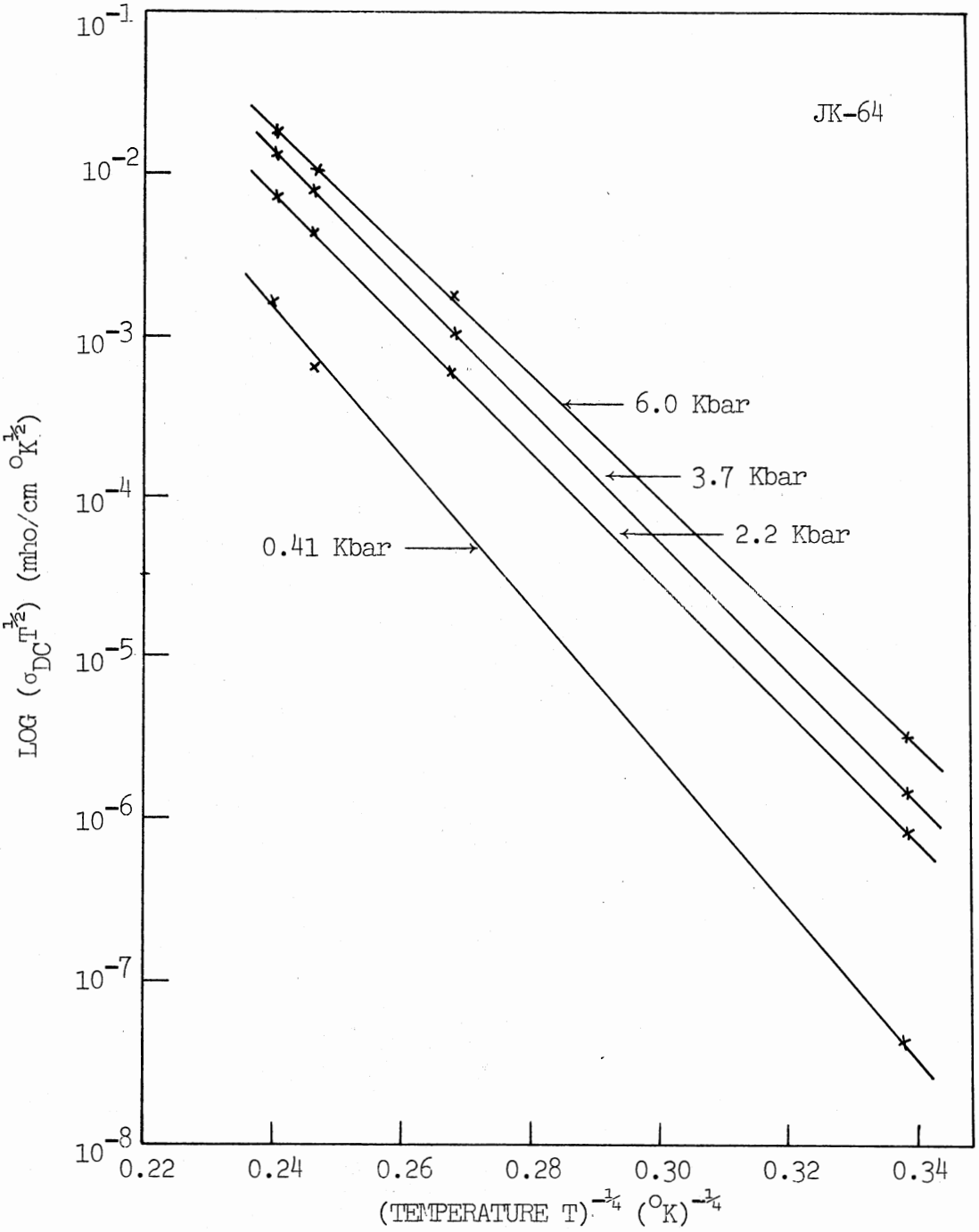

Figure 46. Log ($\sigma_{DC}T^{1/2}$) Versus $T^{-1/4}$
(Polymer JK-64)

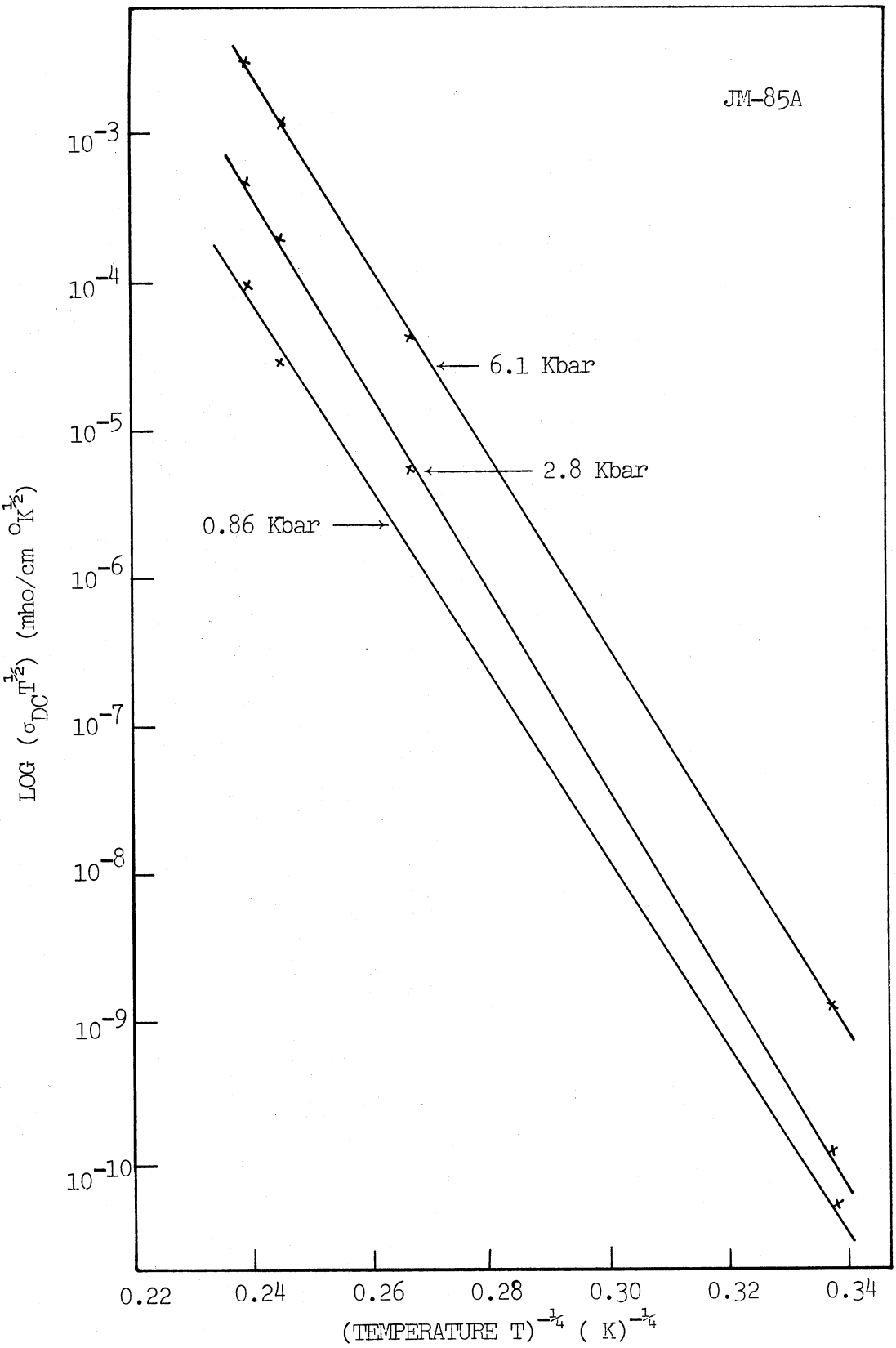

Figure 47. Log ($\sigma_{DC}T^{\frac{1}{2}}$) Versus $T^{-\frac{1}{4}}$ (Polymer JM-85A)

TABLE VIII

DENSITY OF STATES OF SELECTED POLYMERS

Sample Name	Pressure (Kbar)	$(T_o)^{\frac{1}{4}}$ $(^oK)^{\frac{1}{4}}$, the Slope from Log $(\sigma_{DC}T^{\frac{1}{2}})$ Versus $(T)^{-\frac{1}{4}}$ Plot	T_o (^oK)	Density of States N $(eV^{-1}\ cm^{-3})$
DP-1A	0.46	163	7.02×10^8	2.61×10^{17}
	1.1	146	4.58×10^8	4.00×10^{17}
	3.9	136	3.43×10^8	5.35×10^{17}
	8.0	129	2.77×10^8	6.63×10^{17}
JK-64	0.0	111	1.52×10^8	1.21×10^{18}
	0.41	109	1.41×10^8	1.30×10^{18}
	2.2	97.7	9.11×10^7	2.01×10^{18}
	3.7	92.1	7.20×10^7	2.55×10^{18}
	6.0	87.3	5.81×10^7	3.16×10^{18}
JM-85A	0.86	161	6.70×10^8	2.74×10^{17}
	2.8	156	5.94×10^8	3.09×10^{17}
	6.1	152	5.30×10^8	3.46×10^{17}

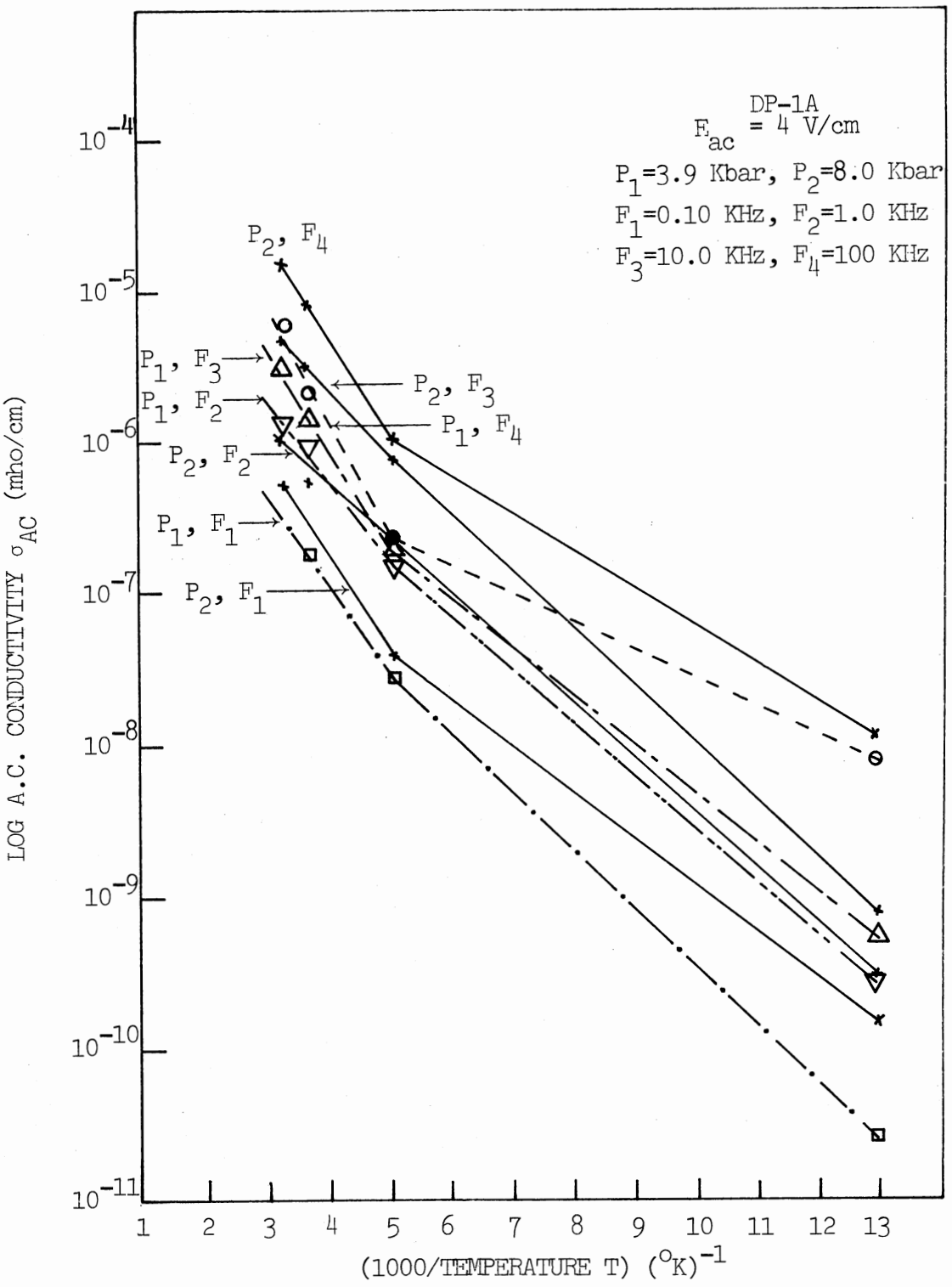

Figure 48. Log (A.C. Conductivity) Versus (1000/Temperature) (Polymer DP-1A at P=3.9 Kbar and 8.0 Kbar)

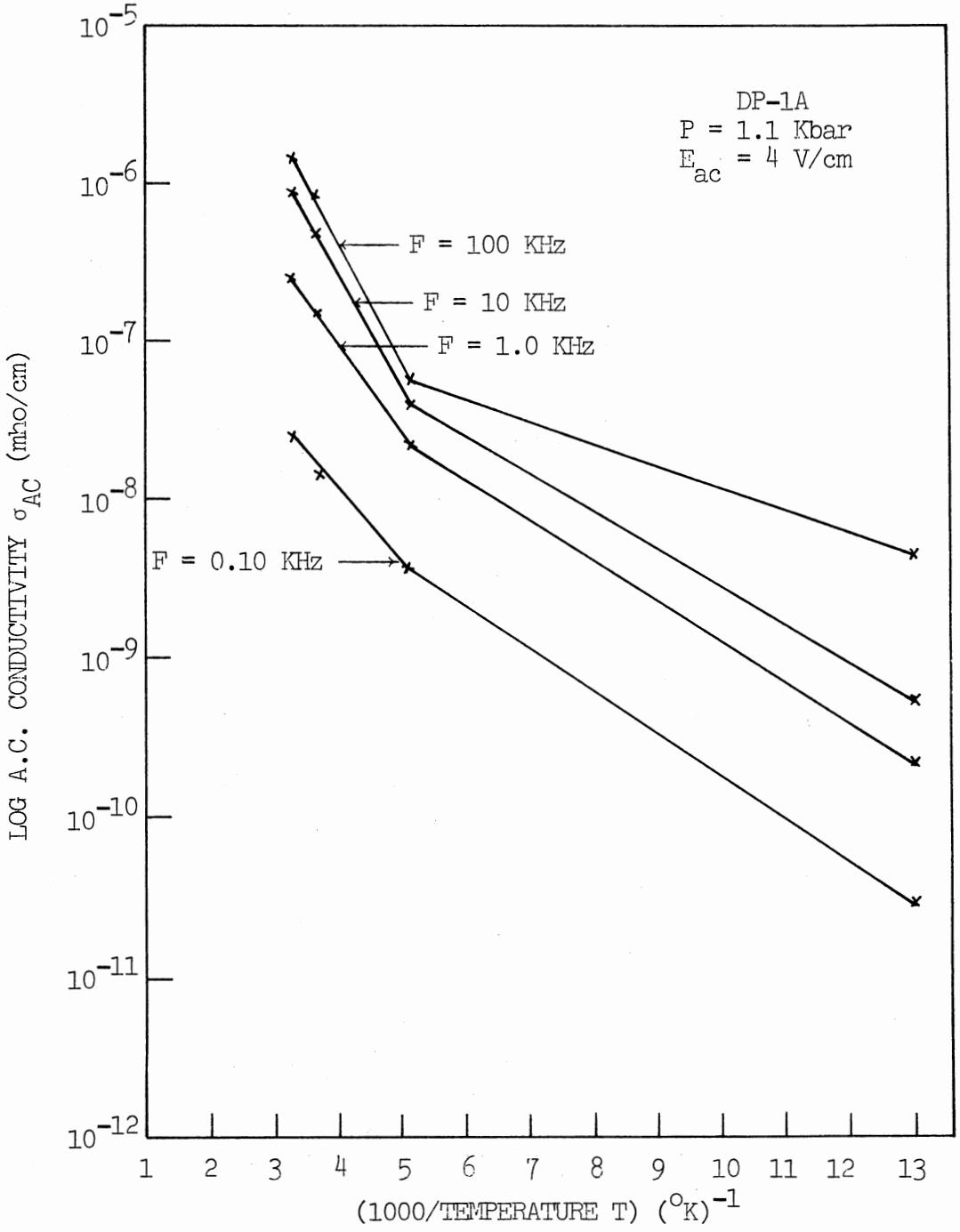

Figure 49. Log (A.C. Conductivity) Versus (1000/Temperature)
(Polymer DP-1A at P=1.1 Kbar)

polymer DP-1A for F = 0.10 KHz, 1.0 KHz, 10.0 KHz and 100 KHz at P = 1.1 Kbar, and in Figure 50 for polymer JK-64 for F = 0.03 KHz, 0.10 KHz, 0.60 KHz, 1.0 KHz, 10.0 KHz, 30.0 KHz, 60.0 KHz, 100 KHz and 150 KHz at 'ambient' pressure P = 0 for temperatures ranging from T = 77°K to 300°K. The a.c. activation energy E_a as given by Equation (25) for these polymers are listed in Table VII.

3.6. Dielectric Constant and Temperature

From Equation (22) in Section 3.3., the relative dielectric constant ε_r increases exponentionally with increasing temperature T. Plots of log (dielectric constant ε_r) versus (temperature T)$^{-1}$ are shown in Figure 51 for polymer DP-1A for frequencies F = 0.10 KHz, 1.0 KHz, 10.0 KHz and 100 KHz at pressures P = 3.9 Kbar and 8.0 Kbar, in Figure 52 for polymer DP-1A for F = 0.10 KHz, 1.0 KHz, 10.0 KHz and 100 KHz at P = 1.1 Kbar, and for F = 0.10 KHz, 1.0 KHz and 10.0 KHz at P = 0.46 Kbar, in Figure 53 for polymer JK-64 for F = 0.03 KHz, 0.10 KHz, 0.30 KHz, 0.60 KHz, 1.0 KHz, 3.0 KHz, 6.0 KHz, 10.0 KHz, 30.0 KHz, 60.0 KHz, 100 KHz and 150 KHz at 'ambient' pressure P = 0, and in Figure 54 for polymer JM-85A for F = 0.15 KHz, 1.0 KHz, 10.0 KHz and 100 KHz at P = 0.86 Kbar, 2.8 Kbar and 6.1 Kbar. The a.c. activation energy E_a (i.e. W_ε) as given by Equation (22) in Section 3.3. for dielectric constant for these polymers are listed in Table VII.

3.7. D.C. Conductivity and D.C. Electric Field Strength

Rosen and Pohl (1966) have derived a conductivity which takes into account the effect of electric field strength as

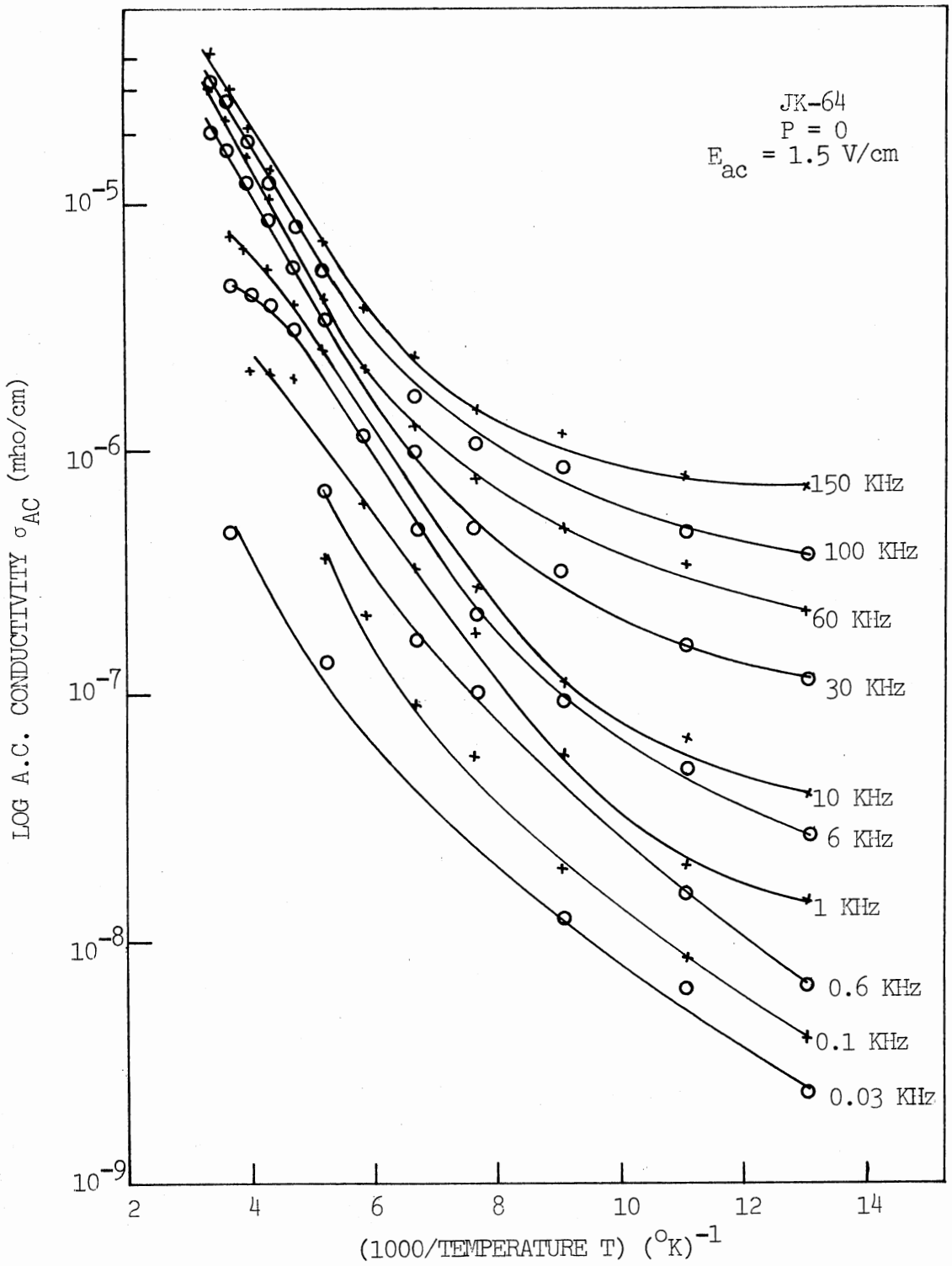

Figure 50. Log (A.C. Conductivity) Versus (1000/Temperature) (Polymer JK-64 at P=0)

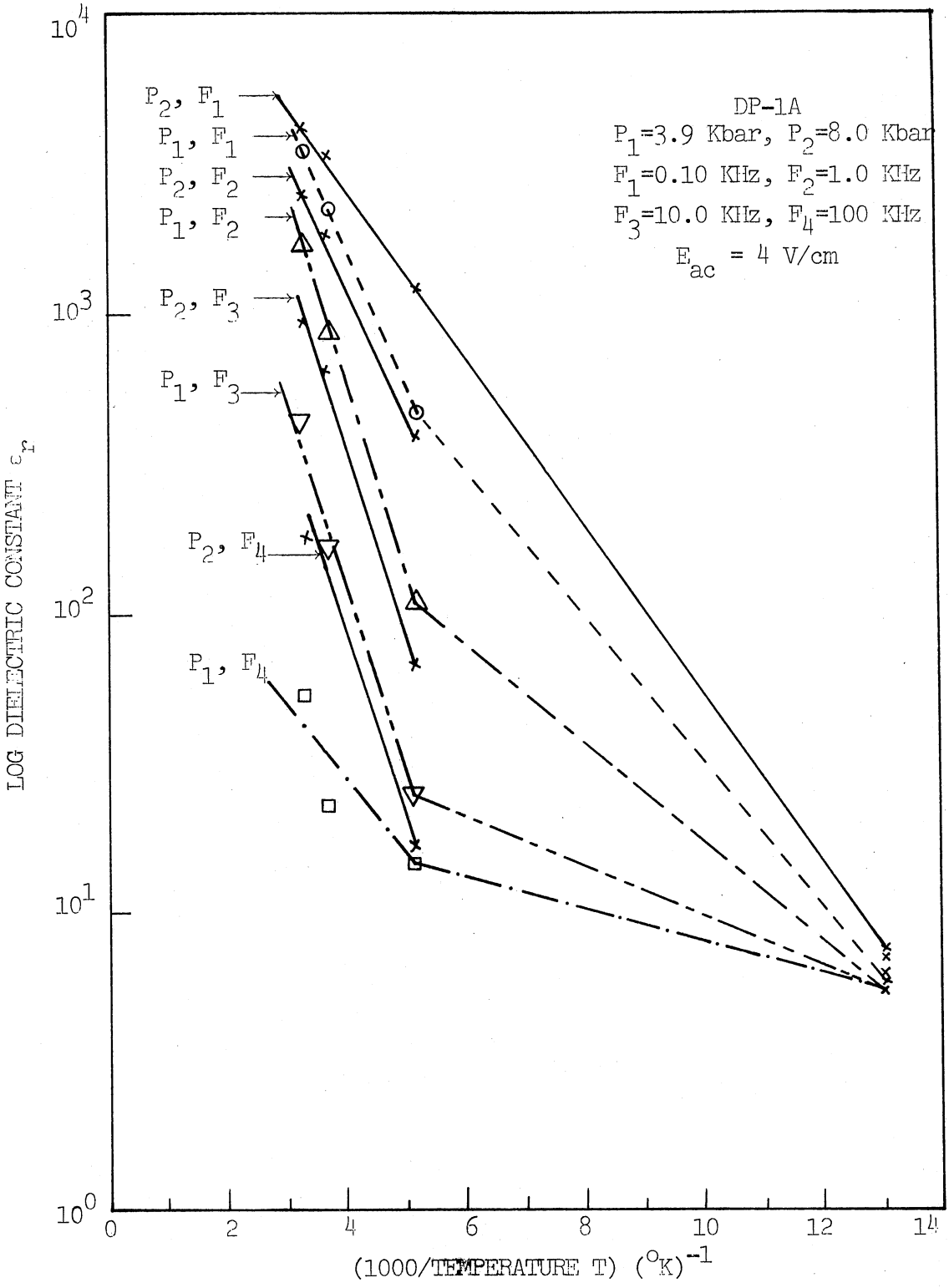

Figure 51. Log (Dielectric Constant) Versus (1000/Temperature) (Polymer DP-1A at P=3.9 Kbar and 8.0 Kbar)

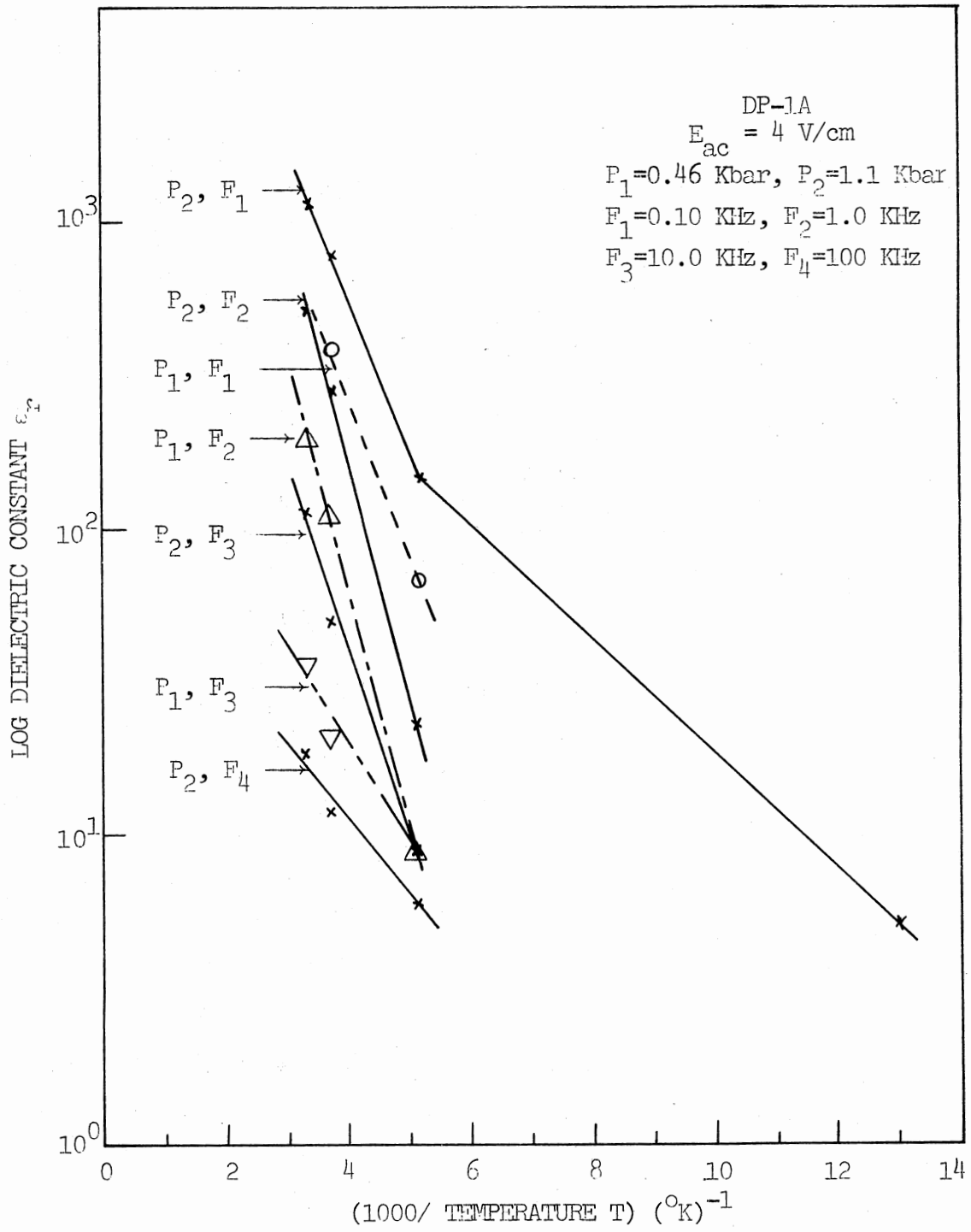

Figure 52. Log (Dielectric Constant) Versus (1000/Temperature) (Polymer DP-1A at P=0.46 Kbar and 1.1 Kbar)

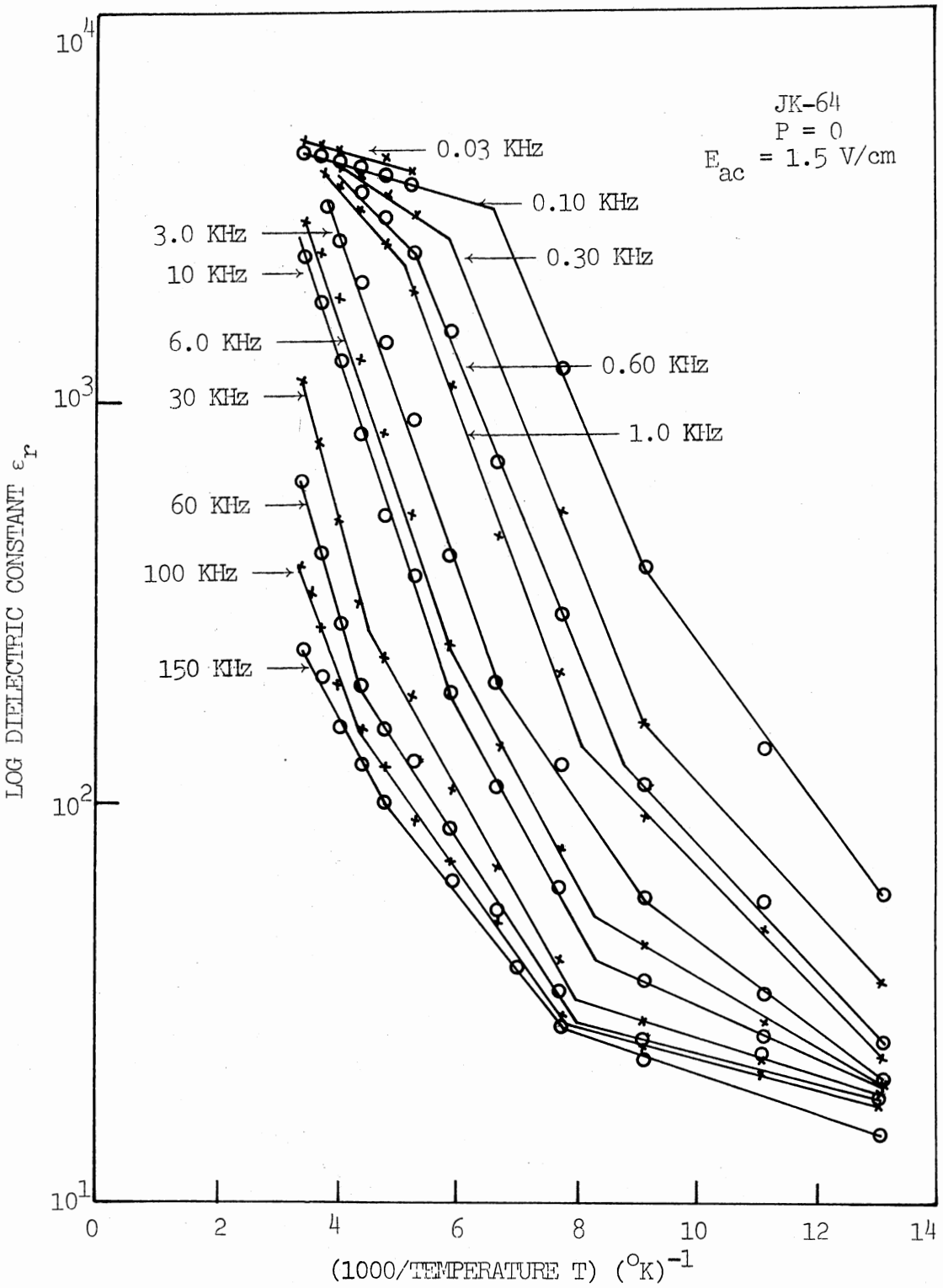

Figure 53. Log (Dielectric Constant) Versus (1000/Temperature) (Polymer JK-64 at P=0)

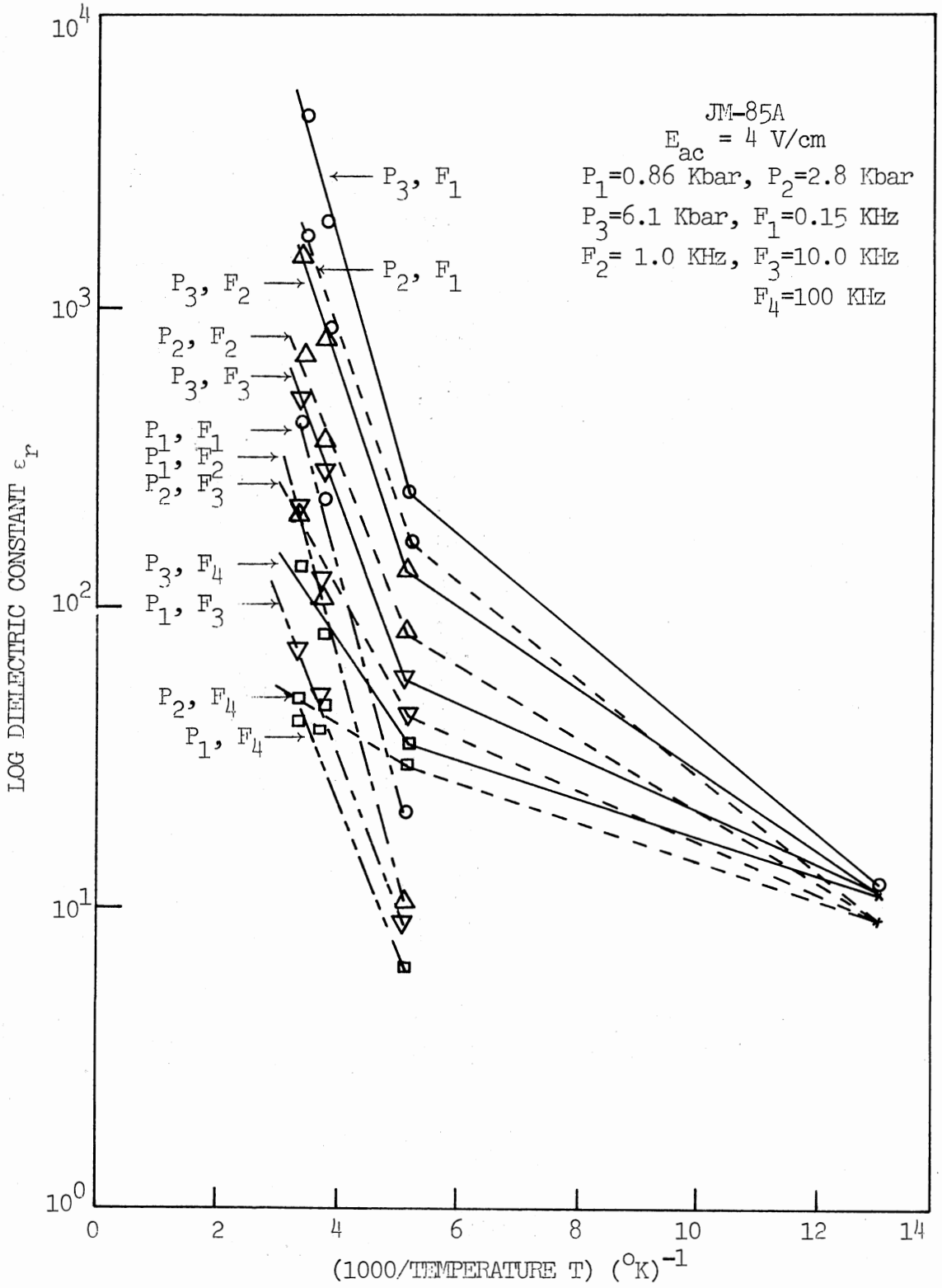

Figure 54. Log (Dielectric Constant) Versus (1000/Temperature) (Polymer JM-85A)

$$(\sigma_{DC}/\sigma_o)_{P,T} = (2kT/eEL)\ \{\exp\ (eEL/2kT) - 1\} \qquad (26)$$

where E = d.c. electric field strength and L = molecular length. For small electric fields this can be written as

$$\{(\sigma_{DC}/\sigma_o) - 1\} = \{eEL/(4kT)\} \qquad (27)$$

Figure 55 shows plots of d.c. conductivity σ_{DC} versus d.c. electric field strength E_{DC} and $\{(\sigma_{DC}/\sigma_o) - 1\}$ versus E_{DC} for polymer JK-64 at pressure P = 0.41 Kbar and temperature T = 300°K, and Figure 56 shows plots of σ_{DC} versus E_{DC} and $\{(\sigma_{DC}/\sigma_o) - 1\}$ versus E_{DC} for polymer JK-64 at P = 0.41 Kbar and T = 273°K. Figure 57 shows the plots of $\{(\sigma_{DC}/\sigma_o) - 1\}$ versus E_{DC} for polymer DP-1A at P = 0.46 Kbar and at temperatures T = 303°K, 273°K and 195°K, and for polymer JM-85A at P = 0.86 Kbar and at temperatures T = 300°K and 273°K, from which the molecular lengths can be calculated and these are listed in Table IX.

3.8. Dielectric Constant

3.8.1. Dielectric Relaxation

Pohl and Wyhof (1972a) showed that the frequency of the maximum a.c. conduction-polarization response is a thermally activated one for these polymers of the form

$$\nu_{max} = \nu_o(T)\ \{\exp\ (-E_\nu/kT)\} \qquad (28)$$

where ν_{max} is the average frequency of maximum response of charge pairs, i.e., the arc maximum of ε_r'' $(\sigma_{AC}/\omega\varepsilon_o)$ versus ε_r' Cole-Cole plots (Cole and Cole, 1941).

Table X lists ν_{max} for polymer DP-1A at pressure P = 1.1 Kbar, and for polymer JK-64 at 'ambient' pressure P = 0 in the temperature range

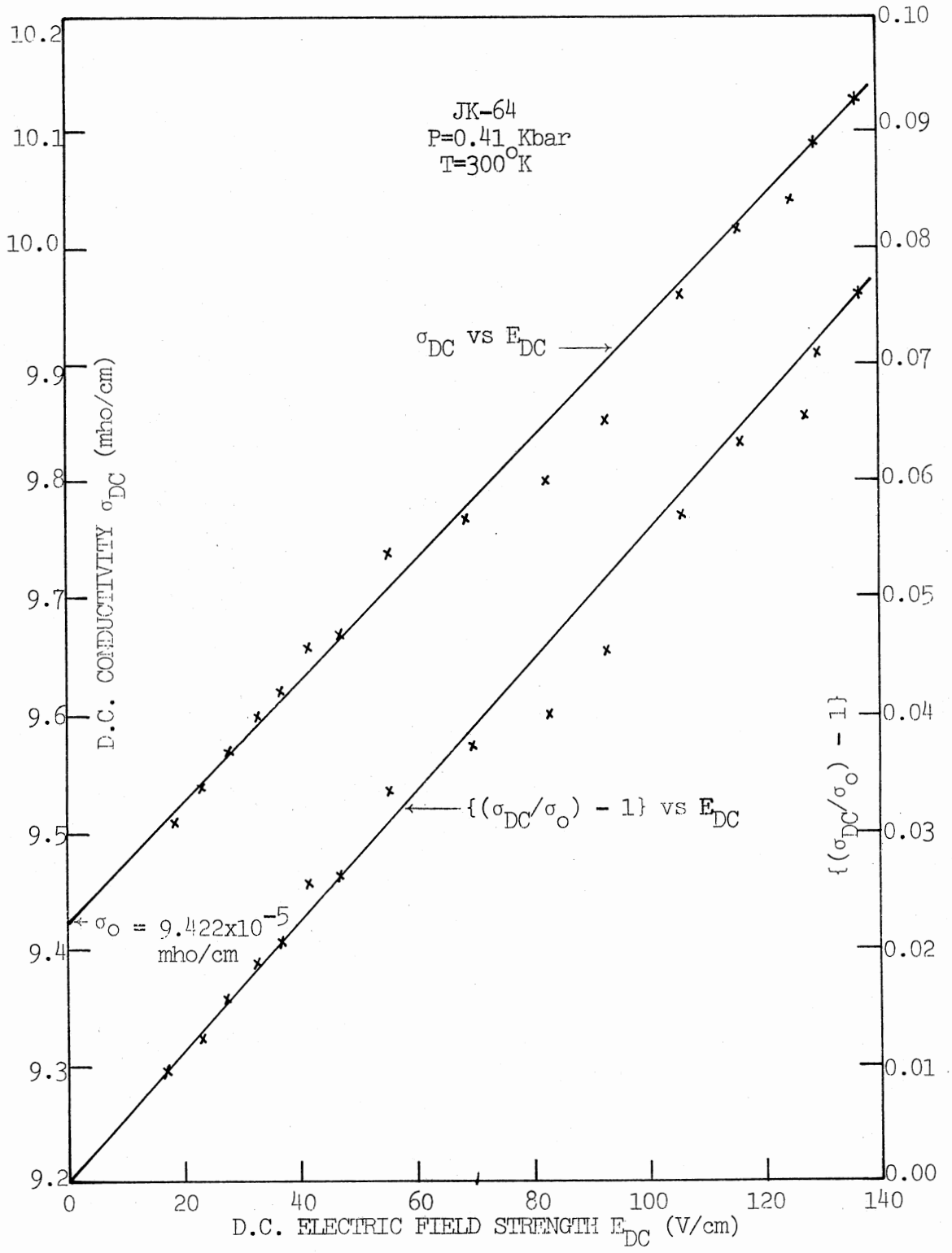

Figure 55. D.C. Conductivity and $\{(\sigma_{DC}/\sigma_o) - 1\}$ Versus D.C. Electric Field Strength (Polymer JK-64 at P=0.41 Kbar and T=300°K)

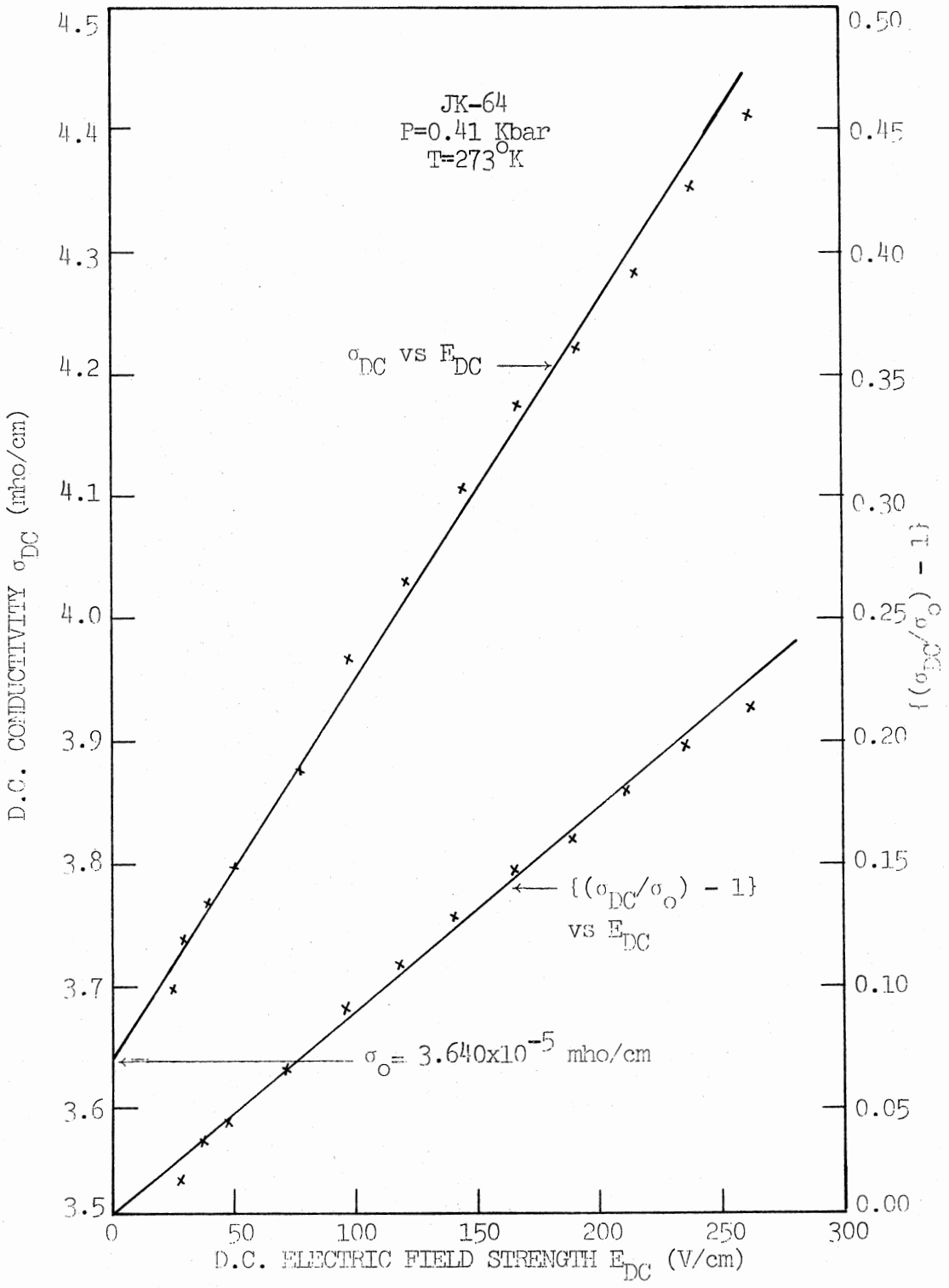

Figure 56. D.C. Conductivity and $\{(\sigma_{DC}/\sigma_o) - 1\}$ Versus D.C. Electric Field Strength (Polymer JK-64 at P=0.41 Kbar and T=273°K)

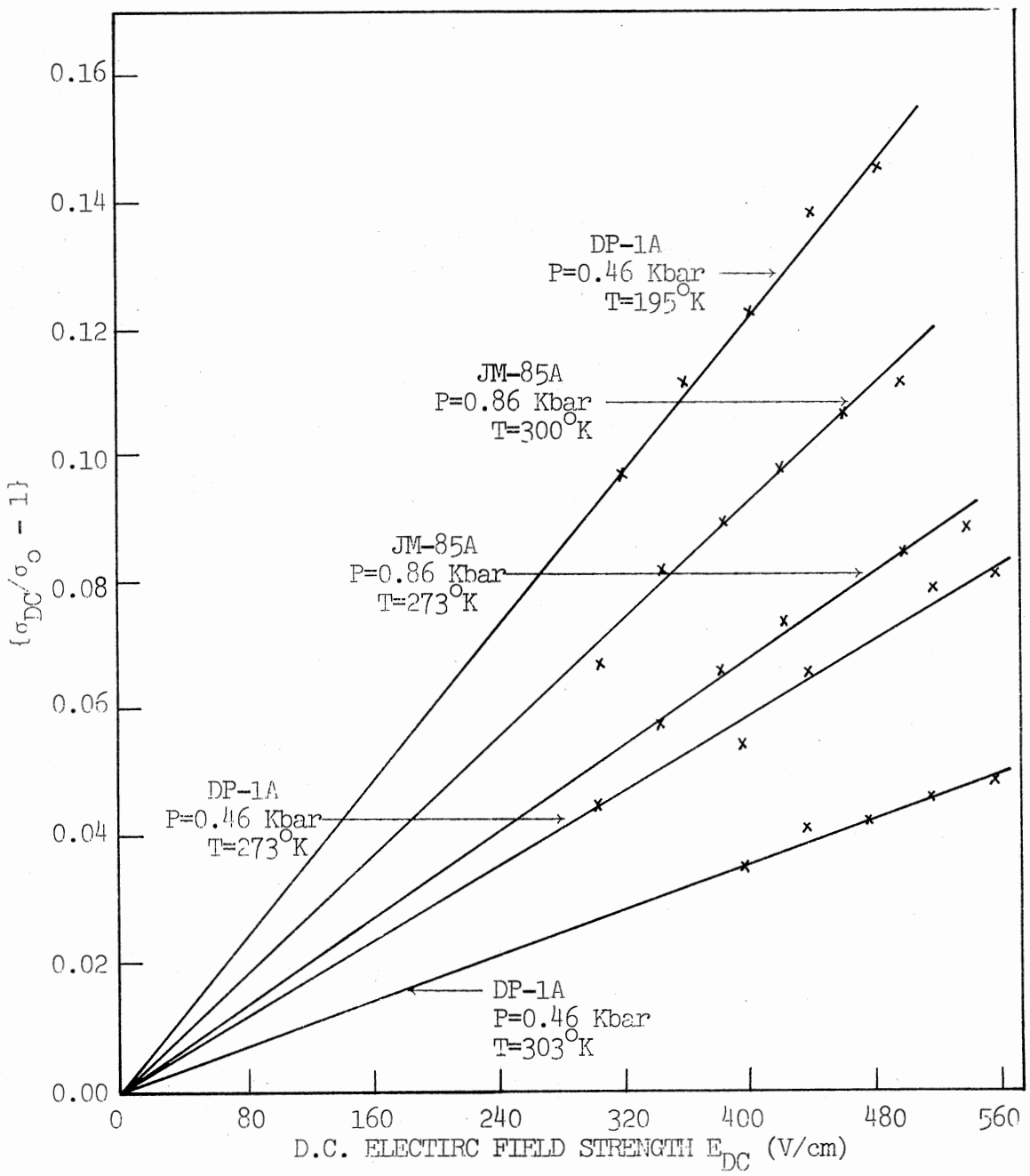

Figure 57. $\{(\sigma_{DC}/\sigma_o) - 1\}$ Versus D.C. Electric Field Strength E_{dc} (Polymers DP-1A and JM-85A)

TABLE IX

AVERAGE MOLECULAR LENGTHS OF SELECTED POLYMERS

Sample Name	Pressure (Kbar)	Temperature (^{o}K)	ε_r (Experimental)	Molecular Length L (Angstroms)		
				From Pohl-Pollak Theory $\varepsilon_r \propto L^2$	From Slope of $\{(\sigma_{DC}/\sigma_o)-1\}$ Versus E_{DC}	From Saturation of Polarization by E_{AC}
DP-1A	0.46	303	1070 (f=0.01 KHz)	245 x 15 = 3700	900	1400 (E_{sat}=600 V/cm)
		273	1000 (f=0.01 KHz)	283 x 15 = 4200	1400	1300 (E_{sat}=700 V/cm)
				Av L = 3900	Av L = 1100	Av L = 1300
JK-64	0.0	294	4510 (f=0.03 KHz)	500 x 15 = 7500	5000 (P=0.41 Kbar)	-
		270	4410 (f=0.03 KHz)	583 x 15 = 8700	8200 (P=2.2 Kbar)	-
				Av L = 8100	Av L = 6600	
JM-85A	0.86	300	420.7 (f=0.15 KHz)	155 x 15 = 2300	2400	1100 (E_{sat}=1000 V/cm)
		273	232.8 (f=0.15 KHz)	134 x 15 = 2000	1500	-
				Av L = 2100	Av L = 1900	Av L = 1100

TABLE X

EXPERIMENTAL VALUES OF DIELECTRIC RELAXATION
OF SELECTED POLYMERS

Sample Name	Pressure (Kbar)	Temperature (^{o}K)	1000/T $(^{o}K)^{-1}$	ν_{max}(Hz) From Cole-Cole Plots of ε_r'' Versus ε_r'	ν_{max} x 1000/T $(Sec^{-1}\ {}^{o}K^{-1})$
DP-1A	1.1	303	3.30	1000	3300
		273	3.66	600	2200
		195	5.13	100	510
		77	13.1	<10	130
JK-64	0.0	294	3.41	8000	27300
		270	3.70	6000	22200
		250	4.00	4000	16000
		230	4.35	3000	13000
		210	4.76	2000	9520
		190	5.26	1500	7890
		170	5.88	1000	5880
		150	6.67	600	4000
		130	7.70	300	2300
		110	9.10	100	910
		90	11.1	<10	110
		77	13.1	<10	60

$T = 77^{o}K$ to $300^{o}K$. Figure 58 shows the plots of log ($\nu_{max} T^{-1}$) versus T^{-1} for these two polymers from which the activation energy E_{ν} can be calculated. For polymer DP-1A $E_{\nu} = 0.089$ eV, and for polymer JK-64 $E_{\nu} = 0.054$ eV. E_{ν} is interpreted as the hopping energy associated with the charge carriers in the long molecular domains of the polymers while within them.

3.8.2. Frequency and D.C. Electric Field Strength Dependence

The dielectric constant ε_r decreases with increasing frequency ω as

$$\varepsilon_r(\omega) \simeq B\,\omega^{-p} \qquad (29)$$

where $p = (1 - s)$.

Plots of log (dielectric constant ε_r) versus log (frequency F) are shown in Figure 59 for polymer DP-1A at pressure P = 3.9 Kbar and at temperature $T = 303^{o}K$ for various d.c. bias electric field strengths E_{dc} = 0 V/cm, 40 V/cm, 80 V/cm and 160 V/cm in the frequency range F = 0.01 KHz to 150 KHz, in Figure 60 for polymer DP-1A at P = 3.9 Kbar and $T = 273^{o}K$ for E_{dc} = 0 V/cm, 40 V/vm, 80 V/cm and 160 V/cm in the frequency range F = 0.01 KHz to 150 KHz, in Figure 61 for polymer DP-1A at P = 0.32 Kbar, 1.1 Kbar and 3.3 Kbar, and $T = 303^{o}K$ in the frequency range F = 1.0 MHz to 100 MHz, in Figure 62 for polymer JK-64 at 'ambient' pressure P = 0 and at $T = 77^{o}K$, $90^{o}K$, $110^{o}K$, $130^{o}K$, $150^{o}K$, $170^{o}K$, $190^{o}K$, $210^{o}K$, $230^{o}K$, $250^{o}K$, $270^{o}K$ and $293^{o}K$ in the frequency range F = 0.03 KHz to 150 KHz, in Figure 63 for polymer JK-64 at 'ambient' pressure P = 0 and $T = 300^{o}K$ for E_{dc} = 1.5 V/cm, 15 V/cm, 74 V/cm and 148 V/cm in the frequency range 100 Hz to 100 MHz, and in Figure 64,

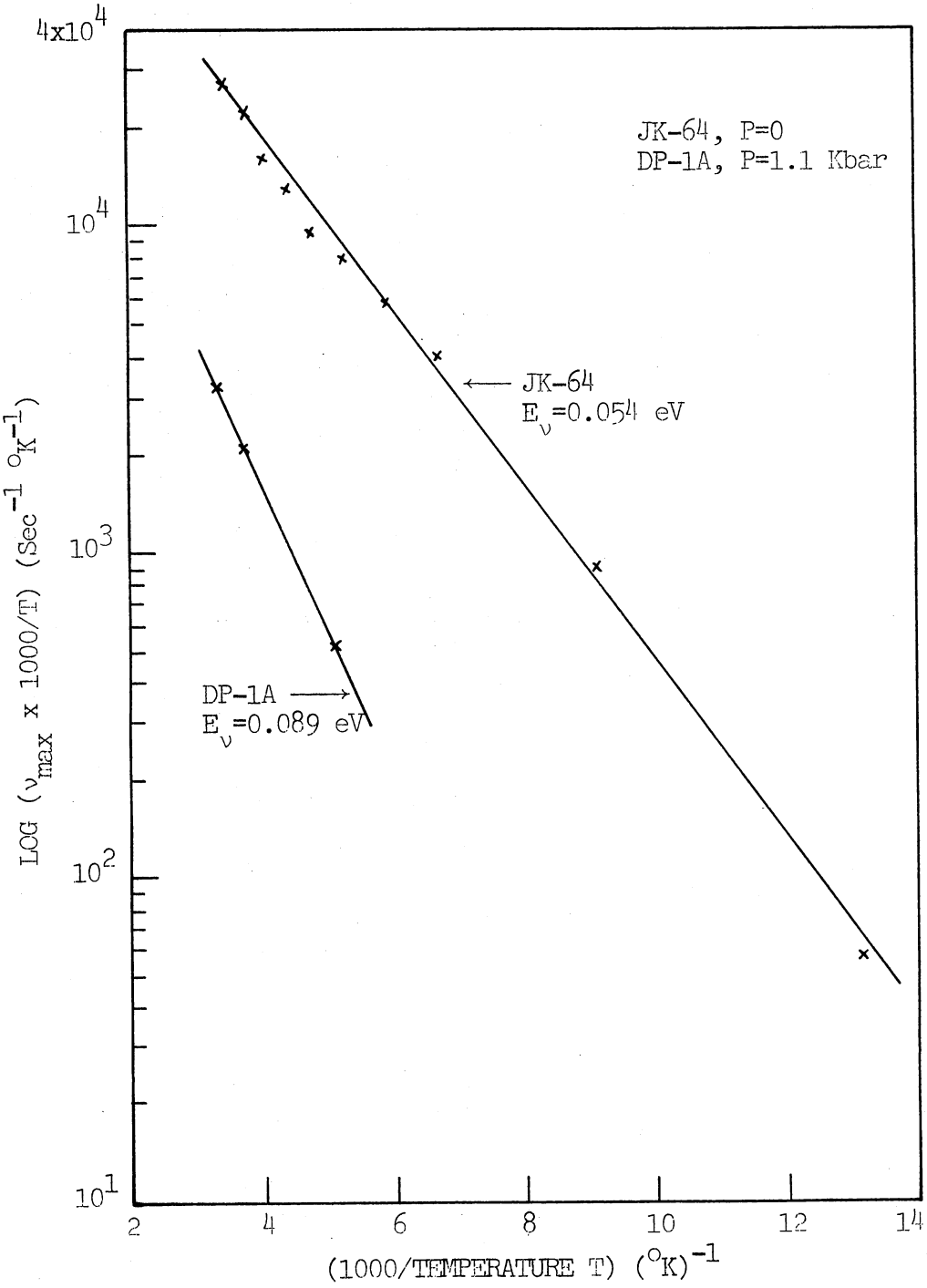

Figure 58. Log (ν_{max} x 1000/T) Versus (1000/T)

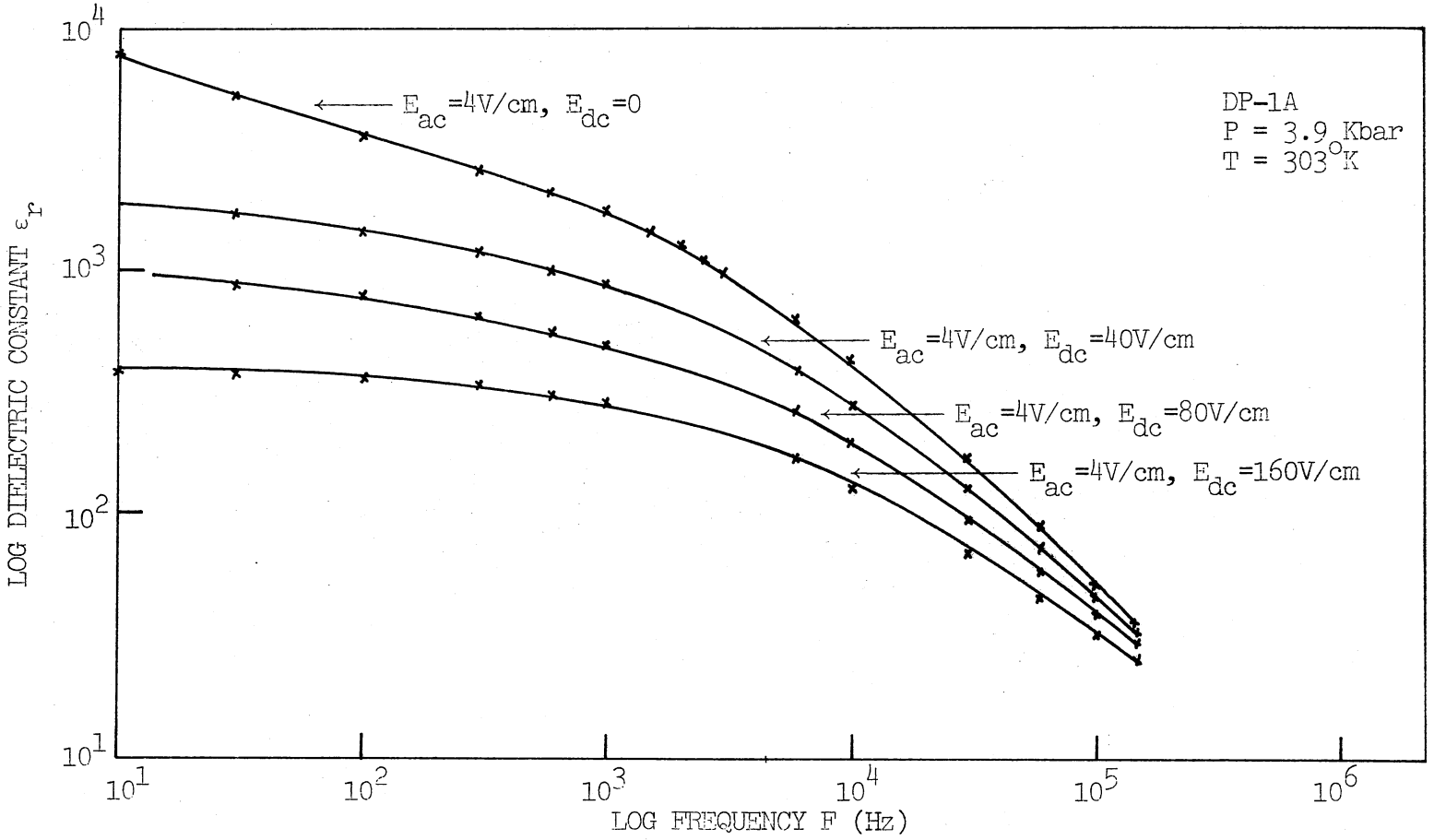

Figure 59. Log (Dielectric Constant with D.C. Bias Electric Field Strength) Versus Log (Frequency) (polymer DP-1A at P=3.9 Kbar and T =303°K)

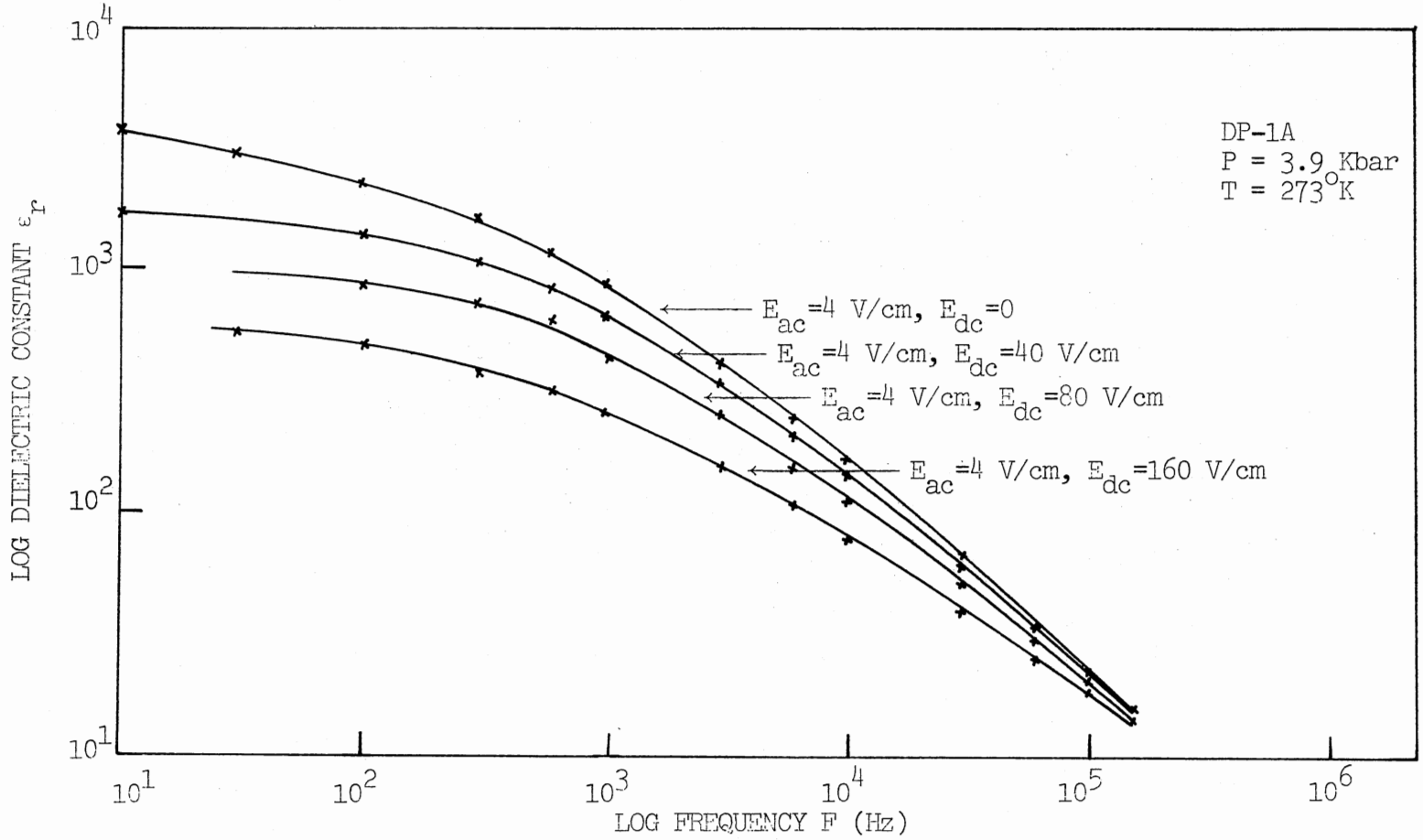

Figure 60. Log (Dielectric Constant with D.C. Bias Electric Field Strength) Versus Log (Frequency) (Polymer DP-1A at P=3.9 Kbar and T=273°K)

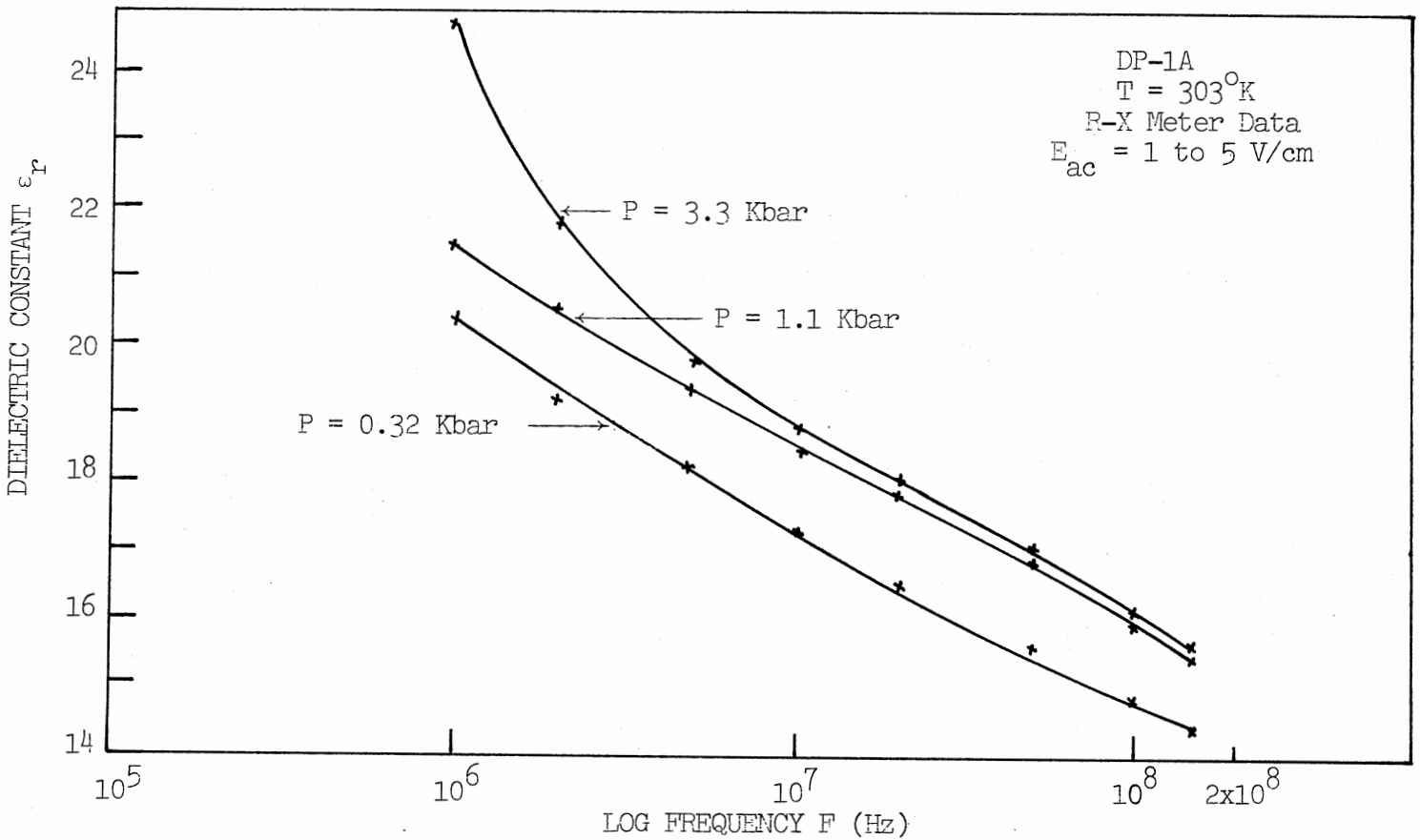

Figure 61. Dielectric Constant Versus Log (Frequency) (Polymer DP-1A at T=303°K, Frequency Range from F=1.0 MHz to 100 MHz)

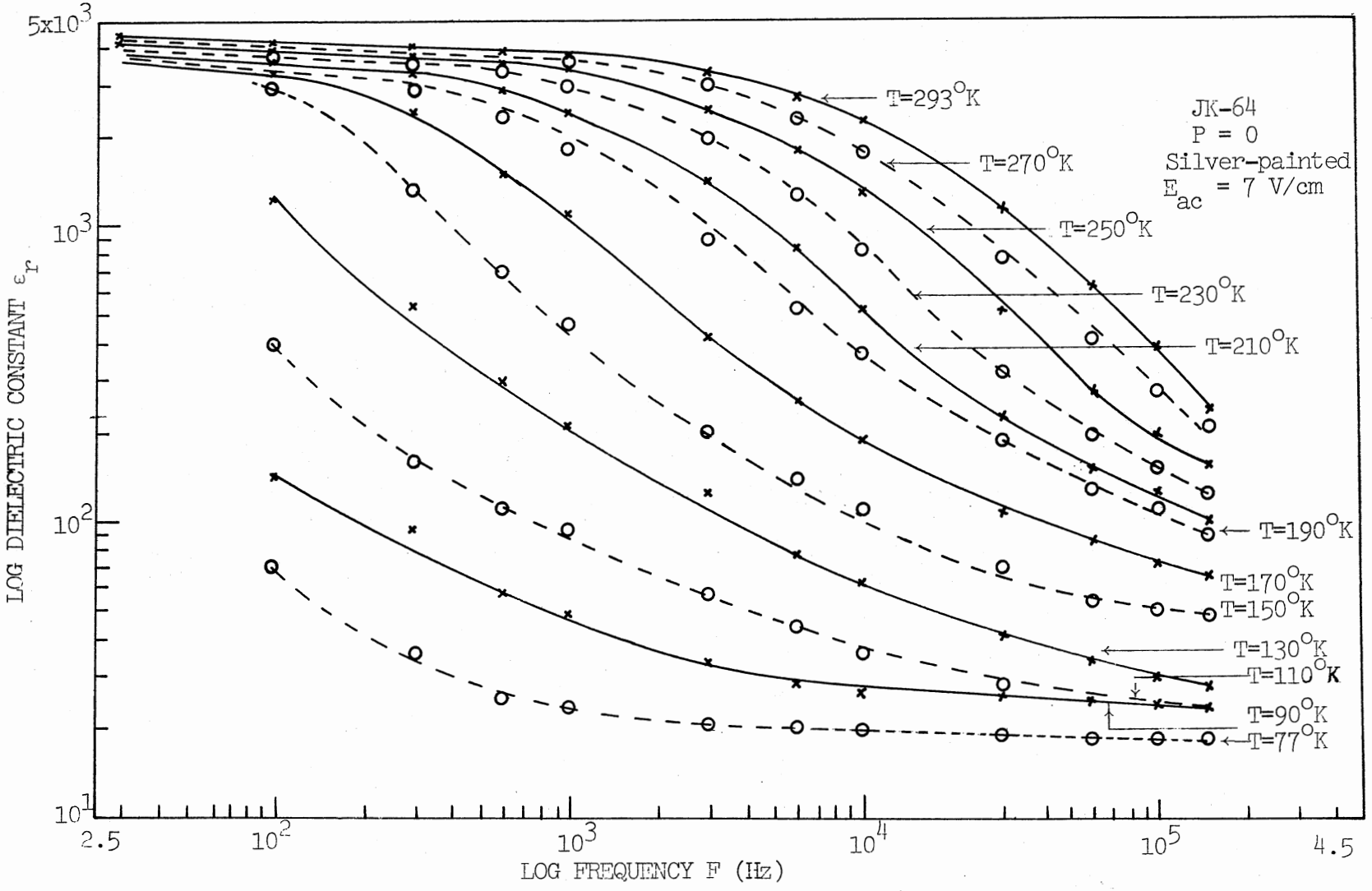

Figure 62. Log (Dielectric Constant) Versus Log (Frequency) (Polymer JK-64 at P=0)

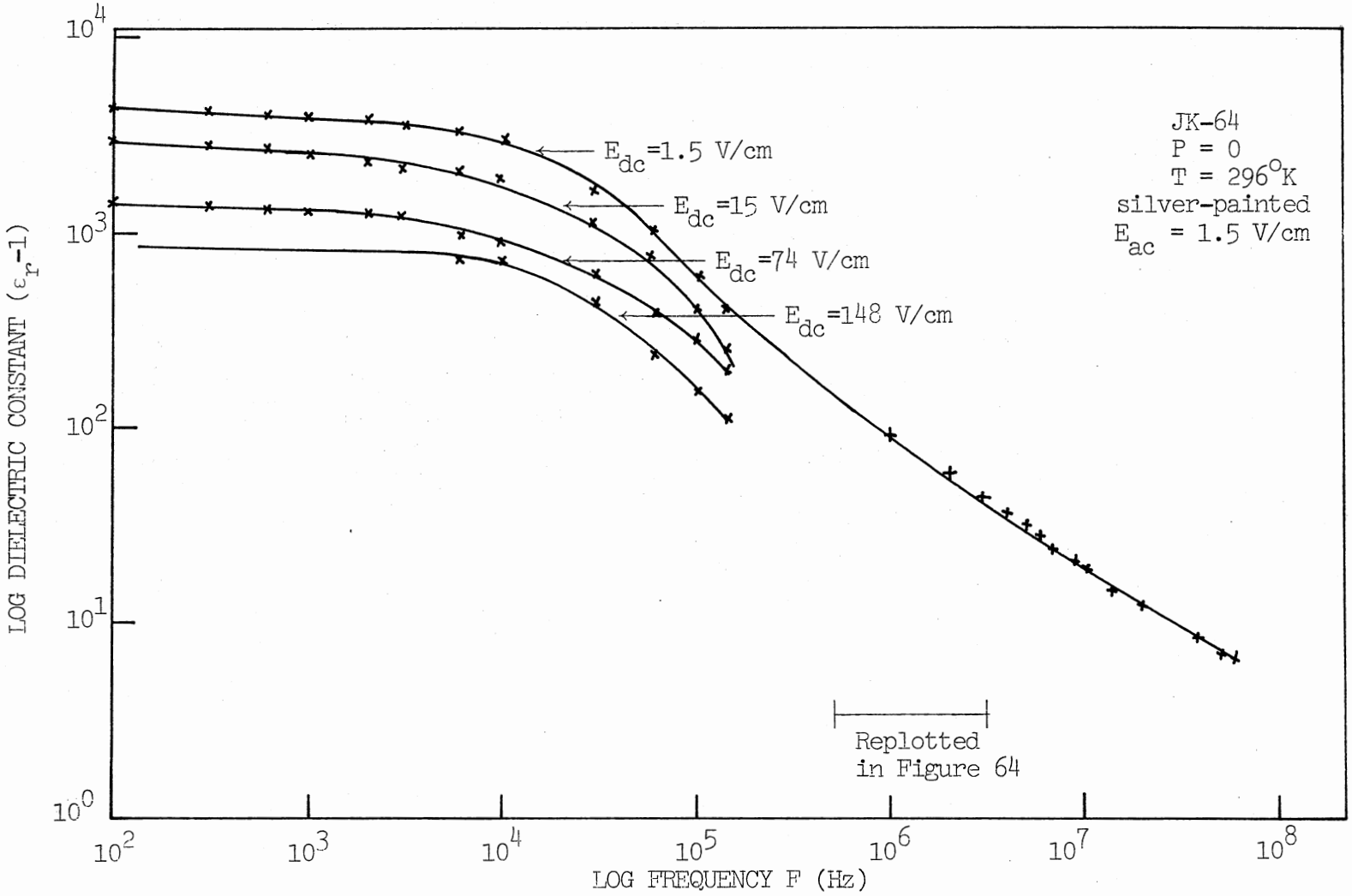

Figure 63. Log (Dielectric Constant with D.C. Bias Electric Field Strength) Versus Log (Frequency) (Polymer JK-64, at P=0)

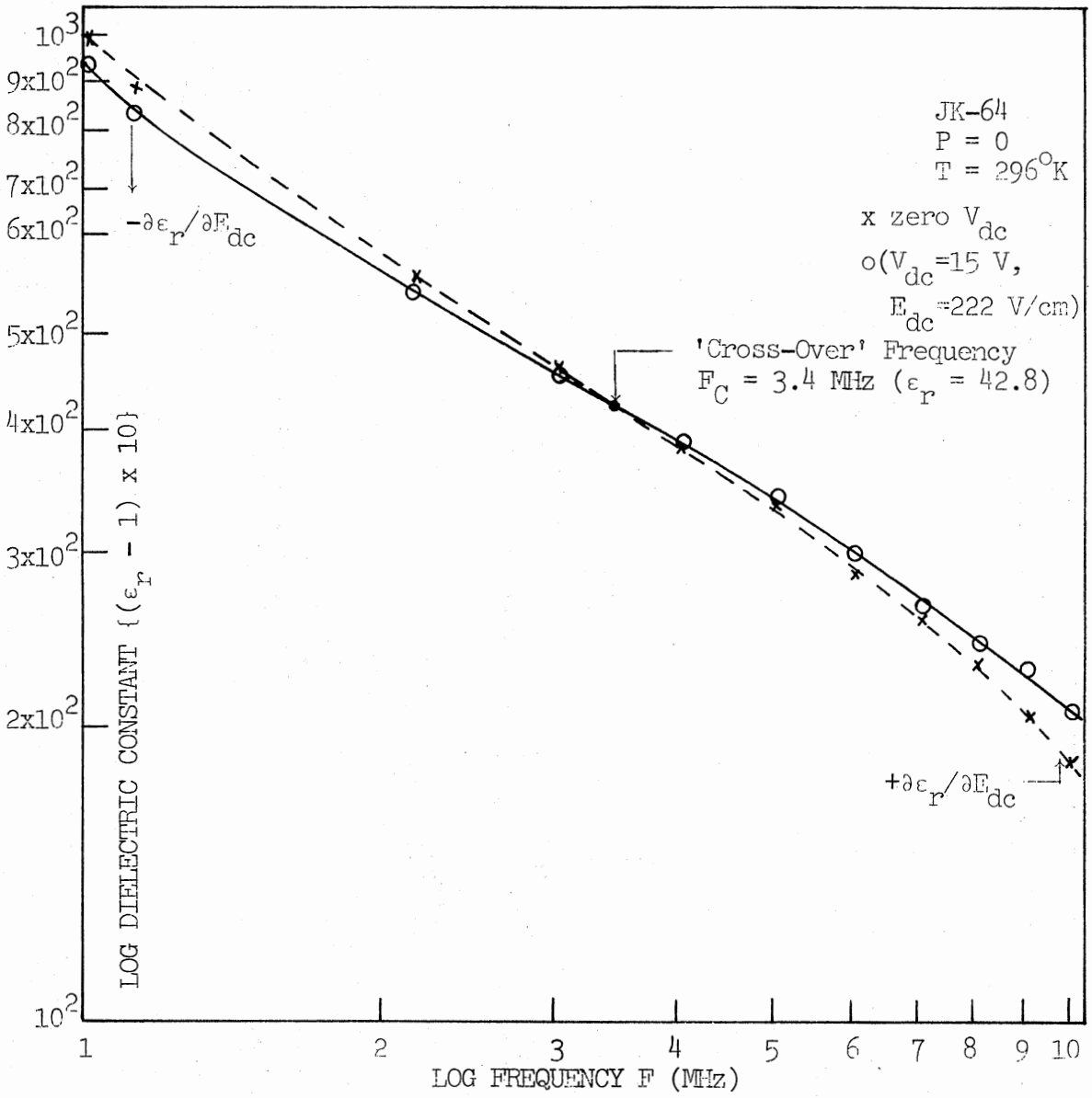

Figure 64. Log (10 x Dielectric Constant with D.C. Bias Electric Field Strength) Versus Log (Frequency) (Polymer JK-64 at P=0, Frequency Range F=1.0 MHz to 10.0 MHz)

which is an expanded plot of Figure 63, in the frequency range F = 1.0 MHz to 10 MHz for polymer JK-64 at 'ambient' pressure P = 0 and T = 296°K for E_{dc} = 0 V/cm and 222 V/cm. Figure 64 also shows the d.c. bias electric field strength induced reversal of dielectric constant from $-\partial\varepsilon_r/\partial E_{dc}$ to $+\partial\varepsilon_r/\partial E_{dc}$ at a 'cross-over' frequency F_C of 3.4 MHz with a relative dielectric constant ε_r of 42.8.

3.8.3. AC/DC Electric Field Strength Dependence

Based on the dielectric theory proposed by Pohl and Pollak (1977), the static dielectric constant as given by Equation (15) in Section 1.2.2., the theoretical plots of log dielectric constant (ε_r) versus log (a.c. electric field strength E_{ac}) (d.c. electric field strength E_{dc} = 0, i.e., 'total'), and log dielectric constant (ε_r) versus log (E_{dc}) (E_{ac} = small, i.e., 'differential') were shown in Figure 7. Experimental results are shown in Figure 65 for polymer DP-1A at pressure P = 3.9 Kbar and at temperature T = 303°K as plots of ε_r versus log E_{ac} (E_{dc} = 0) in the range of 1 to 800 V/cm, and ε_r versus log E_{dc} (E_{ac} = 4 V/cm) in the range of 1 to 200 V/cm at frequencies F = 0.10 KHz and 1.0 KHz; in Figure 66 for polymer DP-1A at P = 3.9 Kbar and T = 273°K as plots of ε_r versus Log E_{ac} (E_{dc} = 0) in the range of 1 to 800 V/cm, and ε_r versus log E_{dc} (E_{ac} = 4 V/cm) in the range of 1 to 400 V/cm at F = 0.10 KHz and 0.30 KHz; in Figure 67 for polymer JK-64 at P = 0.41 Kbar and T = 300°K as plots of ε_r versus log E_{ac} (E_{dc} = 0) in the range of 1 to 300 V/cm, and ε_r versus E_{dc} (E_{ac} = 7 V/cm) in the range of 1 to 90 V/cm at F = 10.0 KHz; in Figure 68 for polymer JK-64 at P = 0.41 Kbar and T = 300°K as plots of ε_r versus log E_{ac} (E_{dc} = 0) in the range of 1 to 300 V/cm, and ε_r versus log E_{dc} (E_{ac} = 7 V/cm) in the range of 1 to 80

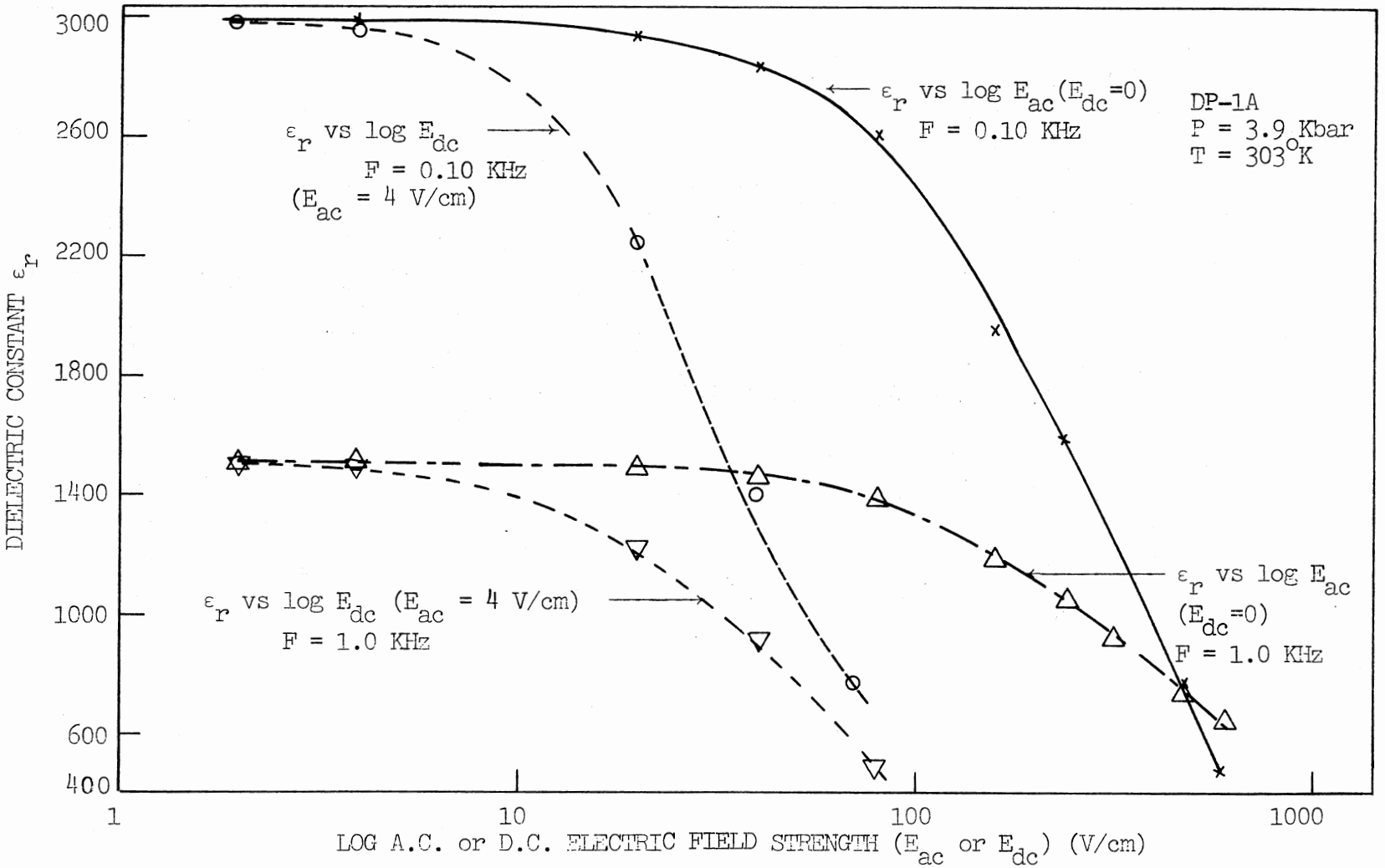

Figure 65. Dielectric Constant Versus Log (AC/DC Electric Field Strength) (Polymer DP-1A at P=3.9 Kbar, T=303°K, at F=0.10 KHz and 1.0 KHz)

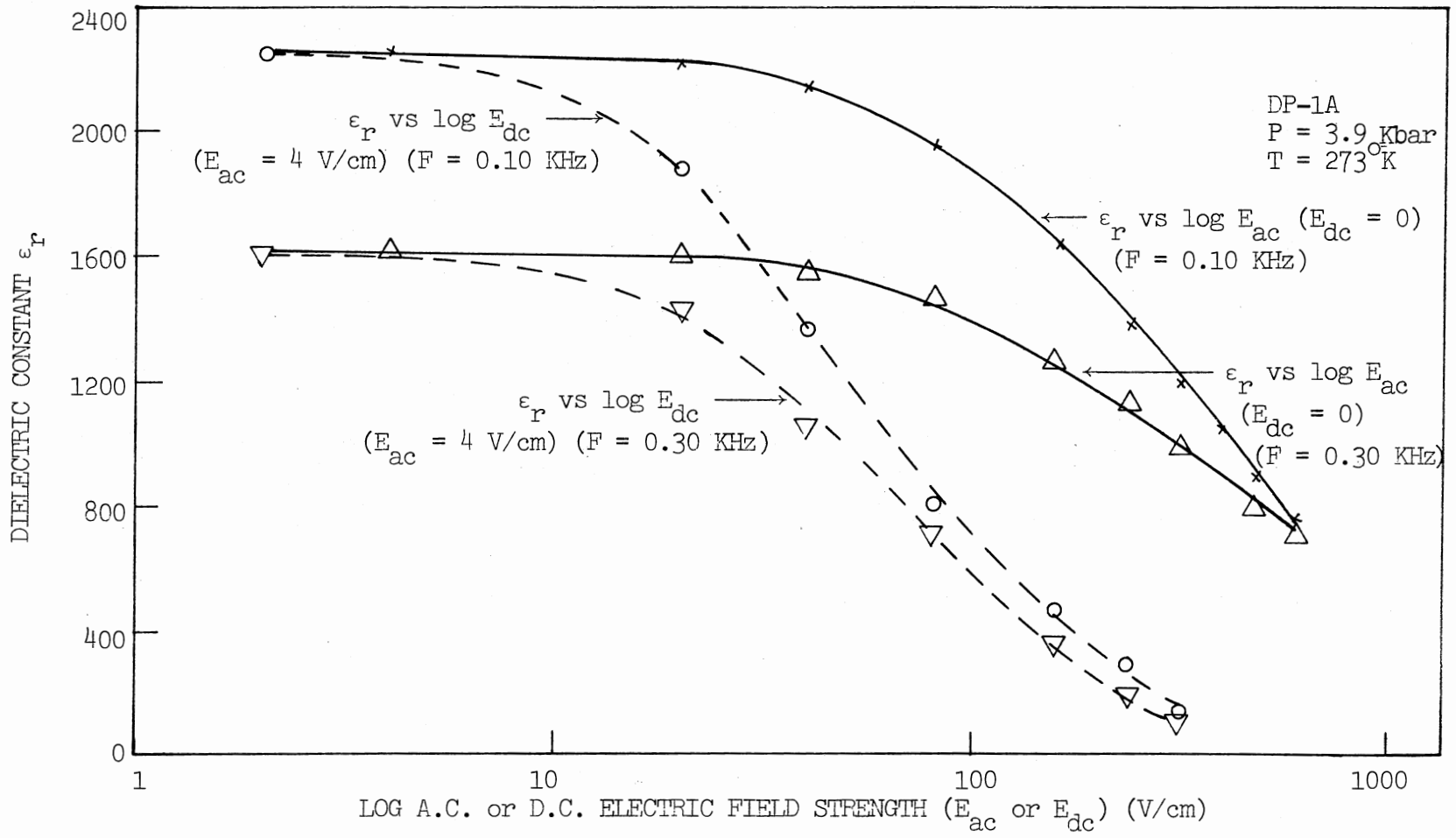

Figure 66. Dielectric Constant Versus Log (AC/DC Electric Field Strength) (Polymer DP-1A at P=3.9 Kbar, T=273°K, and F=0.10 KHz and 0.30 KHz)

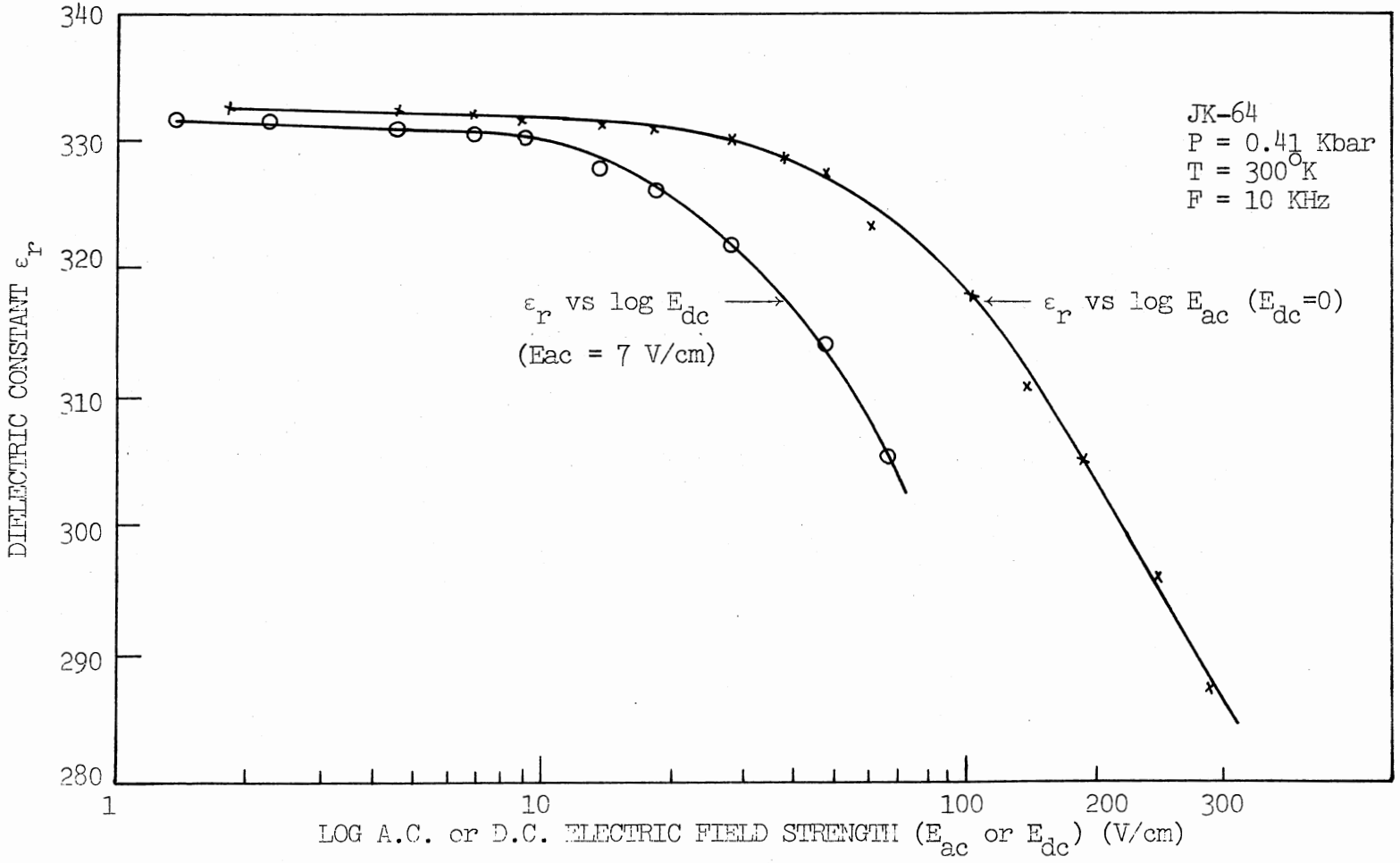

Figure 67. Dielectric Constant Versus Log (AC/DC Electric Field Strength)
(Polymer JK-64 at P=0.41 Kbar, T=300°K and F=10.0 KHz)

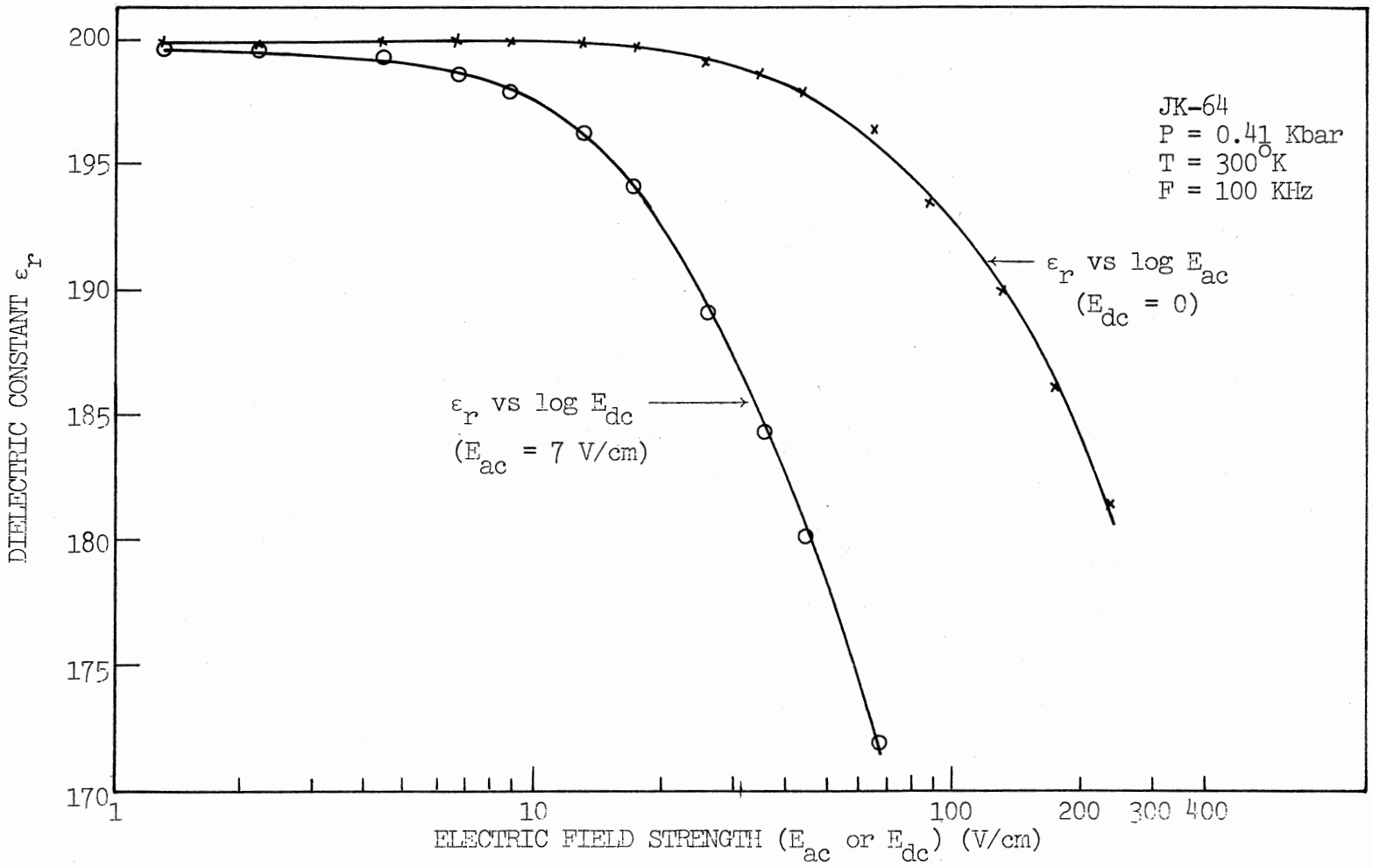

Figure 68. Dielectric Constant Versus Log (AC/DC Electric Field Strength) (Polymer JK-64 at P = 0.41 Kbar, T=300°K and F= 100 KHz)

V/cm at F = 100 KHz; in Figure 69 for polymer JK-64 at P = 0.41 Kbar and T = 273°K as plots of ε_r versus log E_{ac} (E_{dc} = 0) in the range of 1 to 800 V/cm, and ε_r versus log E_{dc} (E_{ac} = 7 V/cm) in the range of 1 to 100 V/cm at F = 1.0 KHz and 10.0 KHz; in Figure 70 for polymer JK-64 at P = 0.41 Kbar and T = 273°K as plots of ε_r versus log E_{ac} (E_{dc} = 0) in the range of 1 to 300 V/cm, and ε_r versus log E_{dc} (E_{ac} = 7 V/cm) in the range of 1 to 150 V/cm at F = 100 KHz; in Figure 71 for polymer JK-64 at P = 0.41 Kbar and T = 195°K as plots of ε_r versus log E_{ac} (E_{dc} = 0) in the range of 1 to 700 V/cm, and ε_r versus log E_{dc} (E_{ac} = 7 V/cm) in the range of 1 to 200 V/cm at F = 1.0 KHz; in Figure 72 for polymer JK-64 at P = 0.41 Kbar and T = 195°K as plots of ε_r versus log E_{ac} (E_{dc} = 0) in the range of 1 to 700 V/cm, and ε_r versus log E_{dc} (E_{ac} = 7 V/cm) in the range of 1 to 500 V/cm at F = 10.0 KHz; in Figure 73 for polymer JK-64 at P = 0.41 Kbar and T = 77°K as plots of ε_r versus log E_{ac} (E_{dc} = 0) in the range of 1 to 500 V/cm, and ε_r versus log E_{dc} (E_{ac} = 7 V/cm) in the range of 1 to 700 V/cm at F = 0.15 KHz.

3.8.4. Polarization and A.C. Electric Field Strength

Figure 74 shows plots of log (polarization P) versus a.c. electric field strength (E_{ac}) for polymer DP-1A at pressure P = 3.9 Kbar and temperature T = 303°K for frequencies F = 0.01 KHz, 0.03 KHz, 0.10 KHz, 0.30 KHz, 0.60 KHz, 1.0 KHz, 3.0 KHz, 6.0 KHz and 10.0 KHz for E_{ac} ranging from 5 to 1000 V/cm. It also shows the saturation of polarization $\{P = (\varepsilon_r - 1)\varepsilon_o E_{ac}\}$ for relatively small a.c. field strengths of few hundred V/cm. Pohl (1974) has shown that by balancing the field force on a carrier moving along a chain of length L and within it, with the

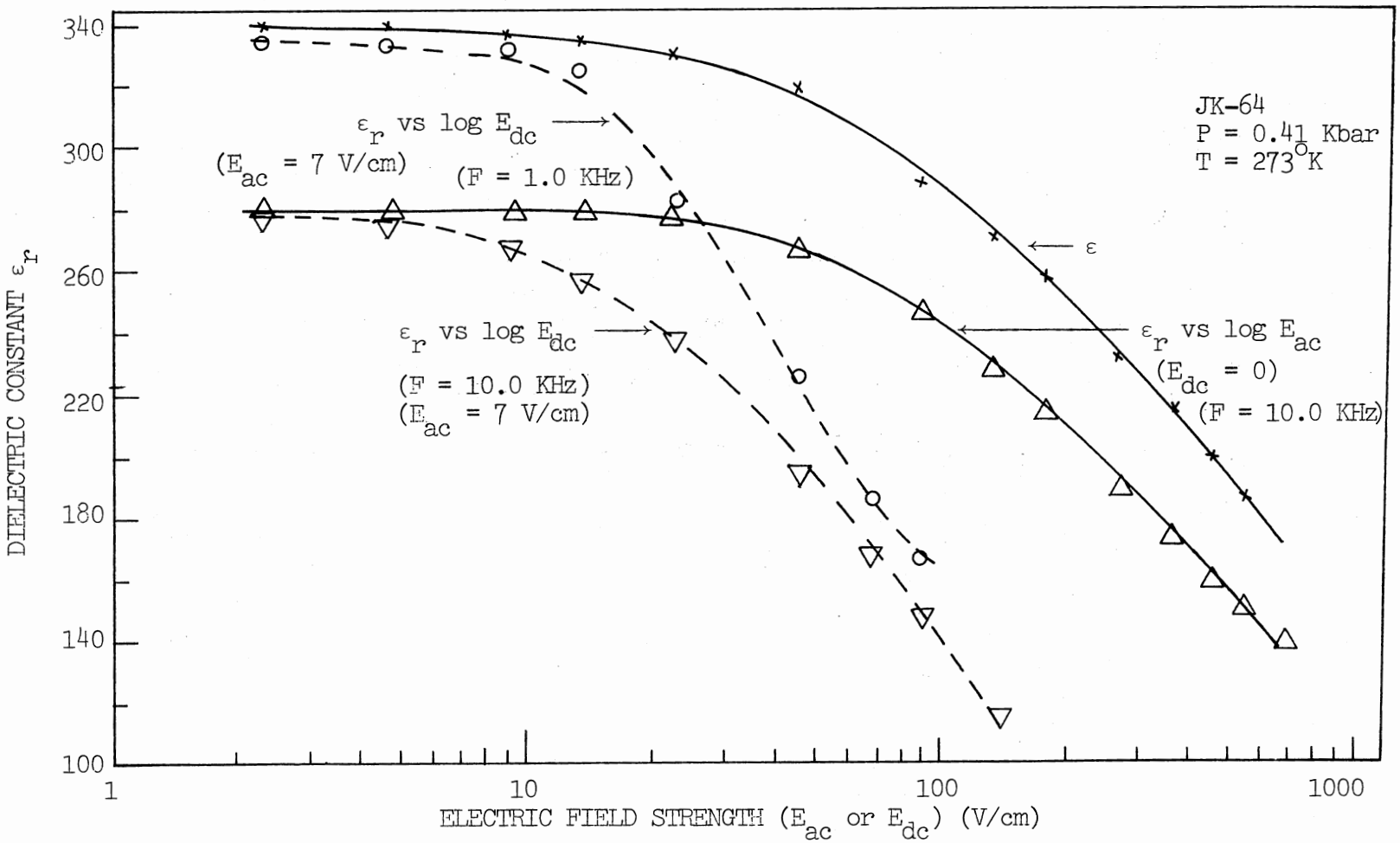

Figure 69. Dielectric Constant Versus Log (AC/DC Electric Field Strength) (Polymer JK-64 at P=0.41 Kbar, T=273°K, at F=1.0 KHz and 10.0 KHz)

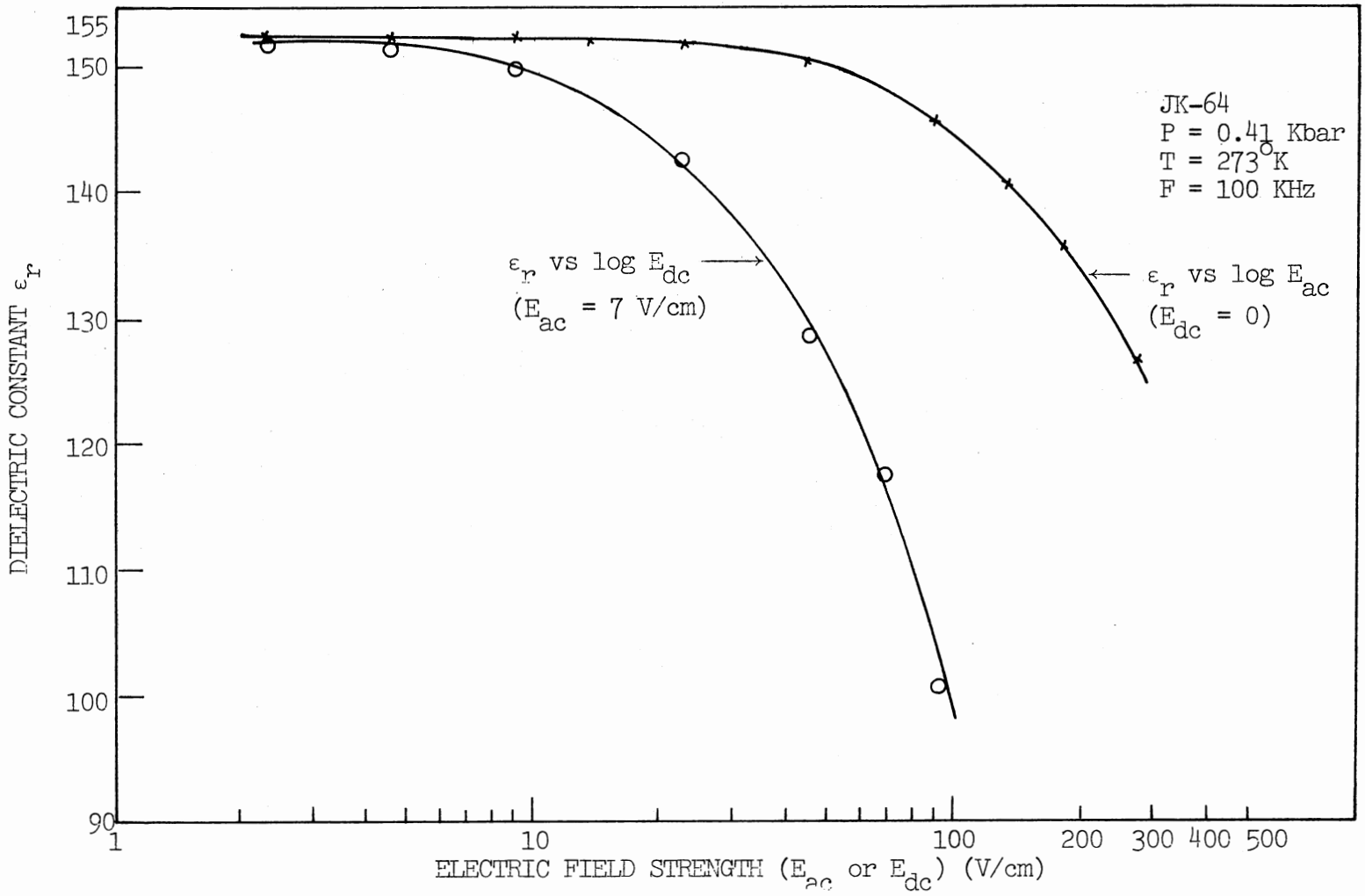

Figure 70. Dielectric Constant Versus Log (AC/DC Electric Field Strength)
(Polymer JK-64 at P=0.41 Kbar, T=273°K and F=100 KHz)

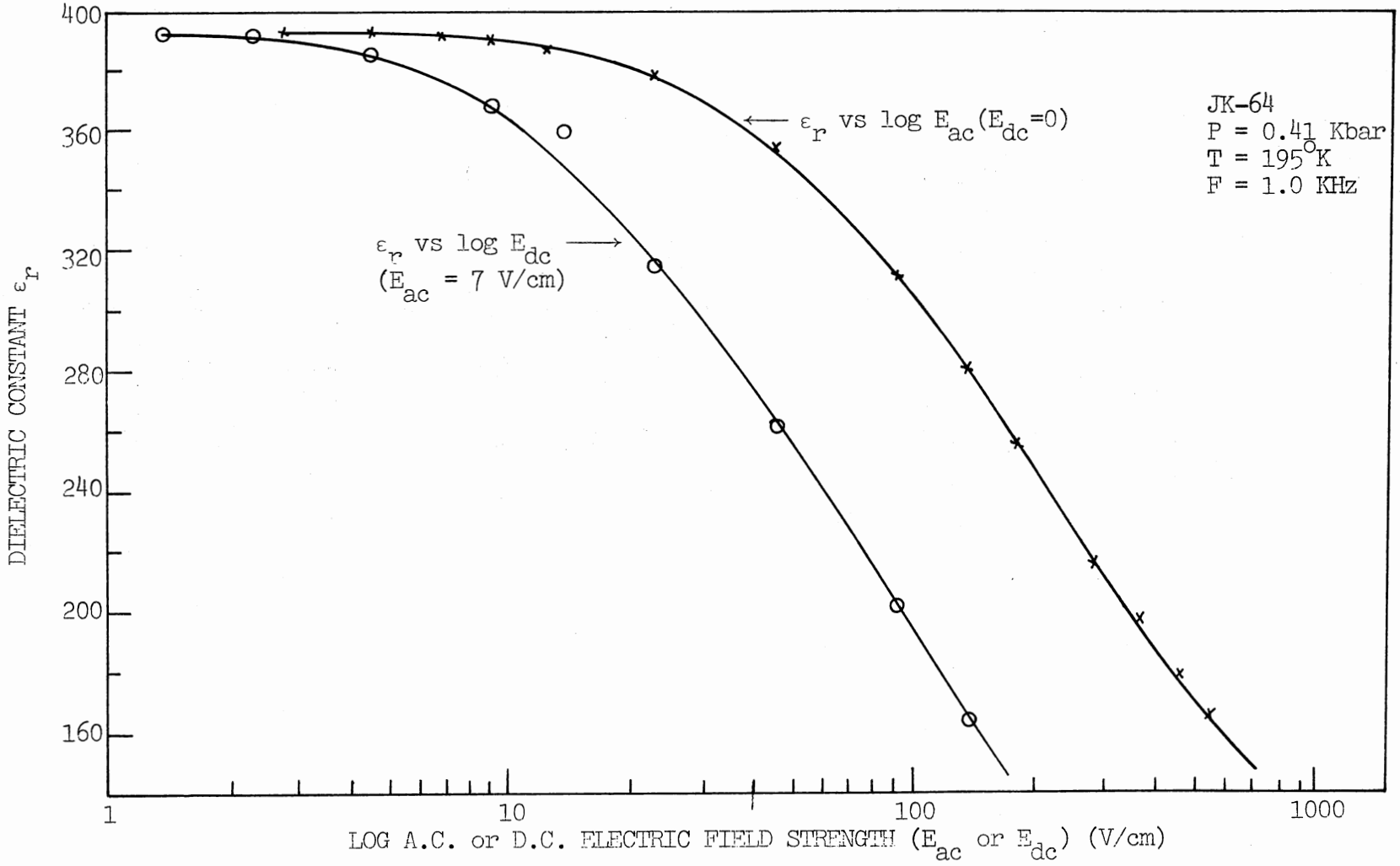

Figure 71. Dielectric Constant Versus Log (AC/DC Electric Field Strength)
(Polymer JK-64 at P=0.41 Kbar, T=195°K and F=1.0 KHz)

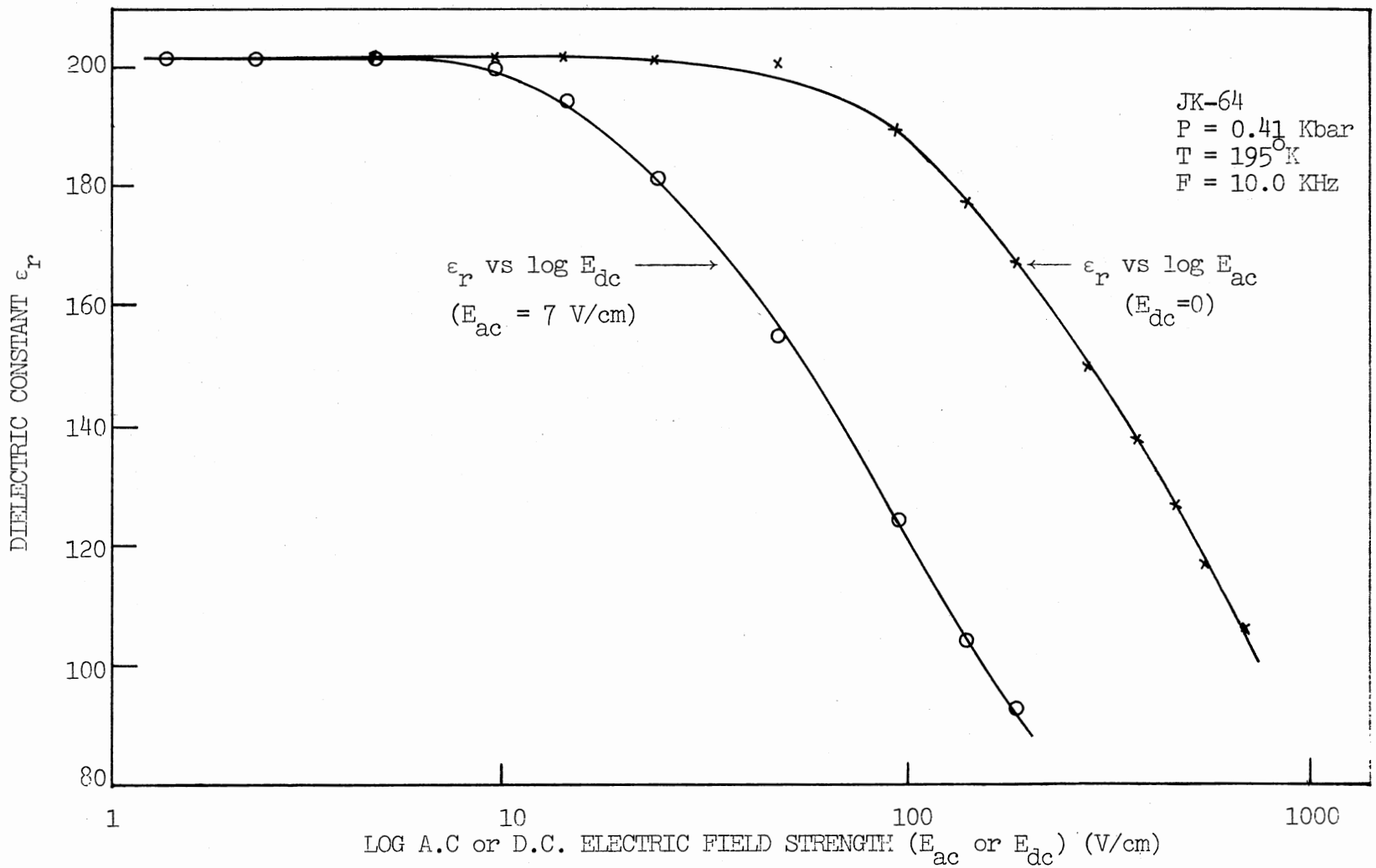

Figure 72. Dielectric Constant Versus Log (AC/DC Electric Field Strength)
(Polymer JK-64 at P=0.41 Kbar, T=195°K and F=10.0 KHz)

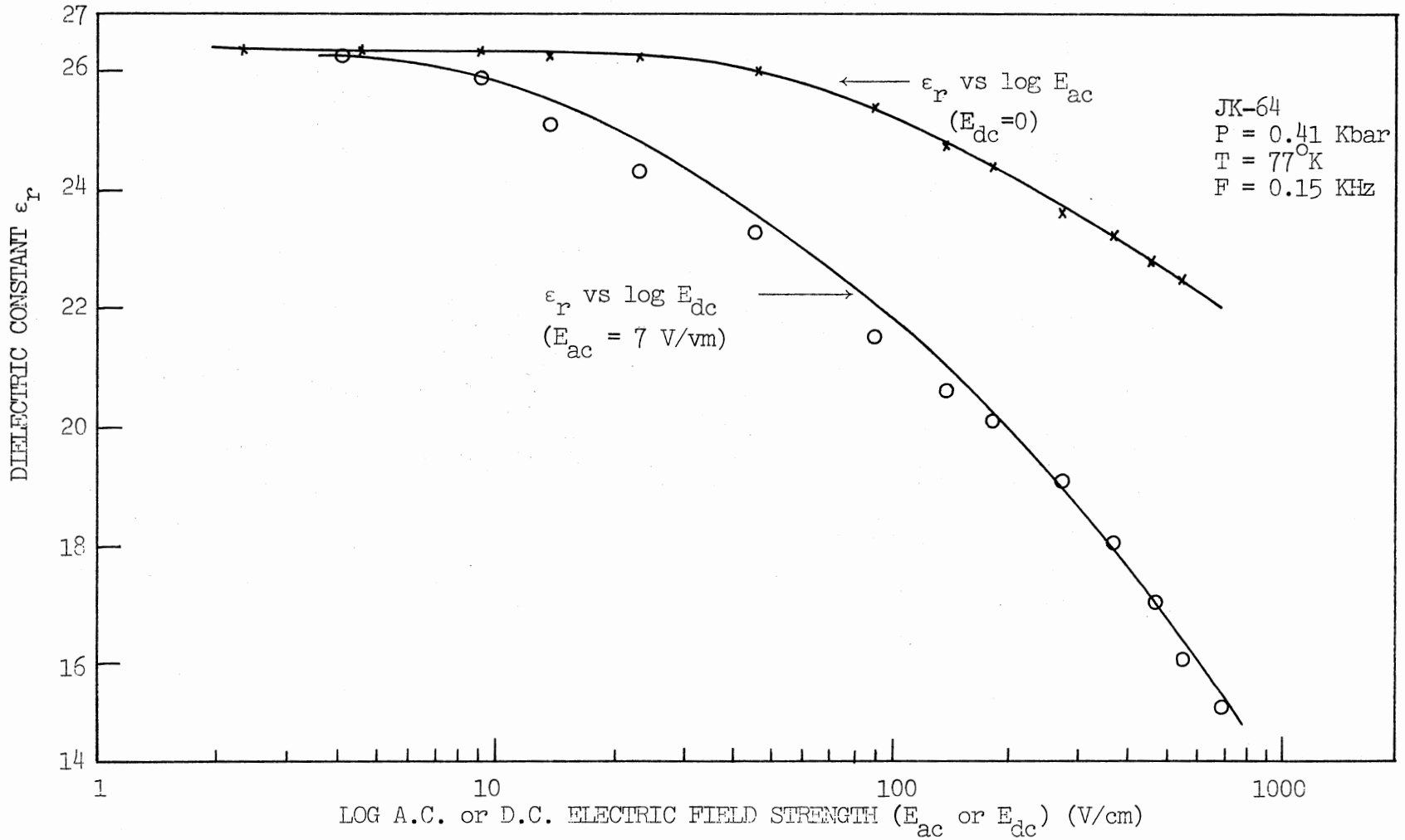

Figure 73. Dielectric Constant Versus Log (AC/DC Electric Field Strength) (Polymer JK-64 at P=0.41 Kbar, T=77°K and F=0.15 KHz)

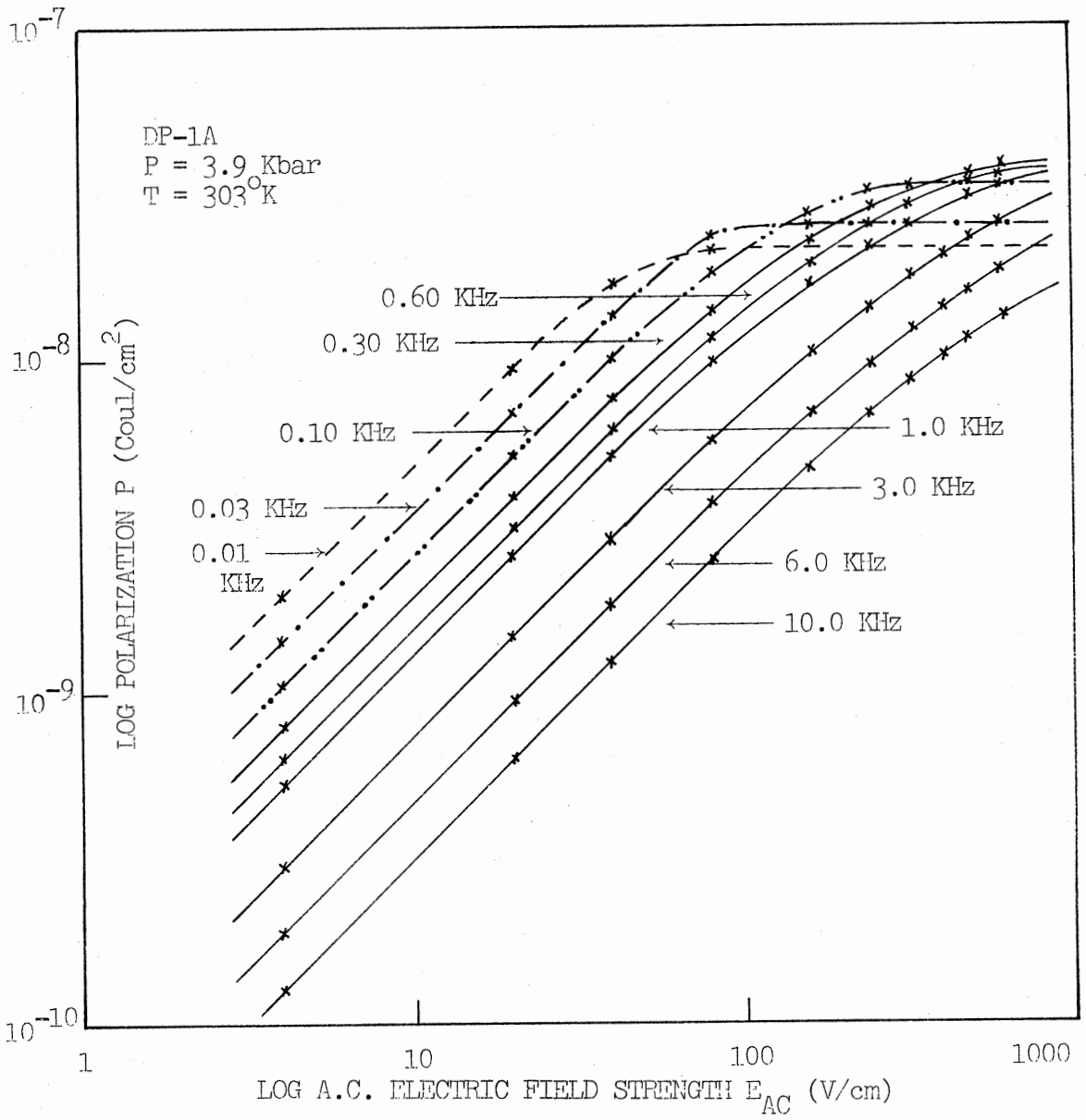

Figure 74. Log (Polarization) Versus Log (A.C. Electric Field Strength) (Polymer DP-1A at P=3.9 Kbar and T=303°K)

coulombic force due to opposite member in another chain (assumed fixed), the molecular length L is given by

$$L = \frac{8.0 \times 10^4 \ A^o}{\{\varepsilon_r \ E_{sat}(V/cm)\}^{\frac{1}{2}}} \tag{30}$$

where E_{sat} = a.c. electric field strength at the saturation of polarization. The molecular lengths calculated by this method are listed in Table IX.

3.9. A.C. Conductivity

3.9.1. Frequency and D.C. Electric Field Strength Dependence

Pollak and Geballe (1961) introduced a 'variable range mechanism' for the a.c. conductivity for crystalline silicon in the impurity conduction range. The frequency dependence is expressed by increasing a.c. conductivity σ_{AC} with increasing frequency ω as

$$\sigma_{AC}(\omega) = A \ \omega^s \tag{31}$$

where s ranges from $0.7 < s < 1$. The loss mechanism considered in the component of polarization which is lagging the applied field by 90^o, and Debye loss is due to hopping between pairs of centers at a distance R from each other with an energy difference W. At frequency ω, the contribution to $\sigma_{AC}(\omega)$ by any pair of centers would be

$$\sigma_{AC}(\omega) \propto \frac{1}{kT} \ \frac{e^2R^2}{(1 + \omega^2\tau^2)} \ \frac{1}{\tau} \{\exp(-W/kT)\} \tag{32}$$

Significant contribution came from pairs such that $W \simeq kT$ and $\omega\tau \simeq 1$, so that to a first approximation $\sigma_{AC}(\omega) \simeq \omega$.

Plots of log (a.c. conductivity σ_{AC}) versus log (frequency F) are shown in Figure 75 for polymer JK-64 at 'ambient' pressure P = 0 for temperatures T = 77°K, 90°K, 110°K, 130°K, 150°K, 170°K, 190°K, 210°K, 230°K, 250°K, 270°K and 293°K in the frequency range F = 0.15 KHz to 150 KHz, in Figure 76 for polymer DP-1A at P = 3.9 Kbar and T = 303°K for various d.c. bias electric field strengths E_{dc} = 0 V/cm, 40 V/cm, 80 V/cm and 160 V/cm in the frequency range F = 0.03 KHz to 150 KHz, in Figure 77 for polymer DP-1A at P = 3.9 Kbar and T = 273°K for E_{dc} = 0 V/cm, 40 V/cm, 80 V/cm and 160 V/cm in the frequency range 0.03 KHz to 150 KHz, and in Figure 78 for polymer JK-64 at 'ambient' pressure P = 0 and T = 303°K for E_{dc} = 0 V/cm and 222 V/cm in the frequency range 1.0 MHz to 100 MHz, and for polymer DP-1A at P = 0.32 Kbar, 1.1 Kbar and 3.3 Kbar at T = 303°K at E_{dc} = 0 V/cm in the frequency range 1.0 MHz to 100 MHz.

3.10. Comparison of Experimental Results with Pohl-Pollak Dielectric Theories

3.10.1. Pollak and Pohl Dielectric Theory (1975)

The frequency and electric field dependence of the real part of dielectric constant due to hyperelectronic (nomadic) polarization predicted by Pollak and Pohl (1975) is given by Equation (1) in Section 1.2.1. Figure 5 shows the theoretical plots of log (dielectric constant ε_r) versus log (frequency ω) based on Equation (1) for N = 300 and for electric field strength parameter K = 0.1 and K = 10 (K = eEL/kT).

As discussed in Section 1.2.1., for low electric field strengths

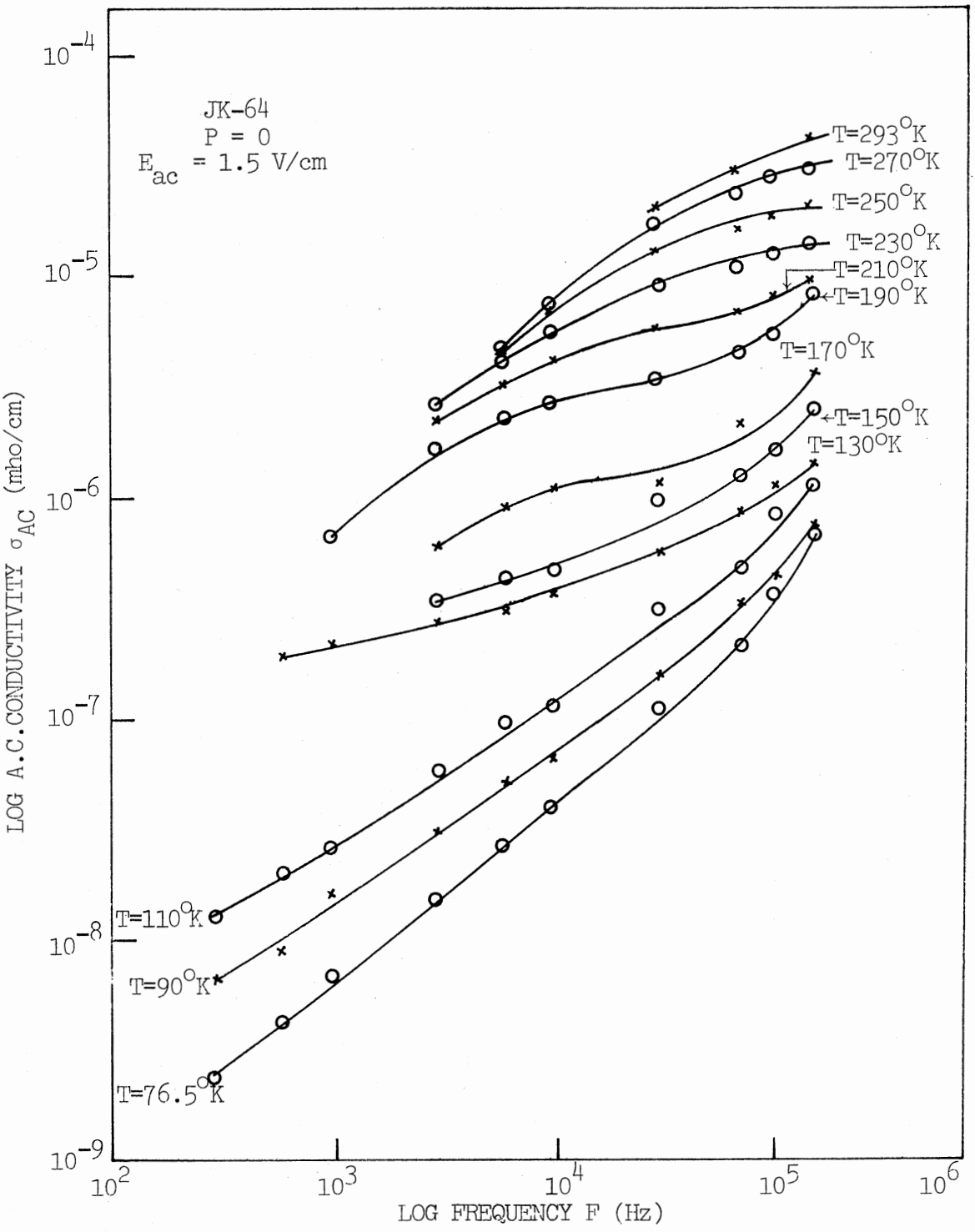

Figure 75. Log (A.C. Conductivity) Versus Log (Frequency) (Polymer JK-64 at P=0)

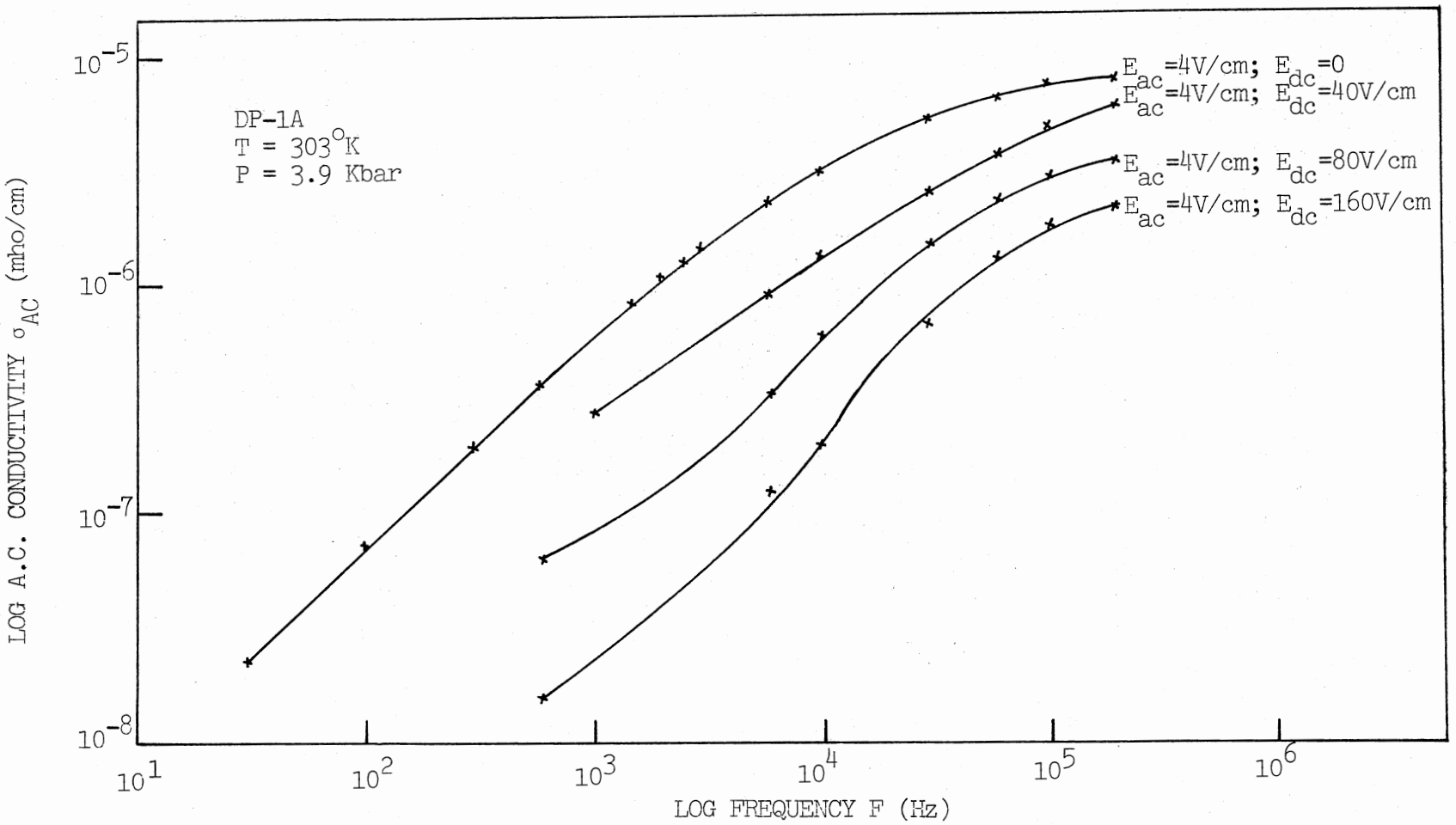

Figure 76. Log (A.C. Conductivity with D.C. Bias Electric Field Strength) Versus Log (Frequency) (Polymer DP-1A at P=3.9 Kbar and T=303°K)

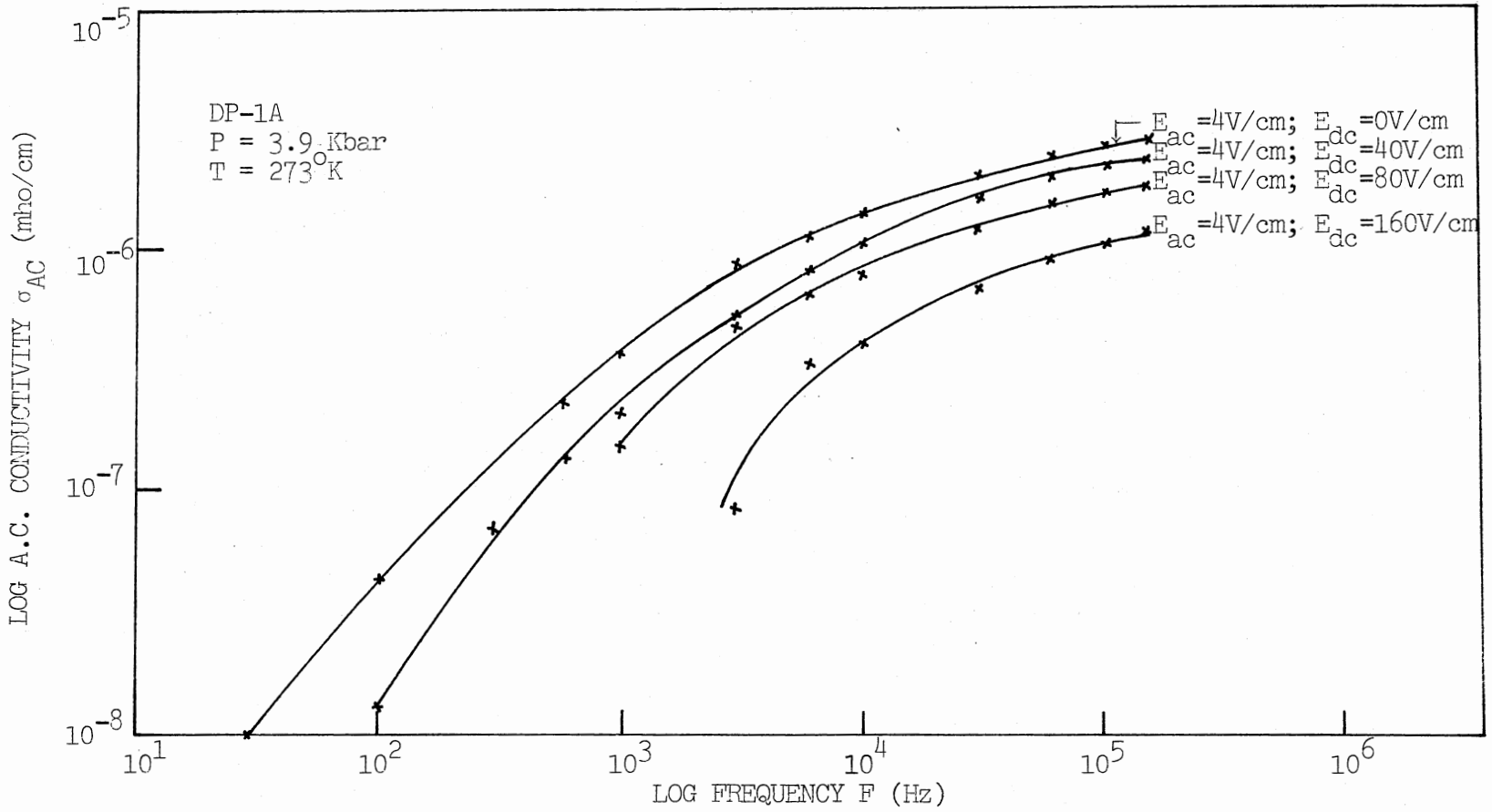

Figure 77. Log (A.C. Conductivity with D.C. Bias Electric Field Strength) Versus Log (Frequency) (Polymer DP-1A at P=3.9 Kbar and T=273°K)

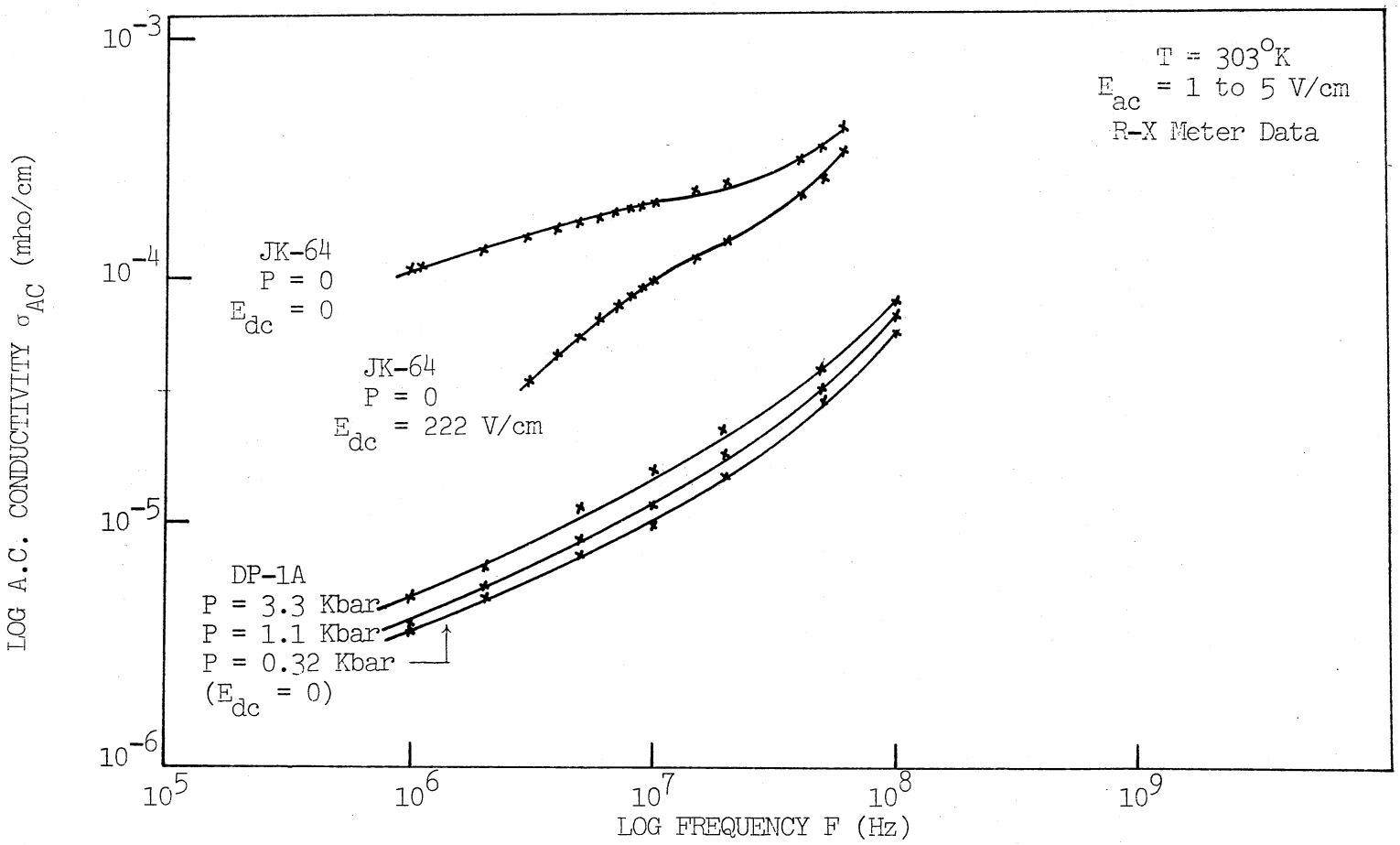

Figure 78. Log (A.C. Conductivity with D.C. Bias Field Strength) Versus Log (Frequency) (Polymers DP-1A and JK-64, Frequency Range from F=1.0 MHz to F=100 MHz)

(e.g., K = 0.1), the dielectric constant decreases with increasing frequency because the dipoles are unable to follow the variations of the higher frequency variations. The experimental plots in Figures 59 to 63, and the theoretical plots in Figures 5, 79 and 80 show this. Also the small polaron hopping rate is independent of the low d.c. bias field. Pollak and Pohl (1975) estimate that for the low dispersion frequencies of few KHz at room temperature observed in PAQR class of polymers, e.g., $\tau_1^{-1} \simeq 2\text{x}10^4$ s^{-1} and N = 1000, the hopping rate ω^o is approximately $2\text{x}10^9$ s^{-1} from the relation $\tau_\alpha = N^2/\{\omega^2\pi^2(\overline{K}^2+\alpha^2)\}$, where $\overline{K} = K/2\pi$.

For higher bias field strengths (e.g., K = 10), the decrease in dielectric constant at all frequencies is due to the reduction in the effective length of the polymer, as the bias electric field strength confines the carrier to a limited part of the macromolecule. At higher frequencies it is possible to obtain an increase in dielectric constant due to the enhanced hopping rate of polarons by the higher bias electric field strengths. This reversal of the change of dielectric constant with the higher d.c. bias electric field strength, from $(-\partial\varepsilon_r/\partial E_{dc})$ to $(+\partial\varepsilon_r/\partial E_{dc})$ occurs in Figure 5 at $\omega/\omega^o \simeq 10^{3.5}$, so with a hopping rate $\omega^o \simeq 10^9$ s^{-1}, the 'cross-over' frequency is approximately 15 KHz.

Figures 79 and 80 show the theoretical plots of log (dielectric constant ε_r) versus log (frequency F) based on Equation (1) in Section 1.2.1. In the experiments E_{dc} was kept to less than 1000 V/cm to limit the dissipation of heat in the samples to a minimum (<0.1 watt). In Figure 79 T = 303°K, s = 15 A°, W = 0.1 eV, $n = 8\text{x}10^{17}/cm^3$, hopping rate $\omega^o \simeq 10^8$ s^{-1} for a dispersion frequency ν_m = 3 KHz. It shows plots for N = 100, 300 and 500 for E_{dc} = 0.1 V/cm ($K \simeq 10^{-4}$) and for E_{dc} =

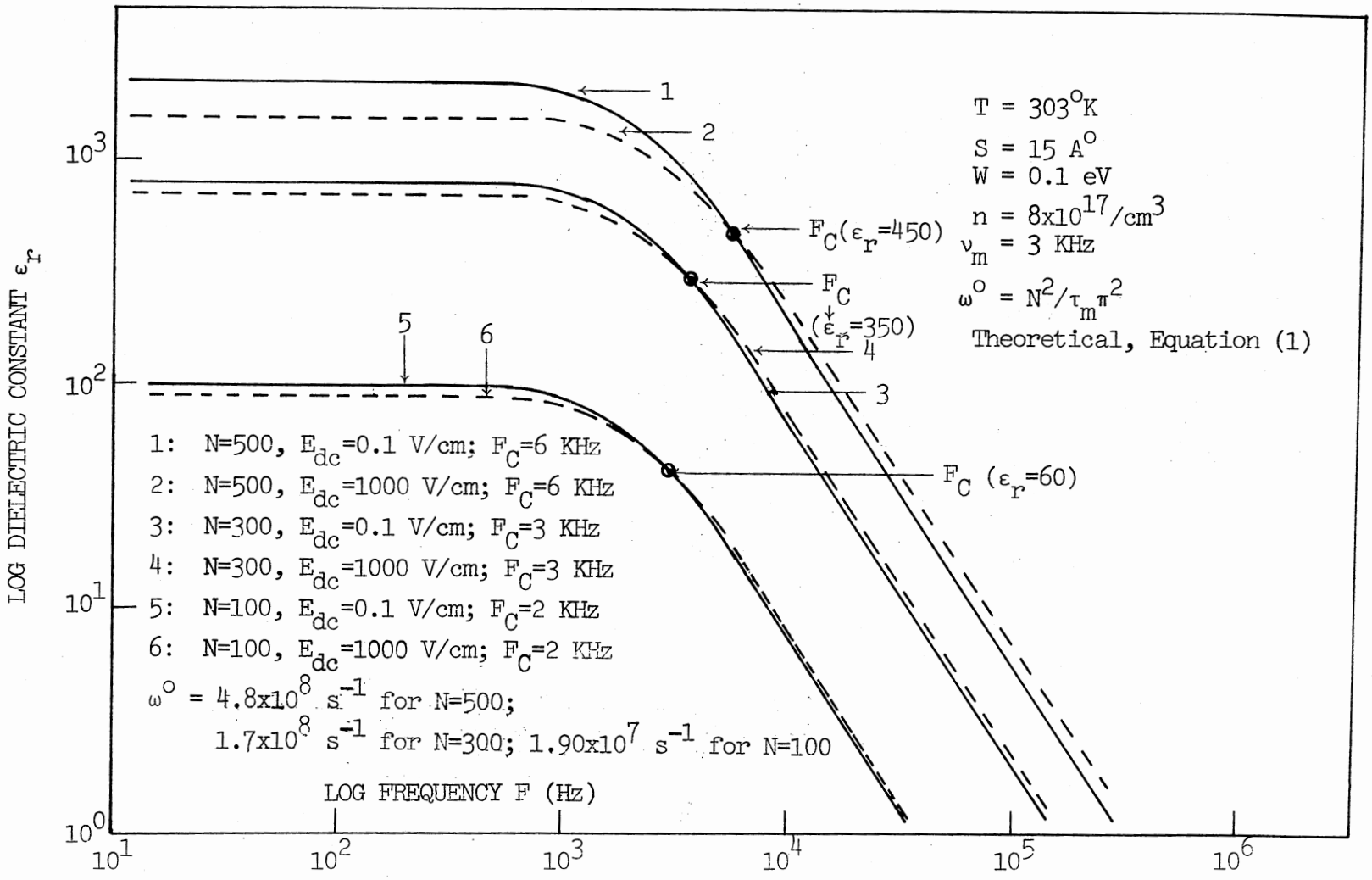

Figure 79. Log (Dielectric Constant with D.C. Bias Electric Field Strength) Versus Log (Frequency) (Theoretical, Equation (1))

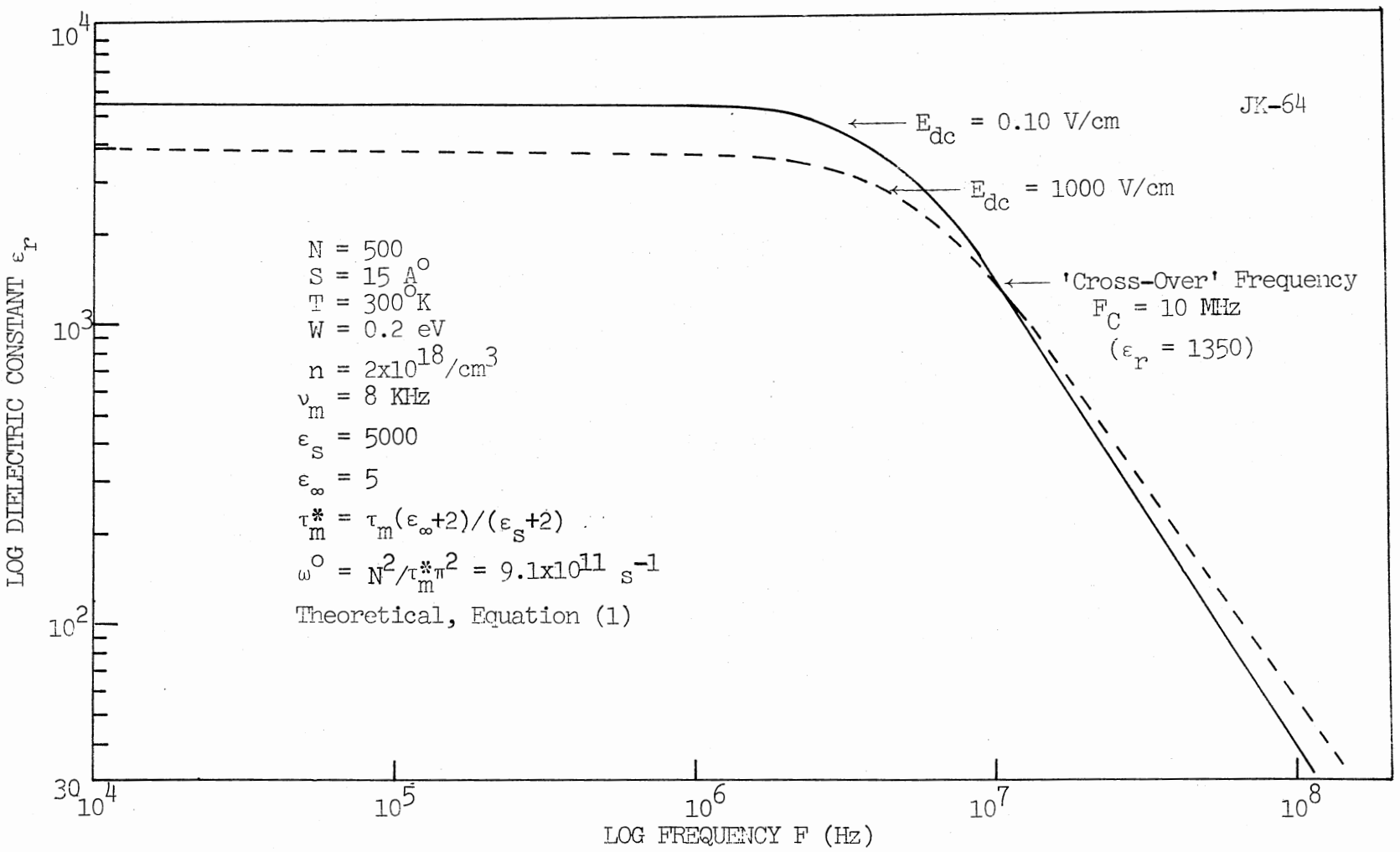

Figure 80. Log (Dielectric Constant with D.C. Electric Field Strength) Versus Log (Frequency) (N=500, T=300°K) (JK-64) (Theoretical, Equation (1))

1000 V/cm (K ≃ 1) giving a 'cross-over' frequency F_C ≃ 3KHz. In Figure 80 T = 300°K, s = 15 A°, W = 0.2 eV, n = $2x10^{18}/cm^3$. To take into account the interaction of polarizable centers and the local electrical field, the relaxation time was modified to $\tau_m^* = \tau_m\{(\varepsilon_\infty+2)/(\varepsilon_s+2)\}$ and the hopping rate $\omega^o = (N^2/\tau_m^*\pi^2)$. With a dispersion frequency of 8 KHz (for JK-64), ε_s = 5000, ε_∞ = 5, $\omega^o = 9x10^{11}$ s^{-1}. Figure 80 shows the theoretical plots for N = 500 for E_{dc} = 0.1 V/cm (K = $2.9x10^{-4}$) and for E_{dc} = 1000 V/cm (K = 2.9) giving a 'cross-over' frequency F_C = 10 MHz.

Figure 64 shows the experimental plots for polymer JK-64 at 'zero' pressure and T = 296°K. This expanded plot of log $\{10(\varepsilon_r-1)\}$ versus log (frequency F) shows a reversal of dielectric constant $(-\partial\varepsilon_r/\partial E_{dc})$ to $(+\partial\varepsilon_r/\partial E_{dc})$ for a change in the d.c. bias field strength E_{dc} from 0 to 200 V/cm, giving a 'cross-over' frequency F_C = 3.4 MHz with ε_r = 42.8.

By comparing Figures 64 and 80, the experimental evidence does show the increase in dielectric constant with higher bias field strengths in certain ranges of frequencies as predicted by Pollak and Pohl (1975). The theoretical 'cross-over' frequency F_C = 10 MHz, where as the experimental 'cross-over' frequency F_C = 3.4 MHz.

Figure 6 shows the theoretical plots of log (a.c. conductivity σ_{AC}) versus log (frequency ω) based on Equation (2) for N = 300 for K = 0.1 and 10. Figure 81 shows the theoretical plots of log (a.c. conductivity σ_{AC}) versus log (frequency F) for N = 100, 300 and 500 at T = 303°K, s = 15 A°, W = 0.1 eV, n = $8x10^{17}/cm^3$, $\omega^o \simeq 10^8$ s^{-1} for E_{dc} = 0.1 V/cm and 1000 V/cm. Figure 82 shows the theoretical plots of log (a.c. conductivity σ_{AC}) versus log (frequency F) for N = 500 at T = 300°K, s = 15 A°, W = 0.2 eV, n = $2x20^{18}/cm^3$, $\omega^o \simeq 9x10^{11}$ s^{-1} for E_{dc} = 0.1 V/cm and 1000 V/cm. For the whole range of frequencies, the a.c. conducti-

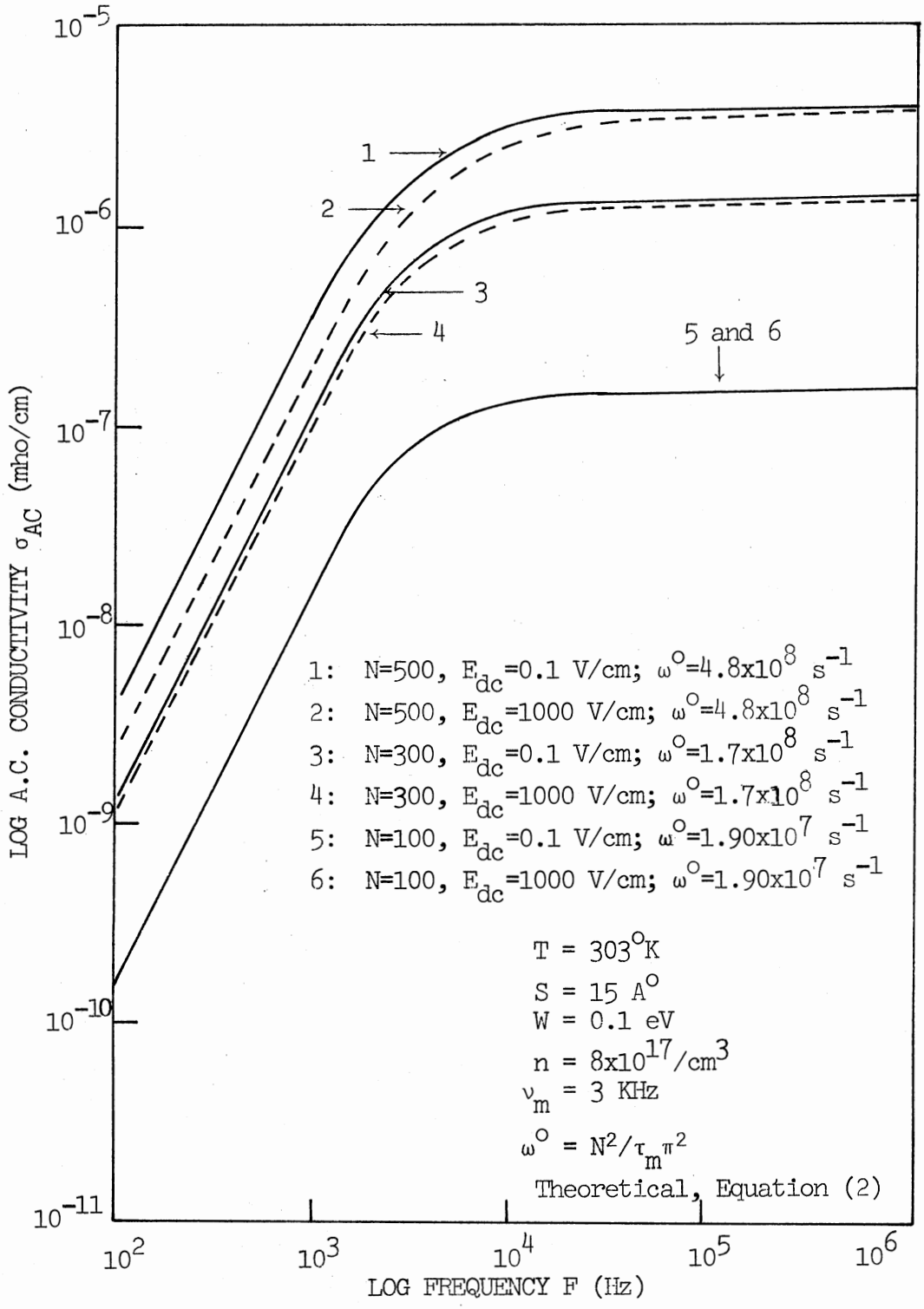

Figure 81. Log (A.C. Conductivity with D.C. Bias Electric Field Strength) Versus Log (Frequency) (Theoretical, Equation (2))

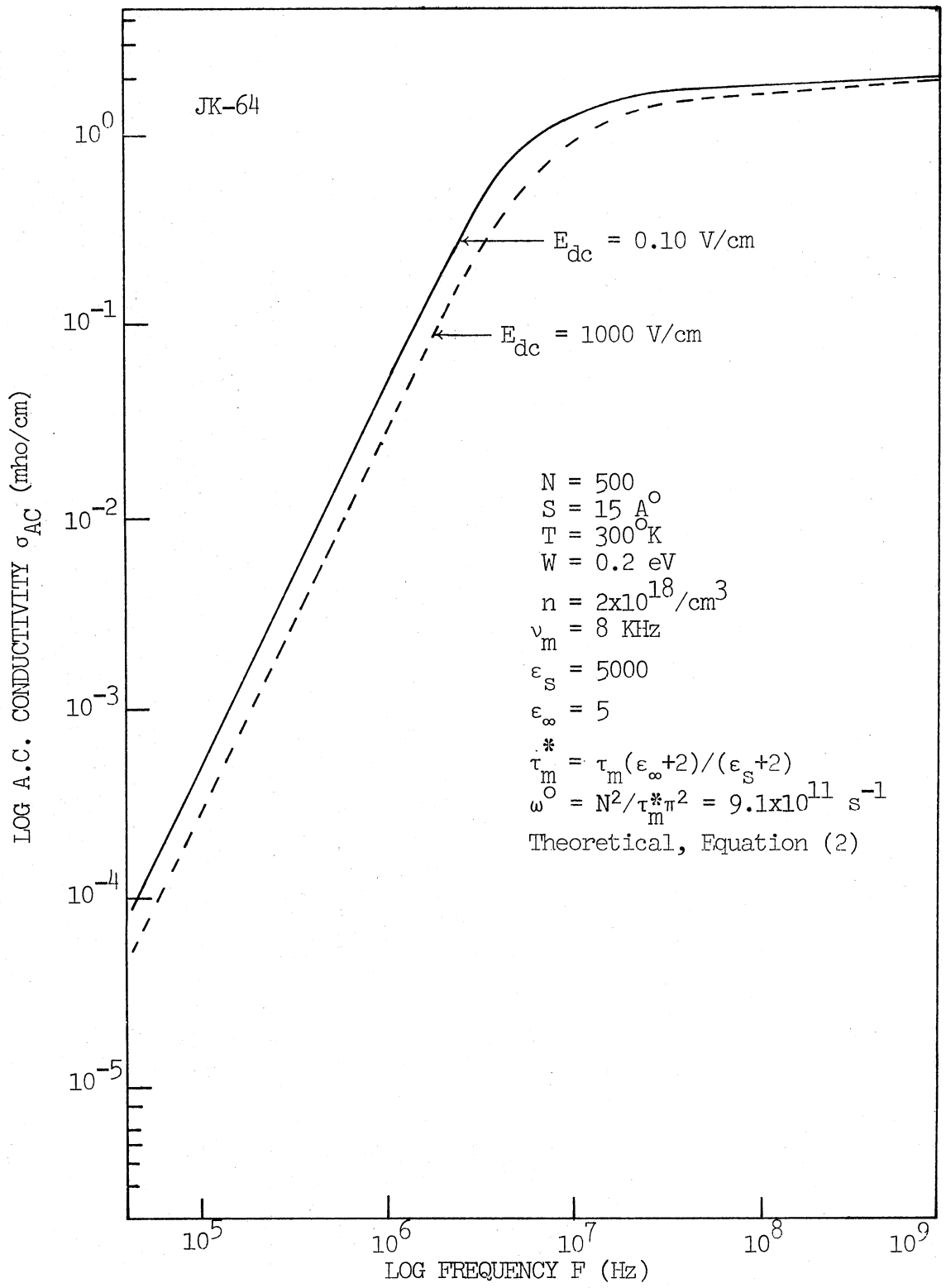

Figure 82. Log (A.C. Conductivity with D.C. Bias Voltage) Versus Log (Frequency) (N=500, T=300°K) (JK-64) (Theoretical, Equation (2))

vity is reduced by the d.c. bias field strength and shows saturation at higher frequencies, as shown also in the experimental plots of Figures 75 to 77.

In comparison it can be said that at least qualitatively, the experiments agree with the Pollak and Pohl dielectric theory (1975).

3.10.2 Pohl and Pollak Dielectric Theory (1977)

Pohl and Pollak (1977) have calculated the contribution of hyper-electronic (nomadic) polarization to the dielectric constant as given by Equation (15) in Section 1.2.2. Figure 7 shows the theoretical plots of log (dielectric constant ε_r) versus log (a.c. electric field strength E_{AC}) (d.c. bias electric field strength $E_{DC} = 0$, i.e., 'total'), and log (dielectric constant ε_r) versus log (d.c. bias electric field strength E_{DC}) (a.c. bias electric field strength E_{AC} = small, i.e., 'differential') based on Equation (15) for N = 100, s = 5 A^o, T = 300^{o}K, W = 0.1 eV and $\varepsilon_o^* = 6$. Figure 83 shows the theoretical plots of dielectric constant ε_r ($\Delta\varepsilon_{t,d}$) versus log (AC/DC electric field strength) for N = 100, s = 15 A^o, T = 303^{o}K, W = 0.1 eV and $\varepsilon_o^* = 5$. Experimental plots are shown in Figures 65 to 73. By comparison it can be said that at least qualitatively experiments agree with the Pohl and Pollak dielectric theory (1977).

Since the static dielectric constant $\varepsilon_r \propto L^2$, this theory gives us one more way to estimate the average molecular lengths of the polymers. Figure 84 shows the theoretical plots of log (dielectric constant ε_r) versus log (N^2) (L = Ns) based on Equation (15) in Section 1.2.2. for temperatures T = 303^{o}K, 273^{o}K and 195^{o}K for s = 15 A^o, W = 0.2 eV, $n = 2\times10^{18}/cm^3$, $\varepsilon_o^* = 5$, E_{ac} = 0.1 V/cm and E_{dc} = 0 V/cm. Table IX lists

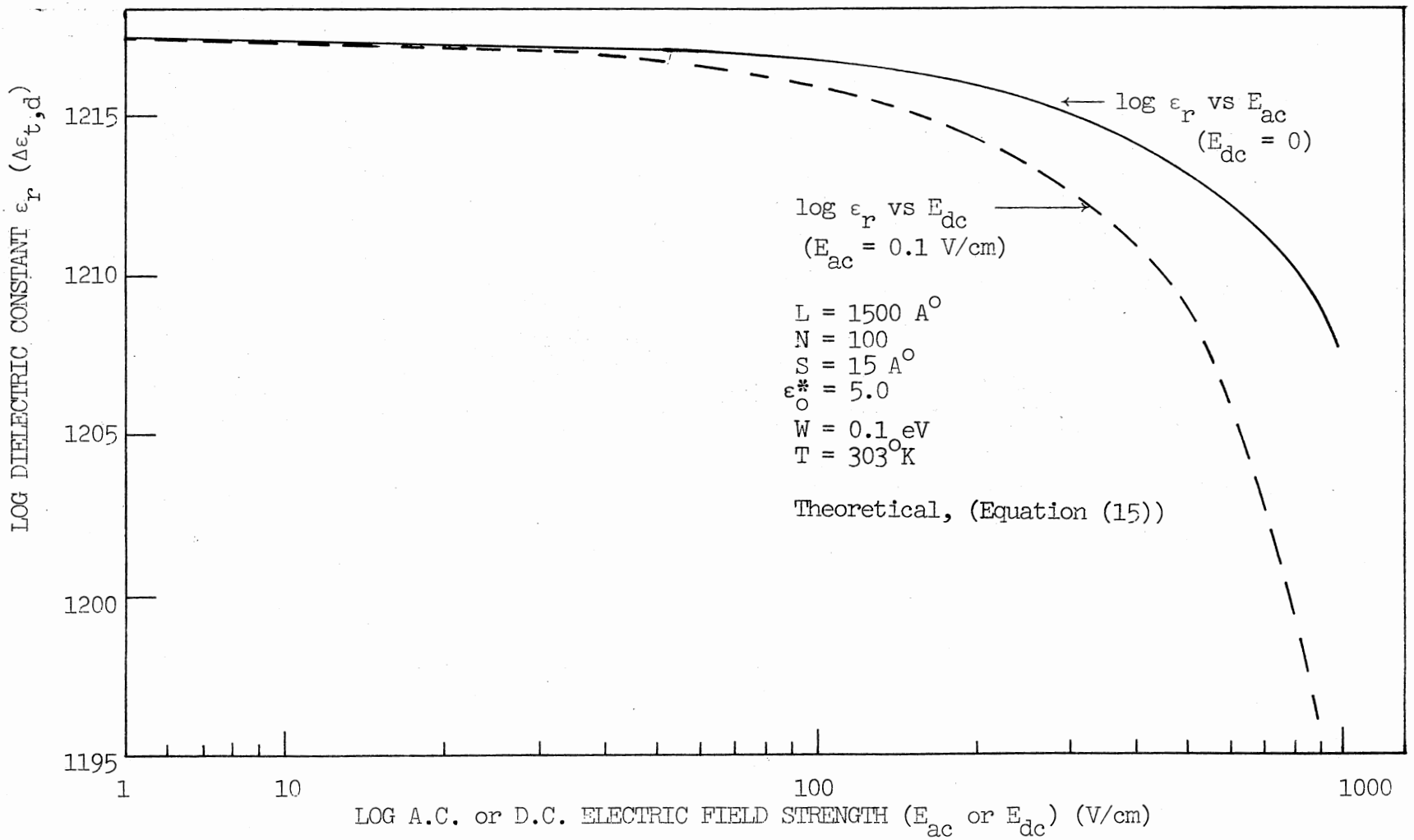

Figure 83. Dielectric Constant Versus Log (AC/DC Electric Field Strength) (N=100, T=303°K) (Theoretical, (15))

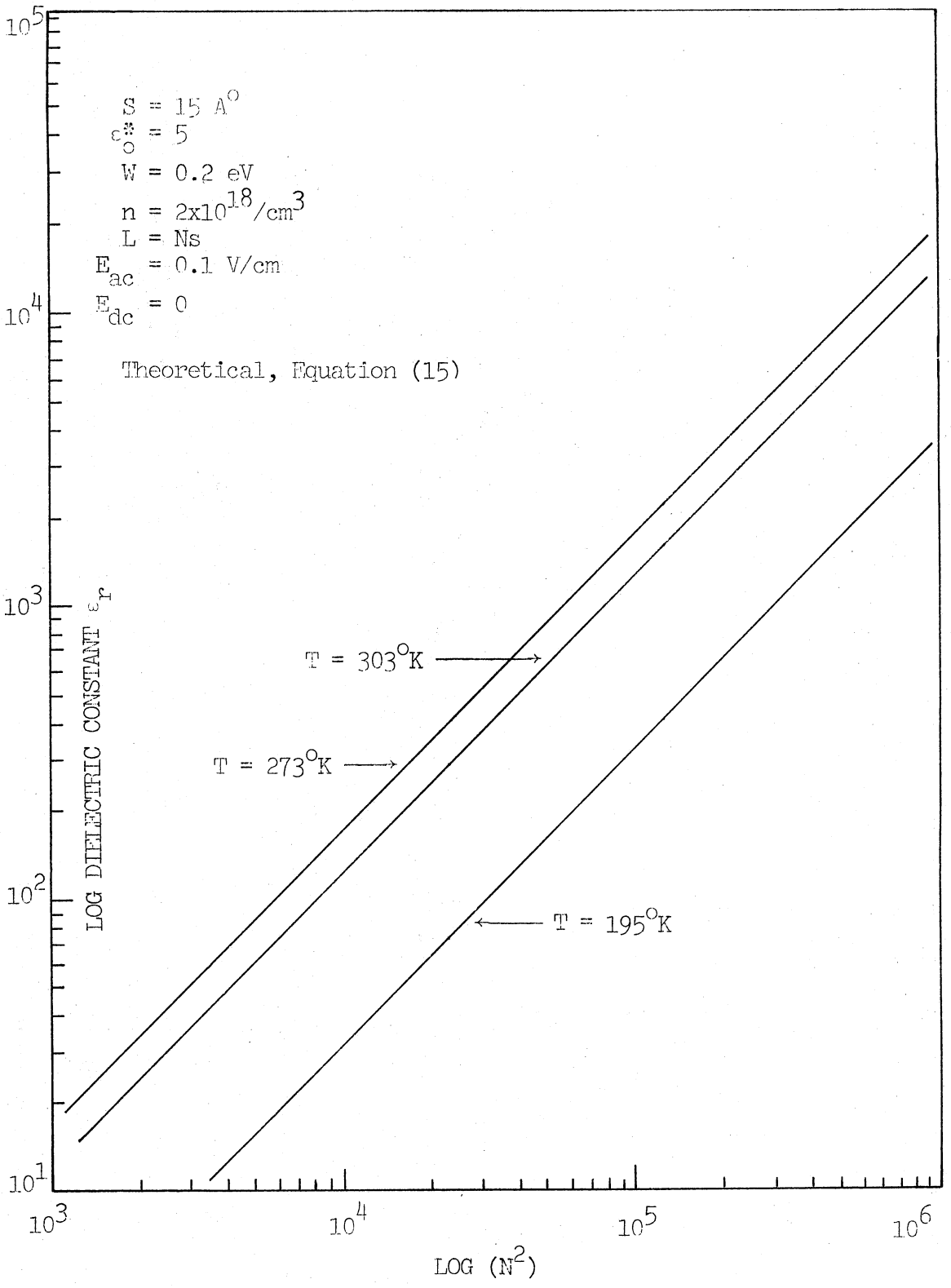

Figure 84. Log (Dielectric Constant) Versus Log (N^2) (Theoretical, Equation (15))

the molecular lengths of selected polymers obtained by this method.

3.11. Average Molecular Length

X-ray diffraction of polymer DP-1A shows a strong 3.5 A^{o} peak characteristic of the Van der Waals spacing between molecules with up to six subsidiary peaks of lesser intensity (Wyhof, 1970). Because of solubility problems, the usual solution techniques such as light scattering, viscosity, etc., cannot be used to estimate the molecular lengths of these polymers. Alternate methods for estimating the molecular lengths are based on the electronic properties of these polymers: (a) From the temperature dependence of electron spin resonance, one can obtain an effective spin density at each temperature, from which the activation energy E_S for unpaired electron formation can be obtained. By assuming that E_S is equal to the energy E needed to promote an electron from the highest occupied molecular orbital to the lowest empty molecular orbital, and that the unpairing energy is so small that $^1E \simeq {}^3E$, one obtains $^1E = h^2/(4m\ell_o Z)$, where molecular length $L = \ell_o Z$, h = Planck's constant, m = electron mass and ℓ_o = C-C bond length of Z atoms in a linear segment (Pohl, 1967; Pohl, 1968; Hartman, 1968; and Wyhof 1970); (b) By the d.c. electric field strength dependence of conductivity (Rosen and Pohl, 1966; Pohl, 1967; Hartman, 1968; Wyhof, 1970; and Equations (26) and (27) in Section 3.7.); (c) From the observed saturation of a.c. electrical polarization with a.c. electric field strength (Pohl, 1974; and Equation (30) in Section 3.8.4.); and (d) From the absolute dielectric constant based on the dielectric theories by Pollak and Pohl (1975) (Equation (1) in Section 1.2.1.), and Pohl and Pollak (1977) (Equation (15) in Section 1.2.2.). Table IX lists the average

molecular lengths of the selected polymers obtained from the above mentioned methods (b), (c) and (d).

3.12. Thermoelectric Power

The detailed theory for the thermoelectric power of a simple band type intrinsic semiconductor was given by Johnson and Lark-Horowitz (1953) and by Johnson (1956). The thermoelectric power S is given by

$$S = \frac{k}{e}\left\{\frac{(\mu_e/\mu_h) - 1}{(\mu_e/\mu_h) + 1}\right\}\left\{\frac{E_g}{2kT} + 2 + \frac{a}{2k}\right\} \qquad (33)$$

where μ_e and μ_h are the electron and hole mobilities, E_g is the width of band gap and $E_g \simeq E_o + aT$.

For the two polymers DP-1A and JK-64, Figure 85 shows plots of thermoelectric emf ΔV versus temperature gradient ΔT, and Figure 86 shows plots of thermoelectric power S ($\Delta V/\Delta T$) versus mean temperature T. The thermoelectric power (Seebeck coefficient) was found to be positive at the cold electrode, indicating holes (p-type) as the dominant carriers for both the polymers DP-1A and JK-64. Table XI lists the thermoelectric power results for the two polymers.

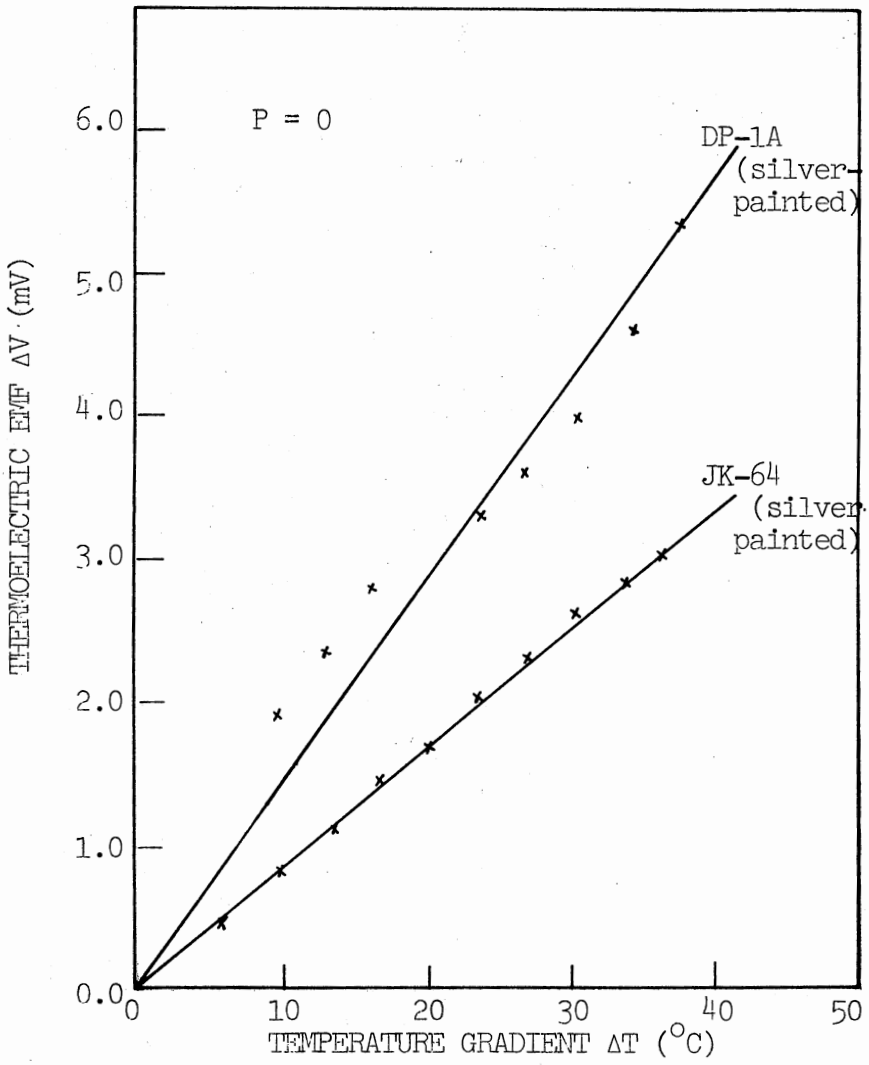

Figure 85. Thermoelectric Emf Versus Temperature Gradient (Seebeck Coefficient S $=\Delta V/\Delta T$)

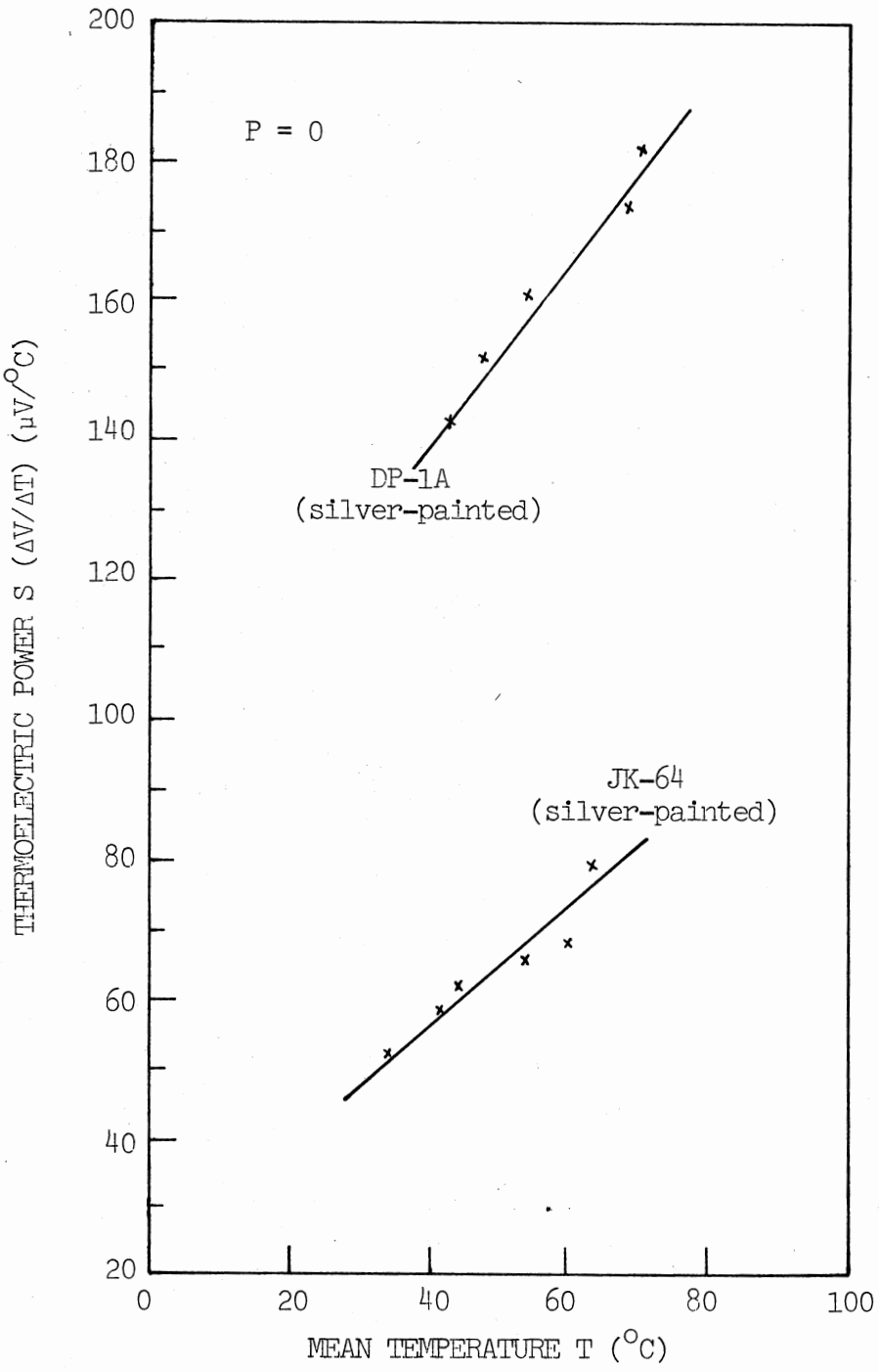

Figure 86. Thermoelectric Power S ($\Delta V/\Delta T$) Versus Mean Temperature

TABLE XI

THERMOELECTRIC POWER OF SELECTED POLYMERS

Sample Name	Pressure (Kbar)	Sample Size	σ_{DC}(mho/cm) at 25°C	Seebeck Coefficient S = $\Delta V/\Delta T$ ($\mu V/^{\circ}C$) at 25°C	dS/dT ($\mu V/^{\circ}C$ /°C)
DP-1A	0.0	d=9.5mm Th=27.8mils Silver-Painted	1.16×10^{-6}	+140, p-type	-1.13
JK-64	0.0	d=4.1mm Th=26.6mils Silver-Painted	3.87×10^{-5}	+82.0, p-type	-0.61

CHAPTER IV

REVIEW OF ELECTRO-ACTIVE PAQR POLYMERS

The polyacenequinone radical (PAQR) class of electro-active semiconducting aromatic polymers have been synthesized, and their electrical properties have been studied by Pohl (1961), Pohl (1962), Pohl and Engelhardt (1962), Pohl and Opp (1962), Pohl et al. (1963), Pohl and Chartoff (1964), Mason et al. (1967), Hartman (1968), Wyhof (1970), Pollak and Pohl (1975), Saha et al. (1976a and 1976b), Pethig and Pohl (1977), Pohl and Pollak (1977), and Burnay and Pohl (1978). Polymeric semiconductors have been reviewed by Seanor (1972), Josefowicz (1973), Williams (1973), Paushkin et al. (1974), Pohl (1974), Kryszewski (1975a and 1975b), Sawa (1975), and Wynne and Street (1982). Organic semiconductors have been reviewed by Fukayama (1974), Karl (1974), Kryszewski (1974), Masuda and Silver (1974), Seki (1974), Goodings (1975) and Silins (1975).

4.1. Syntheses of Electro-Active PAQR Polymers

Aromatic hydrocarbon derivatives/acenes form highly conjugated conductive polymers by a condensation reaction with aromatic acids/anhydrides in the presence of a catalyst (e.g., zinc chloride) at temperatures ranging from approximately 300 to 450^{o}C. The product is then ground and purified by exhaustive extraction with boiling solvents. These PAQR class of polymers are usually hard, black, insoluble (but

swellable in certain aromatic solvents), stable (up to approximately 500°C in vaccum or inert gas), cross-linked, quasi one- and two-dimensional, with spin concentrations of 10^{18} to 10^{20} spins/gm. Table XII lists the compositions of the selected electro-active PAQR polymers.

4.2. Possible Structures of Electro-Active PAQR Polymers

Figure 87 shows three possible structures, as yet unproven, proposed for a typical PAQR class of polymer DP-1A (anthraquinone + pyromellitic dianhydride) by Rosen and Pohl (1966). The monomer unit has a length $s = 12\ell$ ($\simeq 15$ A°), where ℓ = projected C-C bond length = $(\sqrt{3}/2)\ell_0$ and ℓ_0 = C-C bond length (1.4 A°).

4.3. Types of Conjugation

Conjugation is the alternation of single and double bonds in the chemical structures of polymers. The terms 'ekaconjugation' and 'rubiconjugation' have been introduced by Pohl (Pohl and Engelhardt, 1962; and Pohl, 1968) to differentiate structures that favor enhanced electronic properties from those that do not. Ekaconjugated structures possess long range electronic orbital delocalization with least molecular defects, where as, in rubiconjugated structures, defects give rise to limited delocalization. The PAQR class of electro-active polymers are ekaconjugated according to this nomenclature. The importance of long range conjugation to conduction mechanisms was emphasized by Eley (1959), and its special meaning to polymers by Mrozowski (1952a, 1952b, 1953 and 1960), Mark (1957) and Brillouin (1962).

TABLE XII

COMPOSITIONS OF ELECTRO-ACTIVE PAQR POLYMERS

Sample Number	Sample Name	Hydrocarbon Derivative/ Acene	Acid/Anhydride	Reaction Temperature (°C)
1	DP-1A Pohl and Chartoff (1964)	Anthraquinone (a)	Pyromellitic Dianhydride (PMA) (b)	306
2	JK-64 Kho and Pohl (1969)	Pyrene (c)	O-Iodobenzoic Acid (OIBA) (d)	300
3	JM-85A Mason et al. (1967)	Phenothiazine (e)	PMA (b)	295
4	VJ-1	β-Bromonaphthalene (f)	OIBA (d)	306
5	LD-2	β-Chloroanthraquinone (BCAQ) (g)	Tetrachloro-phthalic Anhydride (Cl_4PA) (h)	450
6	LD-3	Pyrene (c)	Cl_4PA (h)	450
7	LD-4-43	Violanthrone (i)	Cl_4PA (h)	450
8	LD-5	Anthraquinone (a)	Tetrabromophthalic Anhydride (Br_4PA) (j)	450
9	LD-6	BCAQ (g)	Br_4PA (j)	450
10	LD-7	Pyrene (c)	Br_4PA (j)	450
11	LD-8	Violanthrone (i)	Br_4PA (j)	450
12	LD-10	BCAQ (g)	PMA (b)	450
13	LD-11	Pyrene (c)	PMA (b)	450
14	LD-12-43	Violanthrone (i)	PMA (b)	450
15	LD-19-41	Tetrachloropyrene (k)	Cl_4PA (h)	450

TABLE XII (Continued)

Sample Number	Sample Name	Hydrocarbon Derivative/ Acene	Acid/Anhydride	Reaction Temperature (°C)
16	LD-20-39	Pyrene (c)	OIBA (d)	450
17	LD-21	Triphenylene (l)	PMA (b)	450
18	LD-22	Chrysene (m)	PMA (b)	450
19	LD-23	Phenazine (n)	PMA (b)	450
20	LD-24	Bianthrone (o)	PMA (b)	450
21	LD-25-64	Acridine (p)	PMA (b)	450
22	LD-27-65	6,13-Dihydrodibenzo-phenazine (DHDBP) (q)	PMA (b)	450
23	LD-28-65	1,10-Phenanthroline (r)	PMA (b)	450
24	LD-29-65	Phenothiazine (e)	PMA (b)	450
25	LD-30-66	Thianthrene (s)	PMA (b)	450
26	LD-31	Acridine (p)	Cl_4PA (h)	450
27	LD-32	2-Chlorophenothiazine (t)	Cl_4PA (h)	450
28	LD-33	DHDBP (q)	Cl_4PA (h)	450
29	LD-34	1,10-Phenanthroline (r)	Cl_4PA (h)	450
30	LD-35	Phenothiazine (e)	Cl_4PA (h)	450
31	LD-36	Thianthrene (s)	Cl_4PA (h)	450
32	LD-37	Acridine (p)	Br_4PA (j)	450
33	LD-38	2-Chlorophenothiazine (t)	Br_4PA (j)	450
34	LD-39	DHDBP (q)	Br_4PA (j)	450

TABLE XII (Continued)

Sample Number	Sample Name	Hydrocarbon Derivative/ Acene	Acid/Anhydride	Reaction Temperature (^{o}C)
35	LD-40	1,10-Phenanthroline (r)	Br_4PA (j)	450
36	LD-41	Phenothiazine (e)	Br_4PA (j)	450
37	LD-42	Thianthrene (s)	Br_4PA (j)	450
38	LD-43	5,12-Naphthaacene-quinone (u)	Cl_4PA (h)	450
39	LD-44	Phenazine (n)	Cl_4PA (h)	450
40	LD-45	Perylene (v)	PMA (b)	450
41	LD-47	Benzanthrone (w)	Cl_4PA (h)	450
42	LD-48	Benzanthrone (w)	Br_4PA (j)	450

Note: The ratio (moles) Acene:Anhydride:Catalyst (Zinc Chloride) is 1:1:1 for polymers JK-64 and VJ-1, and 1:1:2 for the other polymers. The chemical structures of compounds (a) to (w) in Table XII are given below.

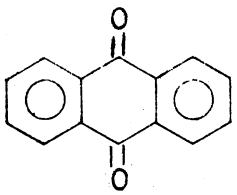

(a) Anthraquinone

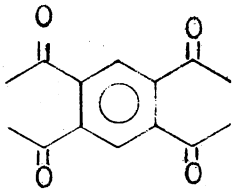

(b) Pyromellitic Dianhydride

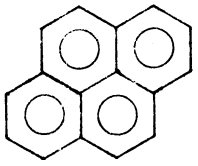

(c) Pyrene

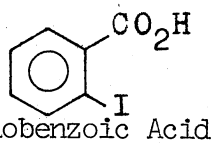

(d) O-Iodobenzoic Acid (OIBA)

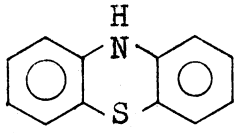

(e) Phenothiazine

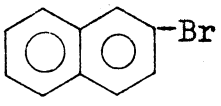

(f) β-Bromonaphthalene

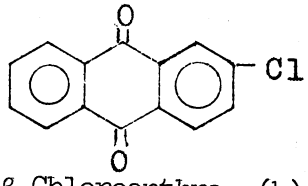

(g) β-Chloroanthraquinone (BCAQ)

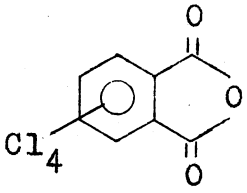

(h) Tetrachloropthalic Anhydride (Cl_4PA)

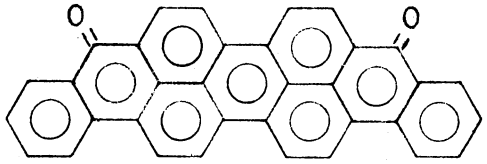

(i) Violanthrone

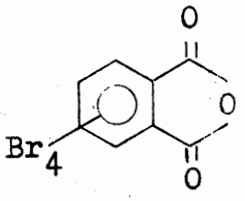

(j) Tetrabromophthalic Anhydride (Br_4PA)

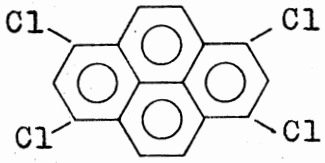

(k) Tetrachloropyrene

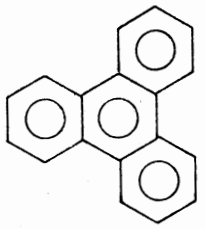

(l) Triphenylene

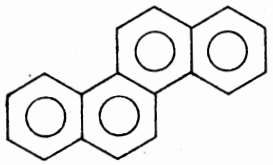

(m) Chrysene

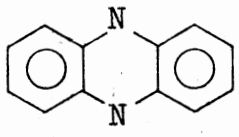

(n) Phenazine

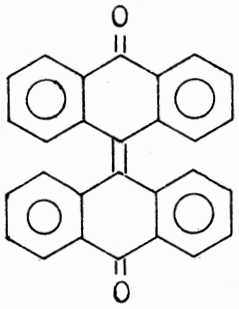

(o) Bianthrone

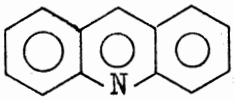

(p) Acridine

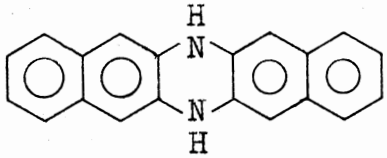

(q) 6,13-Dihydrodibenzophenazine (DHDBP)

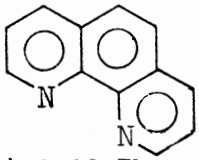

(r) 1,10-Phenanthroline

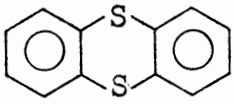

(s) Thianthrene

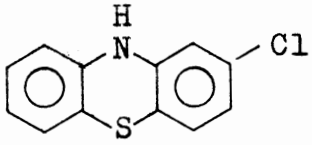

(t) 2-Chlorophenothiazine

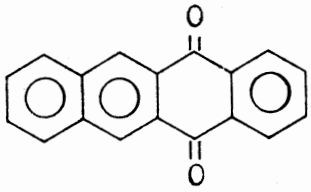

(u) 5,12-Naphthacenequinone

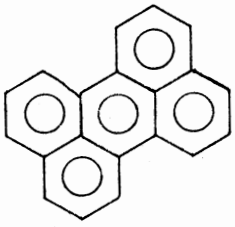

(v) Perylene

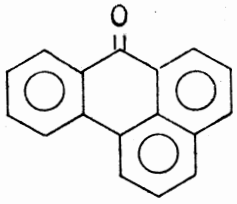

(w) Benzanthrone

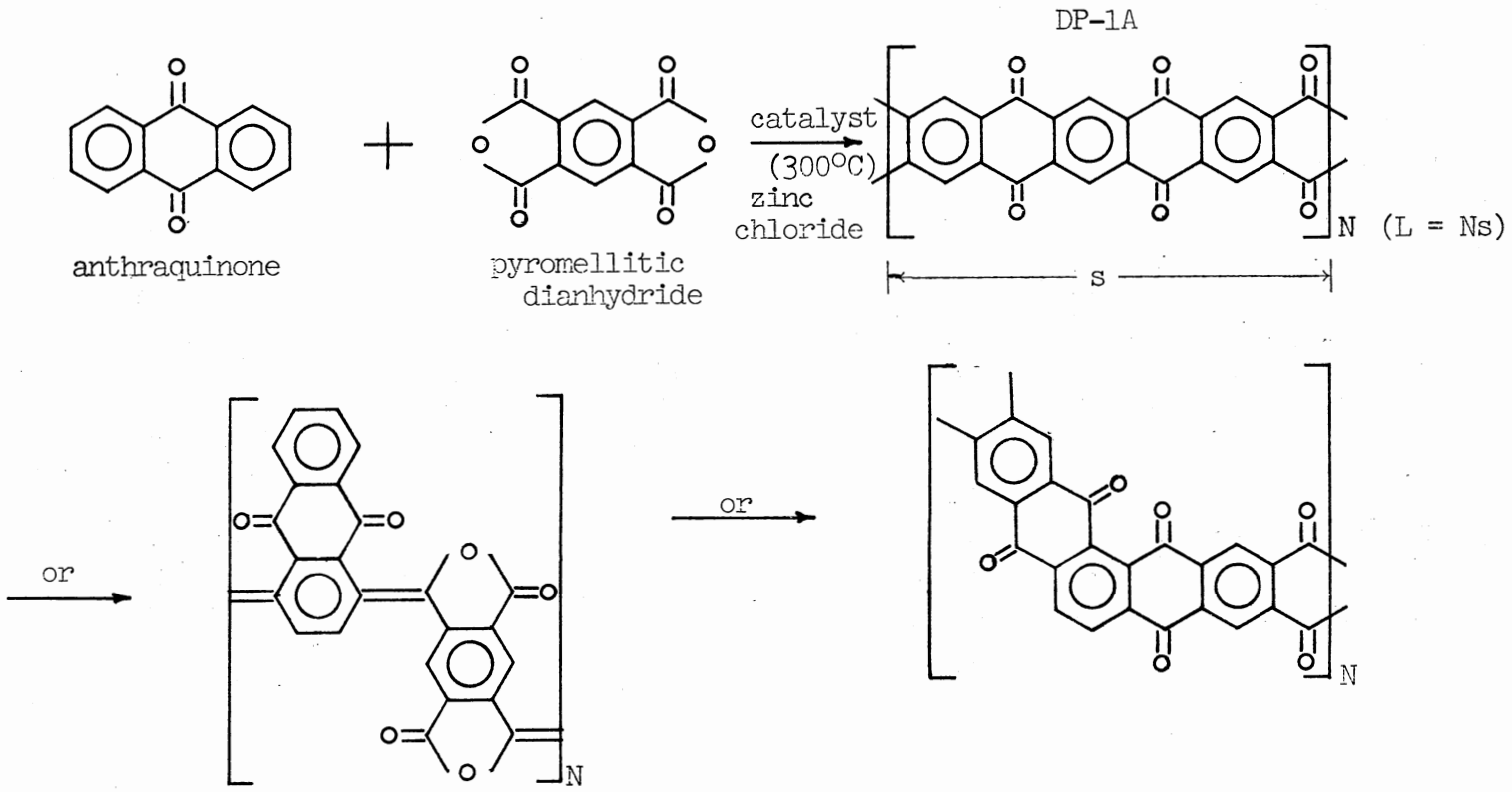

Figure 87. Diagram of Suggested Structures for a typical Electro-Active Polyacenequinone Radical (PAQR) Class of Polymer (DP-1A)

4.4. Purity and Conduction

Unlike inorganic semiconductors (covalent and ionic), impurities in organic semiconductors play a minor role. If one classifies the impurities as 'benign' and 'active', most impurities do not appreciably increase the electronic conduction of conductive polymers (Pohl, 1967; and Kho and Pohl, 1969). This is so, because, electronic conduction in polymers is due to π-electron delocalization associated with special structures (ekaconjugated). For impurity conduction to take place in polymers, the impurities must then have a degree of conjugation greater than that of the host polymer.

4.5. The Disorder Effect

The long range aperiodicity in polymeric semiconductors give rise to 'disorder', and hence the difficulty in formulating theories. Small molecules arranged in three-dimensional structures can give rise to semiconducting or even metallic properties. Inspite of long range 'disorder', short range 'order' may be sufficient to support carrier transport.

4.6. The Size Effect and The π-Electron Hypothesis

The development of the field of organic semiconductors has been attributed to Szent-Gyorgi (1941), who suggested the semiconduction properties due to π-electron transfer from one molecule to another in the field of biochemical metabolism. Eley (1948) and Vartanyan (1948) found that the effect of replacing the two central hydrogen atoms in

phthalocyanine by metals such as Cu, Mg, Zn, etc., had a very small effect on both the conductivity and the energy gap, so that the conductivity may be regarded as an integral part of the conjugated ring structure, most probably involving π-electrons. Inokuchi (1951 and 1952) found that the resistivity (ρ) and the energy interval (ΔE) {where $\rho = \rho_o \exp(\Delta E/kT)$} decreases with the increase of the number of π-electrons for polynuclear hydrocarbons and polyazoaromatic ring systems. This effect for condensed naphthalene, biphenyl system and polyacenes has been illustrated by Okamoto and Brenner (1964). The electrical conductivity of π-electron molecules was found to increase greatly with the number of π-electrons within a molecule for copper phthalocyanine (Epstein and Wildi, 1960) and for donor-acceptor complexes (Akamatu et al., 1956; and Eley et al., 1959).

For a large variety of polymers, it has been shown that increasing the number of fused rings in the hydrocarbons, or increasing the ionization constant of acid monomers, increases the conductivity, whereas, the activation energy interval and the pressure coefficients are decreased (Pohl and Engelhardt, 1962; Gutmann and Lyons, 1967; and Kho and Pohl, 1969). It has also been observed that the increase in spin concentration (spins/gm) results in an increase in both the conductivity (Pohl and Chartoff, 1964; Hartman, 1968; and Wyhof, 1970) and the dielectric constant (Wyhof, 1970).

4.7. Models for Conduction Mechanisms

There are three models for conduction mechanisms (Boguslavskii and Vannikov, 1970; and Pohl, 1967) that can be used to describe the electrical properties of organic semiconductors.

(a) In the 'point defect or impurity' model, point impurities are in continuum and this corresponds to the model used to describe the generation and frequency of carriers hopping between impurity centers in atomic and ionic solids (Pollak and Geballe, 1961; Tanaka and Fan, 1963; Pollak, 1964, 1965, 1970, 1971 and 1972b; Mott, 1969a and 1969b; and Jonscher, 1972).

(b) In the 'heterogeneous' model, the distance between impurities is comparable to impurities themselves and a heterogeneous distribution of conductive material is assumed in a poorly conductive or insulating continuum. The simplest example is the two-layer Maxwell-Wagner condenser (Von Hippel, 1954) and a complicated example is the n-layer model (Koops, 1951). The 'heterogeneous' model for materials of two 'sorts' has been studied by Boguslavskii and Stil'bans, (1963); and Storbeck and Starke, (1965).

(c) In the 'macromolecular' model, the distance between molecules (hopping centers) is smaller than the dimensions of the molecules, and this corresponds to the regions of continuous conjugation separated by thin layers of non-conjugated material. The macromolecular model appears to be relevant to PAQR class of electro-active polymers.

4.7.1. A Macromolecular Model and Carrier Generation

A macromolecular model consisting of macromolecules of an average length L was described in Section 1.2., and in Figures 3 and 4. Since the dissociation to create a 'Mott' (inter-chain) exciton (electron-hole pair) is the promotion of an electron to an energy W, where the Fermi energy $E_F = W/2$, the probability density following the Fermi

statistics is

$$n(W) = \frac{n_o}{\exp\{-(E_F - W)/(kT)\} + 1} = \frac{n_o}{\exp\{(W/2kT)\} + 1} \qquad (34)$$

where n_o = number of electronic states per unit volume at the energy of excitation.

Pohl (Pohl and Opp, 1962; Pohl and Engelhardt, 1962; Pohl, 1964a; and Gutman and Lyons, 1967) offers the following treatment of the carrier generation process based upon the concept of ekaconjugation:

Representing the biradical •R• and its ekaconjugated precursor as R,

$$R \rightleftarrows \bullet R \bullet \qquad (35)$$

$$(\bullet R \bullet)/(R) = K_1 = \exp\{-\Delta F_1/(kT)\} \qquad (36)$$

$$\Delta F_1 = \Delta H_1 - T\Delta S_1 \simeq {}^3E \qquad (37)$$

where ${}^3E$ is the energy of conversion of the singlet bound state to the triplet state biradical. (R) denotes the concentration of R, ΔF_1 is the Helmholtz free energy, ΔH_1 is the enthalpy and $T\Delta S_1$ is the entropy factor for the process. One can roughly estimate ${}^3E$ by the 'metallic' model of linearly conjugated molecules containing Z atoms each contributing a π-electron in the same nodal plane as

$$E_n = h^2n^2/(8mL^2) \qquad (38)$$

where n = 1, 2, ---; L = Zℓ (includes one-half bond length overlap at ends); ℓ = C-C bond distance; and E_n = the energy of a particular state n. The molecule will contain two π-electrons per orbital filled up to Z = 2n in the ground state (Pohl and Engelhardt, 1962; and Lyons et al., 1958). The energy required to excite a frontier electron up to the first unfilled orbital n→n+1, is

$$\underset{(\text{in eV})}{\Delta E} = \frac{h^2(2n+1)}{8m\ell^2Z^2} \doteq \frac{h^2(Z+1)}{8m\ell^2Z^2} = {}^1E = {}^3E = \frac{19.2(Z+1)}{Z^2} \quad (39)$$

For a typical polymer n ≃ 1000, then ΔE becomes equal to the value of kT at room temperature (~ 0.025 eV) and so the excited levels should become thermally populated. Thus one might expect metallic conduction in a true polyene, but only highly crystalline and stereoregular structures show appreciable conductivity. Three reasons for the poor conductivity in polymers are: (a) the large intermolecular barrier; (b) the bonds are not all equal in length but alternate (this Jahn-Teller effect stabilizes the polymer but restricts electron delocalization); and (c) rotation of the chain interrupts conjugation (Goodings, 1975).

The electronic properties of electro-active PAQR polymers can be conveniently divided into two parts (Pohl, 1974): (a) Intra-chain carrier behavior, which considers the origin and kinetics of carriers within long chains, are best analyzed by a.c. phenomenon. Intra-molecular excitons are called 'Frenkel' excitons. The intra-chain motion may be of wave packet drifting type, with thermally activated hopping between small polaron states; and (b) inter-chain carrier behavior, which considers the barrier conduction between molecules, are best analyzed by d.c. phenomenon. The inter-chain carrier transfer is either of the hopping or of the thermally activated tunnelling types.

4.7.2. Types of Transport Mechanisms

For organic semiconductors three distinct types of transport mechanisms have been considered (Paushkin et al., 1974): (a) Band type;

(b) Hopping type; and (c) Tunnelling type.

(a) In band type of conduction, intermolecular π-electron interaction occurs, the energy levels over the whole volume of the polymer form conduction and valence bands separated by an energy gap. An electron on excitation to conduction band leaves a hole in the valence band, either or both carriers can move freely in the bands, giving rise to high mobilities. The greater the width of the band, in general, greater is the mobility. Narrow bands imply a large effective mass and low mobility.

(b) In hopping type of conduction, the carriers hop from one region of polyconjugation (of good conductivity) to another by moving over the barrier separating the two via an activated state. Thus the carriers must overcome poorly conducting dielectric barriers of disordered or nonconjugated structure. The increase in temperature increases the probability of jumps.

(c) Tunnelling type of transport is a quantum mechanical phenomenon, in which an electron passes through a potential energy barrier without acquiring enough energy to pass over the top of the barrier. The energy level of the particle is the same before and after the tunnelling process. The tunnelling probability depends only on the difference between the height of the potential energy barrier and the energy of the particle, and on the width of the barrier.

Ioeffe (1959a and 1959b) has pointed out that especially for organic semiconductors having low mobilities ($< 5\ cm^2/V\text{-}s$), the nominal free path length ($L \propto \mu$) is less than the length of thermal electrons, and is smaller than the lattice spacing. Thus scattering then removes

the possibility of using the band theory notion of mean velocity of carriers and hopping type of conduction mechanism is appropriate. Pollak (1962) has shown that for the band type of conduction where $\sigma_{band}(\omega) \propto \{1/(1+\omega^2\tau^2)\}$ the conductivity will decrease, and for the hopping type of conduction where $\sigma_{hop} \propto \{\omega^2/(1+\omega^2\tau^2)\}$ the conductivity will increase, as the frequency increases.

4.7.3. Anderson's Localization Theorem

Two approximations are used in studies concerning crystalline solids: (a) free electrons (nearly); and (b) tight binding.

Anderson's localization theorem is the extension of the tight binding method to non-crystalline solids (Anderson, 1958). Here, a periodic array of sites with co-ordination number Z is assumed and at each site there is a potential well whose depth (V) is distributed at random over a range V_o. The interaction is between the nearest neighbor sites only. Anderson's theorem then says that, if a parameter defined by $P = V_o/B$ (where B = band width) is greater than some critical value P_o, then a particle placed at zero time in a given potential well at zero temperature will not diffuse away, i.e., the particle will diffuse at a rate exp $(-\alpha r)$, where α depends on V_o/B giving rise to localized states. Detailed treatments of Anderson's localization are given by Miller and Abrahams (1960), Mott and Twose (1961), Economou and Cohen (1970 and 1972), and Freed (1972).

4.7.4. Two Possible Band Models Applicable to Organic Semiconductors

There are two band models which may take into account the

'disorder' field encountered in the PAQR class of polymeric semiconductors. This field could arise due to randomness of range and depth of the aperiodic potential of the lattice.

The Mott-CFO Model. As pointed out by Fritzche (1974), the thermally activated conduction bands are separated by a band gap. Translational and compositional disorders are assumed to cause fluctuations of the potentials of sufficient magnitude that they give rise to localized tail states extending from the conduction and valence bands into the band gap. As noted by Mott (1967, 1969a, 1969b and 1970), the character of wave-function changes at critical energies E_c and E_v which separate the localized and the extended states. At the critical energies, electron and hole mobilities drop sharply from a low mobility band transport at zero temperature between extended states to a thermally activated hopping type between localized gap states which disappears at zero temperature. These so called 'mobility edges' as given by Cohen et al. (1969) define a mobility gap (E_c-E_v) which contains only localized states.

The Davis-Mott Model. In this model proposed by Davis and Mott (1970), the mobility edges still lie at E_c and E_v. A distinction is made between localized states which originate from lack of long range order and others due to structural defects. The first kind of localized states extend from E_c to E_a and from E_v to E_b into the mobility gap. The defect states form longer tails extending from E_a and E_b into the band gap.

4.8. D.C. Conductivity

4.8.1. Pressure Dependence

High pressure techniques are attributed largely to the work of Bridgman (1949). The basic effect of pressure is to increase the overlap of electronic orbitals. This causes delocalization of electrons, a broadening of bands of allowed energy and a decrease of forbidden gap energies. Thus a decrease in resistivity occurs which may ultimately lead to metallic behavior. The second effect of pressure is the relative displacement of one type of orbital with respect to another, which could establish a new ground state of the system or greatly modify the the electronic properties of the ground system due to configuration interaction as shown by Drickamer and Frank (1973).

Pohl et al. (1962) postulated that the carriers tunnelling or hopping between molecular sites be dependent on the molecular orbital overlap, and are reflected in an effective 'area of contact' for the activated state during charge transfer. According to this theory, d.c. conductivity increases with increasing pressure as given by Equations (18), (19) and (20) in Section 3.1.

For organic semiconductors, the effect that conductivity increases with pressure has been associated with the decrease in the activation energy of the formation of carriers as shown by Samara and Drickamer (1962), Aust et al. (1964), and Bentley and Drickamer (1965). The effect that logarithm of conductivity is proportional to the square root of pressure has been observed by Pohl et al (1962), and Samara and Drickamer (1962) for several polymers. Increase in conductivity with pressure has been reported by Paul and Brooks (1954) for

germanium, by Paul and Pearson (1955) for silicon, and by Hamman (1958) for boron. Drickamer and Frank (1973) give a detailed review of the theory of high pressure experiments. For the PAQR class of polymers, the effect of pressure on d.c. conductivity has been studied by Hartman (1968), Kho and Pohl (1969), and Pohl and Wyhof (1972b).

4.8.2. Temperature Dependence

Davis and Mott (1970) and Fritzche (1974) distinguish three principal contributions to conductivity:

Band Conduction. Band conduction of electrons excited above mobility edge E_c or holes below mobility edge E_v written for electrons yields

$$\sigma_{DC} = \sigma_o \exp \{-(E_c-E_F)/(kT)\} \quad (40)$$

which is of the form as Equation (23) in Section 3.4. Assuming a linear dependence as $(E_c-E_F) = \Delta E-\gamma T$,

$$\sigma_{DC} = C \exp (-\Delta E/kT) \quad (41)$$

where $C = e\, g(E_c)\, kT\, \mu_c \exp (\gamma/k)$. If the extended states are not strongly affected by disorder, μ_c (the average value of mobility) might describe the motion of nearly free electrons (or holes) with occasional scattering. In amorphous solids however, $\mu < 5$ cm^2/V-s, which corresponds to a mean free path less than the inter-atomic spacing. In this case, Cohen (1970) suggests that the charge transfer proceeds via diffusion or Brownian motion. Adopting this classical picture for estimating the mobility one considers fast jumps between neighboring sites and obtains $\mu = (1/6)(ea^2/kT)(\nu)$, where a = the inter-atomic spacing and ν = the jump frequency ($\simeq 10^{15}$ s^{-1}).

The d.c. conductivities and associated energy intervals of PAQR polymers have been studied by Pohl et al. (1962), Pohl and Engelhardt (1962), Pohl and Opp (1962), Pohl et al. (1963), Pohl and Chartoff (1964), Rosen and Pohl (1966), Hartman (1968), Kho and Pohl (1969), Pohl and Wyhof (1972a and 1972b), and Saha et al. (1976b).

Thermally Activated Hopping. If the Anderson condition is satisfied everywhere in the band, an electron can move from site to site by thermally activated hopping. The probability that an electron jumps from from one site to another with absorption of phonon energy is of the form given by Mott (1973), $\nu \exp(-2\alpha R - \Delta W/kT)$, where ΔW is the energy difference between two states. One can calculate diffusion coefficient $D = (1/6)\ \nu R^2 \exp(-2\alpha R - \Delta W/kT)$ and using Einstein's relation $\mu = eD/kT$ determine the conductivity $\sigma = ne\mu$. Hence for thermally activated hopping involving energy $(E-E_F)$ needed to raise the electron to the appropriate localized energy E, the conductivity is of the form

$$\sigma_{DC} = \sigma_1 \exp\{-(E-E_F+\Delta W_1)/kT\} \qquad (42)$$

with $\sigma_1 << \sigma_o$.

Hopping Conduction Near Fermi Energy. Conduction is of the form

$$\sigma_{DC} = \sigma_2 \exp(-\Delta W_2/kT) \qquad (43)$$

with $\sigma_2 << \sigma_1$. At sufficiently lower temperature, the number and energy of phonons available for hopping or tunnelling is restricted to seek centers which are not nearest neighbors, but which instead lie energetically close to and with in the range of kT. For this so called 'variable range hopping process', Mott (1969a and 1972) has derived the Equation (24) in Section 3.4.

Mott's equation of variable range hopping conductance near Fermi energy has been observed for amorphous Ge by Clark (1967), Wally and Jonscher (1967), Chittick (1970), Chopra and Bahl (1970), and Allen and Adkins (1972) to hold over a large temperature range; for Ge, Si and C by Morgan and Walley (1971); and for Vanadium Monoxide by Banus et al. (1972). Brodsky and Gambino (1972) found that annealing increases T_o in amorphous Si. The exponent is ¼ for three-dimensional, 1/3 for two-dimensional, and ½ for one-dimensional systems. Knotek et al. (1973) found $T^{-\frac{1}{2}}$ dependence for amorphous Ge films and the results agree well with the analysis of Pollak et al. (1973). Physically unreasonable parameters for Mott's $T^{-\frac{1}{4}}$ law results for the data of Bucker (1973) on pyrolysed phenol-formaldehyde polymer films. Anderson (1975) has suggested a different model for d.c. charge transport for glassy materials. Bernasconi (1973) has proposed that Mott's equation can also be simulated by a 'nearest neighbor model' having an appropriate distribution of activation energies. Using the disordered network type of analysis and percolation theory, one obtains a mean activation energy $E_{act}(T)$ with $\sigma_{DC} = \sigma_o \exp(-E_{act}/kT)$.

Pohl and Wyhof (1972a) report Mott type $T^{-\frac{1}{4}}$ behavior for d.c. conductivity for polymers of PAQR class. Saha et al (1976b) report that to get physically realizable parameters for polymers of PAQR class, one may have to use Bernasconi (1973) type of approach with the mean activation energy $E_{act}(T) \propto T^{3/4}$. At this point one cannot say for certain whether Mott's variable range hopping model or Bernasconi's nearest neighbor hopping model is appropriate. Also, Pohl and Wyhof (1972a) have observed for PAQR class of polymers that the a.c. conductivity also follows $T^{-\frac{1}{4}}$ Mott type equation for certain range of temperatures.

No theory explains this behavior.

4.8.3. D.C. Electric Field Strength Dependence

If electrons in the range ≈kT of the Fermi energy make significant contribution to the conductivity, the hopping probabilities in the direction of electric field and in the opposite direction are proportional to $\nu \exp(-2\alpha R - W/kT \pm eER/kT)$ as given by Mott (1973), where E is the electric field strength, W is the difference in the energies of two states and R is the nearest neighbor distance. If E is not strong, i.e., $E << kT/eR$, the conductivity is given by

$$\sigma_{DC} = e^2 g(E) \nu R^2 \exp(-2\alpha R - W/kT) \qquad (44)$$

Rosen and Pohl (1966) have derived a d.c. conductivity which explicitly takes into account the effect of d.c. electric field strength as given by Equations (26) and (27) in Section 3.7.

4.9. A.C. Conductivity

4.9.1. Pressure Dependence

The a.c. conductivity increases with increasing pressure as given by Equation (21) in Section 3.2.

4.9.2. Frequency and Temperature Dependence

Pollak and Geballe (1961) introduced a 'variable range mechanism' for a.c. conductivity in crystalline silicon in an impurity conduction range, as given by Equations (31) and (32) in Section 3.9.

Austin and Mott (1969) adopted the theory of Pollak and Geballe (1961) to the case where hopping conduction takes place near Fermi

and obtained

$$\sigma_{AC}(\omega) = (\pi/3) \{g(E_F)\}^2 kT e^2 \alpha^{-5} \omega \{\ln (\nu_p/\omega)\}^4 \quad (45)$$

where ν_p is a phonon frequency and α describes the decay with r of the localized wave function exp $(-\alpha r)$ and $g(E_F)$ is the density of states at Fermi energy E_F. The theory of this phenomenon was treated by Pollak (1964, 1965 and 1971) to analyse the hopping motion of electrons between pairs of localized states and also extended hopping over many sites. It was pointed out by Jonscher (1972) that this type of frequency behavior is found not only in disordered, glassy and amorphous solids, but also in ordered molecular solids. It was shown that carriers need not be electrons, but may be polarons, protons or ions and that s is not a constant, but approaches unity at low temperatures and 0.5 or less at high temperatures. Pollak and Pike (1972) raise similar points. Other theoretical treatments of frequency dependent conductivity in hopping systems are given by Mott (1969a), Austin and Mott (1969), and Davis and Mott (1970). Scher and Lax (1973) have extended to a.c. conditions the d.c. theory of Miller and Abrahams (1960), and Butcher (1972).

From the experimental data of Owen (1970), Austin and Garbett (1971), and Taylor et al. (1971) for As_2S_3, Chan and Jonscher (1969) for solid polymeric CS_2, and Nathoo and Jonscher (1971) for stearic acid, one can say that $\sigma_{AC}(\omega)$ varies as ω^n (where $n < 1$) in the low frequency range ($<10^6$ Hz), varies as ω^2 in high frequency range (upto 10^8 Hz) and for very high frequencies it probably saturates. The temperature dependence of ω^n variation is more at low frequencies and less at higher frequencies. ω^2 type variation has very little temperature dependence. A new model for dielectric loss in polymers has been

described by Jonscher (1975).

In PAQR polymers, the a.c. conduction has been studied by Hartman and Pohl (1968), Hartman (1968), Wyhof and Pohl (1970), and Pohl and Wyhof (1972a and 1972b). Saha et al. (1976a) have assumed an a.c. activation energy distribution as $E_{act}(T) = k\,\eta\,T^{3/4}$, where η is related to certain critical percolation concentration based on the percolation theories of hopping transport by Ambegaokar et al. (1972), Pollak (1972a) and Bernasconi (1973). At low frequencies at least, they suggest that Mott's type $T^{-1/4}$ equation can be simulated for the observed a.c. conductivities varying as $T^{-1/4}$ $\{\sigma_{AC} = \sigma_o \exp(-\eta/T^{1/4})\}$ for the two PAQR class of polymers they studied. They found lower values of η for a.c. than for d.c. They also report a saturation of σ_{AC} at low temperatures and that the loss tangent peaks shift to higher temperatures for higher frequencies. The equation for increasing a.c. conductivity with increasing temperature is of the form as given by Equation (25) in Section 3.5.

4.10. Dielectric Constant

4.10.1. Pressure and Temperature Dependence

The pressure and temperature dependence of dielectric constant of PAQR polymers are given by Rosen and Pohl (1966), Hartman and Pohl (1968), Wyhof and Pohl (1970), Pohl and Wyhof (1972a), Pohl (1974), and Equation (22) in Section 3.3.

4.10.2. Frequency Dependence

The dielectric constant decreases with increasing frequency of the

applied electric field as given by Equation (29) in Section 3.8.2. and observed by Rosen and Pohl (1966), Hartman and Pohl (1968), and Pohl (1974). A possible reason for the saturation of polarization comes from the long length of the polymer macromolecules (Wyhof, 1970; and Pohl, 1974). Saturation can be expected when the electrical energy along the molecular domain is comparable to kT. In a randomly interacting dielectric medium, the effect is enhanced because the local electric field is larger than the applied external electric field.

4.10.3. Local Electric Field Strength

Pohl (1974) estimates the local electric field strength in the intra-chains as

$$E_{local} = \frac{e \exp(-W/kT)}{2 a b \varepsilon_1 \varepsilon_o (\varepsilon_r+2)} \qquad (46)$$

where W = activation energy; a, b = cross-sectional dimensions of the polymer chain, ε_1 = local relative dielectric constant in the polymer chain, ε_r = relative dielectric constant of the whole solid and ε_o = permittivity of free space.

4.10.4. Dielectric Relaxation

One may express relative dielectric constant as $\varepsilon_r = \varepsilon_r' - i\varepsilon_r''$, and a.c. conductivity as $\sigma_{AC} = \sigma' + i\sigma''$, then $\sigma' = \omega\varepsilon_r''$ and $\sigma'' = \omega\varepsilon_r'$, where ω is the angular frequency, ε_r' and σ' are in-phase components, ε_r'' and σ'' are the out of phase components.

From the Equation (28) in Section 3.8.1., the relaxation time is thermally activated one of the form as given by Pohl and Wyhof (1972a), and Norrell et al. (1974),

$$\tau_{max} = \tau_o \exp (E_v/kT) \tag{47}$$

From conventional polarization theory of Debye (1912 and 1929), for a single relaxation time τ one can write

$$\varepsilon_r = \varepsilon_r' - i\varepsilon_r'' = \varepsilon_\infty + (\varepsilon_s - \varepsilon_\infty)/(1 + i\omega\tau) \tag{48}$$

where ε_r is the complex dielectric constant, ε_∞ is the optical dielectric constant and ε_s is the static dielectric constant of the material. From this one obtains

$$\varepsilon_r' = \varepsilon_\infty + (\varepsilon_s - \varepsilon_\infty)/(1 + \omega^2\tau^2) \tag{49}$$

$$\varepsilon_r'' = (\varepsilon_s - \varepsilon_\infty)\ (\omega\tau)/(1 + \omega^2\tau^2) \tag{50}$$

and also one can obtain

$$\sigma'(\omega) = \omega\varepsilon_r'' \propto \omega^2/(1 + \omega^2\tau^2) \tag{51}$$

For a distribution of relaxation times, the dielectric constant is given by Frohlich (1958) and Boettcher (1952) as

$$\varepsilon_r = \varepsilon_\infty + (\varepsilon_s - \varepsilon_\infty) \int_0^\infty \frac{G(\tau)}{(1 + i\omega\tau)}\, d\tau \tag{52}$$

where $G(\tau)$ is the distribution function of relaxation such that

$$\int_0^\infty G(\tau)\, d\tau = 1 \tag{53}$$

Fuoss and Kirkwood (1941), Cole and Cole (1941), and Frohlich (1958) have suggested various empirical forms of $G(\tau)$.

Pohl and Wyhof (1972a) showed that the frequency of the maximum a.c. conduction-polarization response is a thermally activated one for the PAQR class of polymers of the form as given by Equation (28) in Section 3.8.1.

4.11. Hall Effect

In the study of organic semiconductors, it is difficult and many times impossible to measure the Hall effect because of the high resistivities.

Within the theoretical framework of band theory, the Hall effect for a semiconductor with a single dominant carrier is described by the Hall constant (Kittel, 1971)

$$R_H = -1/en \tag{54}$$

where n is the concentration of carriers and e is the absolute value of electronic charge. Since the conductivity $\sigma = ne\mu$, one can obtain the Hall mobility from the relation $\mu_H = R_H\sigma$. If the mobilities of the holes and electrons do not differ greatly, one must take into account the contribution of intrinsic carriers and the Hall constant is given by

$$R_H = (-1/e)\ (n\mu_n^2 - p\mu_p^2)/(n\mu_n^2 + p\mu_p^2) \tag{55}$$

Since the concentration of intrinsic carriers in organic semiconductors is generally unknown, calculations from measured values of R_H must be treated with circumspection (Boguslavskii and Vannikov, 1970).

In amorphous materials the Hall mobility is in need of special interpretation (Friedman, 1971). In materials such as the amorphous covalent and ionic semiconductors, it almost always yields a value of Hall mobility in the order of 0.1 $cm^2/V\text{-}s$ and is temperature independent. Moreover, the sign of the Hall effect has been observed to be negative even in materials which has positive thermoelectric powers (Seebeck coefficients). These anomalies have been explained by Friedman (1971) using the random phase model. In this model, the Hall voltage arises

from a magnetic quantum mechanical interference involving three or more sites which can momentarily achieve the same energy state. Then the sign of Hall effect is found to be negative even for hole conduction. This resolved the Hall-Seebeck effects anomaly for amorphous atomic solids. In chain or sheet like structures such as macromolecular solids the anomaly is yet unresolved.

Burnay and Pohl (1978) have observed a 'Friedman-anomalous' negative Hall constant of 130 cm^3/C for a polyphthalocyanine polymer with a positive Seebeck coefficient of 9.5 $\mu V/^oK$ at room temperature. Hermann and Rembaum (1966) report a Hall mobility of approximately 0.4 $cm^2/V\text{-}s$ for a polymeric complex of polyvinylcarbazole with iodine. Pohl and Rosen (1963) report Hall mobilities of 2 to 5 $cm^2/V\text{-}s$ for pyrolysed ion-exchange resins (n-type) with a concentration of carriers of 1 to $3x10^{20}$ $/cm^3$. Pohl and Engelhardt (1962) observed a 'normal' positive Hall constant of 290 cm^3/C for a pyrene-pyromellitic anhydride PAQR polymer (p-type) at room temperature with the mobility estimated to be 0.04 $cm^2/V\text{-}s$ with a concentration of about $2x10^{16}/cm^3$, and a positive Seebeck coefficient of 70 $\mu V/^oC$. Pohl and Laharre (1960) report high mobilities of 120 $cm^2/V\text{-}s$ for nickel-doped pyropolymers.

4.12. Thermoelectric Power

Along with the Hall effect, the thermoelectric power or Seebeck coefficient is a traditional source of information on the nature of conduction and concentration of carriers on semiconductors. The thermoelectric power S is given by Equation (33) in Section 3.12. for a simple band type semiconductor. The value of dS/dT should have the opposite sign to that of S. This has been observed by Pohl and

Engelhardt (1962), and Kho and Pohl (1969) for PAQR class of polymers. Among the earliest studies on polymeric solids were those of Winslow et al. (1955), and on low molecular weight organic solids were those of Fielding and Gutmann (1957). These studies show temperature dependent mobilities as expected of hopping type conduction.

CHAPTER V

SUMMARY AND CONCLUSIONS

In general, the response of matter to an externally applied electric field results in both conduction and polarization. The metallic or semiconducting motion of carriers shows up as conduction response. The blocked or polarized motion of carriers shows up as polarization response.

There are four recognizable modes of electrical polarization in pure substances as shown in Figure 2. They are: (a) Electronic; (b) Atomic; (c) Orientational; and (d) Nomadic. The fifth type (e) Maxwell-Wagner or Interfacial polarization is found in mixtures.

Nomadic polarization is due to the pliant response to an applied electric field acting on unlike charge pairs occupying separate long molecular domains. If the charge carriers are electrons, it is called as hyperelectronic polarization. If the charge pairs are protons, it is called as hyperprotonic polarization. As compared to low dielectric constants (~1.8 to 38) of conventional organic compounds, hyperelectronic polarization can give rise to unusually high dielectric constants (~50 to 100,000) as found in electro-active polyacenequinone (PAQR) class of polymeric semiconductors.

An investigation was made of the enhanced electronic semiconduction and the unusually high dielectric constants due to hyperelectronic polarization as exhibited in certain classes (ekaconjugated) of polyacene-

quinone radical (PAQR) polymers. Forty two polymeric solids were examined. In particular, the theory of Pollak and Pohl for nomadic polarization based on small polaron transport in macromolecular solids was compared with experiment. Variations in experimental parameters such as temperature ($77^{o}K$ to $350^{o}K$); pressure (0 to 8 Kbar); frequency (dc to 100 MHz); and electric field strength (ac/dc., 0 to 1000 V/cm) were examined.

All the polymers investigated in this study were electronic semiconductors with conductivities σ ranging from 10^{-1} to 10^{-8} mho/cm, and relative dielectric constants ε_r ranging from 200 to 300,000 at room temperature. The thermoelectric measurements indicate that the majority carriers are p-type (holes).

The application of pressure enormously increases the d.c. conductivity $\{\sigma_{DC} \propto \exp P^{\frac{1}{2}}\}$ due to increased intermolecular orbital overlap and thus the lowering of potential barrier for pressure activated carrier formation. The a.c. conductivity increases with pressure $\{\sigma_{AC} \propto \exp P^{\frac{1}{2}}\}$ due to increased intermolecular overlap and eased carrier formation. The application of pressure enormously increases the relative dielectric constant $\{\varepsilon_r \propto \exp P^{\frac{1}{2}}\}$ for similar reasons.

The d.c. semiconductivity increases enormously with temperature $\{\sigma_{DC} \propto \exp (-E_a/kT)\}$ due mainly to the increase in thermally activated carrier formation and mobility. The a.c. conductivity increases with temperature $\{\sigma_{AC} \propto \exp (-E_a/kT)\}$ as a consequence of increase in carrier content and mobility. The relative dielectric constant increases enormously with temperature $\{\varepsilon_r \propto \exp (-E_a/kT)\}$ for similar reasons.

The d.c. conductivity follows Mott's 'variable range hopping'

conduction relation $\{\sigma_{DC} \propto \exp(T^{-\frac{1}{4}})\}$, not just up to about $40^{o}K$ as theoretically expected, but over the entire range of temperatures studied ($77^{o}K$ to $350^{o}K$). The Mott model enables one to estimate the density of electronic states as $\sim 10^{17}$ to 10^{18} $eV^{-1}cm^{-3}$ for these solids.

From Cole-Cole plots of ε_r'' versus ε_r', the dominant relaxation times are found to be of the order of $\sim 10^{-3}$ to 10^{-4}s for these polymers. The activation energy E_ν $\{\nu_{max} = \nu_o \exp(-E_\nu/kT)\}$ for the characteristic frequency, ν_{max}, at each temperature is interpreted as the hopping energy associated with the charge carriers in the long molecular domains. The relative dielectric constant decreases with increasing frequency $\{\varepsilon_r \propto \omega^{-p}\}$ because the polaronic dipoles are unable to follow the variations of higher frequency electric fields. The a.c. conductivity increases with frequency $\{\sigma_{AC} \propto \omega^{s}\}$ as characteristic of hopping (polaronic) conduction.

The high dielectric constants observed as a result of hyper-electronic polarization in PAQR class of aromatic polymers are due to: (a) an appreciable density of carriers (pressure, temperature or electric field activated); (b) long molecular domains due to extensive π-electron delocalization; and (c) the ready transport of carriers, probably due to small polaron hopping-type motion within these amorphous solids.

Pollak and Pohl (1975) predicted that the tendency of the applied field to reduce the dielectric constant such as is normal at low frequencies, should reverse at high frequencies, an effect due to enhanced hopping rate by the higher electric field strength. This reversal of dielectric constant from $(-\partial\varepsilon_r/\partial E_{dc})$ to $(+\partial\varepsilon_r/\partial E_{dc})$ as predicted by theory occurs at a characteristic 'cross-over' frequency F_C = 10 MHz

for polymer JK-64 as shown in Figure 80. Figure 64 shows that this reversal of dielectric constant for a change of d.c. electric field strength from 0 to 222 V/cm actually occurs at a 'cross-over' frequency F_C = 3.4 MHz for polymer JK-64 as seen from experiment. The experimental results also agree with theory in the effect of a.c. and d.c. electric field strengths upon the static dielectric constant as proposed by Pohl and Pollak (1977). The theory and experiment also agree with the effect of electric field strength on a.c. conductivity.

One of the necessary parameter for the quantitative evaluation of the Pollak-Pohl dielectric theory is the molecular length. Since these aromatic polymers are insoluble in ordinary solvents, special techniques based on solid state properties were necessary to evaluate average molecular length. These were: (a) the effect of d.c. electric field strength on d.c. conductivity as proposed by Rosen and Pohl (1966); (b) the a.c. electric field strength saturation of polarization as proposed by Pohl (1974); and (c) the dielectric theories proposed by Pollak and Pohl (1975), and Pohl and Pollak (1977). The average molecular lengths for three polymers DP-1A, JK-64 and JM-85A gave comparable results on using these three approximate methods.

This study finds that the hyperelectronic polarization model does account for the unusually high dielectric constants observed in PAQR class of aromatic amorphous polymeric solids.

In broad aspect, the theory to explain electronic conduction and hyperelectronic polarization in polyacenequinone class of polymers is observed to agree well with experiment. Minor deviations observed from the theory can be accounted for by the realization that the theory has been perhaps oversimplified to deal with a complicated phenomena.

A SELECTED BIBLIOGRAPHY

Akamatu, H., H. Inokuchi, and Y. Matsunga, Bull. Chem. Soc. Japan 29, 213 (1956).

Allen, F. and C. J. Adkins. Phil. Mag. 26, 1027 (1972).

Ambegaokar, V., B. I. Halperin, and J. S. Langer, J. Non-Cryst. Sol. 8-10, 492 (1972).

Anderson, J. C., Dielectrics, Reinhold Pubs., Co., N.Y. (1964).

Anderson, P. W., Phys. Rev. 109, 1492 (1958).

Aust. R. B., W. H. Bentley, and H. G. Drickmer, J. Chem. Phys. 41, 1856 (1964).

Austin, I. G. and N. F. Mott, Adv. in Phys. 18, 41 (1969).

Austin I. G. and E. S. Garbett, Phil. Mag. 23, 17 (1971).

Banus, M. D., T. B. Reed, and A. C. Strauss, Phys. Rev. B5, 2764 (1972).

Bentley, W. H. and H. G. Drickamer, J. Chem. Phys. 42, 1573 (1965).

Bernasconi, J., Phys. Rev. B7, 2252 (1973).

Boettcher, C. J. F., Theory of Electric Polarization, Elsevier Pubs., Co., N.Y. (1952).

Boguslavskii, L. I. and L. S. Stil'bans, Dokl. Akad. Nauk SSR 147, 1114 (1963).

Boguslavskii, L. I. and A. V. Vannikov, Organic Semiconductors and Biopolymers, Trans. by B. J. Hazzard, Plenum Press, N. Y. (1970).

Bridgman, P. W., Physics of High Pressure, G. Bell and Sons Ltd., London (1949).

Brillouin, cited in Eley, D. D. and G. D. Parfitt, Horizons in Bio-Chemistry, P. 348, Eds. B. Pullman and Kasha, Academic Press, N.Y. (1962).

Brodsky, M. H. and R. J. Gambino, J. Non-Cryst. Sol. 8-10, 739 (1972).

Brophy, J. J., Physics Today 14(8), 40 (1961).

Bucker, W., J. Non-Cryst. Sol. 12, 115 (1973).

Butcher, P. N., J. Phys. Sol. St. Physics. C5, 1817 (1972).

Burnay, S. G. and H. A. Pohl, J. Non-Cryst. Sol. 30, 221 (1978).

Chan, W. S. and A. K. Jonscher, Phys. Stat. Solidi 32, 749 (1969).

Chittick, R-C., J. Non-Cryst. Sol. 3, 255 (1970).

Chopra, K. L. and S. K. Bahl, Phys. Rev. B1, 2545 (1970).

Clark, A. H., Phys. Rev. 154, 750 (1967).

Cohen, M. H., H. Fritzche, and S. R. Ovshinsky, Phys. Rev. Lett. 22, 1065 (1969).

Cole, K. S. and R. H. Cole, J. Chem. Phys. 9, 341 (1941).

Davis, E. A. and N. F. Mott, Phil. Mag. 22, 903 (1971).

Debye, P., Phys. Zeits. 13, 97 (1912).

Debye, P., Polar Molecules, Chemical Catalog Co., N.Y. (1929).

Drickamer, H. G. and W. Frank, Electronic Transitions and the High Pressure Chemistry and Physics of Solids, Chapman and Hall, London (1973).

Economou, E. N. and M. H. Cohen, Phys. Rev. Lett. 25, 1445 (1970).

Economou, E. N. and M. H. Cohen, Phys. Rev. B5, 2931 (1972).

Eley, D. D., Nature 162, 819 (1948).

Eley, D. D., Research (London) 12, 293 (1959).

Eley, D. D., H. Inokuchi, and M. R. Willis, Disc. Faraday Soc. 28, 54 (1959).

Eley, D. D., Organic Semiconducting Polymers, Chapter 5, Ed. by J. E. Katon, Marcel Dekker Inc., N.Y. (1968).

Epstein, A. and B. S. Wildi, J. Chem. Phys. 33, 324 (1960).

Fielding, P. and F. Gutmann, J. Chem. Phys. 26, 411 (1957).

Frohlich, H., Theory of Dielectrics, Second Edition, Oxford Press (1958).

Freed, K. F., Phys. Rev. B5, 4802 (1972).

Friedman, L., J. Non-Cryst. Sol. 6, 329 (1971).

Fritzche, H., Amorphous and Liquid Semiconductors, Chapter 5, Ed. by J. Tauc, Plenum Press, N.Y. (1974).

Fukayama, H., Bussei 15(10), 492 (1974).

Fuoss, R. M. and J. G. Kirkwood, J. Am. Chem. Soc. 63, 685 (1941).

Gladstone, S., K. J. Laidler, and H. Eyring, Theory of Rate Processes, McGraw-Hill Book Co., N.Y. (1941).

Goodings, E. P., Endeavour 34, 123 (1975).

Greene, R. L., G. B. Street, and L. J. Suter, Phys. Rev. Lett. 34, 577 (1975).

Gutmann, F. and L. E. Lyons, Organic Semiconductors, John Wiley and Sons, Inc., N.Y. (1967).

Hamman, S. D., Aust. J. Chem. 11, 391 (1958).

Hartman, R. D., "Hyperelectronic Polarization and Related Electronic Properties of Macromolecular Solids: Organic Semiconductors", Un-Pub. Ph.D. thesis, Oklahoma State University (1968).

Hartman, R. D. and H. A. Pohl, J. Polym. Sci. A1(6), 1135 (1968).

Hermann, A. M. and A. Rembaum, J. Appl. Phys. 37, 3642 (1966).

Holstein, T. D., Ann. Phys. New York 8, 343 (1959).

Inokuchi, H., Bull. Chem. Soc. Japan 24, 222 (1951).

Inokuchi, H., Bull. Chem. Soc. Japan 25, 28 (1952).

Inokuchi, H. and H. Akamatu, Solid State Physics, pp. 93-148, Eds. F. Seitz and D. Turnbull, Academic Press, N.Y. (1961).

Ioeffe, A. F., Sol. St. Phys. USSR 1, 1 (1959a).

Ioeffe, A. F., Phys. Chem. Sol. 8, 6 (1959b).

Johnson, V. A. and K. Lark-Horowitz, Phys. Rev. 92, 226 (1953).

Johnson, V. A., Prog. in Semiconductors 1, 63 (1956).

Jonscher, A. K., Thin Sol. Films 1, 213 (1967).

Jonscher, A. K., J. Non-Cryst. Sol. 8-10, 293 (1972).

Jonscher, A. K., Electronic and Structural Properties of Amorphous Semiconductors, pp. 329-361, Eds. P. G. Le Comber and J. Mort,

Academic Press, N.Y. (1973).

Josefowicz, M., Fast Ion Transp. Solids, Solid State Batteries Devices, Proc. NATO Adv. Study Inst. 1972, pp. 623-636, Ed. by W. van Gool (1973).

Kanda, S. and H. A. Pohl, Organic Semiconducting Polymers, Chapter 3, Ed. by J. E. Katon, Marcel Dekker Inc., N.Y. (1968).

Karl, N., Festkoerperprobleme 14, 261 (1974).

Kho, J. H. T. and H. A. Pohl, J. Polym. Sci. A1(7), 139 (1969).

Kittel, C., Introduction to Solid State Physics, Fourth Edition, John Wiley and Sons, Inc., N.Y. (1971).

Knotek, M. L., M. Pollak, T. M. Donovan, and H. Kurtzmann, Phys. Rev. Lett. 30, 853 (1973).

Koops, C., Phys. Rev. 83, 121 (1951).

Kryszewski, M., Pr. Nauk Inst. Chem. Org. Fiz. Politech. Wroclaw 7(1), 29 (1974).

Kryszewski, M., J. Polym. Sci., Polym. Symp. (Int. Symp. Macromol. Invited Lect., 1974) 50, 359 (1975a).

Kryszewski, M., Mater. Sci. 1(1), 3 (1975b).

Lakatos, A. I. and M. Abkowitz, Phys. Rev. B3, 1791 (1971).

Last, B. J. and D. J. Thouless, Phys. Rev. Lett. 27, 1719 (1971).

Lyons, L. E., A. Bree, and G. C. Morris, Proc. of the Third Conf. on Carbon, Pergamon, N.Y. (1958).

Marcus, R. A., J. Chem. Phys. 43, 2642 (1965).

Mark, H. F., Proc. of the Symp. on the Role of Sol. St. Phenomena in Electric Circuits, Microwave Research Inst., Poly. Inst., Brooklyn Symp. Ser. Vol. 7, Wiley (Interscience). N.Y. (1957).

Mason, J. W., R. D. Hartman, and H. A. Pohl, J. Polym. Sci. C17, 187 (1967).

Masuda, K. and M. Silver, Energy and Charge Transfer in Organic Semiconductors, Plenum Press, N.Y. (1974).

Miller, A. and S. F. Abrahams, Phys. Rev. 120, 745 (1960).

Mizokuchi, K., E. Tsuchida, and I. Shinohara, Hyomen 13(10), 559 (1975).

Morgan, M. and P. A. Walley, Phil. Mag. 23, 661 (1971).

Mott, N. F. and W. D. Twose, Adv. Phys. 10, 107 (1961).

Mott, N. F., Adv. Phys. 16, 49 (1967).

Mott, N. F., Phil. Mag. 19, 835 (1969a).

Mott, N. F., Festkorperprobleme 9, 22 (1969b).

Mott, N. F., Phil. Mag. 22, 7 (1970).

Mott, N. F., J. Non-Cryst. Sol. 8-10, 1 (1972).

Mott, N. F., Electronic and Structural Properties of Amorphous Semiconductors, pp. 1-51, Eds. P. G. Le Comber and J. Mort, Academic Press. N.Y. (1973).

Mrozowski, S., Phys. Rev. 85, 609 (1952a).

Mrozowski, S., Phys. Rev. 86, 1056 (1952b).

Mrozowski, S., Semiconduction in Molecular Solids, pp. 1-7, H. A. Pohl, Ivy Curtiss Press, Philadelphia (1960).

Nathoo, M. H. and A. K. Jonscher, J. Phys. Sol. St. Phys. C4, L301 (1971).

Norrell, C. J., H. A. Pohl, M. Thomas, and K. C. Berlin, J. Polym. Sci. Polym. Phys. Ed. 12, 913 (1974).

Okamoto, Y. and W. Brenner, Organic Semiconductors, John Wiley and Sons, Inc., N.Y. (1964).

Owen, A. E., J. Non-Cryst. Sol. 4, 78 (1970).

Paul, W. and H. Brooks, Phys. Rev. 94, 1128 (1954).

Paul, W. and G. L. Pearson, Phys. Rev. 98, 1755 (1955).

Paushkin, Ya. M., T. P. Vishnyakova, A. F. Lunin, and N. A. Nizova, Organic Polymeric Semiconductors, Trans. by R. Kondor, Ed. by D. Slutzkin, John Wiley and Sons, Inc., N.Y. (1974).

Pethig, R. and H. A. Pohl, J. Phys. D.: Appl. Phys., 10, 105 (1977).

Pohl, H. A. and J. P. Laherre, Proc. Fourth Conf. on Carbon, p. 259, Ed. by S. Mrozowski, Pergamon Press N.Y. (1960).

Pohl, H. A., Modern Aspects of the Vitreous State, pp. 72-113, Ed. by J. Mackenzie, Butterworth, London (1961).

Pohl, H. A., Organic Semiconductors, pp. 134-141, Eds. J. J. Brophy and J. W. Buttrey, Macmillan Co., N. Y. (1962).

Pohl, H. A. and D. A. Opp, J. Phys. Chem. 66, 2121 (1962).

Pohl, H. A., A. Rembaum, and A. Henry, J. Am. Chem. Soc. 84, 2699 (1962).

Pohl, H. A., C. G. Cogos, and C. Cappas, J. Polym. Sci. A1, 2207 (1963).

Pohl, H. A. and R. Rosen, Proc. Fifth Conf. on Carbon, Vol II, p. 113, Ed. by Mrozowski, Pergamon Press, N.Y. (1963).

Pohl, H. A., Prog. in Sol. St. Chem., I, pp. 317-343, Pergamon Press, N.Y. (1964a).

Pohl, H. A., Electronic Aspects in Biochemistry, pp. 121-127, Ed. by B. Pullman, Academic Press, N.Y. (1964b).

Pohl, H. A. and R. P. Chartoff, J. Polym. Sci. A2, 2787(1964).

Pohl, H. A., J. Polym. Sci. C17, 13 (1967).

Pohl, H. A., Organic Semiconducting Polymers, Chapter 2, Ed. by J. E. Katon, Marcel Dekker Inc., N.Y. (1968).

Pohl, H. A. and J. R. Wyhof, J. Non-Cryst. Sol. 11, 137 (1972a).

Pohl, H. A. and J. R. Wyhof, J. Polym. Sci. A1(10), 387 (1972b).

Pohl, H. A., J. Biol. Phys. 2(3), 113 (1974).

Pohl, H. A. and M. Pollak, J. Chem. Phys. 66(9), 4931 (1977).

Pollak, M. and T. H. Geballe, Phys. Rev. 122, 1742 (1961).

Pollak, M., Physics of Semiconductors (Conf. at Exeter), Inst. of Phys. and the Phys. Soc., London (1962).

Pollak, M., Phys. Rev. 133, A564 (1964).

Pollak, M., Phys. Rev. 138, A1822 (1965).

Pollak, M., Disc. Faraday Soc. 50, 13 (1970).

Pollak, M., Phil. Mag. 23, 519 (1971).

Pollak, M., J. Non-Cryst. Sol. 8-10, 486 (1972a).

Pollak, M., J. Non-Cryst. Sol. 11, 1 (1972b).

Pollak, M. and G. E. Pike, Phys. Rev. Lett. 28, 1448 (1972).

Pollak, M., M. L. Knotek, H. Kurtzmann, and H. Glick, Phys. Rev. Lett. 30, 856 (1973).

Pollak, M. and H. A. Pohl, J. Chem. Phys. 63(7), 2980 (1975).

Rembaum, A., J. Moacanin, and H. A. Pohl, Prog. in Dielectrics 6, 41 (1965).

Rosen, R. and H. A. Pohl, J. Polym. Sci. A1(4), 1135 (1966).

Sachs, S. B. and K. S. Spiegler, J. Phys. Chem. 68, 1214 (1964).

Saha, K., S. C. Abbi, and H. A. Pohl, J. Non-Cryst. Sol. 22, 291 (1976a).

Saha, K., S. C. Abbi, and H. A. Pohl, J. Non-Cryst. Sol. 21, 386 (1976b).

Samara, G. A. and H. G. Drickamer, J. Chem. Phys. 37, 474 (1962).

Sawa, G., Hyomen 13(7), 367 (1975).

Scher, H. and M. Lax, Phys. Rev. B7, 4592 (1973).

Seanor, D. A., J. Polym. Sci. 2, 1187 (1972).

Seki, H., Amorphous Liq. Semicond. Proc. Int. Conf. Fifth, 1973, 2, pp. 1015-1034, Ed. by J. Stuke and W. Brenig, Taylor and Francis, London (1974).

Silins, E., Latv. PSR Zinat. Akad. Vestis. 6, 40 (1975).

Storbeck, I. and M. Starke, Ber. des. Busenges, Phys. Chem. 89, 343 (1965).

Szent-Gyorgi, A., Science 93, 609 (1941).

Tanaka, S. and H. Y. Fan, Phys. Rev. 132, 1516 (1963).

Taylor, P. C., S. G. Bishop, and D. L. Mitchell, Phys. Rev. Lett. 27, 414 (1971).

Vartanyan, A. T., J. Phys. Chem. USSR 22, 769 (1948).

Von Hippel, A. H., Dielectric and Waves, John Wiley and Sons, Inc., N.Y. (1954).

Walley, P. A. and A. K. Jonscher, Thin Sol. Films 1, 367 (1967).

Williams, D. J. Polym. Prepr. Am. Chem. Soc., Div. Polym. Chem. 14(2), 830 (1973).

Winslow, F. H., W. A. Baker, and W. A. Yager, J. Am. Chem. Soc. 77, 4751 (1955).

Wyhof, J. R. "The Nature of Hyperelectronic Polarization", Unpub. Ph.D. thesis, Oklahoma State University (1970).

Wyhof, J. R. and H. A. Pohl, J. Polym. Sci. A2(8), 1741 (1970).

Wynne, K. J. and G. B. Street, Ind. Eng. Chem. Prod. Res. Dev. 21, 23 (1982).

VITA 2

Pormamilla Shamarao Vijayakumar

Candidate for the Degree of

Doctor of Philosophy

Thesis: ELECTRONIC CONDUCTION AND HYPERELECTRONIC POLARIZATION IN ELECTRO-ACTIVE POLYACENEQUINONE CLASS OF POLYMERIC SEMICONDUCTORS

Major Field: Physics

Biographical:

Personal Data: Born in Bangalore, Mysore, India, June 23, 1946, the son of Mr. and Mrs. P. L. Shamarao.

Education: Graduated from National High School, Bangalore, India, in March, 1960; received Bachelor of Engineering degree in Electrical Engineering from University of Mysore in 1969; received Bachelor of Technology degree in Electronics Engineering from Madras Institute of Technology in 1970; received Master of Arts degree in Physics from Indiana State University, Terre Haute, Indiana in 1973; completed requirements for the Doctor of Philosophy degree at Oklahoma State University in July, 1983.

Professional Experience: Graduate teaching assistant, Department of Physics, Indiana State University, 1971-72; graduate teaching assistant, Department of Physics, Oklahoma State University, 1973-80; consultant, Engineering Energy Laboratory, Department of Electrical Engineering, Oklahoma State University, 1981-82; graduate research assistant, Department of Physics, Oklahoma State University, 1982-83.